N.M.R. RELAXATION STUDIES OF THALLIUM COMPOUNDS.

A thesis submitted by

MARK JULIEN FORSTER

in candidature for the degree of Doctor of Philosophy of the University of London.

The Bourne Laboratory,
Royal Holloway College,
University of London,
Egham Hill,
Egham,
Surrey.

July 1984.

exchange phenomena but at high field severe line broadening of undetermined origin was observed.

The observed effects of spin-lattice relaxation on the spectra of coupled nuclei were discussed. The proton spectra of aqeuous dimethylthallium(III) cation at 400 MHz and dineopentylthallium(III) chloride at 360 MHz were reproduced using a chemical exchange formalism.

Preliminary measurements on aqueous thallium(I) ion in the presence of dissolved oxygen taken with previous studies showed an inverse dependence of R_1 on frequency. This was interpreted in terms of scalar relaxation and enabled estimation of the electronic relaxation times.

ACKNOWLEDGEMENTS

The author would like to thank Dr Duncan Gillies for his guidance, enthusiasm and encouragement during the course of this work. Thanks are also due to Dr Ray Matthews for the supply of thallium compounds and use of the Bruker WP80 spectrometer. Dr Geoff Hawkes and Mr Malcolm Buckingham are thanked for experiments performed on the Bruker WH400 under the University of London Intercollegiate Research Services Scheme. The help of Mr Charles Galsworthy in the preparation of some of the samples studied is gratefully acknowledged.

The receipt of a research studentship from the Science and Engineering Research Council is thankfully acknowledged.

Finally the author wishes to thank his family for their support over many years, and Mrs Sylvia Partin for typing this thesis.

****

T O   N I N A

****

CONTENTS.

CONTENTS - continued

CONTENTS - continued

CONTENTS - continued

CONTENTS - continued

LIST OF FIGURES.

LIST OF FIGURES - continued.

LIST OF FIGURES - continued

LIST OF TABLES.

LIST OF TABLES - continued.

LIST OF TABLES - continued.

CHAPTER ONE - INTRODUCTION.

Section 1.1. Introduction to NMR.

1.1.1 Applications of NMR.

Nuclear magnetic resonance is a spectroscopic technique based upon the interaction of atomic nuclei with radiofrequency electromagnetic radiation in the presence of a magnetic field. The first observations of the NMR phenomenon were made independently by the research groups of Bloch[1] and Purcell[2]. Since these pioneering studies, expansion of the field has continued unabated and this technique is now one of the major experimental tools in many branches of modern science.

NMR has found a plethora of uses and applications in chemical studies including compound identification, structural determination, solvation phenomena, hydrogen bonding, exchange and molecular rate processes. More physically inclined investigations include the areas of molecular electronic structure, phase phenomena, intermolecular and intramolecular interactions and relaxation studies which provide information on molecular reorientational, diffusional and internal motions. In addition the NMR method now looks set to achieve considerable advances in the areas of *in vivo* biochemistry and medical imaging.

The property of nuclear spin relaxation, whereby the nuclear spin system returns to equilibrium following a perturbation, is intimately connected with the feasibility and understanding of the NMR experiment.

Relaxation measurements became routinely possible following the introduction of the pulsed Fourier transform method in the early 1970's. Relaxation phenomena are dynamic in nature and provide information on the motion of the molecules that carry the observed spins. This thesis presents some investigations of the spin relaxation behaviour of the thallium nucleus and the derivation of motional information for the cases that allow this.

The basic NMR experiment may be described in terms of classical and quantum mechanical formalisms. A brief discussion of the principles of the NMR experiment will now be given for both methods.

1.1.2. Quantum mechanical approach.

Many nuclei possess the property of spin angular momentum. This property is described quantum mechanically by the spin angular momentum operator $\hat{\underline{I}}\hbar$, which is a vector operator with Cartesian components $\hat{I}_x\hbar$, $\hat{I}_y\hbar$, and $\hat{I}_z\hbar$. Elementary quantum theory shows that the spin wave functions, denoted $|I,m\rangle$ in Dirac notation, are eigenfunctions only of the square of the angular momentum operator $\hat{I}^2\hbar^2$ and of a unique Cartesian component; which by convention is $\hat{I}_z\hbar$. The corresponding eigenvalue equations are

$$\hat{I}^2 |I,m\rangle = I(I+1)|I,m\rangle , \qquad \{1\text{-}1A\}$$

$$\hat{I}_z |I,m\rangle = m |I,m\rangle . \qquad \{1\text{-}1B\}$$

The integer or half integer I is called the spin quantum number and is a characteristic of a given nucleus. The eigenvalue m may take any of the 2I+1 values I,I-1....-I. Thus the absolute value and the value of the z component of the nuclear spin angular momentum, are equal to $\sqrt{I(I+1)}\hbar$ and $m\hbar$ respectively; $\hbar$ is used as the unit of quantum mechanical angular momentum.

Nuclei with non zero spin angular momentum possess a colinear and proportional magnetic moment described by the magnetic moment operator.

$$\hat{\underline{\mu}} = \gamma \hbar \hat{\underline{I}}. \qquad \{1 - 2\}$$

The proportionality constant γ is called the gyromagnetic ratio and is characteristic of each nucleus. The interaction between the magnetic moment and the applied field is given in terms of the Zeeman Hamiltonian

$$\hat{H} = -\hat{\underline{\mu}}.\underline{B}_o \quad . \qquad \{1 - 3\}$$

If the static field is applied along the Z axis then

$$\hat{H} = -\gamma\hbar B_o \hat{I}_z \qquad \{1 - 4\}$$

where B_o is the magnetic flux density in Teslas.
Thus it can be seen that each spin wavefunction $|I,m\rangle$ with distinct eigenvalues m of $\hat{I}_z$ will possess a different energy in the presence of the applied field. It is between these energy levels that transitions occur, due to interaction with the perpendicular component of an oscillating RF field, thus constituting the NMR experiment. Using the Einstein formula

$$\Delta E = h\nu \qquad \{1 - 5\}$$

It is easily seen that for a spin having $I = \frac{1}{2}$ with allowed values for m of $\pm \frac{1}{2}$, transitions are induced by the RF field when the resonance condition is met, i.e.

$$\nu_{RF} = \nu_o = \gamma B_o / 2\pi \qquad \{1 - 6\}$$

where ν_o is the nuclear resonance frequency in MHz.
At a more advanced level the quantum mechanical approach provides a deep insight into relaxation phenomena. However for an elementary appreciation the classical approach is preferred due to its relative simplicity.

1.1.3. Classical approach and spin relaxation.

The classical description of NMR is based upon the phenomological differential equations of Bloch(3). The rate of change of the classical angular momentum $\underline{P}$ of a spinning nucleus in a magnetic field $\underline{B}$, is related to the magnetic moment $\underline{\mu}$ by

$$\frac{d\underline{P}}{dt} = \underline{\mu} \times \underline{B} \qquad \{1 - 7\}$$

The gyromagnetic ratio is defined by the relationship

$$\underline{\mu} = \gamma \underline{P}, \qquad \{1 - 8\}$$

thus

$$\frac{d\underline{\mu}}{dt} = \gamma(\underline{\mu} \times \underline{B}). \qquad \{1 - 9\}$$

This equation may be solved by adopting a rotating frame of reference (4). For a lone static field of magnitude B_o parallel to the z axis, the solution to equation {1-9}shows that the magnetic moment precesses at the Larmor frequency.

ABSTRACT.

The thallium-205 spin relaxation behaviour of several thallium compounds have been investigated as a function of temperature and frequency.

For the aqueous dimethylthallium(III) cation there were significant contributions from both the chemical shift anisotropy (CSA) and spin rotation (SR) mechanisms at low fields but at high fields the former was dominant. Reorientational and angular momentum correlation times were obtained and their values were rationalised in terms of a structure limited motional model. Thallium-205 spin rotation constants and an absolute shielding scale were also determined.

In the aqueous glycerol medium CSA was found to be the only significant relaxation mechanism for the dimethylthallium(III) cation at both high and low field. At high field the reorientational motion was outside extreme narrowing and an R_1 maximum was observed. This allowed simultaneous determination of the motional parameters and of the shielding anisotropy as 5550 $\pm$ 32 ppm. Again a structure limited reorientational model was appropriate. The motional dependence of the ratio R_2/R_1 was as expected for a single correlation time model, extrapolating to 7/6 at extreme narrowing.

Dimethylthallium(III) chloride in DMSO-d^6, dineopentylthallium(III) chloride in pyridine-d^5 and neat thallium(I) ethoxide all showed significant CSA relaxation. Low field thallium(I) ethoxide spectra were dominated by

$$\nu_o = \gamma B_o / 2\pi \qquad \{1 - 10\}$$

For an ensemble of non interacting spins the magnetisation vector is the vector sum of the magnetic moments

$$\underline{M} = \Sigma_i \, \underline{\mu}_i \qquad \{1 - 11\}$$

This leads to the equation of motion of the magnetisation

$$\frac{d\underline{M}}{dt} = \gamma(\underline{M} \times \underline{B}) \qquad \{1 - 12\}$$

This equation describes the behaviour of the magnetisation in the presence of the static magnetic field $\underline{B}_o$, and the magnetic vector $\underline{B}_1$ of the perturbing RF. At equilibrium, there is no transverse phase coherence, but, due to the differing populations of the allowed energy states, or allowed orientations of each magnetic moment, there is a finite magnetisation parallel to the static field

$$\underline{M} = (0,0,M_o). \qquad \{1 - 13\}$$

The foregoing equations take no account of nuclear spin relaxation processes. Bloch[3] assumed that the return to equilibrium of the longitudinal and transverse components of the magnetisation, following a perturbation, may be described by first order processes with the constants T_1 and T_2 respectively. Thus the full Bloch equations in vector form are

$$\frac{d\underline{M}}{dt} = (\underline{M} \times \underline{B}) + \left[\frac{-M_x}{T_2} , \frac{-M_y}{T_2} , \frac{-(M_z - M_o)}{T_1} \right]. \qquad \{1 - 14\}$$

These equations allow a simple description of the relaxation process for non interacting spins.

Bloembergen, Purcell and Pound[5] gave the first explanation of nuclear spin relaxation in molecular rather than macroscopic terms. The physical picture proposed is one in which relaxation processes are stimulated by microscopic, time dependent, electric and magnetic fields at the nucleus. These typically arise from the modulation by molecular motion of magnetic and electrical interactions of the observed nucleus with its environment and other nuclei. The modulation of these various interactions leads to a number of so called relaxation mechanisms, each of which can contribute to the observed relaxation. Thus before information on an individual mechanism can be obtained one must establish its contribution to the total relaxation rate. This process is aided by the measurement of relaxation rates as a function of both temperature and frequency, and sometimes also by double irradiation methods. The investigation of the frequency dependence of the spin relaxation has been called "Relaxation Spectroscopy" by Noack[6]. If the relaxation rate(s) for a given mechanism are found, then a knowledge of the magnitude of the interaction. will allow the derivation of the motional correlation time(s) characterising the molecular motion. This idea will be further elaborated in the following chapter.

Section 1.2. Thallium NMR.

The thallium nucleus has two naturally occurring isotopes, ^{203}Tl and ^{205}Tl, both of which are magnetically active with spin ½, the natural abundances are 29.5% and 70.5% respectively. The gyromagnetic ratios and hence the resonance frequencies of the two isotopes are in the ratio $(^{205}Tl)/(^{203}Tl) = 1.0098$. For the majority of purposes ^{203}Tl and ^{205}Tl NMR will provide the same information, hence ^{205}Tl is the isotope observed due to its greater natural abundance. For a reference sample of aqueous dimethylthallium(III) nitrate at 41°C, the extrapolated infinite dilution ^{205}Tl resonance frequency has been reported as $\nu_o(^{205}Tl)=57,887,037$ Hz [10]. This frequency is scaled to a field strength for which the ^{1}H resonance frequency of $Si(CH_3)_4$ is exactly 100 MHz. The receptivity of the ^{205}Tl nucleus is 0.1355 relative to that of the proton, thus ^{205}Tl is the third most receptive spin ½ nucleus after ^{1}H and ^{19}F.

The nuclear properties discussed above suggest that the ^{205}Tl nucleus should be readily amenable to study by NMR, this is indeed the case. The first liquid and solid state thallium NMR spectra were both reported in 1953, by Gutowsky and McGarvey[8], and Bloembergen and Rowland[9] respectively. Thallium exists in stable +1 and +3 oxidation states and both states have been extensively studied by thallium NMR.

The thallium (I) ion has a $d^{10}s^2$ outer electronic structure and an ionic radius of about 140 pm, making it similar to the Na(I) and K(I) ions. Hence thallium (I) ion has been used as a probe for the study of the function of alkali metal cations in biological systems [14-22]. The ^{205}Tl shift range is very large being of the order of 7000 ppm and the ^{205}Tl shift is known to be a sensitive monitor of the thallium electronic environment. There have been numerous studies of the effects on the ^{205}Tl shift of anion, concentration, solvent composition and interactions with cryptands and crown ethers[23-42], thus leading to information on ion-solvent, ion-ion, and complexation interactions. The spin relaxation behaviour of the thallium(I) ion in solution has been widely investigated. The concentration, anion, field strength and dissolved oxygen dependence have been studied in aqueous solution[43-45], as have the effects of temperature[46] and of the presence of other paramagnetic species[23,47]. The ^{205}Tl(I) ion relaxation has also been found to be strongly solvent dependent[43-45]. Finally a number of thallium relaxation measurements have been reported in biological ionophore complexes of Tl(I) [21-22].

Thallium(III) compounds are usually most stable in the form of organothallium(III) derivatives. Solution state ^{205}Tl chemical shifts have been reported for the compounds $(CH_3)_3Tl$[28,48,49], $(C_2H_5)_3Tl$[28], $(CH_3)_2Tl^+$ [28,43] and CH_3Tl^{2+} [50] as well as for some

thallium(III) complexes[27,51]. ^{205}Tl shifts have also been measured for Ph_2TlCl_2 and its complexes with PPh_3 and pyridine in pyridine and methanol solvents[28], Ph_2TlCl in liquid ammonia[49], Ph_2TlBr in DMSO[28], Ph_3Tl in ether[28] and a series of substituted arylthallium(III) bis-trifluoroacetates in a number of solvents[28]. In addition the thesis of Brady[13] contains previously unreported ^{205}Tl chemical shift measurements for a number of organothallium(III) compounds. The ^{205}Tl shift of dimethylthallium(III) and monomethylthallium(III) cations has been studied as a function of solvent, concentration, anion and temperature[52,53,50,10]. The dimethylthallium(III) cation in aqueous solution has a strongly temperature dependent ^{205}Tl chemical shift ($\simeq$ 0.44 ppm/K), but it is almost independent of concentration. These properties make it convenient to use the ^{205}Tl shift of this sample for temperature measurement in ^{205}Tl NMR spectra. The majority of the variable temperature relaxation studies to be presented in this thesis utilise this method.

Brady[13] has reported variable temperature, solution state, ^{205}Tl spin lattice relaxation measurements for a number of mono and diorganothallium(III) compounds. Previously the only ^{205}Tl spin lattice relaxation study of organothallium(III) compounds had been the report of Reeves[43] of the effect of dissolved O_2 on the dimethylthallium(III) cation in aqueous solution. It has been reported in two recent reviews[7,11] that the thallium

relaxation of this species is independent of concentration, anion, substitution of H_2O for D_2O, substitution of ^{203}Tl for ^{205}Tl, and of the resonance frequency. This statement is not fully correct, Reeves in fact only observed this to be true for the Tl(I) ion. Measurements to be described in Chapter Four show that the resonance frequency has a dramatic effect on the spin lattice relaxation of the dimethylthallium(III) cation.

Large numbers of coupling constants are available in the literature characterising the interaction between ^{203}Tl, ^{205}Tl and the ^{1}H, ^{19}F, ^{13}C and ^{31}P nuclei[7,12,13]. It is relevant to note that measurement of coupling constants to thallium from splittings in, for instance, proton spectra are often complicated by overlap of ^{205}Tl and ^{203}Tl features. At high fields accuracy is in most cases further reduced by line broadening effects caused by enhanced relaxation of the thallium nuclei.

The thallium alkoxides present a problem which shows the value of ^{205}Tl and ^{203}Tl NMR in the elucidation of the structure of thallium compounds. The early work of Schneider and Buckingham[48] confirmed the tetrameric structure $\{Tl(OR)\}_4$ of thallium(I) ethoxide in the liquid state and in cyclohexane solution. Subsequent ^{205}Tl NMR measurements by Gillies et al[55] have shown that this is also the case for several other thallium(I) alkoxides in toluene and benzene solution.

The above discussion only describes some of the thallium NMR literature that is relevant to this

thesis, further information is available in the reviews of Hinton, Metz and Briggs[7], Dechter[12] and the theses of Brady[13], and Burke[54].

The measurements to be described in the following chapters represent an effort to characterise and analyse the ^{205}Tl relaxation behaviour of some thallium compounds. In each case the aim has been to obtain a quantitative separation of the total relaxation rate into the rates due to individual mechanisms, therefore allowing a more informed discussion of the properties and features of each relaxation mechanism. It is hoped that this will then allow a more general appreciation of thallium NMR spectroscopy and allow the optimisation of future NMR experiments for thallium and other nuclei. In addition if molecular interaction constants are known or can be measured these relaxation measurements can provide information on molecular motion in the studied sample and may be used to add to our understanding of liquid state dynamics.

REFERENCES - CHAPTER ONE

1. F.Bloch, W.H.Hansen and M.Packard, Phys.Rev. 70, 474 (1946).
2. E.M.Purcell, H.C.Torrey and R.V.Pound, Phys.Rev.69, 37 (1946).
3. F.Bloch, Phys.Rev. 70, 460 (1946).
4. A.Abragam, "The Principles of Nuclear Magnetism", O.U.P,(1961).
5. N.Bloembergen, E.M.Purcell and R.V.Pound, Phys.Rev. 73, 679 (1948).
6. F.Noack in "NMR Basic Principles and Progress", Vol.3, Springer Verlag (1971).
7. J.F.Hinton, K.R.Metz and R.W.Briggs, Ann.Rep.NMR Spectry., 13, p.211 (1982).
8. H.S.Gutowsky and B.R.McGarvey, Phys.Rev., 91, 81 (1953).
9. N.Bloembergen and T.J.Rowland, Acta Metal, 1, 731 (1953)
10. P.J.Burke, R.W.Matthews and D.G.Gillies, J.C.S.Dalton, 1, 132 (1981).
11. J.F.Hinton and R.W.Briggs in NMR and the Periodic Table, Editors R.K.Harris and B.Mann, Academic Press (1978).
12. J.J.Dechter, Prog.Inorg.Chem., 29, 285 (1982).
13. F.Brady, Ph.D.Thesis, Polytechnic of North London (1980).
14. J.Reuben and G.J.Kayne, J.Biol.Chem. 246, p.6227 (1971).
15. F.J.Kayne and J.Reuben, J.Amer.Chem.Soc., 92, p.220 (1970).
16. J.F.Hinton, G.L.Turner and F.S.Millett, J.Magn. Reson., 45, p.42 (1981).
17. J.F.Hinton, G.Young and F.S.Millett, Biochemistry, 21, p.651 (1982).

18. J.F.Hinton, G.L.Turner and F.S.Millett, Biochemistry, 21, p.646 (1982).

19. R.W.Briggs, F.A.Etzkorn and J.F.Hinton, J.Magn.Reson., 37, p.523 (1980).

20. R.W.Briggs and J.F.Hinton, J.Magn.Reson., 32,p.155 (1978).

21. R.W.Briggs and J.F.Hinton, J.Magn.Reson., 33, p.363 (1979).

22. R.W.Briggs and J.F.Hinton, Biochemistry, 17, p.5576 (1981).

23. R.P.H.Gasser and R.E.Richards, Mol.Phys.,2, 357 (1959)

24. R.Freeman, R.P.H.Gasser, R.E.Richards and D.H.Wheeler, Mol.Phys. 2, 75 (1959).

25. R.Freeman, R.P.H.Gasser and R.E.Richards, Mol.Phys., 2, 301 (1959).

26. R.W.Vaughan and D.H.Anderson, J.Chem.Phys.,52, 5287 (1970).

27. S.Hafner and N.H.Nachtrieb, J.Chem.Phys., 42, 631 (1965).

28. H.Koppel, J.Dallorso, G.Hoffman and B.Walther, Z.Anorg.Allg.Chem., 427, p.24 (1976).

29. J.J.Dechter and J.I.Zink, Inorg.Chem., 15, 1690 (1976).

30. J.J.Dechter and J.I Zink, J.Amer.Chem.Soc., 97 2937 (1975).

31. J.J.Dechter and J.I.Zink, J.Chem.Soc.Chem.Comm., 96 (1974).

32. J.F.Hinton and R.W.Briggs,J.Magn.Reson.,19, 393 (1975)

33. J.J.Dechter and J.I.Zink, J.Amer.Chem.Soc., 98, 845 (1976).

34. J.F.Hinton and R.W.Briggs, J.Magn.Reson., 25, 379 (1977).

35. R.W.Briggs, K.R.Metz and J.F.Hinton, J.Solution Chem., 8, 479 (1979).

36. J.F.Hinton and K.R.Metz, J.Solution Chem., 9, 197 (1980).

37. R.W.Briggs and J.F.Hinton, J.Solution Chem., 6, 827 (1977).

38. R.W.Briggs and J.F.Hinton, J.Solution Chem., 7, 1 (1978).

39. R.W.Briggs and J.F.Hinton, J.Solution Chem., 8, 519 (1979).

40. D.Gudlin and H.Schneider, Inorg.Chim.Acta, 33, 205 (1979).

41. M.Shamispur, G.Rounaghi and A.Popov, J.Solution Chem., 9, 701 (1980).

42. C.Srivanivt, J.I.Zink and J.J.Dechter, J.Amer.Chem.Soc., 99, 5876 (1977).

43. S.O.Chan and L.W.Reeves, J.Amer.Chem.Soc., 96, 404 (1974).

44. M.Bacon and L.W.Reeves, J.Amer.Chem.Soc., 95, 272 (1973).

45. B.W.Bangerter, J.Magn.Reson., 28, 141 (1977).

46. J.F.Hinton and R.W.Briggs, J.Magn.Reson., 25, 379 (1977).

47. B.W.Bangerter and R.N.Schwartz, J.Chem.Phys., 60, 333 (1974).

48. W.G.Schneider and A.D.Buckingham, Disc.Faraday Soc., 34, 147 (1962).

49. K.Hildenbrand and H.Dreeskamp, Z.Phys.Chem., 69, 171 (1970).

50. C.S.Hoad, R.W.Matthews, M.M.Thakur and D.G.Gillies, J.Organomet.Chem., 124, C31 (1977).

51. G.M.Sheldrick and J.P.Yesinowski, J.Chem.Soc.Dalton, 870 (1975).

52. J.F.Hinton and R.W.Briggs,J.Magn.Reson., 22, 447 (1976).

53. P.J.Burke, D.G.Gillies and R.W.Matthews, J.Chem.Res., (5) 124 (1981).

54. P.J.Burke, Ph.D.Thesis, Polytechnic of North London, (1979).

55. P.J.Burke, R.W.Matthews and D.G.Gillies, J.Chem.Soc., Dalton, 1439 (1980).

CHAPTER TWO - THEORETICAL BACKGROUND

Section 2.1. Some important concepts.

2.1.1. Nuclear spin Hamiltonians.

When one seeks to describe the phenomena of magnetic resonance and spin relaxation, the accurate description is of course that given by quantum mechanics.

If it is assumed that the various interactions of the spin system with the lattice and the external fields are independent, then the Hamiltonian operator $\hat{H}_{TOT}$ is given as

$$\hat{H}_{TOT} = \hat{H}_Z + \hat{H}_{RF} + \sum_{\lambda} \hat{H}_{\lambda} \qquad \{2 - 1\}$$

where $\hat{H}_Z$ and $\hat{H}_{RF}$ describe the interaction of the magnetic dipole with the static field and RF field(s) respectively[1]. The $\hat{H}_{\lambda}$ operators describe the return to equilibrium of a perturbed spin system, due to relaxation mechanisms that couple the spin system to the lattice[1]. In general the electric and magnetic interactions which these Hamiltonians describe are anisotropic ,and a tensor description of these interactions allows one to consider all of them in a general manner. Authoritative reviews have been provided by Haeberlen[2] and Spiess[3].

2.1.2. Anisotropic interactions and tensorial treatment.

The relaxation Hamiltonian for any mechanism with the label λ is given by[3]

$$\hat{H}_{\lambda} = C_{\lambda}\ \underline{\hat{I}} \cdot \underline{\underline{R}}_{\lambda} \cdot \underline{\hat{A}} \qquad \{2 - 2\}$$

where C_λ is a constant, $\hat{\underline{I}}$ is the nuclear spin angular momentum operator, the vector operator $\hat{\underline{A}}$ may be the same spin operator (λ= quadrupolar), another spin operator (λ= dipolar and spin spin), or the external magnetic field (λ = shift anisotropy). The second rank tensors $\underline{\underline{R}}_\lambda$ couple every element of $\hat{\underline{I}}$ to every element of $\hat{\underline{A}}$. The second rank tensor may be decomposed into irreducible components of rank 0, 1 and 2[4,5], and it is these that have fundamental physical significance. The irreducible tensors are constructed from the full tensor as follows.

$$R^{(0)}_{ab} = R_{ISO} \quad \delta_{ab} \quad \text{where} \quad R_{ISO} = \frac{1}{3} Tr(\underline{\underline{R}}) \qquad \{2 - 3A\}$$

$$R^{(1)}_{ab} = \tfrac{1}{2} (R_{ab} - R_{ba}) \qquad \{2 - 3B\}$$

$$R^{(2)}_{ab} = \tfrac{1}{2} (R_{ab} + R_{ba}) - R_{ISO}\, \delta_{ab} \qquad \{2 - 3C\}$$

and we have

$$R_{ab} = R^{(0)}_{ab} + R^{(1)}_{ab} + R^{(2)}_{ab} \qquad \{2 - 4\}$$

These are the isotropic, traceless antisymmetric and traceless symmetric part respectively. The spin rotation, chemical shift and spin spin coupling tensors $\underline{\underline{C}}$, $\underline{\underline{\sigma}}$, and $\underline{\underline{J}}$ can contain all three constituents. The dipolar coupling and electric field gradient tensors $\underline{\underline{D}}$ and $\underline{\underline{V}}$, are always traceless and symmetric.

For each interaction there exists a principal axis system in which the symmetric component $\underline{\underline{R}}^{(2)}$ becomes diagonal (Reference 6, Appendix D); then

$$\underline{\underline{R}}^{(0)} + \underline{\underline{R}}^{(2)} = \begin{bmatrix} \rho_{xx} & 0 & 0 \\ 0 & \rho_{yy} & 0 \\ 0 & 0 & \rho_{zz} \end{bmatrix} \qquad \underline{\underline{R}}^{(1)} = \begin{bmatrix} 0 & \rho_{xy} & \rho_{xz} \\ -\rho_{xy} & 0 & \rho_{yz} \\ -\rho_{xz} & -\rho_{yz} & 0 \end{bmatrix}$$

{2 - 5A} {2 - 5B}

$(\underline{\underline{R}}^{(0)} + \underline{\underline{R}}^{(2)})$ and $\underline{\underline{R}}^{(1)}$ are the symmetric and antisymmetric tensors in the principal axis system. The principal axis system is fixed in the molecular or crystal axes. The axes of the principal axis system are labelled according to the following convention

$$\left| \rho_{zz} - R_{ISO} \right| \geq \left| \rho_{xx} - R_{ISO} \right| \geq \left| \rho_{yy} - R_{ISO} \right| \qquad \{2 - 6\}$$

From the irreducible tensors in the principal axis system one may define three new parameters which will later be of use. The delta parameter is defined as

$$\delta = \rho_{zz} - R_{ISO} \qquad \{2 - 7\}$$

This equals $R_{zz}^{(2)}$ in the principal axis system. The assymetry of η is defined as

$$\eta = (\rho_{yy} - \rho_{xx})/\delta \qquad \{2 - 8\}$$

Finally the anisotropy ΔR is defined as

$$\Delta R = \frac{3}{2}\delta = \rho_{zz} - \tfrac{1}{2}(\rho_{xx} + \rho_{yy}) \qquad \{2 - 9\}$$

for an axially symmetric coupling tensor

$$\rho_{xx} = \rho_{yy} = \rho_{\perp} \text{ and } \rho_{zz} = \rho_{\parallel}$$

then

$$\Delta R = (\rho_{\parallel} - \rho_{\perp}) \qquad \{2 - 10\}$$

Note also that $\eta = 0$ in the axially symmetric case. Further discussion will later be given on axially symmetric shielding and spin rotation tensors in the linear dimethylthallium(III) cation.

In high resolution fluid NMR, one observes the trace of the $\underline{\underline{\sigma}}$ and $\underline{\underline{J}}$ tensors as the chemical shift and coupling constant respectively.[2]

$$R^{CS}_{ISO} = \frac{1}{3} Tr (\underline{\underline{\sigma}}) = \sigma_{ISO} \qquad \{2 - 11A\}$$

$$R^{J}_{ISO} = \frac{1}{3} Tr (\underline{\underline{J}}) = J_{ISO} \qquad \{2 - 11B\}$$

Note that R^{D}_{ISO} and R^{V}_{ISO} equal zero, and hence quadrupolar and dipolar interactions are averaged to zero by rapid molecular motion. The spin rotation tensor C has a non zero isotropic component C_{ISO}, spin rotation coupling is observed in gas phase rotational microwave spectroscopy, but lifetimes of rotational states in fluids are so short that the coupling is collapsed and not observed. This may be compared with the collapse of spin spin coupling between two nuclei when one is rapidly relaxing.

Thus it is the isotropic part of the coupling tensor that are observed in the steady state NMR spectrum but the symmetric and antisymmetric parts may induce relaxation. A return to this topic will be made, after a discussion of the theories of how molecular motion modulates the relaxation Hamiltonians.

2.1.3. Correlation function formalism.

Studies of molecular dynamics in fluids may be carried out by several experimental techniques such as infrared spectroscopy, Raman spectroscopy, neutron scattering, NMR relaxation and others. The results of these investigations are usually discussed in terms of time correlation functions, which allow motions to be described formally and in a physically understandable way. The normalised time autocorrelation function of a function f(t) is defined as[6]

$$G(t) = \frac{\langle f(0) \cdot f^{*}(t) \rangle}{\langle f(0)^{2} \rangle} \quad , \qquad \{2 - 12\}$$

where * denotes complex conjugation and < > denotes an ensemble average.

One calls the autocorrelation function stationary if it is independent of the time origin. The autocorrelation function measures the persistence of molecular fluctuations in the medium. Its value at zero time is unity and it decays to zero at long time.[7] It must also satisfy the inequality

$$-1 \leq G(t) \leq 1. \qquad \{2 - 13\}$$

The time dependent functions f(t) of practical interest in NMR relaxation are the normalised spherical harmonics $Y_{lm}(\theta, \phi)$ [6,8]. The angles θ and ϕ are time dependent relative to some laboratory fixed axes, because of molecular reorientation.

The spectral density function $J(\omega)$ is the Fourier transform of the autocorrelation function.

$$J(\omega) = \int_{-\infty}^{\infty} G(t) \exp(i\omega t) dt \qquad \{2 - 14\}$$

This function is the frequency spectrum for molecular fluctuations. The correlation time τ_c is half the zero frequency spectral density, or equivalently the area under the autocorrelation function.

$$\tau_c = \tfrac{1}{2}J(0) = \int_{0}^{\infty} G(t) dt \qquad \{2 - 15\}$$

One often considers an exponential correlation function

$$G(t) = \exp(-|t|/\tau_c) \qquad \{2 - 16\}$$

Then the correlation time τ_c is simply the exponential decay time, and the spectral density function is Lorentzian.

$$J(\omega) = \frac{2\tau_c}{1 + \omega^2 \tau_c^2} \qquad \{2 - 17\}$$

Typically ω_o is in the megahertz range and τ_c is a few picoseconds, then

$$\omega_o \tau_c << 1 \qquad \{2 - 18\}$$

This is the so called extreme narrowing condition, it will later be seen that interesting properties arise outside this region.

It is sometimes necessary to consider a continuously variable range of liquid state environments within the fluid. One may then envisage a distribution of exponential correlation times. This is described by a distribution function g (τ). This must be normalised

$$\int_{0}^{\infty} g(\tau) d\tau = 1 \qquad \{2\text{-}19\}$$

Then our correlation function is a weighted average

$$f(t) = \int_0^\infty g(\tau) \exp\{-t/\tau\}\, d\tau \qquad \{2 - 20\}$$

The most widely used distribution is that due to Cole and Davidson [54]

$$g(\tau) = \frac{\sin(\beta\pi)}{\pi} \left[\frac{\tau}{\tau_o - \tau}\right]^\beta \quad \text{for } 0 \leqslant \tau < \tau_o \qquad \{2 - 21A\}$$

$$g(\tau) = 0 \quad \text{for } \tau \geqslant \tau_o \qquad \{2 - 21B\}$$

where τ_o is the limiting correlation time, and β the distribution width has a value between 0 and 1. The average correlation time is then

$$\bar{\tau} = \beta\tau_o. \qquad \{2 - 22\}$$

Another quantity of interest in NMR relaxation is the angular momentum correlation time τ_J

$$\tau_J = \int_0^\infty \frac{\langle \underline{J}(t) \cdot \underline{J}(0) \rangle}{\langle \underline{J}(0)^2 \rangle}\, dt\,, \qquad \{2 - 23\}$$

Where J (t) is the molecular angular momentum at time t. Many models of molecular motion predict a relationship between τ_c and τ_J, thus measurement of these two correlation times allows a test of the relevant model. The table below indicates several experimental techniques and the correlation function(s) studied.[7,9]

Technique	Quantity measured	Correlation function(s)
Far IR and dielectric relaxation	Fluctuations of electric dipole moment	Reorientation auto & cross correlation functions for Y_1
Near IR	Fluctuations of dipole with vibration	Vibrational and reorientational $< Y_1(0)Y_1(t)>$
Polarised vibrational Raman	Fluctuations of mean polarizability with vibration	Vibrational correlation function
Depolarised vibrational Raman	Fluctuations of anisotopic polarizability	Vibrational and $<Y_2(0)Y_2(t)>$ rotational
NMR	Spin rotation relaxation	τ_J
	CSA, DD, Quadrupolar relaxation	τ_2 = area under $<Y_2(o)Y_2(t)>$
	Spin echo decay.	Translational correlation time τ_{TRANS}

TABLE 2 - 1. Motional information obtained by various experimental methods.

These methods have different advantages and disadvantages[9,10]; Far IR and dielectric methods depend upon both single and two particle correlation functions. Both Raman and near IR methods provide a mixture of vibrational and reorientational correlation functions, whereas NMR can provide pure reorientational information but usually only on correlation times.

Section 2.2. Models of molecular reorientation.

As previously described it is modulation of magnetic and electrical interactions by molecular motion that induces spin relaxation. In spin relaxation we are most often concerned with reorientational motions, and to a lesser extent translational motions. In order to facilitate discussion of relaxation results let us now discuss some of the accepted models for molecular reorientation.

2.2.1. Isotropic rotational diffusion

This model was proposed by Debye[11] in connection with dielectric relaxation of polar molecules. The molecule in solution is considered as a sphere in a continuous viscous medium, acted upon by fluctuating torques due to the Brownian motion of the molecules of the medium; this is analogous to Einstein's picture of translational diffusion. The picture of reorientation that this model produces is one of a rotational random walk of infinitesimal step size. Thus a large number of collisions are necessary for an appreciable change in molecular reorientation. This is equivalent to assuming that $\tau_J \ll \tau_c$. The reorientational random walk over the surface of a sphere is described by a probability function $P(\theta,\phi,t)$, that some vector fixed in the molecular axis system has polar angles θ and ϕ at time t. This probability equation obeys the rotational diffusion equation[6,8,9]

$$\frac{1}{D}\ \frac{\partial P}{\partial t} = \nabla^2 P\ , \qquad \{2 - 24\}$$

where D is the diffusion constant in $rad^2 s^{-1}$ and ∇^2 is the Laplacian operator.

It can be shown (Reference 6, Appendix H) that in this model the autocorrelation function for a spherical harmonic of order ℓ decays exponentially to zero.

$$G_{\ell m}(t) = \frac{< Y_{\ell m}(0).\ Y_{\ell m}^{*}(t) >}{< Y_{\ell m}(0).\ Y_{\ell m}^{*}(0) >} = \exp\{ -D\ell(\ell+1)t \} \qquad \{2-25\}$$

where it is the orientational angles θ and ϕ that are time dependent. In IR and dielectric relaxation studies one is interested in the correlation function for $\cos\ \theta(t) = Y_{10}(\theta, \phi)$ we find

$$G_1(t) = \exp(-2Dt) = \exp(-t/\tau_1) \qquad \{2 - 26\}$$

In NMR relaxation and Raman band shape analysis the relevant function is the second order spherical harmonic (1,14)

$$\tfrac{1}{2}\{3\cos^2\theta(t) - 1\} = Y_{20}(\theta, \phi) \qquad \{2 - 27\}$$

from equation 2 -25

$$G_2(t) = \exp(-6Dt) = \exp(-t/\tau_2) \qquad \{2 - 28\}$$

hence

$$\tau_2 = 1/6D \qquad \{2 - 29A\}$$

$$\tau_1 = 3\tau_2 \qquad \{2 - 29B\}$$

and the mean squared angle swept out by molecular reorientation is

$$<\Delta\theta^2> = 4Dt. \qquad \{2 - 30\}$$

As expected for isotropic diffusion the molecular reorientation is independent of the angle ϕ , and

we need only consider the spherical harmonics $Y_{\ell m}$ with m=O. This will be found not to be the case for anisotropic motion. In the diffusional limit Hubbard[12] derived an equation relating the angular momentum correlation time τ_J, to the reorientational correlation times τ_ℓ.

$$\tau_J \tau_\ell = \frac{I}{\ell(\ell+1)kT} \qquad \{2 - 31\}$$

where I is the moment of inertia and T the absolute temperature. This is the Hubbard equation. This relationship will later be tested for the dimethylthallium(III) cation in aqueous solution.

By comparison between rotational and translational diffusion, Debye[11] suggested that the rotational diffusion constant for a sphere of radius a in a medium of shear viscosity η should be given by the Stokes-Einstein relationship.

$$D = \frac{kT}{8\pi a^3 \eta} \qquad . \quad \{2 - 32\}$$

Then the reorientational correlation times τ_L are given as

$$\tau_\ell = \frac{1}{\ell(\ell+1)D} = \frac{1}{\ell(\ell+1)} \frac{8\pi a^3 \eta}{kT} \quad . \{2 - 33\}$$

This equation implies that the temperature dependence of τ_ℓ is equal to that of (η/T), we will further investigate this point later.

Gierer and Wirtz[15] removed the restrictive assumption of a continuous hydrodynamic medium. They calculated the microviscosity for a solute molecule of radius a_o, in a medium of spherical solvent molecules

of radius a_s and found the rotational diffusion constant D to be

$$D = \frac{1}{f} \quad \frac{kT}{8\pi a_o^3 \eta} \quad , \qquad \{2 - 34\}$$

where f is the microviscosity factor defined as

$$f = \{6a_s/a_o + 1/(1 + a_s/a_o)^3\}^{-1}. \quad \{2 - 35\}$$

then for pure liquids $a_s = a_o$ then $f = 1/6.125$ and τ_ℓ is correspondingly shorter than for the Debye equation.

The influence of viscosity on correlation times is described by equation {2 -33 }for the Debye model. Experiments on a wide variety of organic liquids [16] have shown τ_ℓ proportional to η/T but the slope does not match that given by equation {2 - 33.} The microviscosity theory is one attempt to account for this discrepancy. Another approach is to generalise equation {2 - 33} for $\ell = 2$, we have [17,18].

$$\tau_2 = A\eta + B \quad , \qquad \{2 - 36\}$$

where A and B are constants.

B has been found to be similar to the classical free rotor reorientation time[19].

$$\tau_{FR} = \frac{2\pi}{9} \left(\frac{I}{kT}\right)^{\frac{1}{2}} \qquad \{2 - 37\}$$

where I is the moment of inertia.

When A equals the value $\frac{4}{3}\pi a^3/kT$ given by the Debye equation, it is considered as at the "perfect stick" limit. Here we are assuming that at the surface of the molecule the continuum fluid rotates with the molecule. For a spherical molecule A may vary from the the value of $4\pi a^3/3kT$ in the perfect

stick limit, to zero in the 'perfect slip' limit, where the fluid at the molecular surface is stationary, and the reorientation is inertial or free rotational.[17,18]

2.2.2. Anisotropic rotational diffusion.

In the case of anisotropic molecular reorientation, the motions about different axes have different rates. One must then consider the reorientational correlation times τ_{2m} given as the areas under the auto-correlation functions of the spherical harmonics $Y_{\ell m}$, where $m= 0,1,2$. The τ_{2m} are called the spherical tensor correlation times. In the isotropic case only $m=0$ need be considered.

NMR relaxation is induced by Brownian motional modulation of electric or magnetic interactions. The relaxation vector is, for example, the internuclear vector in the dipole dipole case, or the principal axis of the electric field gradient tensor in the quadrupolar interaction. If the principal symmetry axis of the molecule undergoes reorientation, and α is the angle between this and the relaxation vector, then the correlation time for motional modulation of the relaxation vector is given as[20]

$$\tau_2^{EFF} = \tau_{20} \{\frac{3}{2}\cos^2\alpha - \tfrac{1}{2}\}^2 + \tau_{21}\{3\sin^2\alpha\cos^2\alpha\} + \tau_{22}\{\frac{3}{4}\sin^4\alpha\} \qquad \{2-38\}$$

This is a general result and applies even outside the diffusional limit.

In the diffusional limit, anisotropic reorientation is described by a diffusion tensor $\underline{\underline{D}}$, which

in diagonal form describes the rate of reorientation about the three principal axes of the tensor. The theory for an asymmetric diffuser was developed and applied to the case of quadrupolar relaxation by Huntress.[21]

The relationship between the diffusion constants for a symmetric top molecule, and the correlation time for a given relaxation vector was derived by Woessner[22] and later extended to include internal rotation.[23] In a symmetric top molecule such as the dimethylthallium(III) cation[24], we have diffusion constants ($D_{\parallel}$ and $D_{\perp}$) parallel and perpendicular to the principal symmetry axis. The effective correlation time for a relaxation vector at an angle α to this axis is a function of $D_{\parallel}$, $D_{\perp}$ and α.[22]

$$\tau_2^{EFF} = \{\frac{\frac{3}{2}\cos^2\alpha - \frac{1}{2}\}^2}{6\,D_{\perp}} + \frac{3\cos^2\alpha\,\sin^2\alpha}{5D_{\perp} + D_{\parallel}} + \frac{\frac{3}{4}\sin^4\alpha}{2D_{\perp} + 4D_{\parallel}} \qquad \{2 - 39\}$$

This is a special case of equation 2 - 38, the above equation will later be of great use in describing how correlation times for various relaxation mechanisms depend upon the motion.

Just as the isotropic diffusion model has been extended to anisotropic motions then the generalised hydrodynamic theories can be used to describe the same motions. The diffusion constant D about a given axis is related to the friction coefficient γ by

$$D = kT/\gamma. \qquad \{2 - 40\}$$

Perrin[16] has calculated the friction coefficients in the stick limit for prolate and oblate spheroids. These lead to equations for τ_ℓ similar to equation 2 - 33 but which involve functions of the ratio of the axial lengths. Later Hu and Zwanzig calculated the ratio of the friction coefficients for the slip limit to that in the stick limit, for the oblate and prolate spheroids.[28]

These results allow a calculation of the viscosity dependence of reorientational correlation times for symmetric top molecules in both the slip and stick limits.

2.2.3 Extended diffusion model.

The major assumption of the diffusional models is that of an infinitesimal reorientation step, i.e. that $\tau_J << \tau_\ell$. The extended diffusion model is an attempt to incorporate inertial or large step reorientational effects such as those expected in dilute gases. This model was proposed by Gordon[25] for linear molecules; and extended to spherical tops[26,27], and symmetric tops[28-33] by other workers. A comprehensive review has been provided by McLung[13].

In the extended diffusion model the step size between collisions is treated as a continuous variable. The collisions are considered as instantaneous events which randomise the molecular angular momentum. Two limits of the extended diffusion model exist. In the J diffusion model the collisions randomise both the direction and magnitude of the angular momentum; in the M diffusion

limit only the direction of the angular momentum is changed. The time between collisions is assumed to have a Poisson distribution with mean time τ_J. The relationship between τ_J and τ_ℓ in this model is discussed in terms of the reduced correlation times

$$\tau_J^* = (kT/I)^{\frac{1}{2}}\tau_J \qquad \{2 - 41A\}$$

$$\text{and} \quad \tau_\ell^* = (kT/I)^{\frac{1}{2}}\tau_\ell \qquad \{2 - 41B\}$$

where I is the molecular moment of inertia.

The τ_J^*, τ_ℓ^* relationship may now be discussed independently of any particular system and experimental work compared to the predictions of the model.

Both the M and J diffusion models enable the calculation of τ_ℓ^* as a function of τ_J^*, for a given inertial symmetry. These are integral functions too complicated to reproduce here, but may be found in the aforementioned review.[13] The limiting behaviour of the J and M models are of interest, in the limit of large reorientational steps $\tau_J^* >> 0$, both the M and J models approach the perturbed free rotor model[34]. In the limit of small reorientational steps $\tau_J^* \to 0$ and the J diffusion model approaches the Hubbard relationship

$$\tau_J^* \tau_\ell^* = 1/\ell(\ell+1) \qquad \{2 - 42\}$$

Thus the diffusional reorientation model may be considered as a limiting case of the J diffusion model.

2.2.4. Structure limited models.

This class of motional models regards reorientational motion as a perturbation of the behaviour of the solid state. The reorientational behaviour of the molecule studied then depends not only upon the properties of the molecule itself but also upon structural relaxation of the environment around the molecule. The structural relaxation time plays a role analogous to the period between collisions in the extended diffusion model. The timescale for alterations in the environment may then control the timescale for the loss of orientational correlation. These models are likely to be applicable to highly structured fluids such as associated liquids and hydrogen bonded systems.

The jump diffusion model was proposed by Ivanov[35] and applied by Litovitz et al.[36,37] The reorientation is assumed to take place in the following stages:

(1) A molecule in the liquid is stationary or oscillates about an equilibrium position which is unchanged for A mean time τ_{RES}.

(2) The structural relaxation allows free rotation to a new equilibrium position.

(3) Molecular reorientation takes place by a repetition of these steps.

The correlation functions for this model are found to be exponential.

$$G(t) = \exp\{-t/\tau_{\ell}\} \qquad \{2 - 43\}$$

and the correlation time τ_ℓ is related to the residence time τ_{RES} by[36]

$$\tau_\ell = \tau_{RES} + \frac{1}{\ell(\ell+1)D} \qquad \{2 - 44\}$$

where D is the rotational diffusion coefficient. Two limiting cases of the jump diffusion model may be distinguished:

(1) $\tau_{RES} >> D^{-1}$. Then all reorientational correlation times τ_ℓ are equal to τ_{RES}

$$\tau_1 = \tau_2 = \tau_{RES} \qquad \{2 - 45\}$$

(2) If $\tau_{RES} << D^{-1}$ then the reorientational motions approach the rotational diffusion limit.

$$\tau_2 = 3\tau_1 \qquad \{2 - 46\}$$

Litovitz et al have measured the ratio τ_2/τ_1 for some associated liquids.[36,37,39,40] In glycerol they found $\tau_2/\tau_1 = 1.1$ and concluded that jump diffusional reorientation is operative in this liquid. They also made the connection between structural relaxation effects and the existence of a distribution of dielectric (τ_1) correlation times.[36] They suggested that a distribution of reorientational (τ_2) correlation times might also exist. The existence of this distribution and the presence of the jump diffusion mechanism for glycerol have been confirmed by the ^2H relaxation studies of Jonas.[41]

A related model is the defect diffusion model proposed by Glarum[42] and developed by Powles.[43] This model describes molecular reorientation as a cooperative process with the reference molecule interacting

with its near neighbours.

The reference molecule in the body of the liquid undergoes small step rotational diffusion until a free volume defect or vacancy arrives at the molecule which then undergoes large angle reorientation until the defect moves on. These free volume defects are assumed to diffuse throughout the liquid. Limiting cases of this model are discussed elsewhere.(44)

Litovitz et al. have discussed free volume effects on the viscosity of liquids.(45)

The Ivanov theory has been extended to anisotropic reorientation by O'Reilly.(55) It is assumed that fast reorientation takes place for a time τ_i following a hard collision, whilst in the time τ_s between collisions no significant reorientation occurs. Using this model O'Reilly has shown that the product of the reorientational and angular momentum correlation times is a function of the mean squared angle of the reorientation step. For a spherical top

$$\tau_2 \tau_J = \frac{I\langle \theta^2 \rangle}{6kT\,(1-\exp\{-\langle\theta^2\rangle\})}, \qquad \{2 - 47A\}$$

where

$$\langle\theta^2\rangle = \langle \theta_x^2\rangle + \langle \theta_y^2\rangle + \langle \theta_z^2\rangle$$

and $\langle \theta_i^2\rangle$ is the mean squared angular displacement about the ith axis. For a linear molecule or a nucleus on the symmetry axis of a symmetric top, the formula given for an asymmetric top reduces to

$$\tau_2 \tau_J = \frac{I_\perp \langle \theta_\perp^2\rangle}{2kT(1-\exp\{-3\langle\theta_\perp^2\rangle\})} \qquad \{2 - 47B\}$$

In the limit of small mean squared angular jumps both of these expressions reduce to the Hubbard equation.

The conditional inertial rotation model of Atkins et al.[56] assumes that molecular reorientation in liquids occurs only when the immediate environment of the molecule obtains an "expanded lattice configuration", during this time quasi-free inertial rotation takes place. O'Reilly[55] has recast this model in terms of his own model and observed two interesting consequences. Firstly he suggested that the activation energy of τ_2 will equal that of τ_s, i.e. that it equals that of the process inducing the large angle reorientational step. Secondly, the mean squared jump angle should be only weakly temperature dependent. This implies that although τ_2 and τ_J change with temperature the product of the two should be constant over a range of temperatures. This is a somewhat different result to that obtained with O'Reilly's assumption of hard collision induced reorientation , where it is suggested that the mean squared jump angle varies as the square of the absolute temperature.[58,59]

Some of the properties of these models will later be tested on the reorientational motion of the dimethylthallium(III) cation in aqueous and aqueous glycerol media.

Section 2.3. Relaxation mechanisms.

In order to use spin relaxation studies to probe molecular motions in solution, it is necessary to have a quantitative understanding of how the motional modulation of electric and magnetic interactions contribute to spin relaxation for each mechanism. Firstly a description will be given in general terms of how the modulation of a perturbation Hamiltonian leads to a transition probability that is proportional to the spectral density at the transition frequency. Each mechanism will then be described in more specific terms.

2.3.1. Transition probability for spin relaxation.

Consider a spin ½ nucleus in a static magnetic field B_o, described by the independent spin wave functions $|\alpha\rangle$ and $|\beta\rangle$. A time dependent perturbation Hamiltonian $\hat{H}_1$ acting upon this system will mix these states leading to a wave function of the form

$$|\psi\rangle = C_\alpha(t)\exp(-iE_\alpha t/h)|\alpha\rangle + C_\beta(t)\exp(-iE_\beta t/h)|\beta\rangle . \qquad \{2 - 48\}$$

This must obey the time dependent Schrodinger equation

$$i\hbar \frac{\partial|\psi\rangle}{\partial t} = \hat{H}|\psi\rangle \quad , \qquad \{2 - 49\}$$

where the total Hamiltonian is a sum of static and time dependent parts

$$\hat{H} = \hat{H}_0 + \hat{H}_1 \quad . \qquad \{2 - 50\}$$

differentiating equation 2 - 48 with respect to time and substituting into 2 - 49 one finds

$$i\hbar\,\dot{C}_\alpha = \exp\{i(E_\alpha - E_\beta)t/\hbar\}\,\langle\alpha|\hat{H}_1|\beta\rangle\,C_\beta, \qquad \{2-51A\}$$

and $$i\hbar\,\dot{C}_\beta = \exp\{i(E_\beta - E_\alpha)t/\hbar\}\,\langle\beta|\hat{H}_1|\alpha\rangle\,C_\alpha \qquad \{2-51B\}$$

where $\dot{C}_\alpha = (\partial C_\alpha/\partial t)$ etc.

Now assume that this system is in the ground state at time zero and

$$C_\alpha(0) = 1 \qquad C_\beta(0) = 0.$$

then equation 2 - 51A is zero, and integrating 2 -51B the following expression is obtained.

$$C_\beta(t) = \frac{1}{i\hbar}\int_0^t \exp\{i(E_\beta - E_\alpha)t/\hbar\}\langle\beta|\hat{H}_1|\alpha\rangle\,dt \qquad \{2-52\}$$

The population of the state $|\beta\rangle$ is $C_\beta^*\,C_\beta$ and the transition probability $W_{\alpha\beta}$ at time t is given as

$$W_{\alpha\beta} = \frac{d\,(C_\beta^*\,C_\beta)}{dt} = C_\beta\,\frac{dC_\beta^*}{dt} + C.C., \qquad \{2-53\}$$

where C.C. implies complex conjugate. Defining

$$\omega_{\alpha\beta} = (E_\alpha - E_\beta)/h = -\omega_{\beta\alpha}\ , \qquad \{2-54\}$$

from above, it is found that

$$W_{\alpha\beta} = \frac{1}{\hbar^2}\int_0^t \langle\alpha|\hat{H}_1(t)|\beta\rangle\langle\beta|\hat{H}_1(t')|\alpha\rangle\,\exp(+i\omega_{\alpha\beta}(t'-t))\,dt' + C.C. \qquad \{2-55\}$$

Now if $\hat{H}_1(t)$ is time dependent due to motional modulation of the interactions, then the observed transition probability is an ensemble average.

$$\overline{W}_{\alpha\beta} = \frac{1}{\hbar^2}\int_0^t \overline{\langle\alpha|\hat{H}_1(t)|\beta\rangle\langle\beta|\hat{H}_1(t')|\alpha\rangle}\,\exp\{+i\omega_{\alpha\beta}(t'-t)\}\,dt' + C.C. \qquad \{2-56\}$$

The function under the bar is the autocorrelation function $G_{\alpha\beta}$ of the matrix element $\langle\alpha|\hat{H}_1(t)|\beta\rangle$.
This should depend only on the time difference $t-t' = \tau$

then

$$\overline{W}_{\alpha\beta} = \frac{1}{\hbar^2} \int_0^t G_{\alpha\beta}(\tau)\exp\{-i\omega_{\alpha\beta}\tau\}d\tau + C.C., \qquad \{2 - 57A\}$$

or

$$\overline{W}_{\alpha\beta} = \frac{1}{\hbar^2} \int_{-t}^{t} G_{\alpha\beta}(\tau)\exp\{-i\omega_{\alpha\beta}\tau\}d\tau \quad . \qquad \{2 - 57B\}$$

If the time limit t is much larger than the reciprocal transition frequency, then these limits may be replaced by $\pm\infty$

$$\overline{W}_{\alpha\beta} = \frac{1}{\hbar} \int_{\infty}^{\infty} G_{\alpha\beta}(\tau)\ \exp\{-i\omega_{\alpha\beta}\tau\}d\tau. \qquad \{2 - 58\}$$

This is the Fourier transform of the correlation function, or the spectral density function at the transition frequency,

$$\overline{W}_{\alpha\beta} = \frac{J_{\alpha\beta}(\omega_{\alpha\beta})}{\hbar^2} \quad . \qquad \{2 - 59\}$$

This is the desired result and shows that the observed transition probability for spin relaxation, depends upon the density of motional fluctuations at the resonance frequency

Therefore spin lattice relaxation expressions for mechanisms involving a single spin will only contain terms at the resonance frequency. Mechanisms that rely on the coupling of two spins may contain zero and double quantum terms. Relaxation by the chemical shift anisotropy mechanism is a single spin process, and is of particular relevance to this work. Spin-spin relaxation

however involves mutual quanta exchange and hence a zero quantum term is expected.

2.3.2 Chemical shift anisotropy (CSA) relaxation.

The Zeeman Hamiltonian for the interaction of a nuclear spin operator $\hat{\underline{I}}$ with a static magnetic field $\underline{B}_o$ is given as [1,6]

$$\hat{H}_z = -\gamma\hbar\underline{B}_o\cdot(\underline{\underline{1}} - \underline{\underline{\sigma}})\cdot\hat{\underline{I}} \qquad \{2 - 60\}$$

where

γ is the nuclear gyromagnetic ratio in rad $s^{-1}T^{-1}$,

$\underline{\underline{1}}$ is the second rank unit tensor

$\underline{\underline{\sigma}}$ is the chemical shift tensor of the nucleus .

As discussed in Section Two, $\underline{\underline{\sigma}}$ may be decomposed into irreducible components.

$$\underline{\underline{\sigma}} = \underline{\underline{\sigma}}^{(1)} + \underline{\underline{\sigma}}^{(2)} + \underline{\underline{\sigma}}^{(3)} \qquad \{2 - 61\}$$

The Zeeman Hamiltonian then becomes

$$\hat{H}_z = -\gamma\hbar\,(1 - \sigma_{ISO})\underline{B}_o\cdot\hat{\underline{I}} + \gamma\hbar\underline{B}_o\cdot(\underline{\underline{\sigma}}^{(1)})\cdot\hat{\underline{I}} + \gamma\hbar\underline{B}_o\cdot(\underline{\underline{\sigma}}^{(2)})\cdot\hat{\underline{I}} \qquad \{2 - 62\}$$

The trace of the tensor determines the isotropic shift and the rank one and two components may induce relaxation.

For a nucleus in which the first rank antisymmetric component is zero, the spin relaxation times are given in the extreme narrowing limit as[1]

$$R_{1\,CSA} = T_{1\,CSA}^{-1} = \frac{2}{15}\gamma^2 B_o^2 \Delta\sigma^2 (1+\eta^2/3)\tau_2 \qquad \{2 - 63A\}$$

$$R_{2\,CSA} = T_{2\,CSA}^{-1} = \frac{7}{45}\gamma^2 B_o^2 \Delta\sigma^2 (1+\eta^2/3)\tau_2 \qquad \{2 - 63B\}$$

where $\Delta\sigma$ and η are the anisotropy and asymmetry of the shielding tensor respectively. Note that both $R_{2\,CSA}$

and $R_{1\ CSA}$ are proportional to B_o^2 and therefore

$$R_{2\ CSA}/R_{1\ CSA} = T_{1\ CSA}/T_{2\ CSA} = \frac{7}{6} \qquad \{2 - 64\}$$

For situations which are outside extreme narrowing the full expression given by Spiess[3] should be used

$$R_{1\ CSA} = \frac{1}{15}\gamma^2 B_o{}^2 \Delta\sigma^2 (1 + \eta^2/3) \left[\frac{2\tau_2}{1 + \omega^2\tau_2^2}\right] \qquad \{2 - 65A\}$$

$$R_{2\ CSA} = \frac{1}{15}\gamma^2 B_o{}^2 \Delta\sigma^2 (1 + \eta^2/3) \left[\frac{4\tau_2}{3} + \frac{\tau_2}{1 + \omega^2\tau_2^2}\right] . \qquad \{2 - 65B\}$$

Thus $R_{1\ CSA}$ contains a single quantum spectral density and $R_{2\ CSA}$ contains both zero and single quantum terms. It should be noted that the ratio $R_{2\ CSA}/R_{1\ CSA}$ is a function of τ_2 and of ω and only approaches 7/6 in the limit $\omega\tau_2 << 1$; away from extreme narrowing $R_{2\ CSA}/R_{1\ CSA} > 7/6$. The above expressions will be of great use in the interpretation of results to be presented later.

If the antisymmetric component of the shielding tensor, $\underline{\sigma}^{(1)}$ is non zero, then there exist additional contributions to the total CSA relaxation rate given as[3]

$$R'_{1\ CSA} = \frac{2}{3}\gamma^2 B_o{}^2 \Delta\sigma_a{}^2\ \tau_1/(1 + \omega^2\tau_1{}^2) \qquad \{2 - 66A\}$$

$$R'_{2\ CSA} = \frac{1}{3}\gamma^2 B_o{}^2 \Delta\sigma_a{}^2\ \tau_1/(1 + \omega^2\tau_1^2) \qquad \{2 - 66B\}$$

within extreme narrowing $\omega\tau_1 << 1$ and these reduce to

$$R'_{1\ CSA} = \frac{2}{3}\gamma^2 B_o{}^2 \Delta\sigma_a{}^2 \tau_1 \qquad \{2 - 67A\}$$

$$R'_{2\ CSA} = \frac{1}{3}\gamma^2 B_o{}^2 \Delta\sigma_a^2\ \tau_1 \qquad \{2 - 67B\}$$

where $\Delta\sigma_a^2 = \{\sigma_{xy}^2 + \sigma_{xz}^2 + \sigma_{yz}^2\}$ {2 - 68}

and σ_{xy}, σ_{xz} and σ_{yz} are the components of $\underline{\underline{\sigma}}^{(1)}$ in the principal axis. The total CSA relaxation rate is the sum of the rates due to symmetric and antisymmetric constituents.

$$R_1^{TOT}{}_{CSA} = R_{1\ CSA} + R_{1\ CSA}^{'} \qquad \{2 - 69\}$$

$$R_2^{TOT}{}_{CSA} = R_{2\ CSA} + R_{2\ CSA}^{'} \qquad \{2 - 70\}$$

where the prime indicates antisymmetric, the ratio $R_{2\ CSA}^{'}/R_{1\ CSA}^{'}$ is equal to 1/2 independent of ω and of τ_1. Thus if it is found that $R_2^{TOT}{}_{CSA}/R_1^{TOT}{}_{CSA} < 7/6$ then one may be detecting relaxation by the antisymmetric component of the shielding tensor.(47) The requirement for a non zero $\underline{\underline{\sigma}}^{(1)}$ is that the local nuclear symmetry contains not more than one plane of symmetry which must be perpendicular to any axis of symmetry.(46)

The antisymmetric component of the shielding tensor has recently been observed by ^{59}Co relaxation studies of low symmetry cobalt complexes(57), the effects of its existence on solid state spectra have been discussed by Haeberlen.(2) From the symmetry arguments above, one expects $\underline{\underline{\sigma}}^{(1)} = 0$ in the linear dimethylthallium(III) cation, and we can disregard relaxation due to this component.

Using a density matrix approach Hull and Sykes(54) have derived relaxation expressions for a nucleus with an asymmetric shift tensor ($\eta \neq 0$) in a molecule undergoing symmetric top diffusion, for the case where the principal axes of the shielding and diffusion tensors do not coincide. This is analogous to the quadrupolar

relaxation theory of Huntress[21], except that extreme narrowing and an axially symmetric interaction have not been assumed. They have however disregarded the anti-symmetric component of the shielding tensor.

2.3.3. Transient CSA relaxation.

This relaxation mechanism was first proposed by Schwartz[47], for spin ½ heavy metal ions in solution. Due to the transient nature of the solvated ion fluctuations in solvent number, reorientation of the distorted ion and transient ion pair formation led to an anisotropic electronic environment. These collision induced fluctuations modulate the magnitude and direction of the principal axes of the shielding tensor, and provide a mechanism for spin relaxation. Schwartz has shown that the spin relaxation rates may be expressed using the same formulae as for static CSA. At extreme narrowing

$$R_{1\ CSA} = \frac{6}{7}\ R_{2\ CSA} = \frac{2}{15}\ \gamma^2 B_o^2 \Delta\sigma^2 (1 + \eta^2/3)\tau\ , \quad \{2 - 71\}$$

where $\Delta\sigma$ and η are the transient anisotropy and asymmetry, the correlation time τ is given as

$$\frac{1}{\tau} = \frac{1}{\tau_2} + \left[\frac{n}{n-1}\right] \frac{1}{\tau_D} \qquad \{2 - 72\}$$

where τ_2 is the reorientational correlation time
τ_D is the lifetime of a distortion,
and n is the primary solvation number.
Therefore the two contributions expected for transient CSA may be summarised as
A: reorientation of a distorted solvated ion
B: formation of transient ion pairs.

One would then expect the elucidation of the operative contribution(s) to be possible from the concentration dependence of the relaxation.

2.3.4. Spin rotation relaxation.

This spin relaxation mechanism arises from a coupling between the nuclear spin and the molecular rotational angular momentum. The spin rotation Hamiltonian is

$$\hat{H}_{SR} = \hat{\underline{I}} \cdot \underline{\underline{C}} \cdot \hat{\underline{J}} \qquad \{2 - 73\}$$

All three terms are time dependent; $\hat{\underline{I}}$ because of change of nuclear spin state due to relaxation; $\underline{\underline{C}}$ because it is expressed in the laboratory frame and is time dependent due to reorientation; and $\hat{\underline{J}}$ changes with the molecular rotational state.

In the liquid phase the eigenstates of $\hat{\underline{J}}$ are broadened by intermolecular interactions and the molecular rotation may be regarded as non quantised. As mentioned earlier the very short lifetime of the rotational states leads to the collapse of any observable line splitting due to the trace of the spin rotation tensor $\underline{\underline{C}}$.

The correlation time that governs this mechanism is the spin rotation correlation time τ_{SR}. This of often tacitly assumed to be synonymous with the angular momentum correlation time τ_J; the relationship between these two has been discussed by Kivelson[48]. The spin rotation correlation time may be defined as

$$\tau_{SR} = \int_0^\infty \frac{\langle \hat{\underline{I}}(t) \cdot \underline{\underline{C}}(t) \cdot \hat{\underline{J}}(t)\ \hat{\underline{I}}(0) \cdot \underline{\underline{C}}(0) \cdot \hat{\underline{J}}(0) \rangle}{\langle (\hat{\underline{I}} \cdot \underline{\underline{C}} \cdot \hat{\underline{J}})^2 \rangle} dt, \qquad \{2 - 74\}$$

where the ensemble average includes the appropriate wave functions. If $\hat{\underline{I}}$, $\underline{\underline{C}}$ and $\hat{\underline{J}}$ behave independently then we can average separately,

$$\tau_{SR} = \int_0^\infty \frac{\langle \hat{\underline{I}}(t)\ \hat{\underline{I}}(0)\rangle \langle \underline{\underline{C}}(t)\cdot\underline{\underline{C}}(0)\rangle \langle \hat{\underline{J}}(t)\cdot\hat{\underline{J}}(0)\rangle}{\langle \hat{\underline{I}}^2\rangle \langle \underline{\underline{C}}^2\rangle \langle \hat{\underline{J}}^2\rangle} dt. \qquad \{2 - 75\}$$

If it is now assumed that the rotational angular momentum decays far more rapidly than the other two variables then as an approximation

$$\underline{\underline{C}}(t) \simeq \underline{\underline{C}}(0) \qquad \{2 - 76A\}$$

$$\hat{\underline{I}}(t) \simeq \hat{\underline{I}}(0) \qquad \{2 - 76B\}$$

and we have

$$\tau_{SR} = \int_0^\infty \frac{\langle \hat{\underline{J}}(t)\cdot\hat{\underline{J}}(0)\rangle}{\langle \hat{\underline{J}}(0)^2\rangle}\ dt = \tau_J \qquad \{2 - 77\}$$

Thus it is seen that τ_J and τ_{SR} are only equivalent if the angular momentum varies rapidly with respect to the $\underline{\underline{C}}$ term which varies only as the reorientational correlation time. This is equivalent to the rotational diffusion assumption, $\tau_J << \tau_\ell$ [48]

For a spherical diffuser at extreme narrowing with the relaxing nucleus at the centre of symmetry, the spin rotation relaxation rate has been derived as[50]

$$R_{1\ SR} = T_{1\ SR}^{-1} \quad \frac{2IkT}{\hbar^2}\ C^2\ \tau_{SR} \qquad \{2 - 78\}$$

where I is the moment of inertia and

$C = C_{xx} = C_{yy} = C_{zz}$ is the isotropic spin rotation constant. Unlike the reorientational correlation times, τ_{SR} increases with increasing temperature, hence $R_{1\ SR}$ increases and this is a unique feature of this

mechanism.

For a symmetric top molecule at extreme narrowing the spin rotation relaxation rate has been given by Spiess[3] as

$$R_{1SR} = \frac{2kT}{3\hbar^2}\left[2I_\perp C_\perp{}^2 \tau_{SR\perp} + I_\parallel C_\parallel^2 \tau_{SR\parallel} \right] , \quad \{2 - 79\}$$

where $C_\parallel$ and $C_\perp$ are elements of the diagonalised spin rotation tensor, and $\tau_{SR\parallel}$ and $\tau_{SR\perp}$ are correlation times for the parallel and perpendicular components of the spin rotation correlation function.

Thus evaluation of the spin rotation correlation times τ_{SR} from spin rotation data requires a knowledge of the relevant spin rotation constants. It will later be shown how to obtain these for the ^{205}Tl nucleus in the dimethylthallium(III) cation.

Complicated formulae exist relating τ_J to R_{1SR} for all inertial symmetries in the extended diffusion model.[13]

2.3.5 Transient spin rotation relaxation.

The transient spin rotation mechanism was proposed by Schwartz[48] along with his proposal of transient CSA. The modulation of the spin rotation Hamiltonian arises from two sources. Firstly molecular reorientation of the distorted ion modulates the anisotropic part of $\underline{\underline{C}}$ and secondly, the magnitude and direction of the rotational angular momentum $\underline{J}(t)$ may change as a result of collisions. Analysis of this model under conditions of extreme narrowing leads to the result

$$R_{1SR} = R_{2SR} = \frac{2IkT}{\hbar^2} C^2 \tau_{SR} \quad , \qquad \{2 - 80\}$$

where C is the isotropic spin rotation constant. As before τ_{SR} and hence R_{1SR} and R_{2SR} are expected to increase with temperature.

2.3.6. Quadrupolar relaxation.

Any nucleus with spin quantum number $I \geq 1$ will possess an electric quadrupole moment, which interacts with the electric field gradient at the nuclear site. Reorientational modulation of this interaction provides a mechanism for relaxation.

The perturbation Hamiltonian is

$$\hat{H}_Q(t) = C^Q \hat{\underline{I}} \cdot \underline{\underline{V}} \cdot \hat{\underline{I}} \qquad \{2 - 81\}$$

C^Q is a constant and $\underline{\underline{V}}$ is the second rank, traceless symmetric electric field gradient tensor. Evaluation of the contribution of this mechanism at extreme narrowing leads to[1]

$$R_{1Q} = R_{2Q} = \frac{3}{40} \frac{(2I + 1)}{I^2(2I-1)} \left[1 + \frac{\eta^2}{3} \right] \frac{e^2Qq}{\hbar^2} \tau_2 \, , \qquad \{2 - 82\}$$

$(e^2Qq/\hbar^2)$ is the quadrupole coupling constant in Hz, η is the asymmetry in the field gradient tensor, the field gradient eq and asymmetry η are analogous to the anisotropy and asymmetry of the anisotropic shielding interaction.

2.3.7. Dipole-dipole relaxation.

Dipole-dipole relaxation is a common relaxation mechanism for spin ½ nuclei and ^{13}C-^{1}H

dipolar interactions usually dominate ^{13}C relaxation[52].

The relaxation Hamiltonian for a coupling between two spin operators $\underline{I}$ and $\underline{S}$ is

$$\hat{H}_{DD}(t) = \hat{\underline{I}} \cdot \underline{\underline{D}}(t) \cdot \hat{\underline{S}} \quad , \qquad \{2 - 83\}$$

$\underline{\underline{D}}$ is the traceless symmetric second rank dipolar coupling tensor. This interaction may be modulated by the relative translation and/or reorientation of the two nuclei. One must distinguish between intermolecular and intramolecular mechanisms; translational motion does not contribute to the latter. In the intramolecular case, at extreme narrowing, and considering only the contribution from directly bonded nuclei, we have for the I spin[52]

$$R_{1D} = R_{2D} = \left(\frac{\mu_o}{4\pi}\right)^2 \frac{n_s \gamma_I^2 \gamma_S^2 \tau_2}{r^6} \qquad \{2 - 84\}$$

where μ_0 is the permeability of free space and equals $4\pi \times 10^{-7}$ H m^{-1}, n_s is the number of directly bonded S nuclei, and r is the internuclear distance. A special case of the intermolecular dipole dipole mechanism is relaxation by paramagnetic impurities in solution.

2.3.8 Scalar relaxation.

The modulation of the spin-spin coupling interaction by either chemical exchange or relaxation leads to scalar relaxation of the first and second kinds respectively[1]. The interaction Hamiltonian is,

$$\hat{H}_{SC}(t) = J\, h\, \hat{\underline{I}} \cdot \hat{\underline{S}} \qquad \{2 - 85\}$$

where J is the scalar coupling constant and equals

one third of the trace of the $\underline{\underline{J}}$ tensor. The relaxation rates for the I spin are[1]

$$R_{1SC} = \frac{8\pi^2 J^2 S(S+1)}{3} \frac{\tau_{SC}}{1 + (\omega_I - \omega_S)^2 \tau_{SC}^2} \qquad \{2 - 86\}$$

$$R_{2SC} = \frac{R_{1SC}}{2} + \frac{4\pi^2 J^2 S(S+1)}{3} \tau_{SC} \qquad \{2 - 87\}$$

ω_I and ω_S are resonance frequencies in rad s^{-1}. S is the quantum number of the coupled spin. τ_{SC} is the chemical exchange time for scalar relaxation of the first kind; or is proportional to the relaxation time T_{1S} for scalar relaxation of the second kind. Typically scalar relaxation only contributes to R_2 relaxation, since the large value of the term $\Delta\omega^2\tau_{SC}$ makes R_{1SC} small. Exceptions to this occur when $\omega_I \simeq \omega_S$ as in $^{13}C-^{79}Br$ relaxation or at very low fields as in a $T_1\rho$ experiment.

Scalar contributions to R_2 from scalar relaxation of the second kind are particularly important for spin ½ nuclei coupled to rapidly relaxing nuclei.

The case of rapid relaxation of a quadrupolar nucleus is well known[1] but this is a more general phenomenon and examples where the rapid relaxation is due to CSA relaxation at high field, will be presented later.

REFERENCES - CHAPTER TWO.

1. A.Abragam, "The Principles of Nuclear Magnetism", O. U. P. (1961).
2. U.Haeberlen, Adv.Magn.Reson., Supplement 1 (1976).
3. H.W.Spiess, "Rotation of Molecules and Nuclear Spin Relaxation in NMR. Basic Principles and Progress", Vol.15. Springer Verlag.
4. D.M.Brink and D.R.Satchler, "Angular Momentum", O. U. P., (1968).
5. A.R.Edmonds,"Angular Momentum in Quantum Mechanics" Princeton Univ.Press, 2nd Ed. (1969).
6. A.Carrington and A.D.McLachlan,"Introduction to Magnetic Resonance" Harper and Row. (1967).
7. G.Williams, Time Correlation Functions and Molecular Motion, Chem.Soc. Rev., 7, 89 (1978).
8. A.R.Bullock, Nuclear Magnetic Relaxation in Fluids in Transfer and Storage of Energy by Molecules, Vol.3. Rotational Energy, J.Wiley (1970).
9. J.H.R.Clarke, Band Shapes and Molecular Dynamics in Liquids. Adv.Infra Red and Raman Spec., 4, 109 (1978).
10. R.G.Gordon, Adv.Magn.Reson., 3, 1 (1963).
11. P.Debye, Polar Molecules, Chapter 5, Dover Publications (1945).
12. P.S.Hubbard, Phys.Rev. 131, 1155 (1963).
13. R.E.D.McLung, Adv.Mol.Relaxation and Interaction Processes, 10, 83 (1977).
14. W.A.Steele, Adv.Chem.Phys., 34, 1 (1976).

15. A.Gierer and K.Wirtz, Z.Naturforsch A 8, 532 (1953).

16. F.Perrin, J.Phys.Radium, 5, 497 (1934), 7, 1 (1936).

17. C.Hu and R.Zwanzig, J.Chem.Phys. 60, 4354 (1984).

18. D.R.Bauer, J.I.Brauman and R.Pecora, J.Amer.Chem.Soc., 96, 6840 (1974).

19. F.J.Bartoli and T.W.Litzovitz, J.Chem.Phys. 56, 404 (1972); 56, 413 (1972).

20. R.E.D.McLung, Chem.Phys.Lett., 19, 304 (1973).

21. W.T.Huntress Jr., Adv.Magn.Reson., 4,1, (1970).

22. D.E.Woessner, J. Chem.Phys., 37, 647 (1962).

23. D.E.Woessner, J.Chem.Phys., 50, 719 (1969).

24. D.G.Gillies, P.J.Burke and R.W.Matthews, J.Organomet. Chem., 118, 129 (1976).

25. R.E.Gordon, J.Chem.Phys., 44, 1830 (1966).

26. R.E.D.McLung, J.Chem.Phys., 51, 3842 (1969); 54, 3248 (1971); 57, 2596 (1972); 55, 3459 (1971).

27. R.D.Mountain, J.Chem.Phys., 54, 3243 (1971).

28. M.Fixman and K.Rider, J.Chem.Phys., 51, 2425 (1969).

29. W.A.Steele and A.G.St.Pierre, J.Chem.Phys., 54, 3243 (1972).

30. R.E.D.McLung, J.Chem.Phys., 57, 5478 (1972).

31. F.Bliot, C.Abbar and E.Constant, Mol.Phys., 24, 241 (1972).

32. F.Bliot and E.Constant, Chem.Phys.Lett., 18, 253 (1973).

33. T.E.Eagles and R.E.D.McLung, Chem.Phys.Lett., 18 253 (1973).

34. M.Bloom et al., Can.J.Phys., 45, 3533 (1967).

35. E.N.Ivanov, Sov.Phys. JETP., 18, 1041 (1964).

36. D.A.Pinnow, S.J.Candau, T.A.Litovitz, J.Chem.Phys., 49, 347 (1968).

37. C.J.Montrose and T.A.Litovitz, Relaxation Spectroscopy in Liquids. Proc.4th Inelastic Neutron Scattering Symposium (1968).

38. R.Kno, T.W.Litovitz and G.E.McDuffie, J.Chem.Phys., 45, 1790 (1966).

39. T.A.Litovitz and G.E.McDuffie, J.Chem.Phys., 39, 729 (1963).

40. T.A.Litovitz and G.E.McDuffie, J.Chem.Phys., 37, 1699 (1962).

41. M.Wolfe and J.Jonas, J. Chem.Phys., 71,3252 (1979).

42. S.H.Glarum, J.Chem.Phys., 33, 1371 (1960).

43. B.I.Hunt and J.G.Powles, Proc.Phys.Soc., 88, 513 (1966).

44. C.Brot, Dielectric and related molecular processes, Chem.Soc.Specialist Periodical Reports, 2, 1 (1975).

45. P.B.Macedo and T.A.Litovitz, J.Chem.Phys., 42, 245 (1965).

46. R.M.Lynden Bell, Mol.Phys. 29, 301 (1975).

47. R.N.Schwartz, J.Magn.Reson., 24, 321 (1974).

48. D.Kivelson, Mol.Phys., 28, 321 (1974).

49. D.K.Green and J.G.Powles, Proc.Phys. Soc., London, 85, 87 (1965).

50. D.M.Grant, C.H.Wang, J.R.Lyera Jr., J.Chem.Phys., 55, 4674 (1971).

51. D.M.Grant, C.H.Wang, J.R.Lyera Jr., J.Chem.Phys., 55, 4676 (1971).

52. D.M.Grant and J.R.Lyera Jr., M.T.P. Int.Rev.Series, Vol.4, Chapt.5.

53. D.W.Davidson and R.H.Cole, J.Chem.Phys., 19, 1484 (1951).

54. W.E.Hull and B.D.Sykes, J.Mol.Biol., 98, 121 (1975).

55. D.E.O'Reilly, J.Chem.Phys., 57, 885 (1972).

56. P.W.Atkins, A.Lowenstein and Y.Margalit, Mol.Phys., 17, 329 (1969).

57. S.C.F.Au Yeung, B.J.Builst and D.R.Eaton, J.Magn.Reson., 55, 24 (1983).

58. D.E.O'Reilly, J.Chem.Phys., 63, 3177 (1975).

59. D.E.O'Reilly, J.Chem.Phys., 60, 1607 (1974).

CHAPTER THREE - EXPERIMENTAL

Section 3.1. Spectrometer systems.

Three spectrometers have provided the majority of the results to be presented in this thesis. In this laboratory a modified Varian HA-60 interfaced to a PDP-11/20 computer was used to observe ^{205}Tl at 34.7 MHz (B_o=1.41T). This system was developed by D.G.Gillies and the software written by I.D.Cresshull and I.C.Moon; this spectrometer has been described previously[1], and the only major change has been the replacement of DEC TU-16 dual cassette storage by DEC RX-01 dual floppy disk drives.

High field (B_o= 9.40T) measurements have been carried out at 231 MHz on the Bruker WH-400 spectrometer situated at Queen Mary College, operating under the University of London Intercollegiate Research Services (ULIRS) scheme. This is a commercial instrument and need not be described in detail here. It does however have a 10 mm dedicated thallium probe and RF circuitry, since the highest frequency covered by the broad band circuitry is 160 MHz, the ^{31}P frequency.

The HA-60 system has subsequently been replaced by a Varian XL-100/15 spectrometer. This is a multinuclear, variable field electromagnet system offering the possibility of variable field relaxation studies. This instrument was used in the gyrocode observe mode to observe ^{205}Tl at 21.9 MHz (B_o= 0.89T). Field/frequency lock was achieved by locking to the ^{31}P resonance of 85% ortho phosphoric acid at 15.4 MHz;

this is the frequency used for ^{2}H lock when operating at 2.35T.

CW proton decoupling was available at 37.9 MHz by using a Schlumberger FSX 3006S frequency synthesiser, this signal was passed through an attenuator, a broad band amplifier (Amplifier Research 10 LA), and a band pass filter (Texscan 3BD 38), before being applied to the probe.

The ^{205}Tl observation frequency was measured by a frequency counter (Hewlett Packard Type 52452), which was referenced to the 1 MHz crystal in the FSX frequency synthesiser. Thus the ^{205}Tl resonance frequency can be related to the proton decoupling frequency supplied by the synthesiser.

The spectrometer was interfaced via a 10 bit analogue to digital converter, to the digital PDP-11/20 (28K RAM) computer previously used on the Varian HA-60 system. Dual DEC RX01 floppy disk drives were used for storage. The software allowed up to ten FID's to be stored under one file name. Acquisition was performed using a phase alternated pulse sequence. After digitisation the usual cosine apodisation, exponential multiplication and a Fourier transform of up to 8K points were applied. The spectra were displayed on an oscilloscope for phasing, and a Bryans XY plotter used for hard copy. The pulse timer unit consisted of five digital timers controlling the 180^{o} pulse length, 90^{o} pulse length, period τ between these two pulses, digitisation rate, and experimental period.

Different pulse sequences are generated by manually changing the pulse lengths and interconnection of timer units. The timer controlling the relaxation period τ was under software control.

Section 3.2. Temperature measurement.

3.2.1 Introduction and problems.

When information about spin relaxation mechanisms and molecular motion is sought by relaxation experiments, it is necessary to have a knowledge of the sample temperature. It is evident that when variable temperature studies are carried out, any error in the sample temperature will manifest itself as an error in the derived values of the activation parameters. The problem is exacerbated when comparing results from different spectrometers with different probe geometries. For these reasons one should seek to know the sample temperature as accurately as is practically and routinely possible.

The most usual method of temperature indication and control is to have a thermocouple or resistance thermometer immersed in the gas stream which heats the sample. This method has the disadvantage that it is not actually monitoring the temperature within the sample.

Alternatively one can halt the experiment and insert a thermocouple into the sample, but this technique is cumbersome and may perturb the temperature of the sample.

Additional problems arise from the use of high power decoupling fields; some authors[2,3] have noted large increases in sample temperature with lossy samples, such as solutions of electrolytes, or molecules having large electric dipole moments. These inductive

heating effects are due to an interaction between the electric component of the decoupling RF field, and the electric dipole moment of the molecules or ions of the electrolyte[2]. These effects increase with increasing decoupler frequency and are larger for electrolytes than for polar molecules. In this laboratory a temperature rise of about 50K has been observed for the dimethyl-thallium/water system using 5W of decoupler power at 400 MHz. For heavy metal nuclei the temperature coefficients of the resonance frequency are typically large (~ 0.5 ppm K^{-1}) and significant linebroadening and degradation of lineshape have been observed in this laboratory in proton decoupled thallium spectra at high field.

In an attempt to minimise the inductive heating effect of the decoupler Alderman and Grant[4] have proposed a decoupler coil design which reduces unnecessary heating of the sample. In addition McNair[3] has suggested that sample tubes and inserts,machined from polycrystalline beryllium oxide,will reduce heating effects and temperature gradients; since the high thermal conductivity of this material allows rapid thermal equilibriation with the gas stream.

A popular method of obtaining the sample temperature is to calibrate and then observe the frequency or shift of a resonance that is strongly temperature dependent, a brief discussion of these methods will now be given.

3.2.2 NMR thermometers.

Several authors have reported the use of a temperature dependent shift or resonance frequency as a thermometric property. Measurement of the shift difference between two peaks is often experimentally more convenient on account of the difficulty in measuring an exact resonance frequency.

The peak separation between the aliphatic and hydroxylic protons in both methanol and ethylene glycol (ethane 1,2 diol) have been calibrated at 60 MHz and used as ^{1}H NMR thermometers by Van Geet[5,6] as the temperature increases the extent of hydrogen bonding diminishes and the OH proton signal moves down frequency towards the methyl or methylene resonance.

More recent calibrations of these compounds have been carried out by Becker et al.at 220 MHz[7] ,the conclusions drawn are that the Van Geet equations can be scaled to higher fields with no significant increase in error.

In addition a Pt resistance thermometer assembly for use in multinuclear NMR experiments has been described by Merbach et al.[8] and has been shown to agree within $\pm$ 0.5K with the results of Van Geet.

Some ^{13}C NMR thermometers have been proposed by various authors[9-11], Bailey et al.[12] have suggested the use of either aqueous or organic solutions of Co^{3+} compounds, as a high sensitivity ^{59}Co NMR thermometer for use in broadband or dedicated ^{13}C probes. This technique has the advantages of a high sensitivity

nucleus, a large temperature dependence of the resonance and may be used without probe retuning.

Bornais and Brownstein[13] have used a sample of toluene and hexafluorobenzene in fluorodichloromethane solvent as a low temperature thermometer for use in ^{1}H, ^{19}F and ^{13}C NMR. Calibration data are provided from ambient temperatures down to -145°C. A ^{31}P NMR thermometer has been proposed by Gupta and Gupta[14]. This method monitors the chemical shift differences between the αP and βP resonances in neutral pH solutions of MgATP, this is found to be independent of ionic strength and small pH variations. A linear calibration is provided over the temperature range 0°C to 60°C.

3.2.3 ^{205}Tl NMR thermometer.

The temperature dependence of the ^{205}Tl resonance frequency has been carefully studied for dimethylthallium(III) derivatives in various solvents[15]. The temperature coefficients of the resonance frequencies lie between 0.25 ppm/K and 0.46 ppm/K, with the resonance moving up frequency with increasing temperature.

Dimethylthallium(III) nitrate in D_2O has been the most often used ^{205}Tl NMR thermometer, its calibration and use will be described, and then a quantitative comparison made with the glycol ^{1}H NMR thermometer at 400 MHz.

The following scheme was used to calibrate the ^{205}Tl NMR thermometer.

1. Calibrate thermocouple against N.P.L. standard thermometers.
2. Allow attainment of thermal equilibrium of non decoupled sample, then measure resonance frequency.
3. Move thermocouple from position just above sample level into sample and find temperature.
4. Remove thermocouple to above fluid and remeasure frequency.
5. Repeat measurements at other temperatures.
6. Fit frequency vs. N.P.L. temperature to a linear or a polynomial function.

The sample was non spinning and frequency differences between steps 2 and 4 were usually zero. If the sample was degassed the resonance frequency was assumed unchanged.

Since the shift of dimethylthallium(III) nitrate in aqueous solution is almost independent of concentration[15], sample concentration is not a critical factor in the accuracy of the ^{205}Tl NMR thermometer.

The above calibration scheme was carried out at ^{205}Tl frequencies of 34.73 MHz using the HA-60 spectrometer; and 21.96 MHz using the XL-100. Sample concentrations were 0.164 M and 0.807 M respectively.

The following calibration equations were obtained

<u>at 34.7 MHz</u>

$$t(^{o}C) = 6.95 \times 10^{-9}x^3 - 5.98 \times 10^{-6}\, x^2 + 0.0611\, x + 1.590 \qquad \{3 - 1\}$$

where $x = \nu_o\{^{205}Tl\} - 34731500$ Hz

and ^{2}H lock frequency = 9209392 Hz (Lock D_2O solvent)

at 21.96 MHz

$$t(^{o}C) = 2.492 \times 10^{-5} x^2 + 0.01817 x - 60.299 \quad \{3 - 2\}$$

where $x = \nu_o\{^{205}Tl\}-21962783$ Hz, and the ^{31}P lock frequency was 15.4 MHz using 85% phosphoric acid.

Graphs of these equations are shown in Figures 3-1 and 3-2. These equations imply only a slight non linearity and the mean temperature coefficients of 0.44 ppm/K and 0.43 ppm/K agree excellently with previous studies[15]. The temperature dependence of the lock frequencies may be considered negligible since the ^{31}P shift of H_3PO_4 is almost temperature invariant[16,17] and ^{2}H coefficients are typically 0.01 ppm/K[18].

To establish the field strength more accurately at 21.96 MHz, a $^{205}Tl\ \{^{1}H\}$ double resonance experiment was carried out. Here the ^{205}Tl spectrum is monitored and the ^{1}H CW irradiation frequency varied using the FX 3006 S frequency synthesiser using 1 W of proton RF power, the ^{1}H frequency that gave optimum decoupling was taken as the centre frequency for the protons in dimethylthallium(III) nitrate in D_2O. This was found as

$$\nu_o(^{1}H) = 37943718 \pm 2 \text{ Hz}$$

All frequencies were measured using the HP 52452 counter referred to in Section One.

The comparison of the ^{205}Tl and ^{1}H glycol NMR thermometers was carried out on the Bruker WH-400 spectrometer at a temperature setting of 301K. The proton spectrum was observed via the decoupler coil of

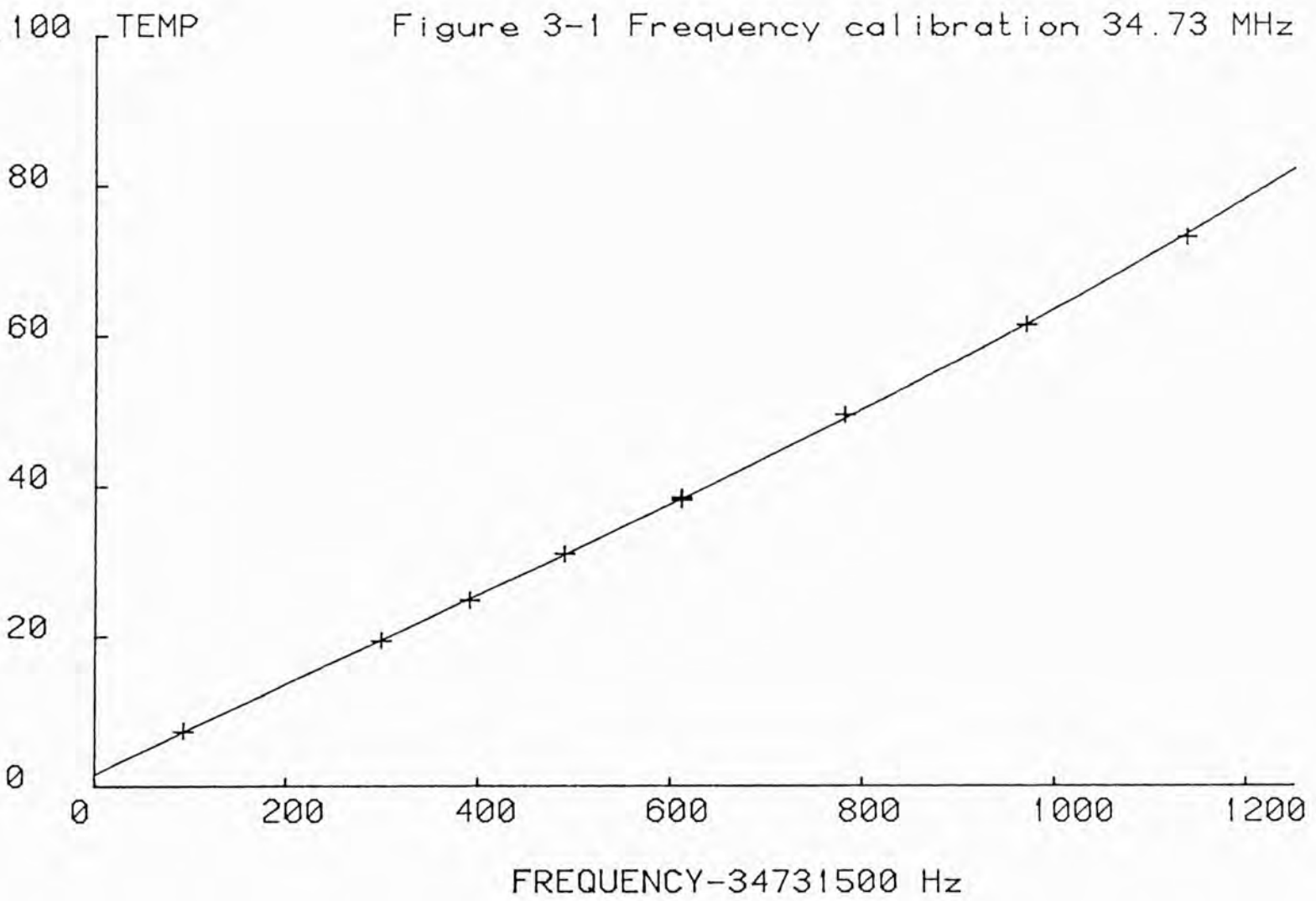

Figure 3-1 Frequency calibration 34.73 MHz

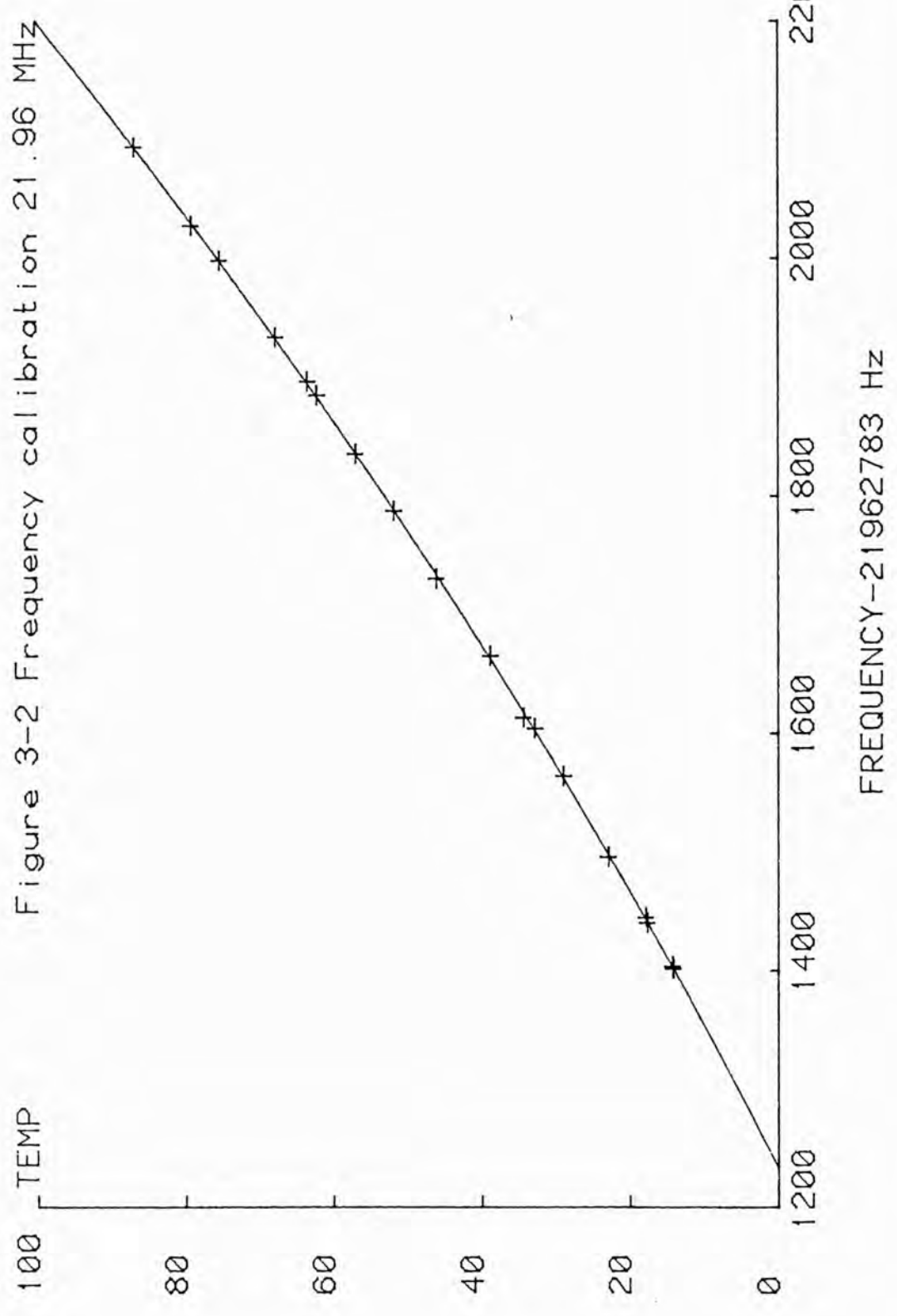

Figure 3-2 Frequency calibration 21.96 MHz

the ^{205}Tl probe, and the frequencies in the spectrum calibrated by placing in the spectrum an RF spike produced by a General Radio frequency synthesiser which was referenced to the 10 MHz master crystal in the spectrometer. The method of connection of this synthesiser is given in Section Three.

The sample was 0.807 M dimethylthallium(III) nitrate in D_2O degassed and sealed in an 8mm tube with an internal capillary of ethylene glycol.

By this method the glycol peak separation was found to be

$$\Delta\nu \text{ (glycol)} = 659.6\text{Hz}.$$

and for dimethylthallium(III) nitrate protons

$$\nu_o(^1H) = 400135835 \text{ Hz}.$$

Using the General Radio synthesiser to produce a spike in the ^{205}Tl spectrum it was found that

$$\nu_o(^{205}Tl) = 231624737 \text{ Hz}.$$

Scaling this down by the ratio of the proton frequencies and using equation 3-2 the ^{205}Tl thermometer indicates a temperature of 297.7 ± 0.5K,

whereas the glycol peak separation indicates[5,7]

$$298.4 \pm 0.3\text{K}.$$

Thus the agreement is within experimental error and under these conditions the set temperature of 301 K is about 3K above the sample temperature.

To summarise, temperature measurement by the ^1H glycol and ^{205}Tl methods may be considered accurate to better than $\pm$ 1K.

Section 3.3 T_1 and T_2 measurement techniques.

3.3.1 T_1 Pulse sequences.

In this section the pulse sequences used to measure the spin lattice relaxation time T_1 will be discussed. All of these methods perturb the equilibrium of the spin system and observe the return of the magnetisation to equilibrium; with knowledge of the nature of the perturbation the relaxation time T_1 may then be found.

The progressive saturation Fourier transform (PSFT) technique was put forward by Freeman and Hill[19,20], a pulse sequence

$$\{90^{o} - (FID) - \tau\}_n \qquad \{3 - 3\}$$

is applied and a steady state allowed to develop. Spectra are obtained as a function of τ and may be shown to obey the expression

$$S_\tau = S_\infty\{1-\exp(-\tau/T_1)\}, \qquad \{3 - 4\}$$

where S_τ and S_∞ are the signal intensities at times τ and infinity respectively. Thus at very short τ the spectra are saturated and S_τ tends to zero, this technique requires no prior knowledge of T_1, but the shortest τ value is limited by the spectral acquisition time. In addition the dynamic range or sensitivity of the technique is only half that of the inversion recovery technique to be discussed shortly.

The saturation recovery Fourier transform (SRFT) technique uses a train of 90^{o} pulses[21], often followed by a field inhomogeneity (homospoil) pulse[22]

to eliminate any residual transverse magnetisation. The magnetisation then recovers exponentially from saturation with a time constant of T_1 seconds, and the signal intensity obeys equation 3 - 4.

This technique also requires no prior knowledge of T_1, but still suffers from the dynamic range disadvantage.

The most widely used technique is the inversion recovery Fourier transform (IRFT) pulse sequence.

$$\{180^{o} - \tau - 90^{o}(FID) - W\}_n, \qquad \{3 - 5\}$$

where W is the waiting or delay time, which allows the spin system to return to equilibrium. This is usually set to equal to or greater than 5 T_1. With perfect pulse angles the recovery curve equation for the magnetisation is

$$S_\tau = S_\infty\{1 - 2\exp(-\tau/T_1)\}. \qquad \{3 - 6\}$$

Inversion of the signal leads to a dynamic range that is twice that of the SRFT and PSFT pulse sequences. In addition an approximate knowledge of T_1 is required to choose appropriate τ values for the experiment. Compared to the SRFT and PSFT sequences the use of a long waiting time W makes the method time inefficient especially for nuclei with low sensitivity and long T_1's (such as ^{13}C).

In an effort to overcome the relatively long time requirement for the IRFT method, Canet et al.[23] have proposed using a waiting time W much less than $5T_1$ but long enough to allow for the decay of transverse

magnetisation. This is called the fast inversion recovery Fourier transform (FIRFT) pulse sequence. A study of the error bounds on T_1 using the FIRFT sequence by Kowalewski et al.[24] suggests that τ values up to $2T_1$ are required for an accurate estimate of T_1, but W may be less than T_1. Studies by Sass and Ziessow[25] on this pulse sequence suggest an optimum waiting time W in the range

$$0.5\ T_1 \leqslant W \leqslant 2T_1 \qquad \{3 - 7\}$$

The pulse sequence(s) used for T_1 determination in this laboratory are the IRFT, and FIRFT technique where necessary.

3.3.2 T_1 Data Analysis.

Having decided on a pulse sequence for the determination of T_1 and having carried out the T_1 experiment, it becomes necessary to address the problem of how to extract T_1 from the set of experimental data. An approach widely used in the analysis of IRFT data has been to rearrange equation 3 - 6 to

$$\ln\{S_\infty - S_\tau\} = \ln\{2S_\infty\} - \tau/T_1 \qquad \{3 - 8\}$$

and to fit the values of $\ln(S_\infty - S_\tau)$ as a function of τ to this equation using a linear technique, the slope obtained is equal to $-1/T_1$. This is called the semi logarithmic plot method. However several authors[24-26] have discussed statistical shortcomings in this method and Sass and Ziessow[25] have suggested fitting to a three parameter expression of the form

$$S_\tau = A_1 + A_2 \exp\{+\tau * A_3\} \qquad \{3 - 9\}$$

where A_1, A_2 and A_3 are the variable parameters. A_1 and A_2 will be the best estimates of S_∞ and $(S_o - S_\infty)$ respectively, and A_3 will be the best estimate for $-1/T_1$. A least squares fit to a function of this form requires an iterative nonlinear estimation technique as discussed in Appendix A and by Leipert and Marquadt[23]. This method has been shown[22] to be superior to the linear regression semilogarithmic plot technique with regard to T_1 error. The exponential regression approach also allows the T_1 error bound to be relatively insensitive to frequency offsets and misadjusted pulse angles. It is also noteworthy that this method can be used to analyse IRFT, FIRFT or SRFT data using a single computer program; only the parameter A_2 will vary for the three different pulse sequences.

To summarise then, T_1 measurements in this laboratory have used the IRFT or FIRFT pulse sequence, and the resulting data analysed by iterative exponential regression using basic programs on BBC Model B and Tektronix 4052 microcomputers, the latter utilising a Tektronix 4662 digital plotter.

An example of a T_1 data set with the file name MFDMTN.AAF is given in Figure 3 - 3. The sample is 0.81 M $(CH_3)_2TlNO_3$ in D_2O; the resonance frequency is 21.9 MHz, and the sample temperature is 28.4°C. The measured peak intensities, τ values and best fit parameters are given on the computer printout (Table 3-1) and a

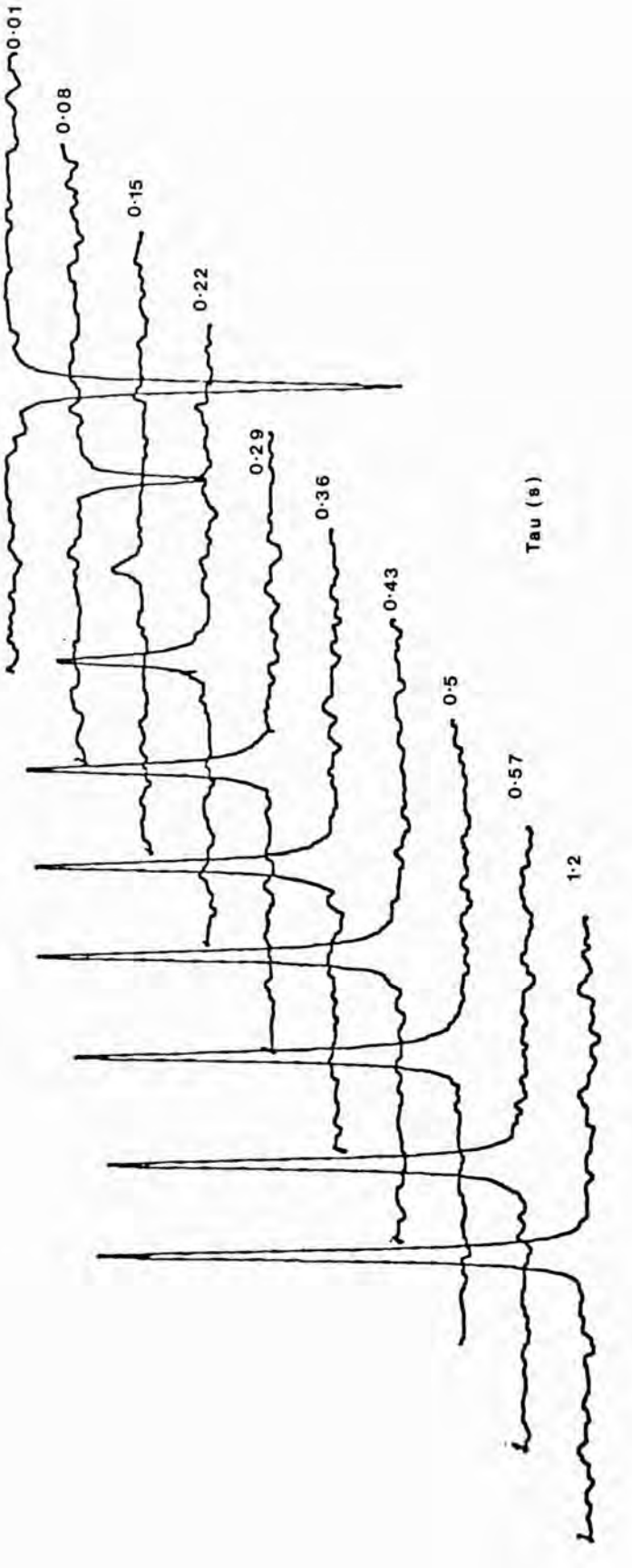

FIGURE 3-3. Proton decoupled ^{205}Tl IRFT spectra of 0.81M $(CH_3)_2TlNO_3/D_2O$ at 21.96MHz. 200 scans, 12.7 Hz linebroadening, temperature 28.4°C.

TABLE 3 - 1:

Best fit parameters for IRFT data.

X(OBS)	Y(OBS)	Y(CALC)
1E-2	-58	-56.6313555
8E-2	-19.5	-21.5762078
0.15	4.5	3.8887063
0.22	22	22.3870407
0.29	36	35.824682
0.36	44	45.5861122
0.43	53	52.6770531
0.5	57	57.8280855
0.57	61.5	61.569921
1.2	72	70.9459603

PARAMETER	VALUE	STD_DEV
1	71.5056038	1.15095351
2	-134.123338	1.49827226
3	4.56601265	0.126798225

parameter 1 =M(infinity)
parameter 2 =M(zero)-M(infinity)
parameter 3 =R1 in /seconds

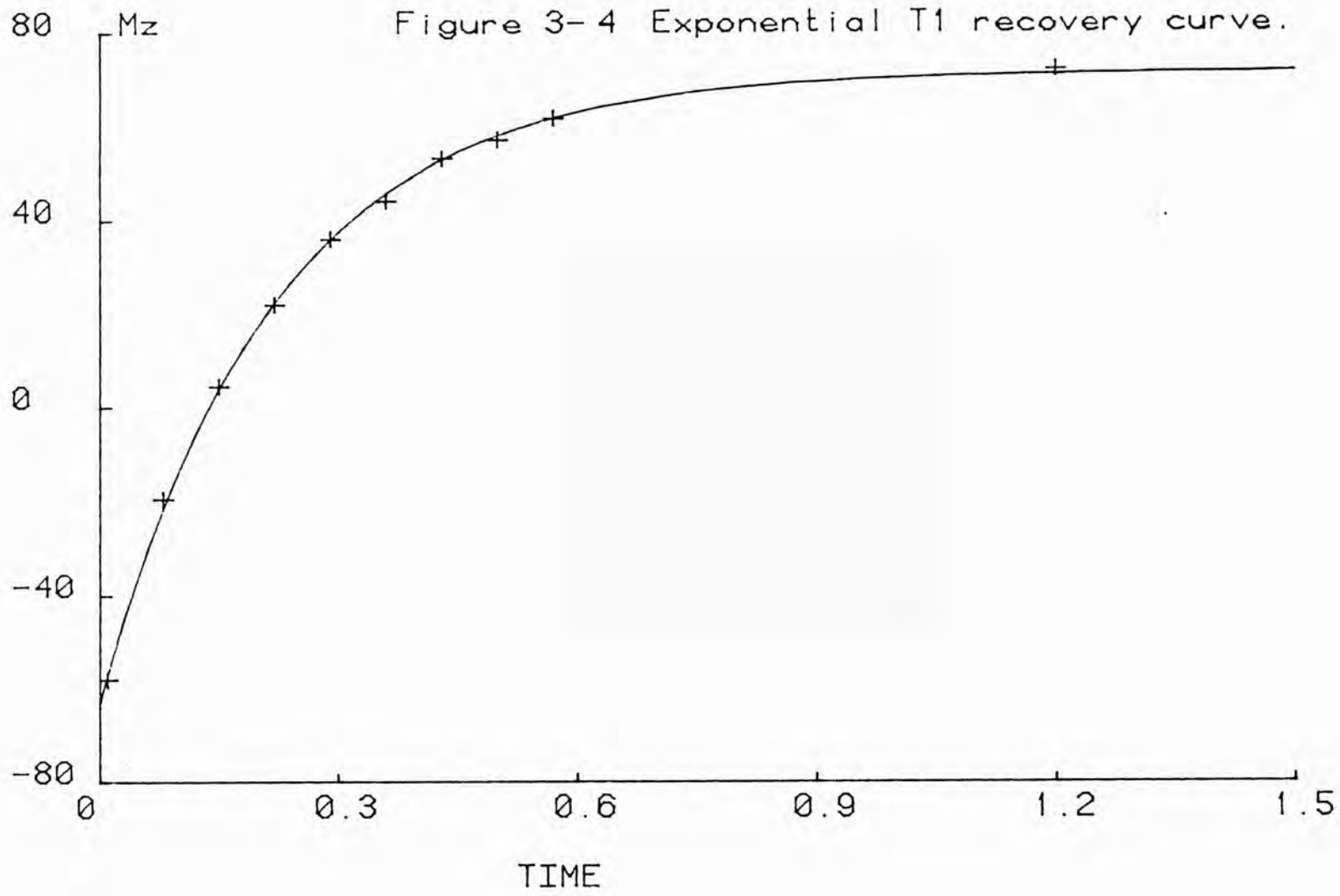

Figure 3-4 Exponential T1 recovery curve.

computer generated plot of the magnetisation recovery curve is shown (Fig. 3 - 4).

3.3.3 T_2 Pulse Sequences and Data Analysis.

Although the majority of the results presented in this thesis are T_1 measurements, a small number of spin-spin relaxation or T_2 experiments have been performed on ^{205}Tl at 231 MHz.

One of the pulse sequences used has been the Hahn spin echo sequence[27], this may be summarised as

$$\{90^{o}(x)-\tau-180^{o}(y)-\tau(ECHO)\}_{n} \; . \qquad \{3 - 10\}$$

The 90^{o} pulse is applied along the x axis of the rotating frame and induces transverse magnetisation along the y axis. A dephasing period of τ seconds is followed by a 180^{o} pulse along the y axis, which causes refocussing of the transverse magnetisation and an echo maximum at time 2τ[28]. The intensity of the transformed spin echo signal decays exponentially to zero as a function of time

$$S_{\tau} = S_{o} \exp\{-2\tau/T_2\} \qquad \{3 - 11\}$$

where S_o is the signal intensity at zero time. In practice phase alternation was used on the 180^{o} pulse in order to minimise the effects of pulse imperfections. The data from these experiments has been analysed using the iterative general least squares procedure discussed previously. The data was fitted to equation 3 - 11 using S_o and T_2 as variable parameters.

In addition to the spin echo T_2 measurements just described, the presaturation technique proposed by

Bain[29], has also been used. To measure T_2 an irradiating field of magnitude B_2 is applied to the spin system at some offset $(\omega-\omega_0)$ from resonance, until a steady state is achieved. The RF is gated off and the resulting Z magnetisation is observed by a 90^o pulse. The signal intensity is a function of B_2, the offset $(\omega-\omega_0)$ and of relaxation times T_1 and T_2; this is equivalent to a saturated CW lineshape. From the Bloch equations[30]

$$M_Z = M_O \frac{1 + T_2^2(\omega-\omega_0)^2}{1 + T_2^2(\omega-\omega_0)^2+\gamma^2B_2^2T_1T_2} \quad \{3 - 12\}$$

A relaxation delay of τ seconds may be allowed between gating off the RF field, and applying the observe pulse. This modifies the equation by allowing relaxation of longitudinal magnetisation[29]. The observed magnetisation as a function of offset may be fitted to equation 3 - 12 using a nonlinear least squares program with $(\gamma B_2)^2T_1T_2$, M_o, and T_2 as variable parameters. Figure 3 - 5 is an example of a ^{205}Tl T_2 determination for the dimethyl-thallium(III) cation in D_2O at a temperature of 306.4K and a resonance frequency of 231.6 MHz. The best fit parameters are

$$M_o = 183.0 \pm 1.8 \text{ mm} \quad \{3 - 13A\}$$

$$T_2 = 2.97 \pm 0.12 \text{ ms} \quad \{3 - 13B\}$$

$$(\gamma B_2)^2T_1T_2 = 3.38 \pm 0.15 \quad \{3 - 13C\}$$

Figure 3 - 6 shows the spectrum of this species following pre-irradiation of the central feature.

These T_2 measurements were carried out on the Bruker WH 400 spectrometer. The ^{205}Tl irradiation

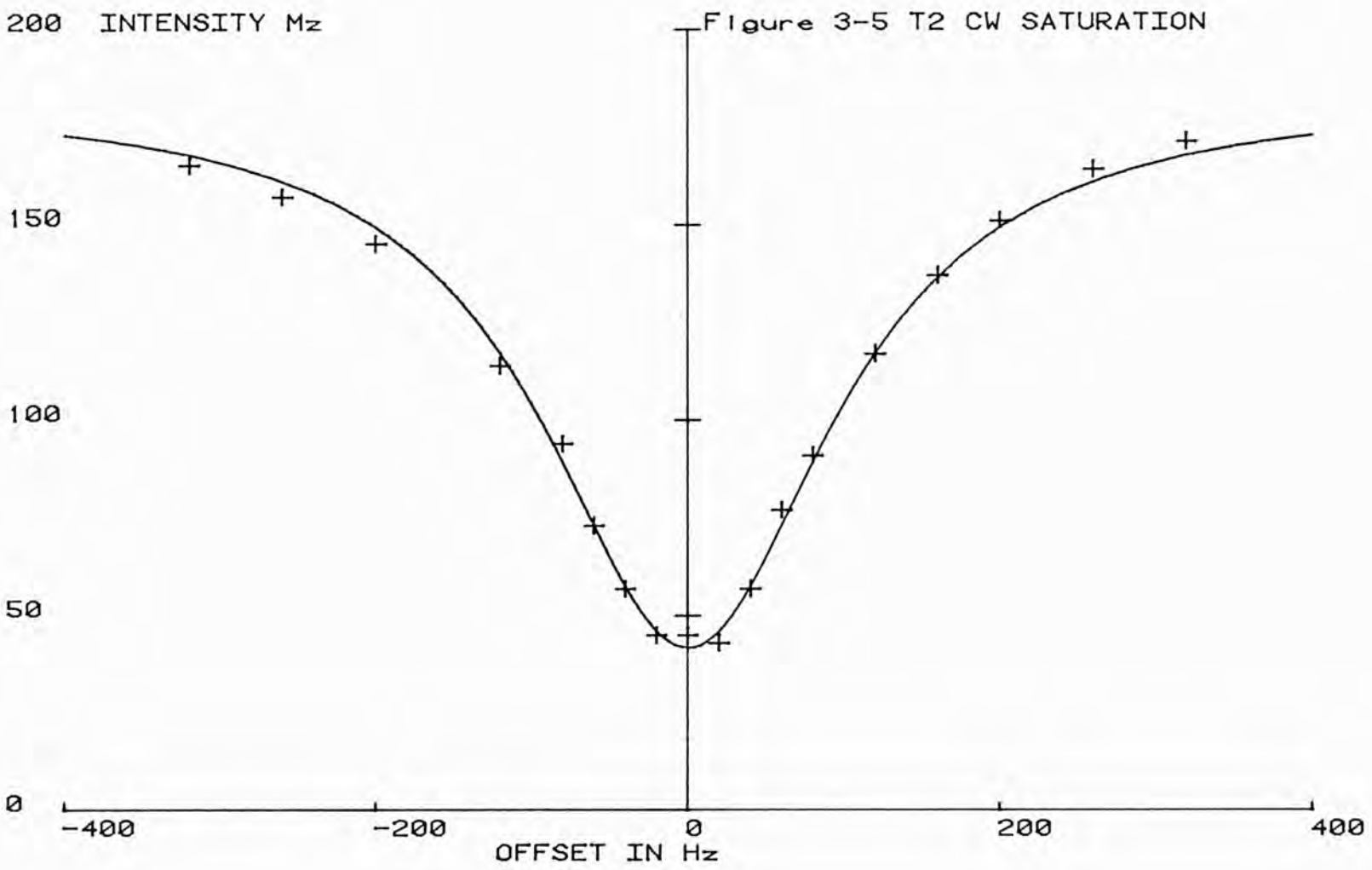
200 INTENSITY Mz
Figure 3-5 T2 CW SATURATION
150
100
50
0
-400
-200
0
200
400
OFFSET IN Hz

FIGURE 3-6 .

^{205}Tl spectrum of 0.81M $(CH_3)_2TlNO_3/D_2O$ at 231.6 MHz following CW irradiation of central feature.
256 scans, 5 Hz linebroadening, temperature 306.4K.

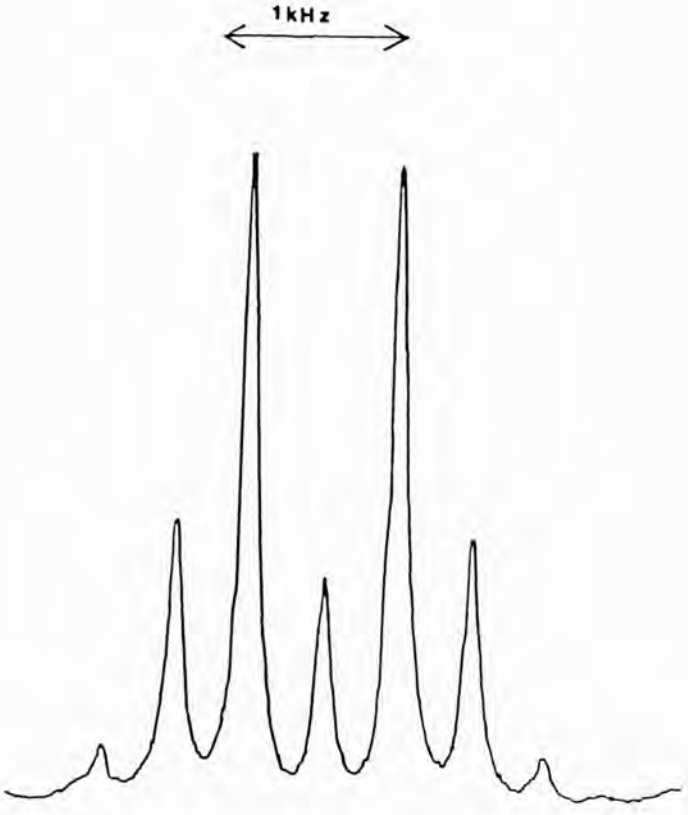

was obtained by
frequency doubling the output of a General Radio type 1061 frequency synthesiser whose 10 MHz reference was the master frequency from the Bruker spectrometer. The output of the synthesiser was gated using two balanced modulators which were controlled by the gated decoupling pulse from the spectrometer. Figure 3 - 7 is a schematic diagram of the arrangement and shows how the frequency was further amplified and applied to the probe. A similar arrangement was used to generate the ^{205}Tl and ^{1}H spikes used for frequency calibration, except that in this instance no power amplification was necessary.

3.3.4 $T_{1\rho}$ Pulse sequence and Data Analysis.

The measurement of $T_{1\rho}$ the spin-lattice relaxation time in the rotating frame, involves the application of a $90^{o}(x)$ pulse to the spins to tip the magnetisation vector along the transverse y axis of the rotating frame. Following this an on resonance RF pulse with magnetic component B_{1y} is applied along the y axis and the magnetisation is spin-locked along this axis for a duration of τ seconds. A Fourier transform of the FID following the release of the spin-locking field results in a signal S_{τ} which is a decaying function of the spin-locking period[28].

$$S_{\tau} = S_{o} \exp(-\tau/T_{1\rho}). \qquad \{3 - 14\}$$

$T_{1\rho}$ is deduced by a non linear fit of the signal intensity data to this function. $T_{1\rho}$ represents the spin-lattice relaxation time in a magnetic field of flux density B_{1y}, thus it is essentially a low field T_{1} experiment and may

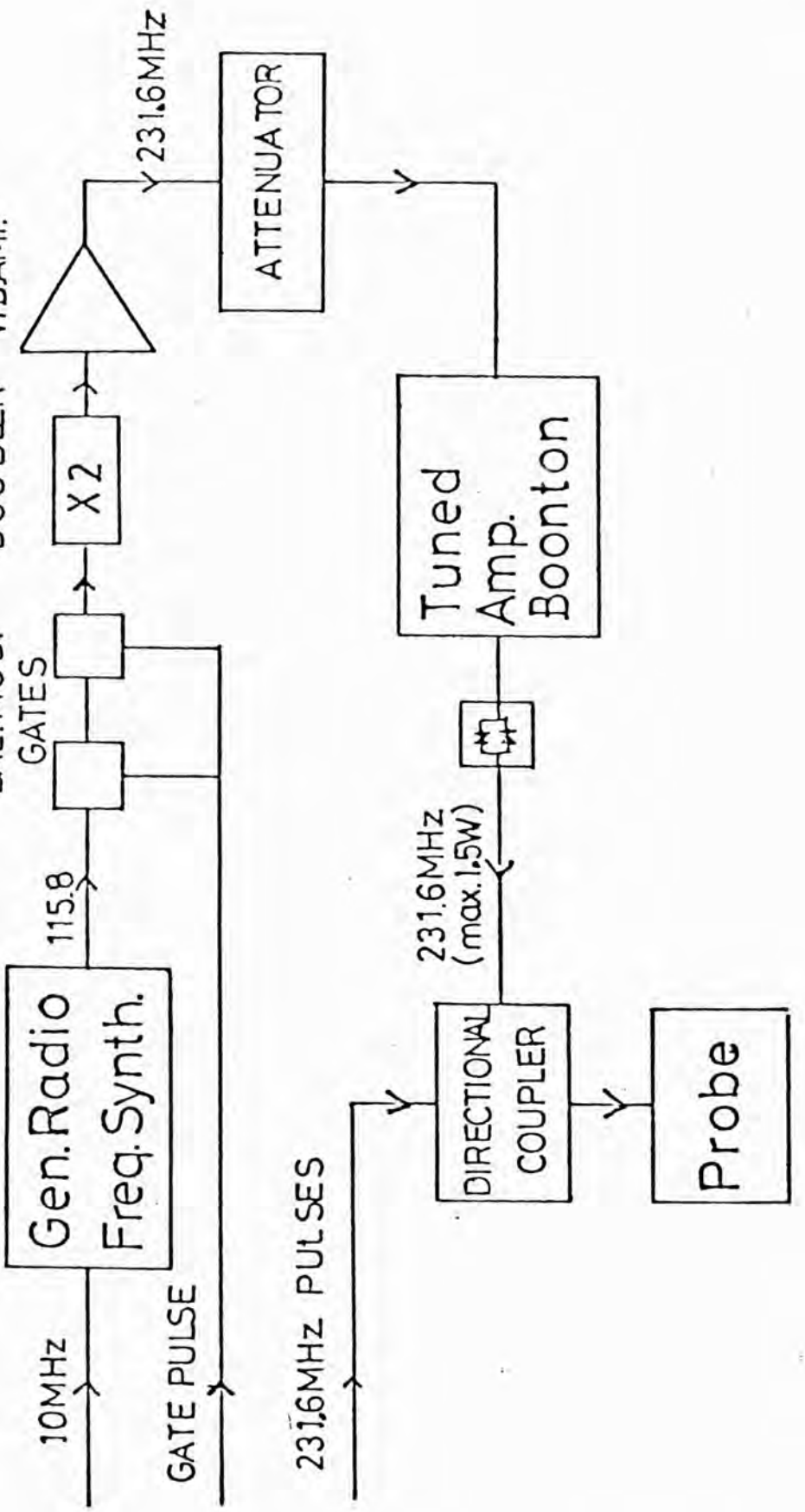

FIGURE 3-7. Scheme for ^{205}Tl presaturation/spike frequency calibration on the Bruker WH -400.

provide useful mechanistic information if T_1 is field dependent.

In practice the spin-locking time, τ, may be limited by the inability of the power amplifier to maintain the power level by the power handling capabilities of the probe. The spin-locking field may be provided by any irradiation field that is phase coherent and of sufficient magnitude to spin-lock all nuclei according to the condition

$$\gamma B_1 >> \Delta\omega \quad , \qquad \{3 - 15\}$$

where $\Delta\omega$ is the spread of frequencies to be spin locked. Since the WH400 spectrometer does not allow software control of B_1 and since the proton decoupler channel is not phase coherent, the $T_{1\rho}$ measurements reported for aqueous $^{205}Tl(I)$ ion have used the Dante sequence(31) to provide a spin-locking field. The Dante sequence consists of a train of m pulses of duration Δt spaced at intervals of τ_r(typically $\Delta t << \tau_r$). The frequency domain excitation spectrum is thus a series of Sinc functions at the carrier frequency and at $\pm 1/\tau_r$, $\pm 2/\tau_r$ etc. The real part of each Sinc function has a selectivity or width between zero crossing points of $1/m\tau_r$ Hz. The effective field B_1^{EFF} is calculated as the product of the duty cycle and B_1 the magnitude of the magnetic component of the RF pulses. The selective $T_{1\rho}$ experiments performed on the aqueous $^{205}Tl(I)$ ion have used effective fields corresponding to ^{205}Tl resonance frequencies in the rotating frame of 35 and 208 Hz. The observed

^{205}Tl linewidth for this sample was 12 Hz. Since the observed $T_{1\rho}$'s were the same within experimental error one may conclude that the spin locking criterion (equation 3 - 15) was satisfied in both cases.

REFERENCES. CHAPTER THREE

1. A.Frangou, PhD Thesis, Royal Holloway College, University of London (1979).
2. J.J.Led and S.B.Peterson, J.Magn. Reson., 32, 1 (1978).
3. D.S.McNair, J.Magn.Reson., 45, 490 (1981).
4. D.W.Alderman and D.M.Grant, J.Magn.Reson., 36, 447 (1979).
5. A.L.Van Geet, Anal.Chem., 40, 2227 (1968).
6. A.L.Van Geet, Anal.Chem., 42, 679 (1970).
7. P.S.Raford, C.L.Fisk and E.D.Becker, Anal.Chem., 51, 2050 (1979).
8. C.Ammann, P.Meier and A.E.Merbach, J.Magn.Reson., 46, 319 (1982).
9. D.R.Vidrine and P.E.Peterson, Anal.Chem., 48, 1301 (1976).
10. S.Combrisson and T.Prange, J.Magn.Reson., 19, 108 (1975).
11. H.J.Schneider, W.Freitay and M.Schommer, J.Magn. Reson., 18, 393 (1975).
12. J.T.Bailey, G.C.Levy and D.A.Wright, J.Magn.Reson., 37, 353 (1980).
13. J.Bornais and S.Brownstein, J.Magn.Reson., 29, 207 (1978).
14. R.K.Gupta and R.P.Gupta, J.Magn.Reson., 40, 587 (1980).
15. P.J.Burke, R.W.Matthews, I.D.Cresshull and D.G.Gillies, J.C.S., Dalton, 132 (1981).
16. M.M.Crutchfield, C.H.Dungon and J.R.van Wazer, Topics in Phosphorus Chemistry, 5, 46 (1967).

17. M.D.Gordan and L.D.Quin, J.Magn.Reson., 22, 149 (1976).

18. I.Y.Slonim, B.M.Arsharva and V.N.Klyuchnikcv, Russ.J.Phys.Chem., 50, No.1 (1976).

19. R.Freeman and H.D.W.Hill, J.Chem.Phys., 54, 3367 (1971).

20. R.Freeman and H.D.W.Hill, J.Chem.Phys. 57, 82 (1972).

21. J.L.Markley, W.H.Horsley and M.P.Klein, J.Chem.Phys., 55, 3604 (1971).

22. G.G.McDonald and J.S.Leigh Jr., J.Magn.Reson, 9, 358 (1973).

23. D.Canet, G.C.Levy and I.R.Peat, J.Magn.Reson., 18, 199 (1975).

24. J.Kowalewski, G.C.Levy, L.F.Johnson and L.Palmer, J.Magn.Reson., 26, 533 (1977).

25. M.Sass and D.Ziessow, J.Magn.Reson. 24, 263 (1977).

26. T.K.Liepert and D.W.Marquadt, J.Magn.Reson., 24, 181 (1976).

27. E.L.Hahn, Phys.Rev., 80, 580 (1950).

28. T.C.Farrar and E.D.Becker, Pulse and Fourier Transform NMR, Academic Press (1971).

29. A.Bain, W.P.Y. Ho, and J.S.Martin, J.Magn.Reson., 43, 328 (1981).

30. A.Abragam, The Principles of Nuclear Magnetism, O.U.P., (1961).

31. G.A.Morris and R.Freeman, J.Magn.Reson., 29, 433 (1978).

CHAPTER FOUR - DIMETHYLTHALLIUM(III) DERIVATIVES.

Section 4.1. Dimethylthallium(III) cation in aqueous solution.

4.1.1. Evidence for existence and structure of cation.

The diorganothallium(III) group R_2Tl- is a relatively stable species and many organometallic compounds with this group are known. Several dimethylthallium(III) derivatives have been studied by infrared and Raman spectroscopy, and the presence of a linear C-Tl-C skeleton has been shown (1,2,3). For $D_{\infty h}$ symmetry (ignoring hydrogens) the C-Tl-C symmetric stretching frequency will be forbidden in the IR spectrum, but should be Raman active, this is in agreement with experiment [1].

A study of the ^{205}Tl shift of dimethylthallium(III) nitrate in H_2O, has shown that the ^{205}Tl shift is almost independent of concentration[4]. This is rationalised by assuming that the equilibrium position for the dissociation

$$(CH_3)_2TlNO_3 \rightleftharpoons (CH_3)_2Tl^+ + NO_3^- \qquad \{4 - 1\}$$

lies well to the right, and that the dissociation is near complete over the concentration studied (up to 1.5 mol % $(CH_3)_2TlNO_3$). This rationalisation is supported by conductivity data (5), which show considerable ionisation in aqueous solution, but only slight ionisation in pyridine. In addition results to be presented shortly will show that the ^{205}Tl R_1 for dimethylthallium(III) nitrate in aqueous solution is independent of concentration - (0.04M to 0.8 M), and independent of anion change from nitrate to acetate,

within experimental error.

Thus the spin relaxation data to be presented in this Chapter will be discussed on the basis of a linear cation structure. The stability and well defined nature of the dimethylthallium(III) cation are in sharp contrast to the relatively ill-defined transient species invoked in a discussion of thallous ion relaxation.

4.1.2. ^{205}Tl spin lattice relaxation studies.

The first ^{205}Tl relaxation studies of the dimethylthallium(III) cation were performed by Chan and Reeves[6], they measured the effect of dissolved molecular oxygen on the ^{205}Tl relaxation of dimethylthallium(III) nitrate in H_2O and several solutions of Tl(I) compounds, at 26°C and 15.1 MHz. It was found that whilst the effect of oxygen on dimethylthallium(III) was greater than that found for other nuclei, it was much smaller than the effect on the Tl(I) ion relaxation. The relaxation rates are linearly related to the oxygen pressure up to 5 atm.

A variable temperature investigation of the ^{205}Tl relaxation of 0.8M dimethylthallium(III) nitrate in D_2O has been carried out by Brady.[7] These measurements were performed on a non degassed sample at 34.73 MHz. It was observed that R_1 decreased as the temperature was increased across the range 25°C to 70°C; after including the relaxation effects due to oxygen the relaxation rate is about five times greater than that reported by Reeves at a corresponding temperature. It will shortly be seen that

these observations are consistent with those to be reported herein. The ^{205}Tl spin lattice relaxation rate R_1 of the dimethylthallium(III) cation in aqueous solution, has been studied as a function of temperature at ^{205}Tl resonance frequencies of 21.96, 34.73 and 231.6 MHz, and as a function of temperature and concentration (0.04M, 0.16M and 0.8M) at 34.73 MHz. The sample temperature for each T_1 experiment was found from the previously calibrated ^{205}Tl resonance frequency as described in Chapter Three. Field/frequency lock was achieved using D_2O solvent at 34.73 MHz and 231.6 MHz; at 21.96 MHz a concentric tube containing 85% H_3PO_4 provided a ^{31}P lock.

The ^{205}Tl R_1 is found to vary strongly as a function of magnetic field strength, typical R_1's at ambient temperature being 4.2 s^{-1}, 9.1 s^{-1} and 375 s^{-1} for resonance frequencies of 21.96 MHz, 34.73 MHz and 231.6 MHz respectively. The ^{205}Tl spin lattice relaxation rate is also a strong function of temperature but almost independent of concentration, this is shown in Figure 4 - 1, which is a plot of $\ln(^{205}Tl\ R_1)$ at 34.73 MHz against inverse temperature, for dimethylthallium(III) nitrate at concentrations of 0.8M, 0.16M and 0.04M and for 0.2M dimethylthallium(III) acetate in D_2O. The data used to generate this plot are given in Table 4 - 1 and are for non-degassed samples, but as will subsequently be shown, paramagnetic oxygen does not greatly contribute to the ^{205}Tl R_1 at this field.

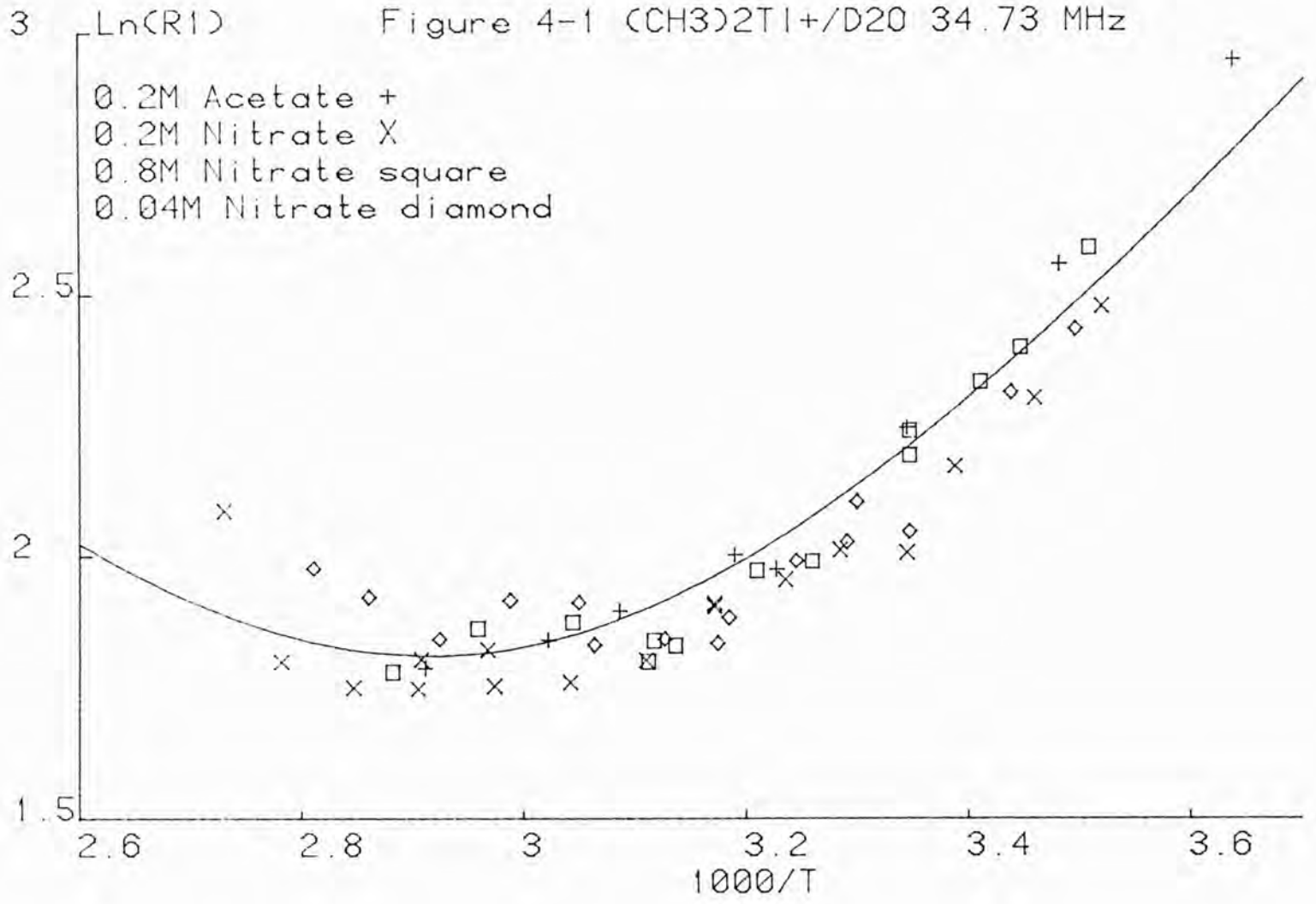
3
Ln(R1)
Figure 4-1 (CH3)2Tl+/D2O 34.73 MHz
0.2M Acetate +
0.2M Nitrate X
0.8M Nitrate square
0.04M Nitrate diamond
2.5
2
1.5
2.6
2.8
3
3.2
3.4
3.6
1000/T

TABLE 4 - 1: Temperature dependence of ^{205}Tl R_1 at 34.73 MHz.

a) 0.16M $(CH_3)_2TlNO_3/D_2O$

Temperature(K)	R_1 (s^{-1})	Temperature(K)	R_1 (s^{-1})
284.3	11.9	328.9	5.81
289.2	10.0	336.4	5.77
295.3	8.77	337.1	6.18
299.1	7.44	344.0	6.07
304.6	7.47	344.4	5.74
309.2	7.06	351.4	5.75
315.4	6.75	359.6	6.04
315.4	6.71	366.4	8.05
321.6	6.06	-	-

b) 0.8M $(CH_3)_2TlNO_3/D_2O$

Temperature(K)	R_1 (s^{-1})	Temperature(K)	R_1 (s^{-1})
285.2	13.3	318.9	6.23
290.3	11.0	320.9	6.29
293.3	10.3	321.4	6.04
298.9	9.39	328.6	6.51
298.9	8.95	338.1	6.43
306.9	7.31	347.1	5.92
311.7	7.18	-	-

TABLE 4 - 1 (continued).

Temperature dependence of ^{205}Tl R_1 at 34.73 MHz.

c) 0.04M $(CH_3)_2TlNO_3/D_2O$

Temperature(K)	R_1 (s^{-1})	Temperature(K)	R_1 (s^{-1})
286.2	11.4	319.9	6.31
291.0	10.1	326.5	6.24
298.9	7.74	328.0	6.76
303.2	8.19	334.8	6.79
304.0	7.59	342.1	6.31
308.3	7.32	349.7	6.83
314.1	6.57	355.9	7.22
315.1	6.26	-	-

d) 0.2M $(CH_3)_2TlOCOCH_3/D_2O$

Temperature(K)	R_1 (s^{-1})	Temperature(K)	R_1 (s^{-1})
275.1	19.0	313.6	7.40
287.4	12.9	324.1	6.65
299.1	9.44	331.0	6.30
310.0	7.20	343.6	5.97

The temperature dependence of the ^{205}Tl R_1 at 34.73 MHz changes sign as a function of temperature and a minimum for R_1 is observed, similar behaviour is observed for both degassed and non degassed samples at 21.96 MHz (Figures 4-2, 4-3 Tables 4-2, 4-3). However at 231.6MHz the ^{205}Tl R_1 decreases steadily with increasing sample temperature (Figure 4-4 and Table 4-4).

The presence of field dependent relaxation with R_1 increasing as a function of field strength is characteristic of a significant contribution from the chemical shift anisotropy (CSA) mechanism. At low field strength and high sample temperature the relaxation data show that the ^{205}Tl R_1 increases with increased sample temperature. This temperature dependence is unique to the spin rotation (SR) mechanism.

Thus a simple qualitative analysis of the ^{205}Tl spin lattice relaxation data implies a temperature dependent mixture of CSA and SR relaxation at low field. The spin lattice relaxation rate contribution from the CSA mechanism, is known to be proportional to the square of the applied field strength within the extreme narrowing limit (equation 2 - 63A). Thus this relaxation mechanism is dominant at 231.6 MHz.

Having shown that CSA relaxation is important for ^{205}Tl, it is useful to discuss this mechanism in a wider context.

TABLE 4 - 2: Temperature dependence of ^{205}Tl R_1 at 21.96 MHz for degassed $(CH_3)_2TlNO_3/D_2O$. (0.81M).

Temperature(K)	R_1 (s^{-1})	Temperature(K)	R_1 (s^{-1})
283.4	5.95	319.2	3.64
288.9	4.97	326.0	3.84
295.1	4.23	334.3	3.91
301.7	4.17	339.2	4.01
306.7	3.87	344.0	4.22
307.2	3.85	352.9	4.44
313.8	3.81	-	-

TABLE 4 - 3: Temperature dependence of ^{205}Tl R_1 at 21.96 MHz for non degassed $(CH_3)_2TlNO_3/D_2O$. (0.81M).

Temperature(K)	R_1 (s^{-1})	Temperature(K)	R_1 (s^{-1})
282.1	6.12	317.9	4.12
295.6	4.69	328.4	4.31
295.9	4.81	336.7	4.56
301.4	4.58	343.8	4.62
306.3	4.38	350.0	4.68
312.1	3.87	345.7	4.37
		356.7	5.02

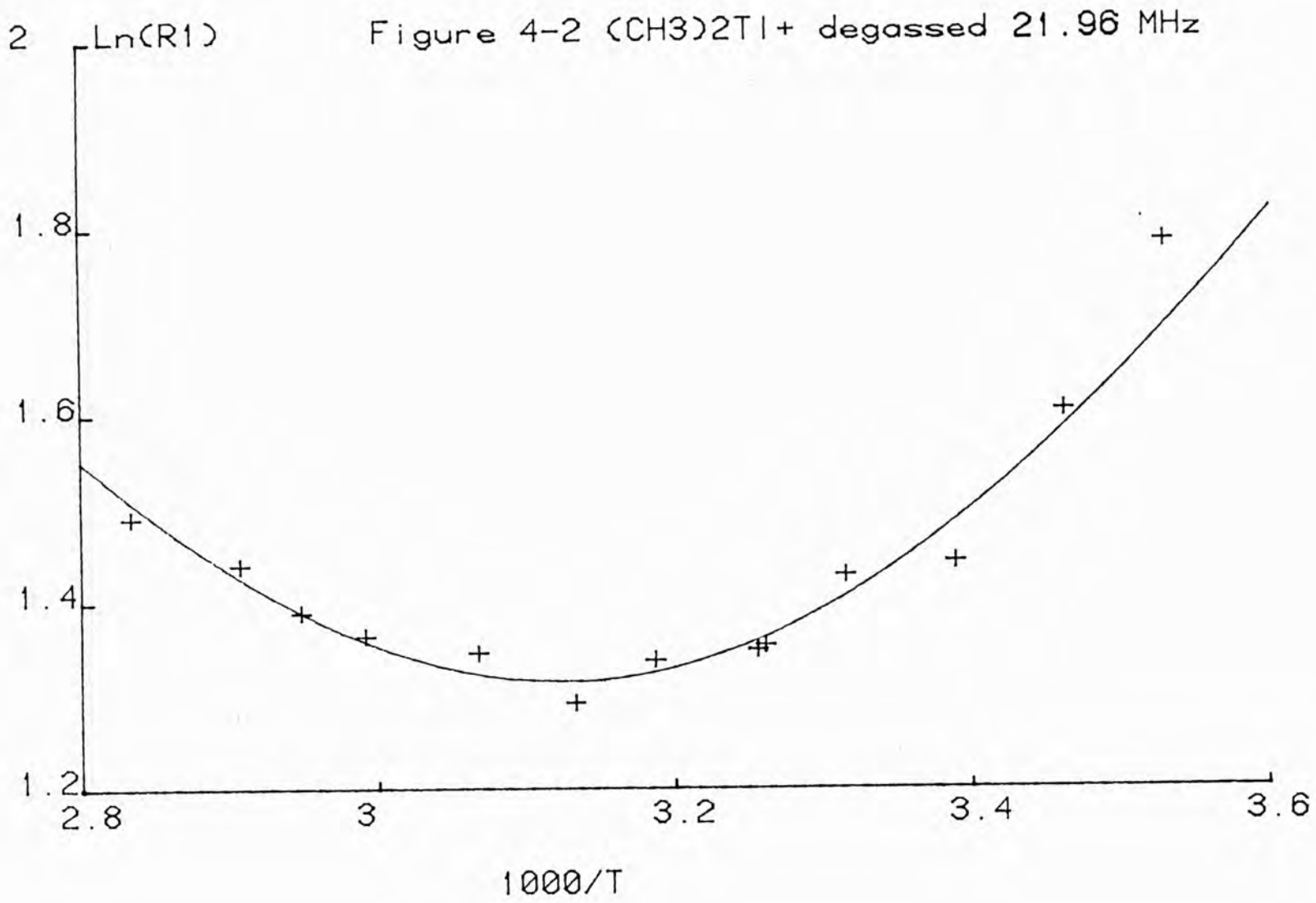

Figure 4-2 (CH3)2Tl+ degassed 21.96 MHz

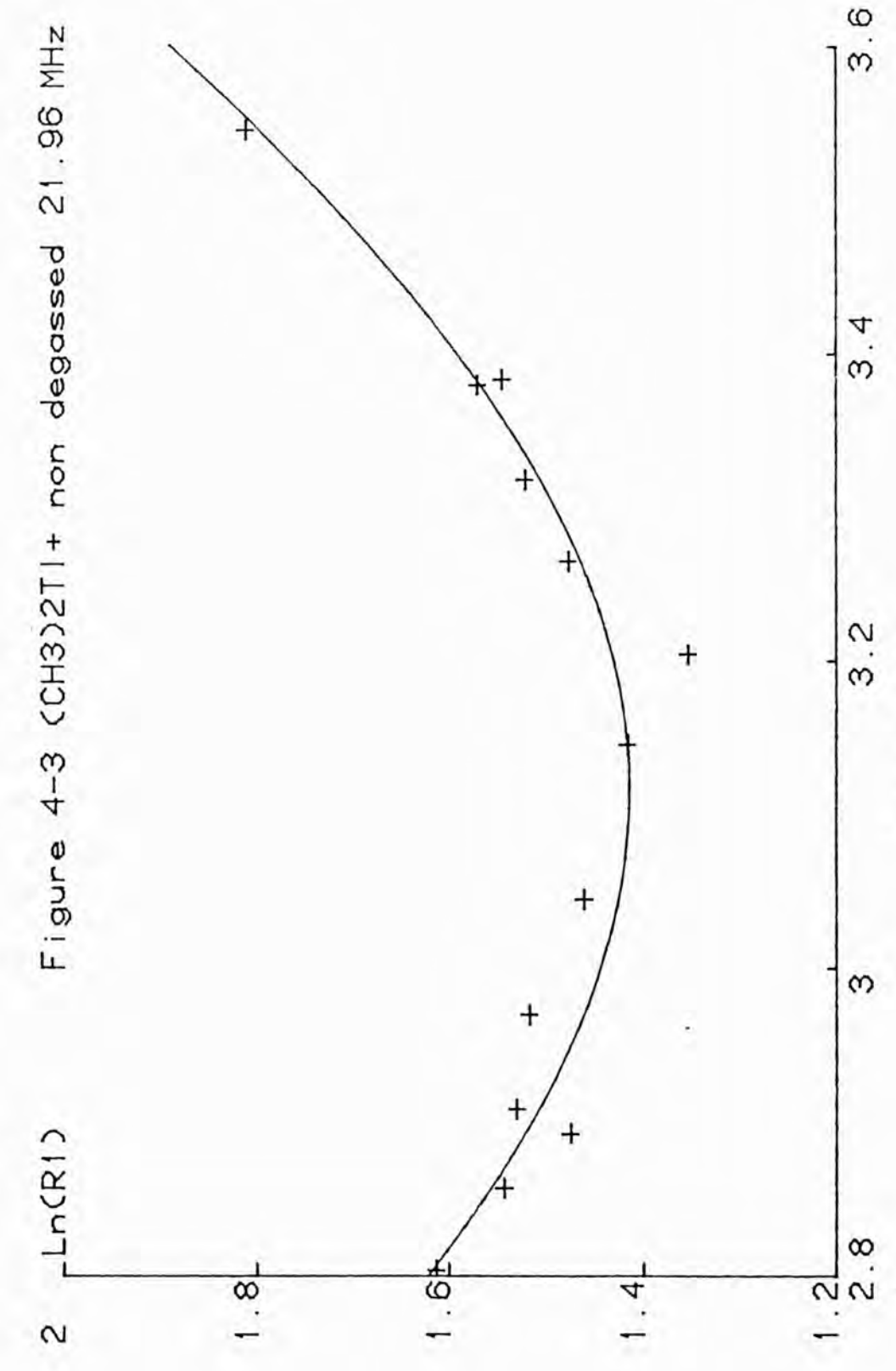

Figure 4-3 (CH3)2Tl+ non degassed 21.96 MHz

TABLE 4 - 4: Temperature dependence of ^{205}Tl R_1 at 231.6 MHz for degassed 0.81M $(CH_3)_2TlNO_3/D_2O$.

Temperature(K)	R_1 (s^{-1})	Temperature(K)	R_1 (s^{-1})
286.9	470	303.0	282
287.0	466	312.3	260
287.8	452	321.6	183
288.0	448	331.3	153
293.4	375	340.3	130
303.0	290	349.3	114

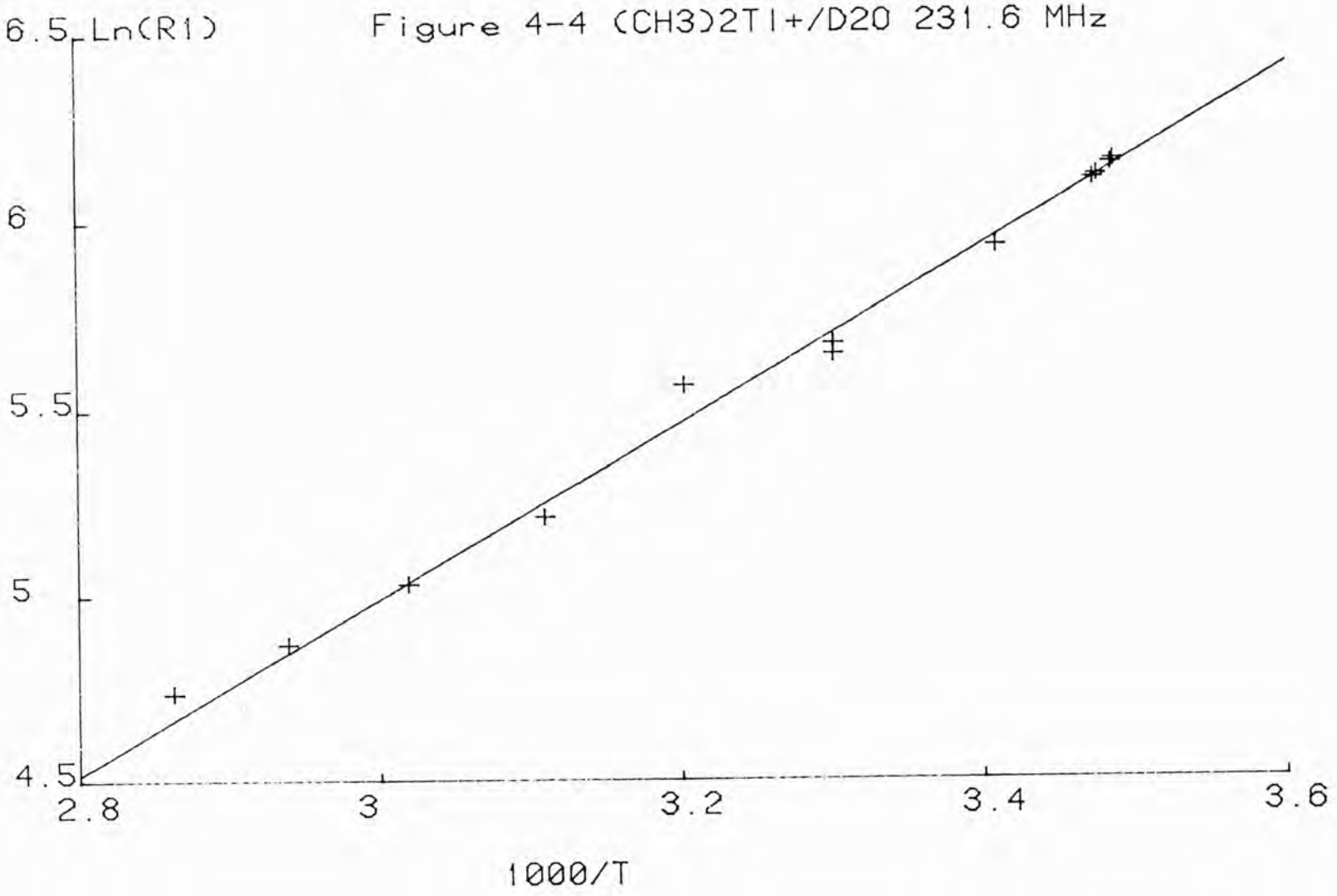
Figure 4-4 (CH3)2TI+/D20 231.6 MHz
6.5 Ln(R1)
6
5.5
5
4.5
2.8
3
3.2
3.4
3.6
1000/T

4.1.3. Some examples of CSA relaxation.

As discussed in Chapter Two the chemical shift anisotropy mechanism will contribute to spin lattice relaxation when reorientational Brownian motion modulates the interaction between the applied static field and an anisotropic shielding tensor. In addition if the anisotropy in the shielding tensor is induced by short timescale processes such as variation in solvation shell structure for ions, or the formation of transient ion pairs; then one may classify the mechanism as transient CSA.

McConnell and Holm[9] considered this mechanism as early as 1956. They compared the fast ^{13}C relaxation in $^{13}CS_2$ relative to that in $^{13}CCl_4$. It was suggested that CSA was operative in $^{13}CS_2$ but not in $^{13}CCl_4$ because of the tetrahedral symmetry and isotropic shielding tensor in the latter. The importance of CSA relaxation for ^{13}C in liquid CS_2 was confirmed by Spiess et al.[10] who carried out temperature dependent T_1 studies at 14 MHz, 30 MHz and 62 MHz. These studies showed that the ^{13}C R_1 was dominated by the spin rotation interaction at low field but by a mixture of SR and CSA at higher fields. Other observations of a CSA contribution to ^{13}C spin lattice relaxation were made by Levy et al.[11] for the inner carbons in diphenyldiacetylene, and by Wehrli for the quaternary carbons in benzonitrile[12]. For ^{13}C the CSA mechanism appears to contribute significantly only for highly anisotropic shielding environments in which there are no directly bonded protons and the dipolar mechanism

is inefficient .

Typical ^{13}C anisotropies are of the order of a few hundred ppm. However for heavier spin ½ nuclei where the chemical shift range may be several thousand ppm, then in anisotropic environments, shift anisotropies may also be large and the CSA mechanism relatively more important.

Sens et al[13] studied the temperature dependence of ^{199}Hg relaxation for dimethyl and divinyl mercury at 2.35 T. They reported an R_1 minimum and concluded that there were CSA and SR contributions. However Lassigne and Wells[14] reported that the ^{199}Hg relaxation of dimethyl mercury was spin rotation dominated at 1.41T, with CSA contributing only about 20%. The value deduced for the anisotropy of 4600 ppm conflicts with values of 7475 ppm [15] and 7325 ppm[16] found by liquid crystal measurements. Gillies et al.[17] have shown CSA to be the dominant relaxation mechanism for ^{199}Hg in diphenylmercury at fields of 2.35T and 7.05T. By measuring the para ^{13}C R_1, the correlation time for motion perpendicular to the molecular axis was found, and this allowed equation 2 - 63A to be used to deduce the shielding anisotropy at 6800 $\pm$ 680 ppm.

Wasylishen et al.[18] have reported ^{199}Hg R_1's for several Hg(II) compounds at 5.875T and 9.40T at a single temperature of 297 $\pm$ 2 K. Field dependent R_1's were used to estimate the shielding anisotropy in the compounds $Hg(CN)_2$, $Hg(CH_3)_2$ and $Hg(C_6H_5)_2$ as 3800,5820 and 5800 ppm

respectively. The errors in these values are reported as at least 10%. The anisotropy value of 5800 ppm for $Hg(C_6H_5)_2$ shows fair agreement with the more comprehensive variable temperature study of Gillies discussed above. The reorientational correlation time τ_2 required to estimate $\Delta\sigma$ was again found by measuring the para ^{13}C R_1. In the case of $Hg(CN)_2$ τ_2 was found by taking a previously reported ^{14}N quadrupole coupling constant and finding the ^{14}N R_1 from the observed linewidth. For $Hg(CH_3)_2$ the τ_2 of 6.7 ps at 300K reported by Lassigne and Wells was used and the anisotropy of 5820 ppm thus found is in poor agreement with previous liquid crystal determinations[15,16]. Wasylishen et al. have also discussed the effect of efficient ^{199}Hg CSA relaxation on the spectra of coupled ^{13}C nuclei but their estimate of the broadening of the ^{199}Hg satellites as $1/\pi T_2(^{199}Hg)$ is incorrect. The correct expression will be given in a later chapter along with a fuller discussion of these phenomena.

The ^{207}Pb spin lattice relaxation in aqueous solutions of $Pb(ClO_4)_2$ was studied by Hawk and Sharp[19] as a function of concentration and temperature at field strengths of 0.656T, 1.17T and 1.69T. They found that for a 3.5M solution spin rotation, chemical shift anisotropy and dipolar contributions were present; whereas for a 1.15M solution spin rotation was the dominant mechanism throughout the liquid range. The shielding anisotropy in the 3.5M solution is due to the presence of $PbClO_4^+$ transient ion pairs. This is the only proven example of transient CSA so far reported. The CSA mechanism has been shown by

Hays et al.[20] to dominate the ^{207}Pb R_1 for Me_3PbCl at 7.05T, whereas spin rotation is the most important mechanism at 2.35T. No field dependent relaxation effects were found for $PbMe_4$ or saturated aqueous $Pb(NO_3)_2$.

Lallemand et al.[21] have observed the disappearance of some ^{195}Pt-^{1}H and ^{195}Pt - ^{13}C coupling constants, and broadening of the ^{195}Pt spectra of Pt(II) complexes at high field. This is rationalised by proposing CSA as the dominant mechanism at high field. Similarly the disappearance of ^{14}N - ^{195}Pt couplings at high field and low temperature for Pt(II) and Pt(IV) amine complexes was observed by Sadler et al.[22], the couplings reappearing at high temperature where CSA relaxation is slower. Broadening of the ^{195}Pt satellites in the ^{1}H spectrum at high fields is also attributable to enhanced CSA relaxation.

The ^{195}Pt shielding anisotropies for $\{(Me_3)Pt(acetylacetonato)\}$, and $\{Me_3Pt\}_2SO_4 2H_2O$ have been found by Doddrell et al.[23], to be of the order of 1000 ppm using ^{1}H - ^{195}Pt cross polarisation techniques in the solid state. Solution state R_1 and R_2 studies at two fields indicated field dependent relaxation, implying an increased CSA contribution at higher field.

Hinton and Ladner[24] have suggested transient CSA as a contributor to the ^{205}Tl relaxation of $TlClO_4$ at high concentration in DMSO-d^6. However, no variable field measurements have been made and this mechanism has been inferred on the basis of concentration and temperature dependent studies. This paper will be discussed in more detail in a later chapter.

Hinton[25] has also studied ^{205}Tl relaxation for thallous ion complexed with a series of ionophoric antibiotics. With the antibiotics nonactin, monactin and dinactin the ^{205}Tl R_1 is deduced to have contribution of 50% spin rotation, 40% dipolar and 10% CSA. This is in contrast with the 90% contribution that is attributed to CSA in the Tl^+/valinomycin complex[26]. However the anisotropy deduced from liquid state relaxation studies is in poor agreement with that found by Hinton[27] from a solid state study of the same complex.

On the basis of temperature dependent studies of the ^{205}Tl R_1 and linewidth Hinton has suggested CSA as the dominant mechanism for ^{205}Tl relaxation in the Tl^+-Lasalocid complex[28]. None of the above mentioned ^{205}Tl studies has however been carried out using more than one field.

Hinton has however noted that in three cases in which the temperature dependence of both the ^{205}Tl R_1 and of the resonance frequency have been measured, the shift is to lower frequency with increasing temperature only when the relaxation is spin rotation dominated.[26] The reasons for this are not yet clear.

A detailed study of CSA relaxation for ^{19}F in fluorotyrosine alkaline phosphatase at 94 MHz and 235 MHz has been presented by Hull and Sykes.[29] The increased shift separation at higher field was matched by an increase in ^{19}F linewidth due to enhanced CSA relaxation. As discussed briefly in Chapter Two, Hull and Sykes used a

density matrix method to derive expressions for ^{19}F relaxation for an asymmetric shielding tensor modulated by a symmetric top diffusion process (i.e. a coupling of internal rotation and overall protein reorientation). Using these expressions and other data they were able to derive overall correlation times for protein reorientation and place limits on the internal mobility of the tyrosine residues.

Eaton et al.[30] have recently reported ^{59}Co relaxation measurements of several low symmetry cobalt complexes at two fields. They have observed a field dependent relaxation term where $R_1 < R_2$; this term is associated with chemical shift anisotropy relaxation involving the antisymmetric component of the ^{59}Co shielding tensor. This appears to be the first observation of chemical shift anisotropy relaxation involving this component.

4.1.4. Separation of ^{205}Tl relaxation mechanisms.

A qualitative discussion of the ^{205}Tl relaxation studies has shown the presence of the CSA and SR mechanisms at low field and the dominance of CSA at high field. In order to extract motional information from these results it is necessary to quantitatively separate the ^{205}Tl R_1 into contributions from each mechanism.

A comparison of the relaxation data for degassed and non degassed solutions at 21.96 MHz, shows that the mean difference between the ^{205}Tl relaxation rates for the two solutions is approximately 0.4 s^{-1}. Thus the oxygen induced contribution to R_1 is less than 10% at 21.9 MHz

and less than 5% at 34.73 MHz. For this reason the effect of sample degassing should be insignificant at 34.73 MHz and higher frequencies.

The high field data are the simplest to analyse. As shown in Figure 4.4 a plot of inverse temperature against ln R_1 is linear within experimental error. This is consistent with relaxation totally dominated by CSA in which the effective reorientational correlation time has an exponential temperature dependence with an activation energy E_{CSA}. Thus with the temperature T in Kelvin $R_1(T)$ is given by,

$$R_1(T) = R_1(298) \exp\left(\frac{E_{CSA}}{R}\left(\frac{1}{T} - \frac{1}{298}\right)\right). \qquad \{4 - 2\}$$

The variable temperature high field relaxation data may be fitted to equation 4 - 2 using a non linear least squares fit procedure with E_{CSA} and R_1 (298K) as variable parameters. This approach is preferred to the linear fit method using inverse temperature, ln R_1 values as x,y points because the estimated error in R_1 (298K) is obtained directly. The best fit parameters obtained for the high field data are

$$R_1\ (298K) = 340 \pm 4\ s^{-1}, \qquad \{4 - 3A\}$$

$$E_{CSA} = 19.6 \pm 0.6\ kJ\ mol^{-1}. \qquad \{4 - 3B\}$$

The errors given are estimated standard deviations. These parameters have been used to generate the linear plot of Figure 4.4.

The separation of the total rate at 21.9 MHz is slightly more involved, for the degassed sample the

preceding discussion has shown contributions from the spin rotation and chemical shift anisotropy mechanisms; if these are the only significant mechanisms then

$$R_{1\ TOT} = R_{1\ CSA} + R_{1\ SR} \cdot \qquad \{4 - 4\}$$

The $R_{1\ CSA}$ term may be calculated at any given temperature by use of the best fit parameters in equation 4 - 3 and scaling down by the ratio of the square of the two fields since the spin rotation relaxation is negligible at high field. Thus $R_{1\ SR}$ may be calculated at every temperature at which $R_{1\ TOT}$ was measured. The temperature dependence of $R_{1\ SR}$ may then be fitted to an equation analogous to equation 4 - 2. The best fit parameters obtained are

$$R_{1\ SR}(298K) = 1.19 \pm 0.04\ s^{-1} \qquad \{4 - 5A\}$$

$$E_{SR} = -17.7 \pm 0.7\ kJ\ mol^{-1}. \qquad \{4 - 5B\}$$

The negative value of E_{SR} shows that the spin rotation mechanism has an opposite temperature dependence to that of the other common relaxation mechanisms. It should be noted that whilst the estimated errors in the measured values of $R_{1\ TOT}$ at this field are $\pm$ 10%, those in $R_{1\ SR}$ are relatively greater. This arises because the total error in any given value of $R_{1\ TOT}$ is equal to that for $R_{1\ SR}$ calculated from equation 4 - 4; since $R_{1\ SR} < R_{1\ TOT}$ it follows that the relative error is increased. This problem is of increased importance at low temperatures where $R_{1\ SR}$ decreases. Thus in deriving the above parameters from the data in Table 4 - 2 the experimental data point at the lowest temperature has been omitted from the least squares

fit following error considerations.

A plot of $\ln(R_{1\ SR})$ against inverse temperature is shown in Figure 4 - 5 along with a line representing $R_{1\ SR}$ calculated from the parameters in equation 4 - 5. The fit is seen to be good in the light of the discussion of relative errors given above.

The separation of the observed ^{205}Tl relaxation rate into contributions from the CSA and SR mechanisms, allows the calculation of the following table of relaxation rates at 21.96 MHz.

T(^{o}C)	$R_{1\ CSA}$	$R_{1\ SR}$	$R_{1\ TOT}$	% CSA
20	3.48	1.06	4.54	76.7
50	1.65	2.07	3.72	44.4
80	0.89	3.63	4.52	19.7

TABLE 4 - 5. ^{205}Tl relaxation rates at 21.96 MHz.

The above table shows directly the temperature dependent variation of the relative importance of the two mechanisms.

Following the procedure used to separate the CSA and SR mechanisms, one might consider the observed ^{205}Tl R_1 of the non degassed sample to be the sum of three terms

$$R_{1\ TOT} = R_{1\ CSA} + R_{1\ SR} + R_{1\ OX} \quad ; \qquad \{4 - 6\}$$

where $R_{1\ CSA}$ and $R_{1\ SR}$ are as previously discussed and $R_{1\ OX}$ is the contribution to the ^{205}Tl R_1 due to mechanisms arising from the presence of molcular oxygen. The terms $R_{1\ CSA}$ and $R_{1\ SR}$ may be calculated from the previously obtained parameters allowing the calculation of $R_{1\ OX}$ from the

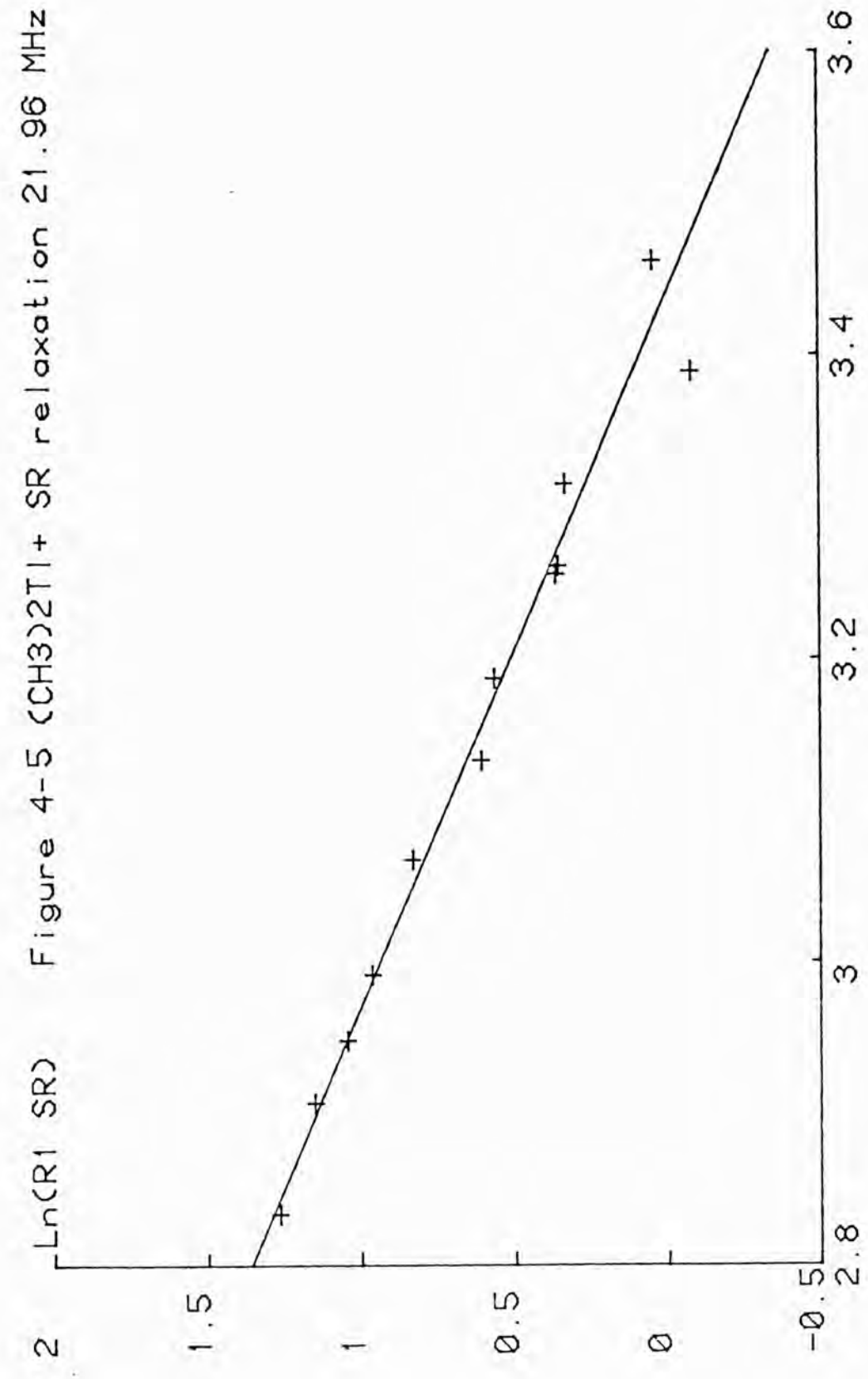

Figure 4-5 (CH3)2Tl+ SR relaxation 21.96 MHz

experimentally observed rate $R_{1\ TOT}$, as a function of temperature. However the method must be treated with considerable caution, since the small contribution of $R_{1\ OX}$ to the observed rate ($\leqslant$10%) leads to large relative errors in the calculated values of $R_{1\ OX}$. Bearing these considerations in mind, a fit of values of $R_{1\ OX}$ as a function of temperature to an equation of the form of equation 4 - 2 leads to the best fit parameters

$$R_{1\ OX}(298K) = 0.42 \pm 0.06\ s^{-1}\ , \qquad \{4 - 7A\}$$

$$E_{OX} = 3.09 \pm 4.26\ kJ/mol. \qquad \{4 - 7B\}$$

These parameters are considered only to approximate the contribution of this mechanism to the observed spin lattice relaxation. The large errors on the parameters in equation 4 - 7 reflect the errors in the values of $R_{1\ OX}$ calculated by this procedure. Thus the characterisation of this mechanism is not nearly as well defined as that of the dominant CSA and SR mechanisms.

Finally the best fit parameters defined in equations 4 - 3, 4 - 5 and 4 - 7 have been used to generate the fitted R_1 curves in Figures 4 - 1 and 4 - 3 in accordance with equation 4 - 6.

4.1.5. ^{205}Tl spin rotation constants and absolute shielding scale.

In the previous section the quantitative characterisation of the chemical shift anisotropy and spin rotation mechanisms has been described. When the shielding anisotropy is known the CSA mechanism provides information on reorientational correlation times. Similarly the spin rotation relaxation mechanism can be used to extract spin rotational correlation times if the relevant spin rotation constants are available.

Previous liquid crystal studies of the dimethylthallium(III) cation in a lyotropic phase have found the magnitude of the ^{205}Tl shielding anisotropy to be 5300 ppm[31], however the value 5550 ppm will be derived in Section 4 - 2 and is used throughout this Chapter. This ^{205}Tl shielding anisotropy will subsequently be used to derive both an absolute ^{205}Tl shielding scale and the values of the ^{205}Tl spin rotation constants in this species.

The spin rotation tensor $\underline{\underline{C}}$ is defined in terms of the spin rotation interaction Hamiltonian discussed in Chapter Two. If a principal symmetry axis for this tensor may be found, and if no antisymmetric component is present the tensor may be described in terms of its three diagonal components. Spin rotation constants in the gas phase may be obtained by molecular beam studies[32] and by microwave spectroscopy.[33]

Another source of spin rotation constants is the relationship between these and the paramagnetic

contribution to the nuclear shielding. The theory was developed for a linear molecule by Ramsey[34], and extended to symmetric and asymmetric tops by Flygare[35]. The subject has been covered in a review by Flygare[36]. Deverell[37,38] had deduced spin rotation constants by this method and has shown them to agree well with values found by molecular beam techniques. Garg, Davidson and Ripmeester[39] have used this relationship to deduce the average value and anisotropy of the ^{19}F rotation tensor for CF_4 in the heavy water clathrate hydrate at 4.2K the ^{19}F shielding anisotropy was found by a fit to the experimental lineshape for a four spin system. The same authors[40], have used this approach to find the ^{19}F spin rotation tensor components for ClO_3F and CCl_3F molecules enclathrated in D_2O hydrates. These constants were then used with ^{19}F and ^{35}Cl spin relaxation data to show the validity of the J diffusion model for these symmetric top molecules.

The derivation of the ^{205}Tl spin rotation constants will be made by a similar procedure, the first step is to obtain the principal elements of the ^{205}Tl shielding tensor. Ramsey[34] has derived an expression for the magnetic shielding of a nucleus in a molecule, due to the motion induced in the electrons by the applied static field. The shielding tensor element σ_{ab} may be written as the sum of two parts

$$\sigma_{ab} = \sigma_{ab}^{d} + \sigma_{ab}^{p} \quad , \qquad \{4 - 8\}$$

the first term describes the unhindered rotation of the electrons about the nucleus, which according to Lenz's law

produces a field which opposes the applied field. This is the diamagnetic term, and for a free atom this is the only term that need be considered. The paramagnetic term is non zero when the electric potential around the nucleus is non spherically symmetric, and is due to a coupling of the ground state wave function with higher states in the presence of the applied field. To evaluate the ^{205}Tl spin rotation constants in the dimethylthallium(III) cation, the 'atom in a molecule' approach, discussed by Deverell[37] will be used. The diamagnetic term will be taken to be that of the free atom and will be constant for all molecules so that differences in the paramagnetic term determine chemical shift differences between molecules. One may write,

$$\sigma_{ab} = \sigma'^{d}_{ab} + \sigma'^{p}_{ab} \quad . \qquad \{4 - 9\}$$

This approach differs from that of Ramsey only in the method of separation of the total shielding into the two terms.

As discussed earlier the linearity of the dimethylthallium(III) cation leads to an axially symmetric ^{205}Tl shielding tensor. When the applied field is parallel to the symmetry axis, unhindered precession of the electrons about this axis will occur and only the diamagnetic term will be non zero, as is the case for the free atom and linear molecules[41]. Thus if the parallel shielding component is diamagnetic only then

$$\sigma'^{p}_{\parallel} = 0 \qquad \{4 - 10\}$$

and

$$\sigma_{\parallel} = \sigma'^{d} \quad . \qquad \{4 - 11\}$$

However the perpendicular shielding tensor element has both diamagnetic and paramagnetic contributions.

$$\sigma_{\perp} = \sigma'^{d} + \sigma'^{p}_{\perp} \qquad \{4 - 12\}$$

The shielding anisotopy $\Delta\sigma$ is defined as

$$\Delta\sigma = (\sigma_{\parallel} - \sigma_{\perp}) = (\sigma'^{p}_{\parallel} - \sigma'^{p}_{\perp}) = -\sigma'^{p}_{\perp} \qquad \{4 - 13\}$$

and the observed paramagnetic shielding is the trace of the paramagnetic shielding tensor

$$\sigma'^{p} = \frac{1}{3}(\sigma'^{p}_{\parallel} + 2\sigma'^{p}_{\perp}) \qquad \{4 - 14\}.$$

Since the paramagnetic term has a deshielding effect it is, by convention, given a negative sign. Furthermore since $\sigma'^{p}_{\parallel}$ is equal to zero one can deduce the important results

$$\sigma'^{p}_{\perp} = -5550 \text{ ppm} \qquad \{4 - 15\}$$

and

$$\Delta\sigma = +5550 \text{ ppm} \qquad \{4 - 16\}.$$

The results in equations 4 - 10 and 4 - 15 will later be used in the derivation of ^{205}Tl spin rotation constants.

An absolute nuclear shielding scale may be defined as one in which the bare nucleus is the chosen reference. Absolute shielding scales have been reported for $^{13}C(36)$, $^{14}N(36)$, $^{17}O(36)$, $^{19}F(37)$, $^{31}P(37,42)$, $^{119}Sn(43)$, $^{199}Hg(14)$ and $^{207}Pb(44)$.

A ^{205}Tl shielding scale relative to the free atom is defined by the condition

$$\sigma'^{p} = 0 \qquad \{4 - 17\}.$$

Using the shielding tensor elements deduced above this ^{205}Tl shielding zero is expected to be 3700 ppm to high shielding (low frequency) of the dimethylthallium(III) cation in aqueous solution.

Hafner and Nachtrieb[45] have proposed a shielding scale in which the reference is the free Tl(I) ion. Their 'best guess' for the free ion frequency is the provisional selection of the lowest resonance frequency observed in any thallium compound. This has been defined in terms of the ratio of the ^{205}Tl resonance frequency to that of the water proton as

$$\nu(^{205}Tl)/\nu(^{1}H) = 0.57664 \qquad \{4 - 18\}.$$

The difference between the Tl(I) ion and Tl atom shielding scales is expected to be small, it may be approximately calculated from the single electron contribution to the diamagnetic shielding given by Schneider and Buckingham[46] as

$$\sigma_{SINGLE}^{d} = 17.8 \times 10^{-6} \frac{(Z_o Z)^{\frac{1}{2}}}{n^2} \qquad \{4 - 19\}$$

where Z is the real nuclear charge, Z_o is the Slater screened nuclear charge and n is the principal quantum number. Schneider and Buckingham have given Z_o as 5.00 for the 6^S electrons in thallium, thus the single electron contribution is about 10 ppm. The difference between the atomic and ionic Tl scales is small enough to be neglected for the purposes considered here.

Köppel et al[47] have shown that the Hafner and Nachtrieb zero is 3790 ppm to high shielding of the aqueous dimethylthallium(III) cation resonance. Thus the difference between the atomic shielding scale proposed herein and the Hafner and Nachtrieb scale is only 90 ppm. This difference is well within the bounds of experimental error, it provides strong evidence for the correctness of

this shielding scale and of the ^{205}Tl shielding anisotropy used to find it.

A recent study of ^{205}Tl and other nuclear shifts in several ternary semiconductors has shown excellent linear correlations between experimental cation shifts and calculated values for the paramagnetic contribution to the chemical shift[48]. In addition near perfect agreement was found between the calculated Tl(I) ion shielding zero and that of Hafner and Nachtrieb, thus providing an independent confirmation of their scale.

If a nuclear shielding scale relative to the free atom has been established and the diamagnetic shielding of that atom is known, then an absolute scale relative to the bare nucleus may be derived. The diamagnetic shielding of the free Tl atom was calculated by Malli and Froese[49] to be

$$\sigma'^{d} = 9894 \text{ ppm} \quad . \qquad \{4 - 20\}$$

Thus the absolute shielding properties of the ^{205}Tl nucleus in the $(CH_3)_2Tl^+$ cation are described by the tensor elements.

$$\sigma_{\parallel} = + 9894 \text{ ppm}, \qquad \{4 - 21A\}$$

$$\sigma_{\perp} = + 4344 \text{ ppm}, \qquad \{4 - 21B\}$$

and by the isotropic value which is the trace of the tensor

$$\sigma = \frac{1}{3} (\sigma_{\parallel} + 2\sigma_{\perp}) = + 6194 \text{ ppm}. \quad \{4 - 22\}.$$

Thus the resonance of the bare Tl nucleus, which is the zero point on the Tl absolute shielding scale is 6194 ppm to low shielding (high frequency) of the dimethylthallium(III) cation in aqueous solution.

Having discussed the ^{205}Tl shielding scale and provided some justification for the paramagnetic shielding tensor elements described by equations 4 - 10 and 4 - 15, the ^{205}Tl spin rotation constants may now be calculated from these values. The relationship between the spin rotation tensor elements and the paramagnetic shielding tensor elements has been used by many authors.[8,14,36-40] It may be expressed in the form

$$\sigma_i'^{p} = A\, C_i I_i \qquad \{4 - 23\},$$

where the subscript i indicates the ith element of the respective diagonalised tensor and A is a constant for a given nucleus. The expression used by Spiess[8], has C in angular frequency units and gives A as

$$A = \frac{\mu_B}{\gamma \hbar^2} \qquad \{4 - 24\}.$$

where μ_B is the Bohr magneton in J T^{-1}, and γ is the nuclear gyromagnetic ratio in rad $s^{-1}T^{-1}$. For the ^{205}Tl nucleus the value of this constant is

$$A = 5.349 \times 10^{36} \text{ rad}^{-1} s^{-1} T^{-1} \qquad \{4 - 25\}.$$

Using a moment of inertia $I_\perp$ of 2.251×10^{-45} kg m^2 (Appendix A) and shielding tensor elements in equations 4 - 10 and 4 - 15 it is found that

$$C_\parallel = 0 \text{ Hz} , \qquad \{4 - 26A\}$$

$$C_\perp = -4.61 \times 10^5 \text{ rad } s^{-1} = -73.4 \text{ kHz}. \qquad \{4 - 26B\}$$

The above ^{205}Tl shielding anisotropy and spin rotation constants have been obtained by liquid state relaxation measurements. These interaction constants will subsequently

be used to obtain reorientational and spin rotational correlation times as a function of temperature.

4.1.6 Test of models of molecular motion.

An anisotropic shielding interaction is a second rank tensorial interaction, hence as discussed in Chapter Two the correlation time governing this interaction is a linear combination of spherical tensor correlation times.

$$\tau_2^{EFF} = \frac{1}{4}\{3\cos^2\alpha - 1\}^2 \tau_{20} + 3\{\sin^2\alpha \cos^2\alpha\} \tau_{21} + \frac{3}{4}\{\sin^4\alpha\}\tau_{22}. \qquad \{4 - 27\}$$

However, since the ^{205}Tl nucleus lies on the symmetry axis of the cation $\alpha = 0$, and it follows that

$$\tau_2^{EFF} = \tau_{\perp} = \tau_{20} . \qquad \{4 - 28\}$$

Thus the information obtained by ^{205}Tl relaxation studies is the area under the reorientational correlation function for the spherical harmonic Y_{20}. Since this is a function of the reorientation angle only, it follows that neither motion about the parallel axis nor internal rotation modulate the anisotropic shielding interaction for ^{205}Tl.

For a symmetric top molecule the principal axes of the diffusion and moment of inertia tensors are coincident[50]. Thus for $(CH_3)_2Tl^+$ these are also coincident with the principal axes of the ^{205}Tl shielding tensor, i.e. parallel and perpendicular to the symmetry axis.

If the reorientational motion is diffusional then the diffusion constant for motion perpendicular to the symmetry axis is

$$D_{\perp} = 1/6\tau_{\perp} \quad . \qquad \{4 - 29\}$$

For an axially symmetric shielding tensor ($\eta = 0$), the CSA relaxation rate within extreme narrowing is found from Chapter Two as

$$R_1^{CSA} = \frac{2}{15}\gamma^2 B_o^2 \Delta\sigma^2 \tau_{\perp} \qquad \{4 - 30\}$$

for a ^{205}Tl shielding anisotropy of 5550 ppm and a ^{205}Tl resonance frequency of 231.6 MHz this becomes

$$R_{1\ CSA} = 8.70 \times 10^{12} \tau_{\perp} \qquad \{4 - 31\} .$$

Using the value of $R_1^{CSA}(298K)$ in equation 4 - 3A one finds

$$\tau_{\perp}(298K) = 39.1 \pm 0.5 \text{ ps} \qquad \{4 - 32\} .$$

Since the activation energy of $\tau_{\perp}$ equals that of $R_{1\ CSA}$ then $\tau_{\perp}$ may be calculated as a function of temperature using a value of 19.6 kJ/mol for E_{CSA} as given in equation 4 - 3B.

The Stokes Einstein equation discussed in Chapter Two predicts that the reorientational correlation time is proportional to η/T where η is the shear viscosity. Taking the values of η_{D_2O} measured at ambient pressure from 10^{o} to $90^{o}C$ by Jonas[51], the activation energy for η/T is found to be 18.8 kJ/mol. This value is equal within experimental error to E_{CSA}. For the reorientation of an ellipsoidal molecule in solution the model proposed by Hu and Zwanzig[52] and discussed by Boeré and Kidd[53], is more appropriate than the Stokes Einstein model. The method involves constructing the smallest right angled box that will enclose the molecule's Van der Waals surface. If the dimensions of this box are $2a < 2b < 2c$, the radial semi-axes of the molecule regarded as ellipsoidal are $a < b < c$.

For a prolate ellipsoid such as the dimethylthallium(III) cation the shape factor

$$\rho_{PROLATE} = (a + b)/2c \qquad \{4 - 33\},$$

allows the calculation of microviscosity f in both the slip and stick limits, hence τ_2 is found as

$$\tau_2 = f \frac{4\pi c^3 \eta}{3kT} \quad . \qquad \{4 - 34\}$$

Using the geometry of the dimethylthallium(III) cation discussed in Appendix 1, in conjunction with the Van der Waals radii given by Bondi[54], the box has the dimensions

$$a = 1.975 \times 10^{-10} \text{ m} \quad , \qquad \{4 - 35A\}$$

$$b = 2.095 \times 10^{-10} \text{ m} \quad , \qquad \{4 - 35B\}$$

$$c = 3.585 \times 10^{-10} \text{ m} \quad . \qquad \{4 - 35C\}$$

Thus the shape factor is

$$\rho_{PROLATE} = 0.567 \qquad \{4 - 36\}.$$

Using linear interpolation between the values of shape parameters and microviscosity factors given in the review of Boeré and Kidd[53] the following microviscosity factors are obtained

$$f_{SLIP} = 0.075, \; f_{STICK} = 0.43. \quad \{4 - 37\}$$

Taking a value of 1.13 cp for ηD_2O at 298K the reorientational correlation times in the two limits are

$$\tau_2^{SLIP} = 4.0 \text{ ps} \; , \qquad \{4 - 38\}$$

$$\tau_2^{STICK} = 22.8 \text{ ps}. \qquad \{4 - 39\}$$

Thus the reorientational motion of the cation appears to lie outside the range of values allowed by the Hu and Zwanzig hydrodynamic model. The correlation times in

equation 4-38,4-39 may be increased by adding solvation water molecules to the cation structure; however the discussion to follow will show that a knowledge of both reorientational and spin rotational correlation times allows a more critical test of models of molecular motion than this approach.

Using the spin rotation constants and spin rotation relaxation data previously discussed, the perpendicular spin rotation correlation time for this species in aqueous solution can be derived. For a symmetric top molecule within extreme narrowing the spin rotation rate $R_{1\ SR}$ may be expressed as[8]

$$R_{1\ SR} = \frac{2kT}{3\ \hbar^2}\left[2I_\perp C_\perp^2 \tau_{SR\perp} + I_\parallel C_\parallel^2 \tau_{SR\parallel}\right]. \quad \{4 - 40\}$$

This expression assumes $\tau_{SR\parallel}, \tau_{SR\perp} < \tau_\parallel, \tau_\perp$, if τ_J and τ_{SR} are taken as equal, as discussed in Chapter Two, and since $C_\parallel = 0$, this becomes

$$R_{1\ SR} = 7.90 \times 10^{11} T \tau_{J\perp} \quad \{4 - 41\}$$

taking the best fit value of $R_{1\ SR}(298K) = 1.195^{-1}$ given in equation 4 - 5 one finds

$$\tau_{J\perp}(298K) = 5.05 \times 10^{-15} \text{ secs} \quad \{4 - 42\}.$$

Thus reorientational and angular momentum correlation times have been calculated at 298K and may be calculated at other temperatures by use of equations 4 - 31 and 4 - 41. In order to do this and make a comparison with the Hubbard equation the low field data in Table 4-2, used to characterise the spin rotation relaxation, will be used again. The reorientational correlation time at any given temperature is calculated from the best fit parameters for the high field relaxation

using equation 4 - 31. The angular momentum correlation time is calculated from the experimental value of $R_{1\ SR}$ at low field, as shown in equation 4 - 4, rather than from the best fit parameters at low field. The results are shown in Table 4 - 6; both correlation times are expressed in reduced form[55],

$$\tau_{\perp}^{*} = \tau_{\perp}(kT/I_{\perp})^{\frac{1}{2}} , \qquad \{4 - 43A\}$$

$$\tau_{J_{\perp}}^{*} = \tau_{J_{\perp}}(kT/I_{\perp})^{\frac{1}{2}} . \qquad \{4 - 43B\}$$

T(K)	$\tau_{\perp}^{*}$	$\tau_{J_{\perp}}^{*} \times 10^{3}$	Product
288.9	66.8	6.11	0.408
295.1	56.9	5.34	0.304
301.7	48.3	7.97	0.384
306.7	42.8	8.08	0.346
307.2	42.3	8.13	0.344
313.8	36.4	9.83	0.358
319.2	32.2	10.2	0.329
326.0	28.0	12.6	0.352
334.3	23.7	14.2	0.336
339.2	21.6	15.3	0.329
344.0	19.7	16.9	0.333
352.9	16.8	18.7	0.314

TABLE 4.6. Reduced correlation times for the dimethylthallium(III) cation.

The data in this table show that across the studied temperature range

$$\tau_{J_{\perp}}^{*} << \tau_{\perp}^{*} \qquad \{4 - 44\}$$

This relationship is often considered a necessary condition for the validity of the rotational diffusion model and the Hubbard equation. The temperature dependence of the correlation times is of considerable interest. It is found that as the temperature is raised, $\tau_{\perp}^{*}$ decreases whilst $\tau_{J_{\perp}}^{*}$ increases and the product of the two is found to be approximately constant. The mean value of the product is thus

$$\tau_{\perp}^{*}\ \tau_{J_{\perp}}^{*} = 0.345 \pm 0.029 \qquad \{4 - 45\}.$$

The constancy of this product is to be expected since E_{CSA} and E_{SR} were found to be opposite in sign and equal within two standard deviations. The data in Table 4 - 6 are presented as a log $\tau_{\perp}^{*}$ vs log $\tau_{J_{\perp}}^{*}$ graph in Figure 4 - 6, the line shown represents the mean value of the product given above.

The relationship between the reorientational and angular momentum correlation times may be compared to the Hubbard equation which in reduced form, and applied to the perpendicular axis is

$$\tau_{\perp}^{*}\ \tau_{J_{\perp}}^{*} = 1/6 = 0.1667 \quad . \qquad \{4 - 46\}$$

The deviation between this result and the one given above, lies well outside the range of experimental error shown by the scatter of the points in Figure 4 - 6. In the light of the fulfilment of the condition $\tau_{J_{\perp}}^{*} << \tau_{\perp}^{*}$, and the non validity of the Hubbard equation, one may conclude that the small step rotational diffusion model is not appropriate for this system.

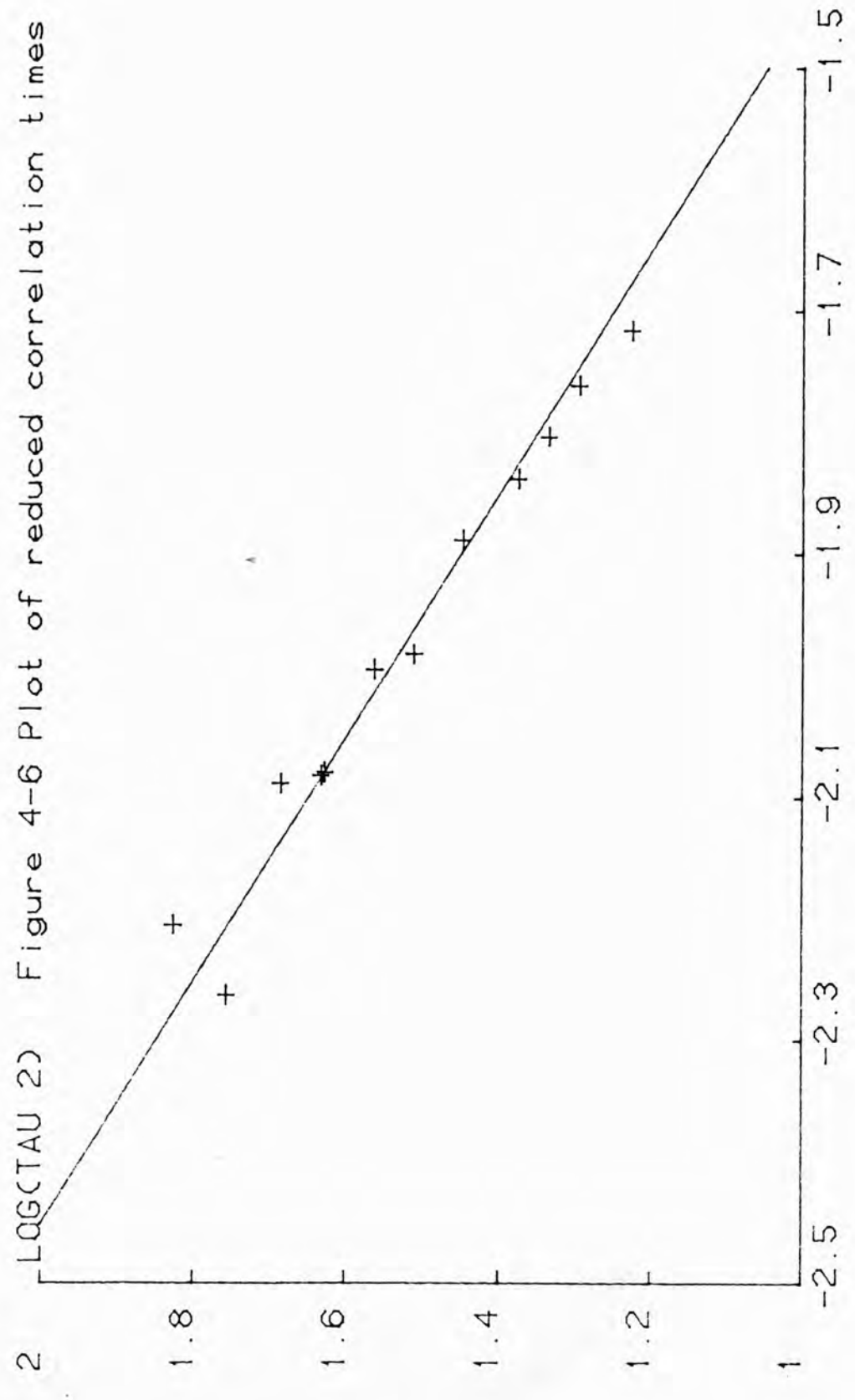

Figure 4-6 Plot of reduced correlation times

It now remains to be shown whether the molecular motion of the dimethylthallium(III) cation can be rationalised on the basis of either the extended diffusion or the solid-like reorientational models discussed in Chapter Two.

The extended diffusion model (55,56) is a gas like model, in which free rotational motion is interrupted by collisions of mean frequency τ_J^{-1}. The collisions may randomise either the magnitude and direction, or only the direction of the rotational angular momentum. These conditions represent the J diffusion and M diffusion limits of the model respectively. In the limit $\tau_J^* << 1$ J diffusion reduces to the rotational diffusion model previously discussed. In this same limit the M diffusion model shows that the product $\tau_\perp^* \tau_{J\perp}^*$ is also a constant, but whose value is a function of the inertial asymmetry ε defined as

$$\varepsilon = (I_\perp - I_\parallel)/I_\parallel \quad . \qquad \{4 - 47\}.$$

This function has a complicated form, involving integration over all values of the molecular orientation and angular momentum. Several values of the function have been presented in graphical form by McLung[56] and are shown in Table 4 - 7. The value ε=0 corresponds to a spherical top and ε=∞ to a linear molecule.

Inertial Asymmetry	$\tau_{\perp}^{*}\ \tau_{J\perp}^{*}$
-0.5	0.40
-0.1	0.44
0	0.50
1	0.54
10	0.79
∞	∞

TABLE 4 - 7. Dependence of the product of reduced correlation times upon inertial asymmetry.

The infinite value for $\tau_{\perp}^{*}\ \tau_{J\perp}^{*}$ reflects the fact that for a linear molecule the τ_{2k} values are infinite in the M diffusion model. The inertial asymmetry of the dimethylthallium(III) cation is calculated in Appendix 1. The value is found to be

$$\varepsilon = 19.96 \ . \qquad \{4 - 48\}$$

Thus if the molecular reorientation is described by the M diffusion model then one expects

$$\tau_{J\perp}^{*}\tau_{\perp}^{*} > 0.8 \ . \qquad \{4 - 49\}.$$

The extended diffusion model allows a range of values for the product $\tau_{\perp}^{*}\ \tau_{J\perp}^{*}$, from 0.167 up to and exceeding 0.8. Hence the value of 0.345 obtained for the dimethylthallium(III) cation lies within this range. The physical interpretation of reorientation that lies between the bounds of the J and M models is that molecular collisions always randomise the direction of angular momentum and may also change its magnitude.

It is of interest to see whether the solid-like or structure limited reorientational models can offer an alternative explanation of the motional behaviour of this species. The failure of the Hubbard relationship is as predicted by the solid-like reorientational model of Kivelson.[57] The physical picture proposed by this model is one in which the observed molecule is "clamped" for τ_0 seconds in a torsional well formed by the surrounding liquid in which the molecule executes rapid oscillations. When random fluctuations in the liquid cause structural relaxation the torsional well is lost, and free rotation takes place for τ_f seconds. The Ivanov model[58] is a limit of the Kivelson model in which the time spent clamped is large, i.e.

$$\tau_f << \tau_0 \quad , \qquad \{4 - 50\}$$

and the angular jumps are large. O'Reilly[59-62] has proposed a model of liquid water in which molecular reorientation occurs in large excursions of short time duration. For times between the large angular reorientations, librational motions occur which do not result in significant net reorientation. This model has been used to rationalise the pressure and temperature dependence of the viscosity and nuclear relaxation times in H_2O and D_2O. Within the framework of this model it is found that the product of the reorientational and angular momentum correlation times is a function of the mean squared angular step size. For a linear molecule or a nucleus on the symmetry axis of a symmetric top this becomes[59,62],

$$\tau_{\perp}^{*}\,\tau_{J_{\perp}}^{*} = \frac{\langle\theta_{\perp}^{2}\rangle}{2\{1-\exp(-3\langle\theta_{\perp}^{2}\rangle)\}} \quad . \qquad \{4 - 51\}$$

In this equation $\langle\theta_{\perp}^{2}\rangle$ is the mean square angular jump about the perpendicular axis. The experimental value of $\tau_{\perp}^{*}\tau_{J_{\perp}}^{*}$ found herein implies

$$\langle\theta_{\perp}^{2}\rangle = 0.589\,\text{rad}^{2} \quad , \qquad \{4 - 52\}$$

or alternatively

$$\langle\theta_{\perp}^{2}\rangle^{\frac{1}{2}} = 44.0^{\circ} \quad . \qquad \{4 - 53\}$$

This root mean square reorientation angle may be compared to an angle of 62° derived by O'Reilly[61] from previous molecular dynamics calculations for water.

Hindman et al.[63,64] have measured the temperature dependence of quadrupolar relaxation in both D_2O and $H_2{}^{17}O$ and found that a double exponential expression was necessary to account for the data. The low temperature-large entropy term was attributed to the cooperative dissolution of a small cluster of hydrogen bonded molecules. The high temperature process was attributed to angular motions larger than those corresponding to the Debye limit. The apparent activation energy was a function of temperature and at $45^{\circ}C$, the mean of the temperature range studied herein, E_{ACT} was about 17.5 kJ mol^{-1} for both liquids. The closeness of these values to E_{CSA} is consistent with the hypothesis of a common reorientational mechanism controlled by breakdown of the hydrogen bonded structure.

Finally, consider the angular momentum correlation time, $\tau_{J_{\perp}}$, which lies in the femtosecond range at ambient

temperatures. It is difficult to explain such a rapid process on the basis of the extended diffusion model. The Kivelson solid-like model, however, offers a simple explanation of such small values.[57] The angular momentum correlation function for cations not trapped in a torsional well will be exponential with a decay time $\tau_{J_\perp\,(FREE)}$ but only a fraction $\tau_f/\{\tau_0 + \tau_f\}$ of the cations are reorienting, and only these will contribute to spin rotation relaxation. For the remaining cations, trapped in torsional wells, the motion will be oscillatory or librational. One would then expect an oscillatory type angular momentum correlation function, having cancelling positive and negative lobes, leading to a $\tau_{J_\perp(TRAPPED)}$ near zero. The observed angular momentum correlation time will be a weighted mean of these terms.

$$\tau_{J_\perp(OBS)} = \tau_{J_\perp(FREE)} \cdot \tau_f/\{\tau_f + \tau_o\} \quad \{4 - 54\}$$

Since raising the sample temperature is likely to increase the fraction of free or non-clamped cations, $\tau_\perp$ would be expected to decrease and $\tau_{J_\perp}$ to increase. Thus the constancy of the product of the correlation times is a manifestation of the fact that they are both controlled by the same physical process, albeit in an opposite sense.

Molecular dynamics calculations have revealed the presence of these librational or oscillatory motions in the calculated reorientational and angular momentum correlation functions in water and aqueous solutions[61,65-67]. Computer simulated water has also been found to have a value of τ_J in the femtosecond range at 34°C.[61]

4.1.7. Proton spin lattice relaxation in the dimethylthallium(III) cation.

The ^{205}Tl relaxation in the dimethylthallium(III) cation has been studied in some detail in order to extract information on motion perpendicular to the symmetry axis. The ^{1}H relaxation in this cation has been studied to try to gain information on the motion of the cation parallel to the symmetry axis and on internal rotation. Similar efforts to study the anisotropy of the reorientational motion have been made for $Hg(CH_3)_2$[14].

In order to separate possible intra and intermolecular dipole-dipole contributions to the ^{1}H R_1, degassed samples of protonated and deuterated dimethylthallium(III) nitrate in D_2O and a 50/50 sample of these were made up. In all cases the concentration of Tl was 0.8M. When studying the ^{1}H relaxation of the deuterated sample one is observing the relaxation of the residual proton in the species $CHD_2CD_3Tl^+$. The proton relaxation in these three samples was measured at a single, instrument indicated, temperature of 301K, on a Bruker WP80 spectrometer at the Polytechnic of North London. The ^{1}H relaxation of the fully protonated species was studied as a function of temperature. The relaxation rates obtained at 301K and the results of variable temperature measurements on the protonated sample are shown in Table 4-8.

The total ^{1}H relaxation rate may be characterised by fitting the data to an equation analogous to equation 4 - 2. The resulting best fit parameters are:

TABLE 4.8 ^{1}H Relaxation rates in the dimethylthallium(III) cation in D_2O

a) variation with sample at 301K

Sample	R_1 (s^{-1})
Protonated	0.408
Mixed	0.436
Deuterated	0.0825

b) temperature dependence of ^{1}H R_1 of $(CH_3)_2Tl^+$ in D_2O

Temperature(K)	R_1 (s^{-1})
301	0.408
316	0.312
331	0.226
346	0.184
356	0.158

$$R_1(298K) = 0.436 \pm 0.008\ s^{-1}\ , \qquad \{4 - 55A\}$$

$$E_{ACT} = 15.5 \pm 0.6\ kJ\ mol^{-1}. \qquad \{4 - 55B\}$$

These parameters lead to the linear plot in Figure 4 - 7. Chemical shift anisotropy relaxation can be discounted due to the small shift anisotropies found for protons[41]. Similarly the temperature dependence of the relaxation implies an insignificant contribution from the spin rotation mechanism. The only likely remaining mechanisms are intramolecular and various intermolecular dipolar contributions. Table 4 - 8 shows that the ^1H relaxation rates for the protonated and mixed samples are equal within experimental error, thus dipolar relaxation between thallium species is insignificant. This leaves only the intramolecular ^1H - ^1H dipolar mechanism and the intermolecular dipolar interaction with solvent deuterons as significant contributors to ^1H relaxation; thus

$$R_1(^1H) = R_{1\ INTER} + R_{1\ INTRA}. \qquad \{4 - 56\}$$

If the molecular correlation time governing the intramolecular dipolar interaction is assumed to be the same in the species $(CH_3)_2Tl^+$ and $(CHD_2)CD_3Tl^+$, then taking into account the different gyromagnetic ratios and spin quantum numbers for ^1H and ^2D and also the 3/2 factor for like spins[69], the intramolecular relaxation rate for the residual proton will be a factor of 24 less than that in the fully protonated species.[14]

The intermolecular contribution however, to the ^1H rate in the above two species would be expected to be the same. Using the results of equation 4 - 56 and Table 4.8a, this may be expressed as

$$0.410 = R_{1\ INTER} + R_{1\ INTRA} \qquad \{4 - 57A\}$$

$$0.0825 = R_{1\ INTER} + R_{1\ INTRA}/24. \qquad \{4 - 57B\}$$

Solving this pair of equations gives the relaxation rates at 301 K as

$$R_{1\ INTRA} = 0.342 \qquad \{4 - 58A\}$$

$$R_{1\ INTER} = 0.0683 \qquad \{4 - 58B\}$$

where $R_{1\ INTRA}$ is the intramolecular contribution to the ^1H relaxation in the fully protonated cation. Thus the intramolecular contribution to the ^1H R_1 in the species $(CH_3)_2Tl^+$ and $(CHD_2)CD_3Tl^+$ are calculated to be 83% and 17% respectively at 301K.

The modulation of the intramolecular ^1H dipolar relaxation in the fully protonated cation, is due to motional modulation of the inter-proton vector of the CH_3 group. This vector is at an angle of 90^o to the symmetry axis of the cation.

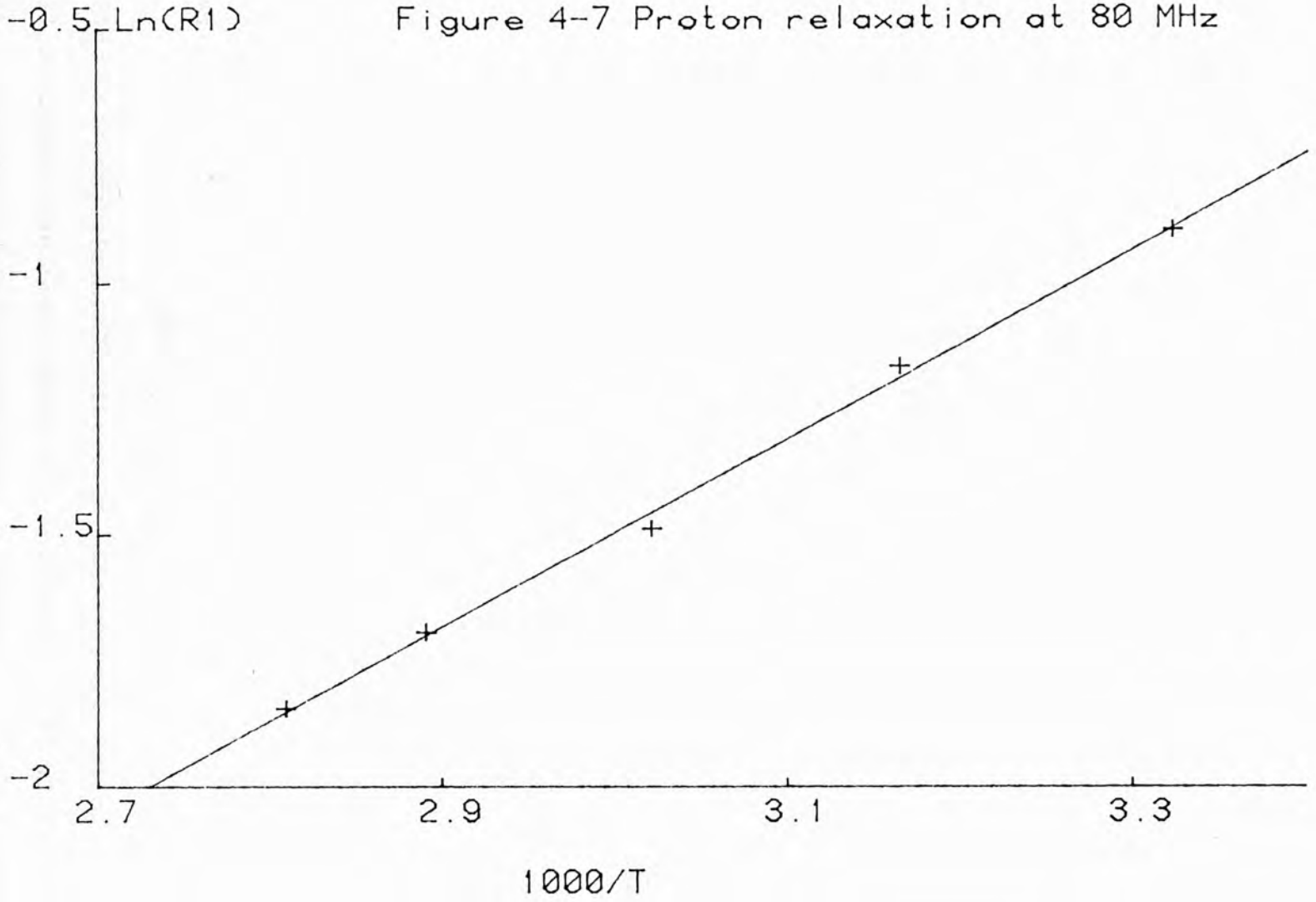

Figure 4-7 Proton relaxation at 80 MHz

In order to obtain the reorientational correlation time τ_{90} from the intramolecular dipolar relaxation rate, the formula of Powles[70] may be used. In SI units this becomes

$$R_{1\ INTRA} = 3\left(\frac{\mu_o}{4\pi}\right)^2 \frac{\gamma_H^4 \hbar^2}{r^6} \tau_{90}. \qquad \{4 - 59\}$$

This equation assumes simple additive interactions and neglects coupled relaxation discussed by Werbelow and Grant[71,72]. Using a value of 1.791×10^{-10} m for the interproton distance r (Appendix 1), this equation becomes,

$$R_{1\ INTRA} = 5.18 \times 10^{10}\ \tau_{90}. \qquad \{4 - 60\}$$

Thus the pertinent correlation time at 301K is

$$\tau_{90}(301K) = 6.60\ ps. \qquad \{4 - 61\}$$

This may be compared to a value of 36.3 ps for $\tau_\perp$ at the same temperature, calculated from equation 4 - 32 giving the ratio of the two correlation times at 301K,

$$\tau_\perp / \tau_{90} = 5.50. \qquad \{4 - 62\}$$

This ratio is however outside the range that is possible for reorientation of a symmetric top. Taking $\alpha = 90^o$ in equation 2 - 38 leads to

$$\tau_{90} = \tfrac{1}{4}\tau_{20} + \tfrac{3}{4}\tau_{22} \quad . \qquad \{4 - 63\}$$

Since $\tau_\perp$ is equal to τ_{20} then the ratio $\tau_\perp / \tau_{90}$ must lie within the range

$$0 < \tau_\perp / \tau_{90} < 4. \qquad \{4 - 64\}$$

Since the experimentally observed value of the ratio $\tau_\perp / \tau_{90}$ lies outside the range shown in equation 4 - 64, it follows that the simplifying assumptions necessary in the calculation

of τ_{90} and the use of instrument indicated temperatures have led to a large error in the value of τ_{90}. In spite of these difficulties the observed ratio of $\tau_{\perp}/\tau_{90}$ still indicates that τ_{22}/τ_{20} is small and that the motion about the parallel axis is fast compared to motion about the perpendicular axis.

It is possible to obtain information on motion about the symmetry axis if two mechanisms are studied which have relaxation vectors at different angles to the symmetry axis. This kind of information could also be obtained by studying the $^{13}C-^{1}H$ dipolar relaxation in $(CH_3)_2Tl^+$, or the ^{2}H quadrupolar relaxation in $(CD_3)_2Tl^+$ since both of these mechanisms possess a relaxation vector that is displaced from the symmetry axis by the tetrahedral angle.

4.1.8. ^{205}Tl Spin-spin relaxation studies.

The ^{205}Tl spin-lattice relaxation of the dimethylthallium(III) cation has been extensively discussed in previous sections, however relatively little comment has been made on the ^{205}Tl spin-spin relaxation time T_2. The mechanisms contributing to T_1 relaxation have been shown to be the spin rotation (SR) and chemical shift anisotropy (CSA) mechanisms; this will also be the case for T_2 relaxation. The presence of a significant CSA contribution to the ^{205}Tl T_2 is evident from the increased ^{205}Tl linewidth at high field. This is shown by the ^{205}Tl spectra at a) 231.6 MHz and b) 34.73 MHz in Figure 4 - 8. Both spectra have the same scale on Hz/cm.[73]

FIGURE 4-8.

Ambient temperature ^{205}Tl spectra of the dimethylthallium(III) cation in aqueous solution at
(a) 231.6 MHz
(b) 34.73 MHz.

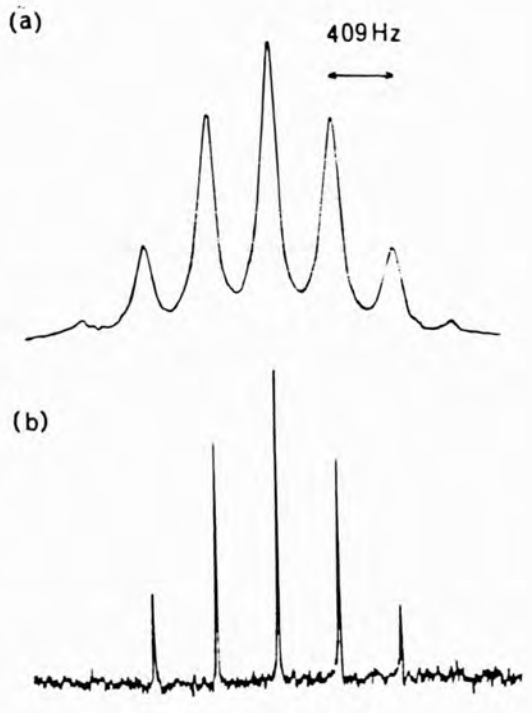

As discussed in Chapter Two the spin rotation mechanism is field independent but CSA relaxation is proportional to B_o^2, within extreme narrowing. Theory shows that the CSA spin-spin relaxation rate is related to the spin lattice relaxation rate as

$$R_{2\ CSA} = (7/6)\ R_{1\ CSA}. \qquad \{4 - 65\}$$

This relationship is well documented but to date no direct experimental verification appears to have been published. In order to attempt to provide such a verification, the ^{205}Tl R_2 of the dimethylthallium(III) cation was measured at high field where CSA is the dominant relaxation mechanism.

Spin-spin relaxation measurements based upon the CPMG pulse sequence[74] were attempted but were not successful. Difficulties arise in the use of this sequence for the measurement of relatively short T_2's such as those for ^{205}Tl in this system, since this requires the application of 180^o refocussing pulses with short inter-pulse delays thus leading to RF induced sample heating and shifting of the thallium resonance.

The Hahn spin echo sequence discussed in Chapter Three uses only a single 180^o refocussing pulse and by choosing a suitably long delay time the sample heating problem could be avoided. This method is more prone to errors due to spin diffusion than is the CPMG sequence[74] but for the measurement of short T_2's this may not be a limiting factor. Measurements of the ^{205}Tl T_2 of $(CH_3)_2Tl^+$ by the Hahn spin echo method have not yet been attempted.

The $T_{1\rho}$ experiment was considered but because the CSA mechanism is field dependent one expects, $T_{1\rho} = T_{1\ SR}$ ~ 0.8 s and hence the spin locking field has to be maintained for about 1 s. The WH-400 spectrometer does not allow for the reduction of B_1 under software control and the experiment would have disastrous effects on the probe. Changes in resonance frequency as a result of sample heating again present a problem.

$T_{1\rho}$ measurements by selective excitation (see Section 3.3.4) were attempted but these were foiled by insufficient effective field to maintain spin locking and by the requirement for rapid pulsing to ensure that there was a single excitation frequency within the thallium multiplet.

Due to these difficulties the ^{205}Tl R_2 in this system has been measured by the presaturation technique of Bain et al.[75] The methodology has been described in Chapter Three. The ^{205}Tl T_2 measurements were carried out at a single temperature of 306.4K, on a non degassed sample of 0.81M $(CH_3)_2TlNO_3$ in D_2O. The sample temperature was found from the ^{205}Tl resonance frequency, using ^{205}Tl and ^{1}H RF calibration spikes as described previously. The ^{205}Tl spin-spin relaxation rates are shown in Table 4 - 9.

Attenuation(dB)	Mo (mm)	T_2(ms)	$R_2(s^{-1})$	$(\gamma B_1)^2 T_1 T_2$
0	183.5	2.85	351	6.54
3	183.0	2.97	337	3.38
5	185.7	3.15	317	0.34
7	187.0	2.78	360	0.11

TABLE 4 - 9. ^{205}Tl R_2 experiments - best fit parameters.

In addition a measurement of the unweighted ^1H coupled linewidth at this temperature gave

$$\Delta\nu_{\frac{1}{2}} = 102.8 \text{ Hz} \; ; \quad \text{hence } R_2^* = 323 \text{ s}^{-1}$$

therefore it would appear that the measured ^{205}Tl R_2 is a function of the attenuation used, albeit not strongly dependent; and that this technique did not give an R_2 value that was significantly less than that found from a simple linewidth measurement.

In order to have a directly comparable ^{205}Tl R_1 this was measured at the same temperature, for the above sample, using both inversion recovery and presaturation recovery pulse sequences (0 dB attentuation). The spin lattice relaxation rates were found to be 254 s^{-1} and 255 s^{-1} respectively. Using the value with the lowest R_2 in Table 4 - 9 the ratio $(R_2/R_1)_{OBS}$ is found to be

$$(R_2/R_1)_{OBS} = 1.24 \qquad \{4 - 66\}$$

This compares with the theoretical ratio of 1.17 for the CSA mechanism within extreme narrowing. Thus within experimental error (taken as $\pm$ 10%) the observed ratio of relaxation rates agrees with the theoretically expected value.

Section 4.2. Dimethylthallium(III) cation in aqueous glycerol solution.

4.2.1. Rationale for study.

A study of the dimethylthallium(III) cation in aqueous solution has shown the dominance of the CSA mechanism at 231.6MHz and temperature dependent contributions from the SR and CSA mechanisms at 21.96 MHz and 34.73 MHz. A correlation time, $\tau_\perp$ of 39.1 ps at 298K was derived. This corresponds to $\omega_0\tau_\perp$ values of 5.39×10^{-3} and 5.69×10^{-2} at 21.96 MHz and 231.6 MHz respectively. Assuming that $\tau_\perp$ is approximately proportional to viscosity, then the choice of a more viscous solvent would shift the value of $\omega_0\tau_\perp$ towards the non-extreme narrowing region especially at high field.

This study of CSA relaxation was motivated by the dipolar[76] and quadrupolar[77] relaxation studies in concentrated aqueous solution and glycerol respectively carried out by Geiger and Hertz. In the first of these two papers a ^1H relaxation study was made in a six molal aqueous solution of ^7LiI and ^6LiI in D_2O, containing a small amount of H_2O. The relaxation studies were carried out at low temperatures and maxima observed for R_1 as a function of temperature. The relaxation maxima confirm that the molecular motion is outside the extreme narrowing region. The relaxation is predominantly dipolar and from the $^{127}I - {}^1H$, $^6Li - {}^1H$ and $^7Li - {}^1H$ contributions, proton-I^- and proton-Li^+ distances in the first coordination sphere are found. Geiger and Hertz have also studied the spin

relaxation of $^{7}Li^{+}$ and $^{133}Cs^{+}$ ions in glycerol and glycerol d^{8}[77], the dominant relaxation mechanism was the intermolecular quadrupolar interaction. In all cases a maximum for the relaxation rate is observed. This maximum occurs at the same temperature as for the proton relaxation rate in the same solution, and Geiger and Hertz concluded that the electrostatic model provides an appropriate description of the origin of the electric field gradient. In both papers the relaxation rate maximum does not occur exactly at $\omega_o\tau = 1$, because of the presence of multiple quantum terms in the spectral density function. This situation arises because the dipolar interaction is a two spin interaction, and in the quadrupolar case neither ^{7}Li or ^{133}Cs are spin ½ nuclei.

However for the CSA relaxation rate of a spin ½ nuclide the spectral density has the form discussed in Chapter Two, and the relaxation maximum will occur at $\omega_o\tau = 1$.

The use of high viscosity solutions to increase the reorientational correlation time and thus to increase R_1, has recently been demonstrated by Bammel and Evilia[78]; they used glycerol for water soluble molecules, and toluene saturated with polystyrene for organic soluble molecules. The objective was to allow acquisition of natural abundance ^{15}N and ^{29}Si spectra in reasonable times. No significant linewidth increases were found, showing the linewidth to be dominated by instrumental factors such as field inhomogeneity etc.

The study of thallium CSA relaxation outside extreme narrowing allows simultaneous determination of the shielding anisotropy and the reorientational correlation time. This is a new method for determination of the shielding anisotropy and is particularly valuable as it pertains to the solution state.

4.2.2. ^{205}Tl spin lattice relaxation measurements.

The ^{205}Tl spin lattice relaxation rate of the dimethylthallium(III) cation has been measured as a function of temperature in an aqueous glycerol solution, at ^{205}Tl frequencies of 21.96 MHz and 231.6 MHz. The solvent used was a glycerol/H_2O mixture with 79% by mass of glycerol. Aqueous glycerol mixtures are a convenient solvent to use since a large range of viscosities is possible by varying the relative amounts of glycerol and water[79]. This solution was used to prepare an approximately 0.07 molal solution of dimethylthallium(III) nitrate. Samples were used non degassed, since the contribution to R_1 from molecular oxygen is only about 5% at low field in aqueous solution; and this is expected to be considerably less in aqueous glycerol solution.

Sample temperatures at high field were found from the ^{205}Tl shift of a solution of dimethylthallium(III) nitrate in D_2O contained in a concentric tube, this also provided the ^{2}H lock signal. As described in Chapter Three RF spikes were used to calibrate the ^{205}Tl and ^{1}H frequencies used in finding the sample temperature. At low field the requirement of a ^{31}P lock to 85% H_3PO_4 contained in another

concentric tube, led to relatively low signal sensitivity using the above temperature measurement technique. Thus this method was not applied directly, the ^{205}Tl shift in aqueous solution was used to calibrate the shift in aqueous glycerol which was subsequently used as the observed thermometric property.

At ambient temperatures the ^{205}Tl resonance in aqueous glycerol is shifted 28.9 ppm to low frequency of that in D_2O, the mean temperature coefficient of the resonance was found to be +0.52 ppm K^{-1}. All spin lattice relaxation rates were measured by the inversion recovery pulse sequence, the temperature and field dependent measurements are summarised in Table 4 - 10. It is observed that at both fields the ^{205}Tl relaxation rate is enhanced in aqueous glycerol solution relative to that in D_2O. At high field R_1 initially increases with increasing temperature but reaches a maximum and decreases thereafter. However, at low field R_1 decreases monotonically with increasing temperature. At any given temperature R_1 increases dramatically with increasing field strength. These observations will be rationalised and discussed in the next Section.

TABLE 4 - 10

^{205}Tl R_1 of $(CH_3)_2Tl^+$ in an aqueous glycerol solution.

a) Temperature dependence at 231.6 MHz.

Temperature(K)	$R_1(s^{-1})$
294.4	2632
299.4	2975
303.1	3046
303.4	2967
312.3	2734
320.7	2145
330.4	1590
340.2	1155
349.4	893

b) Temperature dependence at 21.96 MHz.

Temperature(K)	R_1 (s^{-1})
291.5	118.2
305.5	51.3
316.5	25.9
318.4	27.4
330.4	18.7

4.2.3. Data analysis, CSA relaxation outside the extreme narrowing region.

The ^{205}Tl relaxation rate of the dimethylthallium(III) cation in aqueous glycerol solution has been found to increase strongly with increasing field strength. This is as observed for the cation in aqueous solution and implies a significant contribution to the ^{205}Tl relaxation from the CSA mechanism. The data will be rationalised assuming that this is the only effective mechanism at both field strengths studied. This assumption will later be justified.

The presence of a maximum for R_1 as a function of temperature at high field implies that the extreme narrowing criterion $\omega_o\tau_\perp << 1$ is no longer valid at this field. This may be understood by recalling the CSA relaxation expression given by Spiess,[8] for an axially symmetric shielding tensor the shielding asymmetry equals zero and equation 2 - 65A becomes

$$R_{1\ CSA} = \frac{1}{15}\omega_o^2\ \Delta\sigma^2\ \frac{2\tau_\perp}{1 + \omega_o^2\tau_\perp^2} \quad . \quad \{4 - 67\}$$

In the limit of high temperatures and/or low field $\omega_o\tau_\perp << 1$ hence $R_{1\ CSA}$ is proportional to $\tau_\perp$ and decreases with increasing temperature. At low temperatures at high field $R_{1\ CSA}$ is inversely proportional to $\tau_\perp$ and the opposite dependence is observed. The maximum for $R_{1\ CSA}$ occurs at $\omega_o\tau_\perp = 1$.

In order to analyse the high field data a reference temperature of 298K, and an exponential temperature

dependence of the reorientational correlation time $\tau_\perp$ are assumed.

$$\tau_\perp (T) = \tau_\perp (298K) \exp\left(\frac{E_{CSA}}{R}\left(\frac{1}{T} - \frac{1}{298}\right)\right). \quad \{ 4 - 68 \}$$

Using a non linear least squares procedure with $\Delta\sigma$, $\tau_\perp$ (298K) and E_{CSA} as variable parameters, the temperature dependent high field relaxation data may be fitted directly to equation 4 - 67. The best fit parameters thus obtained are,

$$|\Delta\sigma| = 5550 \pm 32 \text{ ppm} \qquad \{ 4 - 69A \}$$

$$\tau_\perp (298K) = 898 \pm 39 \text{ ps} \qquad \{ 4 - 69B \}$$

$$E_{CSA} = 37.7 \pm 1.4 \text{ kJ/mol} \quad . \qquad \{ 4 - 69C \}$$

The best fit curve and the data points are plotted in the usual way in Figure 4 - 9.

Such a fit procedure is not possible at low field because $\omega_0\tau_\perp << 1$ and all that can be obtained is the product of $\Delta\sigma^2$ and $\tau_\perp$ at a given temperature. Using the above parameters the values of $\omega_0\tau_\perp$ at 298K are 1.31 and 0.123 at high and low field respectively.

The first of these values confirms that the motional narrowing criterion is violated at high field as already shown by the presence of a relaxation rate maximum. The latter value implies that the motional narrowing criterion is approximately valid at low field. This is confirmed by the linearity of the usual logarithmic plot of the low field relaxation data shown in Figure 4 - 10. This diagram shows the experimental data points and the CSA relaxation rate at this field calculated from the parameters in equation 4 - 69. The closeness of the calculated and

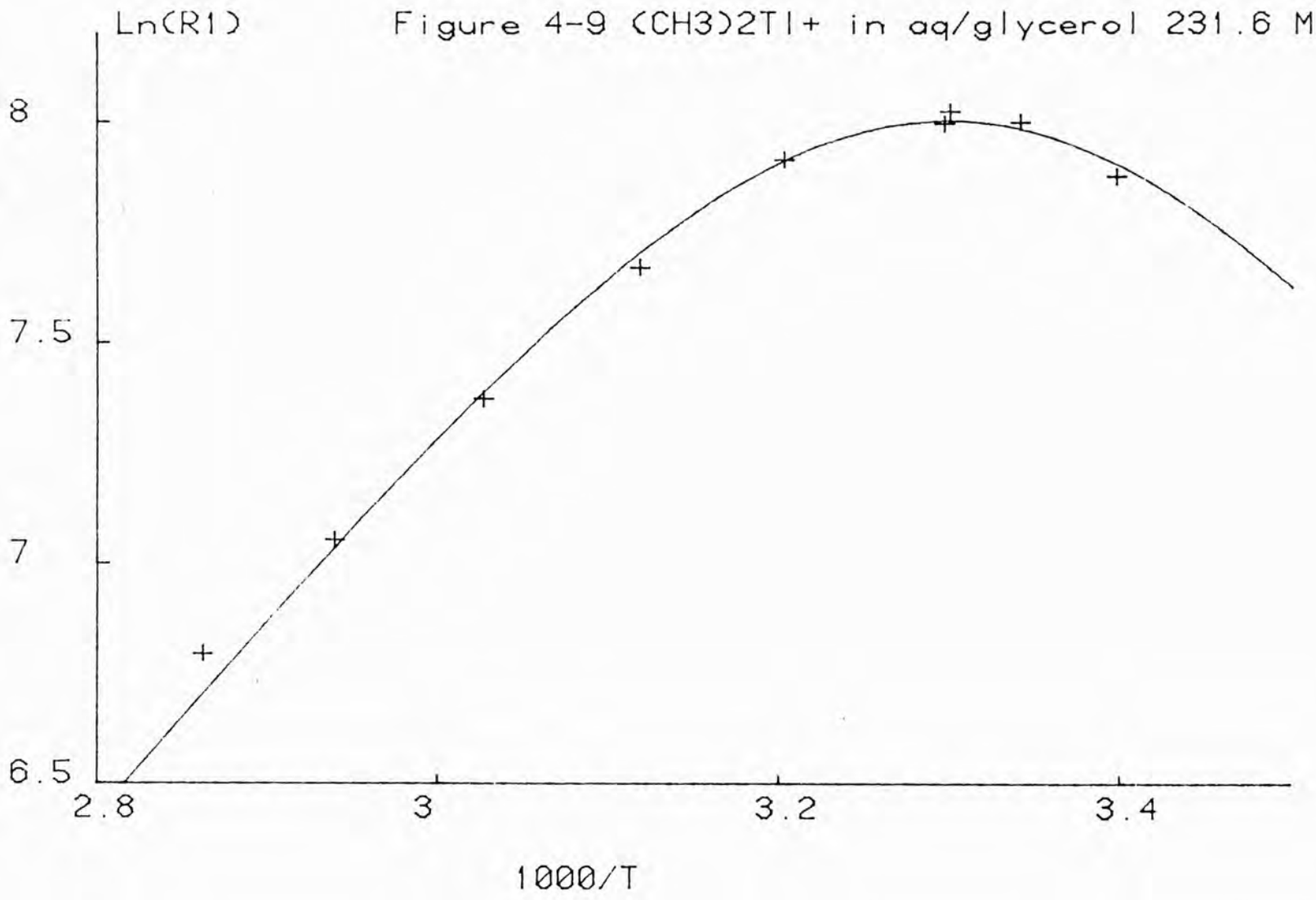
Ln(R1)
Figure 4-9 (CH3)2Tl+ in aq/glycerol 231.6 MHz
8
7.5
7
6.5
2.8
3
3.2
3.4
1000/T

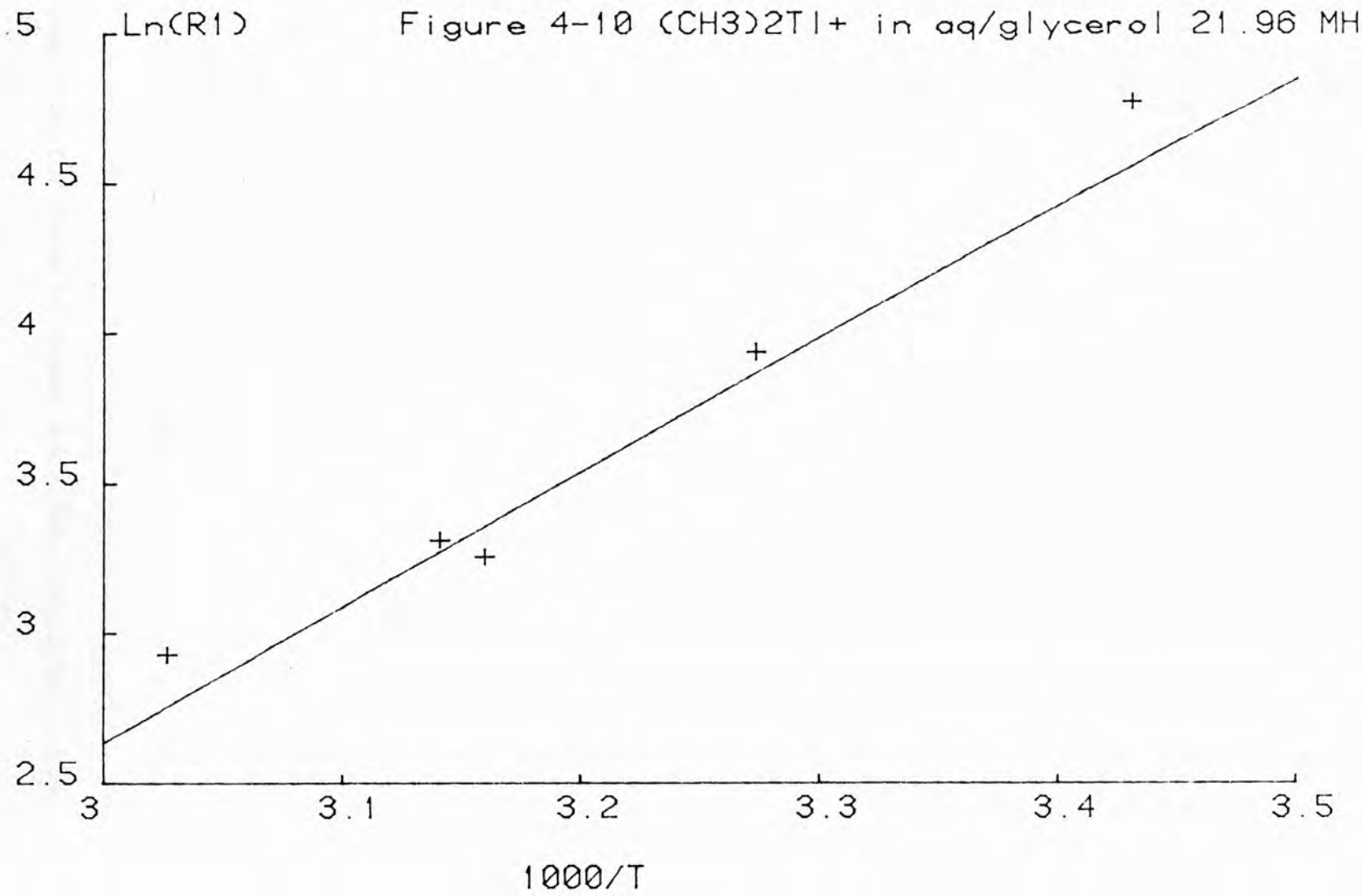
Ln(R1)
Figure 4-10 (CH3)2Tl+ in aq/glycerol 21.96 MHz
5
4.5
4
3.5
3
2.5
3
3.1
3.2
3.3
3.4
3.5
1000/T

observed relaxation rates at low field shows that the CSA mechanism is dominant at both field stengths studied.

This non linear least squares method of deriving an anisotropy is only one of a number of possible methods utilising non extreme narrowing CSA relaxation. Since the relaxation maximum occurs at $\omega_0\tau_\perp = 1$ the reorientational correlation time at this temperature is known, and the anisotropy may be derived from the relaxation rate. This method however uses data at only one temperature and should be considered as less accurate. Alternatively, if the CSA relaxation at the same temperature at two fields is known, and the molecular motion at one of these is near or beyond the spectral density maximum, then from equation 4 - 67 the ratio of the relaxation rates implies τ_2 and hence $\Delta\sigma$.

The application of non extreme narrowing CSA relaxation to the measurement of anisotropies may be possible for many nuclei. Thallium is perhaps the most favourable case, like other heavy metal nuclei it possesses large anisotropies, but of these it has the largest gyromagnetic ratio. The ^{207}Pb and ^{199}Hg nuclei have gyromagnetic ratios that are lower than that of ^{205}Tl by factors of 2.76 and 3.23 respectively. Thus to observe a relaxation maximum the reorientational correlation time will need to increase by these same factors and hence more viscous solutions will be required. Since only 79 % aqueous glycerol solutions have been used here, higher viscosities are possible for this or other solutions which may allow

anisotropy measurements for the above nuclei.

The CSA relaxation mechanism has been observed in the non extreme narrowing region by Hull and Sykes[29], they carried out ^{19}F studies for a trifluoromethyl group in amino acid residues in the protein alkaline phosphatase. This case is more complicated than the ^{205}Tl study presented here. Firstly dipolar relaxation is a significant contributor to ^{19}F relaxation in this case, and secondly the principal axes of the diffusion and shielding tensors are non coincident. Hull and Sykes derived the expression for CSA relaxation under these conditions, and by collecting solid state data from the literature on the orientation and magnitudes of the principal elements of ^{19}F shielding tensors were able to characterise ^{19}F CSA relaxation. Combining this with dipolar relaxation and NOE data they were able to derive the overall tumbling correlation time for alkaline phosphatase and set limits on the internal rotational motion of the tyrosine residues.

A spin lattice relaxation and lineshape study of the ^{31}P spectrum of the β phase of powdered white phosphorøus has been made by Spiess[8] at low temperatures (25K to 126K). The phosphorøus P_4 molecules have a tetrahedral structure and at low temperatures the characteristic powder spectrum for an axially symmetric shielding tensor was found with a ^{31}P anisotropy of 405 ppm. The ^{31}P relaxation is dominated by the CSA mechanism, the anisotropic shielding interaction being modulated by stochastic jumps to other P_4 tetrahedron orientations.

The motion is well outside extreme narrowing and $\omega_o^2\tau_2^2 >> 1$. Thus one finds

$$R_{1\ CSA} = \frac{2}{15}(\sigma_{\parallel} - \sigma_{\perp})^2 \tau_2^{-1}. \qquad \{4 - 70\}$$

By use of this equation Spiess et al. were able to derive jump frequencies τ_2^{-1} and to calculate spectra that agreed well with those found by experiment.

4.2.4. Reorientational motions.

The analysis of the high field ^{205}Tl relaxation data performed in the previous section has shown that the molecular motion is outside the extreme narrowing limit and that the frequency dependence of the relaxation is of the form shown in equation 4 - 67. The term

$$J(\omega) = \frac{2\tau_{\perp}}{1 + \omega^2\tau_{\perp}^2}, \qquad \{4 - 71\}$$

is the spectral density function and describes the frequency dependence of the motional modulation of the anisotropic shielding interaction in this system. The theory discussed in Chapter Two shows that the reorientational correlation function is the Fourier transform partner of the spectral density function. Since the spectral density function given above is Lorentzian in form then the reorientational correlation function must be exponential,

$$G(t) = \frac{\langle Y_{20}(0)Y_{20}(t)\rangle}{\langle Y_{20}(0)^2\rangle} = \exp\{-|t|/\tau_{20}\}, \qquad \{4 - 72\}$$

where the correlation time $\tau_{20} = \tau_2 = \tau_{\perp}$. $\tau_{\perp}$ may be calculated at any temperature by use of equation 4 - 68. Values at three different temperatures are shown in Table 4 - 11 together with values for the D_2O solution discussed previously.

	Aq.glycerol		D_2O	
Temperature(^oC)	$\tau_\perp$ (ps)	$\tau_\perp^*$	$\tau_\perp$ (ps)	$\tau_\perp^*$
20	1155	1549	44.6	59.8
50	275	387	21.1	29.7
80	83.4	123	11.4	16.7

TABLE 4 - 11. Reorientational motion of $(CH_3)_2Tl^+$ in aqueous glycerol and D_2O.

No information on the form of the correlation function is available in aqueous solution since the extreme narrowing criterion is met even at high field.

An exponential reorientational correlation function is the form predicted at the large angle jump limit of the Kivelson solid-like reorientation model[57], and provides further evidence of the applicability of this model to associated liquids. No evidence has been found for a spin rotation contribution to the ^{205}Tl spin lattice relaxation in this system. If the product of the reduced correlation times were approximately constant in different media, then increased viscosity would cause a decrease in $\tau_{J_\perp}$ and suppress spin rotation relaxation as well as enhance chemical shift anisotropy relaxation.

The large angle jump diffusion mechanism has been shown by Wolfe and Jonas[80] to be operative for reorientation of the glycerol molecule in neat glycerol-d^4 $(D_2COH)_2CHOH$ and glycerol-d^3 $C_3H_5(OD)_3$. A study was made of the temperature and pressure dependence of the deuteron spin-lattice

relaxation rate. A Cole-Davidson distribution of correlation times was required to describe intermolecular and intramolecular reorientational motions. The data suggest that the hydrogen bond network in this fluid is relatively insensitive to density but is strongly temperature dependent.

The discussions of dimethylthallium(III) cation reorientation in this Chapter suggest that the reorientation is solvent controlled and that the cation is a reporter of, or takes on, the motion of the surrounding medium. It has not been necessary to invoke a model involving a distribution of correlation times to explain these results. Indeed in Section 4.2.6 where R_2 values are extracted, further confirmation of the adequacy of a single correlation time model is provided by the agreement between theoretical and experimental R_2 behaviour. The adequacy of the simple model for the dimethylthallium(III) cation is not unexpected since it is motionally much less complicated than glycerol itself.

4.2.5. ^{205}Tl shielding tensor in dimethylthallium(III) compounds.

The preceding discussion has shown how observation of CSA relaxation outside the extreme narrowing region has been used to deduce the ^{205}Tl shielding anisotropy of the dimethylthallium(III) cation in an aqueous glycerol solution. Since $R_{1\ CSA}$ is proportional to the square of the shielding anisotropy $\Delta\sigma$, then only the magnitude of $\Delta\sigma$ may be deduced by relaxation studies. In Section 4.2.3

it has been shown that

$$|\Delta\sigma| = 5550 \pm 32 \text{ ppm} , \qquad \{4 - 73\}$$

whilst the discussion in the first half of this Chapter has shown that the paramagnetic shielding tensor elements are

$$\sigma'^{p}_{\perp} = -5550 \text{ ppm} , \qquad \{4 - 74A\}$$

$$\sigma'^{p}_{\parallel} = 0 \text{ ppm} . \qquad \{4 - 74B\}$$

Thus the sign of $\Delta\sigma$ is positive. It is now necessary to consider measurements of the same properties performed by other authors.

In a number of recent papers Hinton et al.[81-83] have measured the ^{205}Tl shielding anisotropy of some Tl(I) and Tl(III) compounds by solid state ^{205}Tl NMR. Using both single crystal rotation studies and powder pattern methods, axially symmetric shielding tensors with $\Delta\sigma$ values of 88 ppm and 117 ppm were reported for the Tl(I) ion in $TlNO_3$ and $TlClO_4$ respectively. More recently $\Delta\sigma$ values of 1975 ppm and 485 ppm have been found by the powder pattern method for $(CH_3)_2TlNO_3$ and $(CH_3)_2TlBr$ respectively[83]. These values vary considerably from the anisotropy reported in Section 4.2.3

Firstly it should be noted that the shielding components reported by Hinton are in fact chemical shifts referenced to the aqueous Tl(I) ion at infinite dilution and hence the positive signs for the dimethylthallium(III) cation are consistent with the resonance being to high frequency of the Tl(I) ion. Hinton reports $\sigma_{\parallel}$ to be to high frequency of $\sigma_{\perp}$. However the displayed powder

pattern spectrum of $(CH_3)_2TlNO_3$ (which has no scale but presumably follows the normal convention of high frequency to the left), shows $\sigma_{\parallel}$ to be to low frequency of $\sigma_{\perp}$. It is important to note that the isotropic shift values reported by Hinton of + 5590 ppm for $(CH_3)_2TlBr$ and + 5072 ppm for $(CH_3)_2TlNO_3$ differ greatly from the solution state values, where δ ranges from + 3305 ppm for $(CH_3)_2TlNO_3$/HMPA to + 3689 ppm for $(CH_3)_2TlI$/pyridine[84]. Previously observed solid/melt/solution state isotropic shift differences were typically less than 500 ppm.[84]

In order to properly characterise solid state ^{205}Tl spectra of thallium compounds with large shielding anisotropies large spectral sweep widths are required. No sweep widths were reported in Hinton's paper but the ^{205}Tl spectrum of $(CH_3)_2TlNO_3$ shown, apparently covered a range of approximately 2500 ppm. If the shielding anisotropy of 5550 ppm reported here is taken as correct, then a sweep width of 10,000 ppm would be appropriate for correct observation of the ^{205}Tl powder pattern. If an insufficient sweep width is used spectral distortions will occur due to aliasing of components of the lineshape outside the observation range. Further requirements are short pulse lengths and short spectrometer dead time. In the light of these difficulties it is easier to detect the more intense $\sigma_{\perp}$ component than the $\sigma_{\parallel}$ component. Assuming the $\sigma_{\perp}$ feature has been correctly identified and taking its sign as negative (i.e. considering shielding elements rather than chemical shifts) the data may be reworked using the following relationship:

$$\sigma_{ISO} = \sigma_{\perp} + \frac{1}{3}\Delta\sigma \qquad \{4 - 75\}$$

Using a $\Delta\sigma$ value of + 5550 ppm the following isotropic shielding values may be calculated

$$\sigma_{ISO}\{(CH_3)_2TlNO_3\} = - 2564 \text{ ppm}, \quad \{4 - 76A\}$$

$$\sigma_{ISO}\{(CH_3)_2TlBr\} = - 3580 \text{ ppm}. \quad \{4 - 76B\}$$

Hence the calculated isotropic shifts of $(CH_3)_2TlNO_3$ and $(CH_3)_2TlBr$ relative to aqueous Tl(I) ion are +2564 ppm and + 3580 ppm respectively.

In the above discussion no account has been taken of reorientational motion in the solid state which would reduce the apparent anisotropy but not alter σ_{ISO}.

The ^{205}Tl shielding anisotropy of $(CH_3)_2Tl^+$ oriented in a lyotropic liquid crystalline phase has been previously measured[31] and found to be 5300 ppm. The agreement between this value and the value derived by relaxation studies is remarkable. Further evidence for the correctness of the value of $\Delta\sigma$ reported herein, is the agreement found between the Hafner and Nachtrieb shift scale[45] and that deduced in Section 4.1.5.

Section 4.2.6. ^{205}Tl Linewidth Studies.

The ^{205}Tl linewidth of the dimethylthallium(III) cation in aqueous glycerol is much greater than that in aqueous solution as is evident from the ^{205}Tl spectrum at 297K and 231.6MHz shown in Figure. 4 -11. The resolved multiplet arises from the aqueous temperature reference solution. The aqueous glycerol spectrum shows broadening sufficient to remove the multiplet structure

arising from the $^{2}J(^{205}Tl - ^{1}H)$ coupling of 403 Hz.

During the course of the variable temperature spin lattice relaxation measurements the observed linewidth decreased strongly with increasing temperature with some evidence of multiplet structure emerging at the highest temperature. A ^{205}Tl linewidth study was made by transforming each of the FIDs taken at long time in the relaxation experiments with no exponental weighting. The linewidth at half height of the multiplet envelope was measured from an expanded plot. The ^{205}Tl R_2 was estimated from this linewidth using a simple numerical spectrum simulation program written in BASIC language on a BBC Model B microcomputer. This program assumes that the ^{205}Tl spectrum is a septet with a binomial intensity distribution using a value of ^{2}J $(^{205}Tl - ^{1}H)$ equal to 403 Hz. A given value of R_2 leads to a coupled multiplet linewidth. The program is then re-run until the computed linewidth is equal to that observed as above. The results of this procedure are shown in Table 4 - 12, along with experimental spin-lattice relaxation rates R_1 and thus the experimentally observed ratio of R_2/R_1.

In order to account for the observed linewidth behaviour the CSA relaxation expressions for an axially symmetric shielding tensor should be recalled, these have been given by Spiess[8] as

$$R_{1\ CSA} = \frac{1}{15}\ \omega_o^{2}\ \Delta\sigma^{2}\left[\frac{2\tau_{\perp}}{1 + \omega_o^{2}\tau_{\perp}^{2}}\right] \qquad \{4 - 77A\}$$

$$R_{2\ CSA} = \frac{1}{15}\ \omega_o^{2}\ \Delta\sigma^{2}\left[\frac{4\tau_{\perp}}{3} + \frac{\tau_{\perp}}{1 + \omega_o^{2}\tau_{\perp}}\right] \qquad \{4 - 77B\}$$

FIGURE 4-11. ^{205}Tl spectra of $(CH_3)_2Tl^+$ at 231.6 MHz in
(a) D_2O
(b) aqueous glycerol solution
512 scans, 50 Hz linebroadening, temperature 297K.

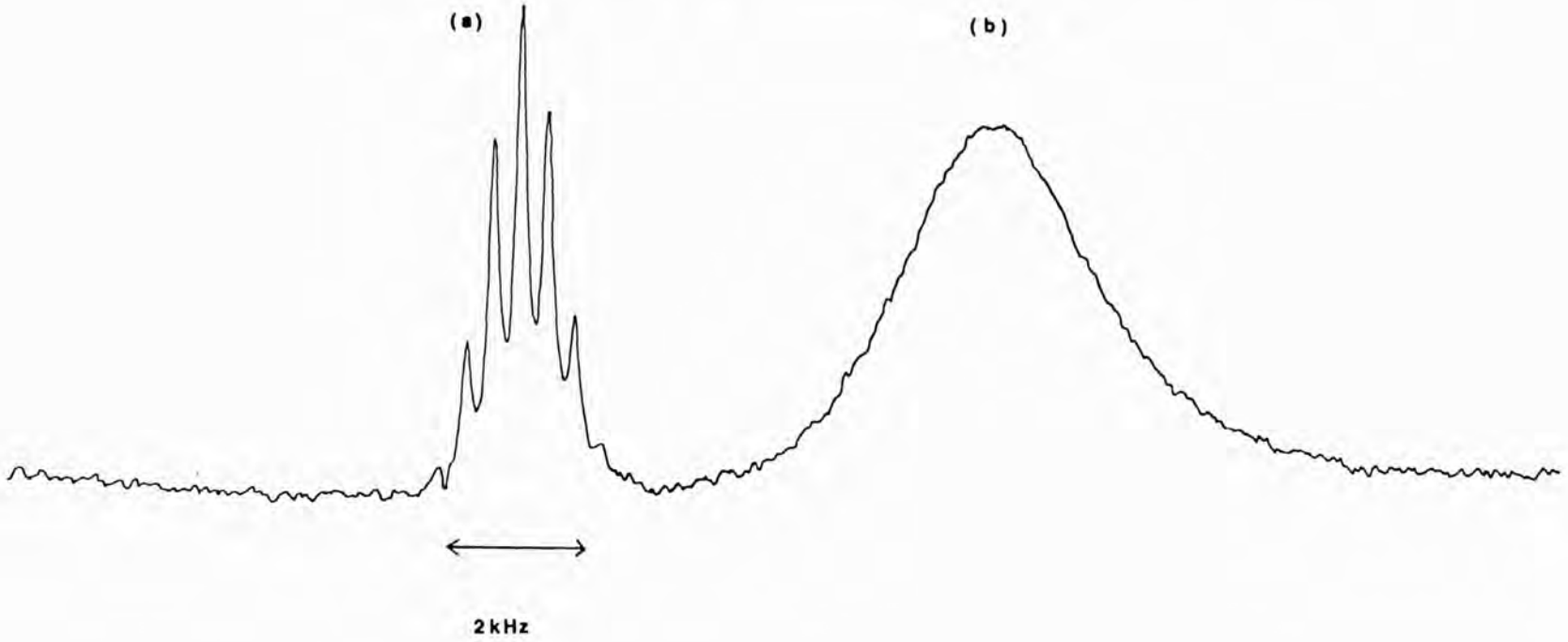

TABLE 4.12 Relaxation rates and linewidths of $(CH_3)_2Tl^+$ in aqueous glycerol. All rates in sec^{-1}.

T(K)	$\Delta\nu_{\frac{1}{2}}$(Hz)	R_2^{EXPT}	R_1^{EXPT}	$(R_2/R_1)^{EXPT}$	R_1^{CALC}	R_2^{CALC}	$(R_2/R_1)^{CALC}$	$\omega_o\tau_\perp$
294.4	3258	8816	2632	3.349	2701	7607	2.817	1.573
299.4	2662	6617	2975	2.224	2926	6301	2.153	1.216
303.1	2382	5525	3046	1.813	2983	5513	1.848	1.011
303.4	2320	5276	2967	1.778	2983	5454	1.828	0.996
312.3	2014	3995	2734	1.461	2727	3952	1.449	0.651
320.7	1786	2973	2145	1.386	2216	2878	1.299	0.445
330.4	1576	2044	1590	1.285	1614	1975	1.224	0.294
340.2	1339	1486	1155	1.287	1136	1355	1.193	0.198
349.4	1164	1185	893	1.327	815	962	1.180	0.139

These expressions show that in the limit $\omega_o\tau_\perp << 1$ R_2/R_1 tends to 7/6, but that this ratio increases dramatically on the slow side of the R_1 maximum when $\omega_o\tau_\perp \geq 1$. Using the above expressions with the best fit parameters in equation 4 - 69 the last four columns of Table 4.12 are obtained. A graphical representation of the data in this Table is given in Figure 4.12, which shows the experimental ratio of R_2/R_1 plotted against $\omega_o\tau_\perp$. The theoretical curve in this diagram is that predicted by the above equations and the value of R_2/R_1 equals the ratio of the spectral density functions.

The vertical bars represent $\pm$ 10% error in the ratio R_2/R_1. Considering the simplicity of the technique used to derive the experimental R_2 values, the agreement is perhaps remarkable. However it is noticeable that nearly all the $(R_2/R_1)^{EXPT}$ values are larger than the calculated values. This may be due to linewidth contributions from mechanisms other that CSA or from temperature inhomogeneity. Figure 4.13 shows the effect of assuming a non-CSA linewidth of 40 Hz, and hence a contribution to the observed R_2 of $40\pi\ s^{-1}$. Nearly all the points then agree with equations 4 - 77 within experimental error . The value of 40 Hz corresponds to a temperature inhomogeneity of approximately 0.4K which is not unreasonable. Possible contributions from intermolecular dipole-dipole relaxation were discounted since no NOE effect was found.

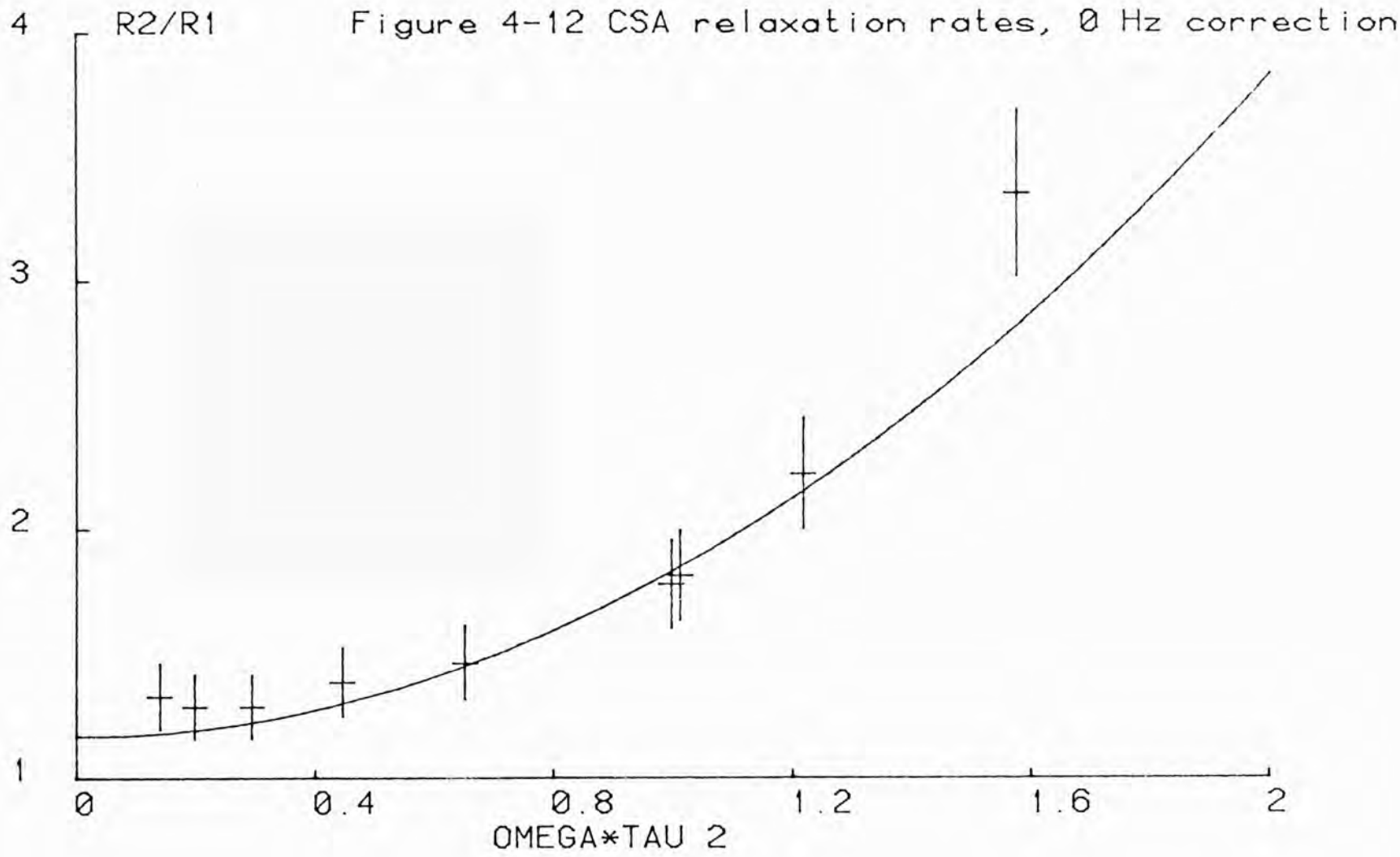

Figure 4-12 CSA relaxation rates, 0 Hz correction

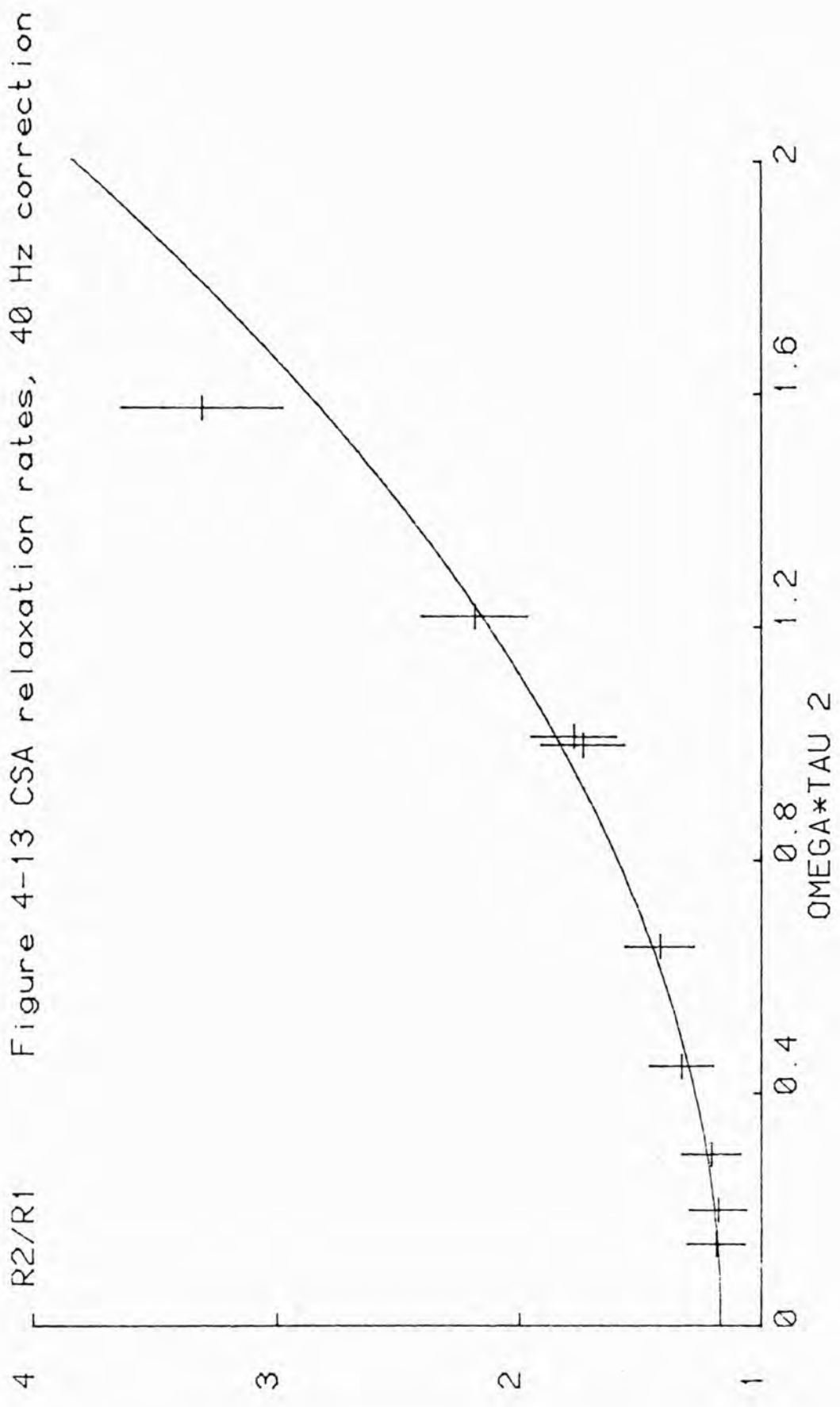

Figure 4-13 CSA relaxation rates, 40 Hz correction

REFERENCES CHAPTER FOUR

1. G.D. Shier and R.S.Drago, J.Organometal.Chem., 5, 330 (1966).
2. P.L.Goggin and L.A.Woodward, Trans.Faraday Soc., 56, 1591 (1960).
3. G.B.Deacon and J.H.S.Green, Spectrochim. Acta, A24, 885 (1960).
4. P.J.Burke, R.W.Matthews, I.D.Cresshull and D.G.Gillies, J.C.S. Dalton, 132 (1981).
5. G.B.Deacon, J.H.S.Green and R.S.Nyholm, J.Chem.Soc., 3411 (1965).
6. S.O.Chan and L.W.Reeves, J.Amer.Chem.Soc., 96, 404 (1974).
7. F.Brady, Ph.D.Thesis, Polytechnic of North London (1980).
8. H.W.Spiess, NMR-Basic Principles and Progress, 15, 55 (1978), Springer Verlag.
9. H.M.McConnell and C.H.Holm, J.Chem.Phys., 25, 1289 (1956).
10. H.W.Spiess, D. Schweitzer, U.Haeberlen, and K.H.Hausser, J.Magn.Reson, 5, 101 (1971).
11. G.C.Levy, J.D.Cargioli and F.A.L.Anet, J.Amer.Chem. Soc. 95, 1527 (1973).
12. F.W.Wehrli, J.Magn.Reson. 32, 451 (1978).
13. M.A.Sens, N.K.Wilson, P.D.Ellis and J.D.Odom, J.Magn.Reson. 19, 323 (1975).
14. C.R.Lassigne and E.J.Wells, Can.J.Chem., 55, 1303, (1977).
15. J.D.Kennedy and W.McFarlane, J.C.S. Faraday II, 1653 (1976).

16. J.Okisaari and P. Diehl , Org.Magn.Reson., 13, 359 (1980).

17. D.G.Gillies, L.P.Blaauw, G.R.Heys, R.Huis and A.D.H. Clague, J.Magn.Reson. 42, 420 (1981).

18. R.E.Wasylishen, R.E.Lekinski and C.Roger, Can.J.Chem., 60, 2113 (1982).

19. R.M.Hawk and R.R.Sharp, J.Chem.Phys., 60, 1522 (1974).

20. G.R.Hays, D.G.Gillies, L.P.Blaauw and A.D.H.Clague, J.Magn.Reson. 45, 102 (1981).

21. J.Y.Lallemand, J.Soulie and J.C.Chottard, J.C.S., Chem.Comm., 436 (1981).

22. I.Ismail, S.Kerrison and P.J.Sadler, Polyhedron, 1, 57 (1982).

23. D.M.Doddrell, P.F.Barron, D.E.Clegg and C.Bowie, J.C.S. Chem.Comm., 575 (1982).

24. J.F.Hinton and K.H.Ladner, J.Magn.Reson., 32, 303 (1978).

25. R.W.Briggs and J.F.Hinton, J.Magn.Reson. 32, 363 (1979).

26. R.W.Briggs and J.F.Hinton, J.Magn.Reson., 32, 155 (1978).

27. R.W.Briggs and J.F.Hinton, J.Magn.Reson., 44, 217 (1981).

28. R.W.Briggs, F.A.Etzkorn and J.F.Hinton, J.Magn.Reson., 37, 523 (1975).

29. W.E.Hull and B.D.Sykes, J.Mol.Biol., 98,121 (1975).

30. S.C.F. au Yeung, R.J.Buist and D.R.Eaton, J.Magn.Reson., 55, 24 (1983).

31. D.G.Gillies, private communication.

32. N.F.Ramsey, Molecular Beams, Oxford University Press, (1956).

33. C.H.Townes and A.L.Schawlow, Microwave Spectroscopy, McGraw Hill (1955).

34. N.F.Ramsey, Phys.Rev., 78, 699 (1950).

35. W.H.Flygare, J.Chem.Phys., 41, 793 (1974).

36. W.H.Flygare, Chem.Rev., 74, 653 (1974).

37. C.Deverell, Mol.Phys., 18, 319 (1970).

38. C.Deverell, Mol.Phys., 17, 551 (1969).

39. S.K.Garg, J.A.Ripmeester and D.W.Davidson, J.Magn.Reson., 36, 325 (1979)

40. S.K.Garg, J.A.Ripmeester and D.W.Davidson, J.Chem.Phys., 72, 567 (1980).

41. B.R.Appleman and B.P.Dailey, Adv.Magn.Reson.,7, 231 (1974)

42. K.T.Gillen, J.Chem.Phys., 56, 1573 (1972).

43. R.R.Sharp, J.Chem.Phys., 57, 5321 (1972).

44. R.M.Hawk and R.R.Sharp, J.Chem.Phys., 60, 1009 (1974).

45. S.Hafner and N.H.Nachtrieb, J.Chem.Phys., 40, 2891 (1964).

46. W.G.Schneider and A.D.Buckingham, Disc.Faraday Soc., 34, 147 (1962).

47. V.H.Köppell, J.Dallorso, G.Hoffman and B.Walther, Z.Anorg.Allg.Chem. 427, 24 (1976).

48. K.D.Becker and U.Berlage, J.Magn.Reson., 54,272 (1983).

49. G.Malli and C.Froese, Int.J.Quant.Chem., 15, 95 (1967).

50. W.T.Huntress Jr., Adv.Magn.Reson., 4, 1 (1970).

51. D.J.Wilbur, T.Defries and J.Jonas, J.Chem.Phys., 65, 1783 (1976).

52. C.M.Hu and R.Zwanzig, J.Chem.Phys., 60, 4354 (1974).

53. R.J.Boeré and R.G.Kidd, Ann.Rep.NMR.Spectry., 13,319 (1983).

54. A.Bondi, J.Chem.Phys., 68, 441 (1964).

55. R.E.D.McLung, Adv.Mol.Relaxation and Interaction Processes, 10, 83 (1977).

56. R.E.D.McLung, J.Chem.Phys., 57, 5478 (1972).

57. D.Kivelson, Mol.Phys., 28, 321 (1974).

58. E.N.Ivanov, Sov.Phys.JETP., 18, 1041 (1964).

59. D.E.O'Reilly, J.Chem.Phys., 63, 3177 (1975).

60. D.E.O'Reilly, J.Phys.Chem., 78, 1674 (1974).

61. D.E.O'Reilly, J.Chem.Phys., 60, 1607 (1974).

62. D.E.O'Reilly, J.Chem.Phys., 57, 885 (1972).

63. J.C.Hindman, J.Zielen, A.Svirmickas and M.Wood, J.Chem.Phys., 54, 621 (1971).

64. J.C.Hindman, J.Chem.Phys., 60 , 4488 (1974).

65. G.I.Szasz and K.Heinzinger, J.Chem.Phys., 79, 3467 (1983).

66. F.H.Stillinger and A.Rahman, J.Chem.Phys., 57, 1281 (1972).

67. P.Bopp, W.Dietz and K.Heinzinger, Z.Naturforsch, 34A, 1424 (1979).

68. G.S.Kell, J.Chem.Eng.Data, 12, 66 (1967).

69. J.H.Noggle and R.E.Schirmer, The Nuclear Overhauser Effect, Academic Press, (1971).

70. J.G.Powles, Ber.Buns.Ges., 67, 328 (1963).

71. L.G.Werbelow and D.M.Grant, Adv.Magn.Reson., 9, 189 (1977).

72. L.G.Werbelow, J.Magn.Reson., 34, 439 (1979).

73. F.Brady, R.W.Matthews, M.J.Forster and D.G.Gillies, Inorg.Nucl.Chem.Letters, 17, 155 (1981).

74. T.C.Farrar and E.D.Becker, Pulse and Fourier Transform NMR. Academic Press, (1971).

75. A.Bain, W.P.Y.Ho and J.S.Martin, J.Magn.Reson., 43, 328 (1981).

76. A.Geiger and H.G.Hertz, J.Solution Chem., 5, 365 (1976).

77. A.Geiger and H.G.Hertz, Adv.Mol.Relaxation Processes, 9, 293 (1976).

78. B.P.Bammel and R.F.Evilia, Anal.Chem., 54, 1318 (1982).

79. G.W.C.Kaye and T.H.Laby, Tables of Physical and Chemical Constants 14th Edition, Longmans (1973).

80. M.Wolfe and J.Jonas, J.Chem.Phys., 71, 3252 (1979).

81. K.R.Metz and J.F.Hinton, J.Amer.Chem.Soc., 104, 6206 (1982).

82. K.R.Metz and J.F.Hinton, J.Magn.Reson., 50, 212 (1982).

83. K.R.Metz and J.F.Hinton, J.Magn.Reson., 53, 131 (1983).

84. J.F.Hinton, K.R.Metz and R.W.Briggs, Ann.Rep.NMR.Spectry., 13, 211 (1983).

CHAPTER FIVE - ^{205}Tl RELAXATION OF OTHER DIORGANOTHALLIUM(III) COMPOUNDS.

Section 5.1. Diphenylthallium(III) chloride.

5.1.1. Introduction.

The ^{205}Tl NMR literature of diarylthallium(III) compounds is relatively sparse compared to the amount of information available for the dialkylthallium(III) compounds. Köppell[1] has investigated the ^{205}Tl NMR of thallium(I) and organothallium(III) compounds and reported the chemical shift of diphenylthallium(III) bromide in DMSO. Also the ^{205}Tl chemical shift of the diphenylthallium(III) chloride in liquid ammonia solvent has been reported by Hildenbrand and Dreeskamp[2]. The thesis of Brady[3] contains further information on the ^{205}Tl shifts of diarylthallium(III) compounds. In addition a number of ^{205}Tl-^{1}H coupling constants are available in the literature.[1-10]

The diphenylthallium(III) halides are stable solids of very high melting or decomposition points[11]. Crystal structures have been determined for the compounds $Ph_2TlS_2CN(C_2H_5)_2$ and Ph_2Tl(tropolonate)[12]. These reveal tetrahedral and pentagonal-bipyramidal thallium geometries, and C-Tl-C angles of 148° and 162.6° respectively.

The solution structures of the diphenylthallium(III) derivatives are a question of considerable importance when interpreting ^{205}Tl NMR parameters in solution. Stegmann et al.[13] have studied the ESR spectra of paramagnetic diphenylthallium(III) semiquinone and semidione complexes. Their results were rationalised

by proposing ion pair formation between the diphenylthallium(III) cation and the paramagnetic anion. Hammond and Pollard[14] have studied substitution reactions of organothallium compounds in pyridine solution. Exchange of phenyl groups was found to occur between diphenylmercury and the diphenylthallium cation, and a study of the kinetics of this reaction suggests a bimolecular transition state.

The ^{205}Tl spin lattice relaxation of diphenylthallium(III) chloride in DMSO-d^6 solution is reported here. The dissociation equilibrium may be written as

$$(C_6H_5)_2TlCl \rightleftharpoons (C_6H_5)_2Tl^+ + Cl^- \qquad 5 - 1$$

It is likely that the diphenylthallium(III) cation thus produced possesses a linear C-Tl-C skeleton like the dimethylthallium(III) cation. Furthermore the diphenylthallium(III) cation is isoelectronic with the diphenyl mercury molecule which is known to be linear.[15] The question of the extent of dissociation in equation 5 - 1 is an important one since if dissociation is not complete, as is the case for the dimethylthallium(III) nitrate in DMSO d^6 [16], then the observed ^{205}Tl resonance frequency and R_1 will be a weighted mean between the two ^{205}Tl environments. This situation will be further discussed later.

5.1.2. ^{205}Tl Spin Lattice Relaxation.

The only previous ^{205}Tl relaxation studies of this class of compounds, appears to be the variable temperature spin lattice relaxation measurements, of 0.2M $(C_6H_5)_2TlCl$ in DMSO-d^6, performed by Brady[13]. These measurements were performed at 34.7 MHz using a non degassed sample and are shown in Table 5.1

Temperature(K)	R_1 (s^{-1})
296.6	15.1
307.6	12.0
323.8	8.00
335.9	6.21
353.8	5.02

Table 5.1 R_1 measurements due to Brady[13].

In Table 5.1 the errors are ± 1K and ± 10% for the temperature and R_1 measurements respectively.

In order to extend the work of Brady, the spin lattice relaxation of an identical sample has been studied at 231 MHz. Initial measurements were performed on a degassed sample and the temperature taken as the instrument set temperature, under non decoupled conditions. These initial measurements have been combined with later studies of a non degassed sample under broadband ^1H decoupled conditions. In this case the sample temperature was found from an internal dimethylthallium(III) nitrate NMR thermometer. As expected the effects of degassing and/or decoupling on

R_1 are negligible at high field; thus the two sets of data are shown together in Table 5.2.

Temperature(K)	$R_1(s^{-1})$
[a] 300	549
[a] 300	526
305.4	449
314.2	355
[a] 320	342
331	254

Table 5.2 $(C_6H_5)_2Tl\text{-}Cl$ ^{205}Tl R_1 measurements at 231 MHz.

[a] indicates WH -400 set temperature, other temperatures found by ^{205}Tl shift thermometer, ^2H locked to DMSO d^6 solvent.

The observed relaxation rates in Tables 5.1 and 5.2 show a dramatic increase in the ^{205}Tl R_1 with increasing field, as was found for the dimethylthallium(III) cation and again indicates CSA relaxation.

5.1.3 Data Analysis and Discussion.

In order to characterise the temperature dependence of the ^{205}Tl R_1 at both fields, the data in Tables 5.1 and 5.2 may be fitted to equation 5-2 using $R_1(298K)$ and the activation energy as variable parameters.

$$R_1(T) = R_1(298K).\ \exp\left(\frac{E_{ACT}}{R}\left(\frac{1}{T} - \frac{1}{298}\right)\right) \quad \{5 - 2\}$$

The following best fit parameters were thus obtained.

	34.7 MHz	231 MHz
R_1(298K) s^{-1}	14.7 ± 0.3	561 ± 14
E_{ACT}kJ/mol	17.9 ± 0.9	19.7 ± 1.6

Table 5.3. ^{205}Tl relaxation parameters for $(C_6H_5)_2TlCl$/DMSO d[6]

The errors given for each parameter are estimated standard deviations. The non linear fit method was used although the data are plotted linearly as ln R_1 vs 1/T as shown in Figure 5.1.

The linearity of this plot shows that the reorientational motion is within the extreme narrowing limit, and thus the CSA mechanism is described by the equation

$$R_1^{CSA} = \frac{2}{15} \gamma^2 B_o^2 \Delta\sigma^2 (1 + \eta^2/3) \tau_2^{EFF} \qquad \{5 - 3\}$$

By use of equation 5.3 it is easily seen that CSA is the dominant mechanism at both fields. There appears to be a small residual non CSA contribution ($\simeq 2$ s^{-1} at 298K), but the quality of the data and the size of this contribution, do not allow a quantitative separation. The near equality of the activation energies in Table 5.3 is further confirmation that CSA relaxation is dominant at both fields.

A comparison of the CSA relaxation rate found here with that for the dimethylthallium(III) cation in aqueous solution, shows that CSA is even more efficient in the dimethylthallium species. This implies a slightly

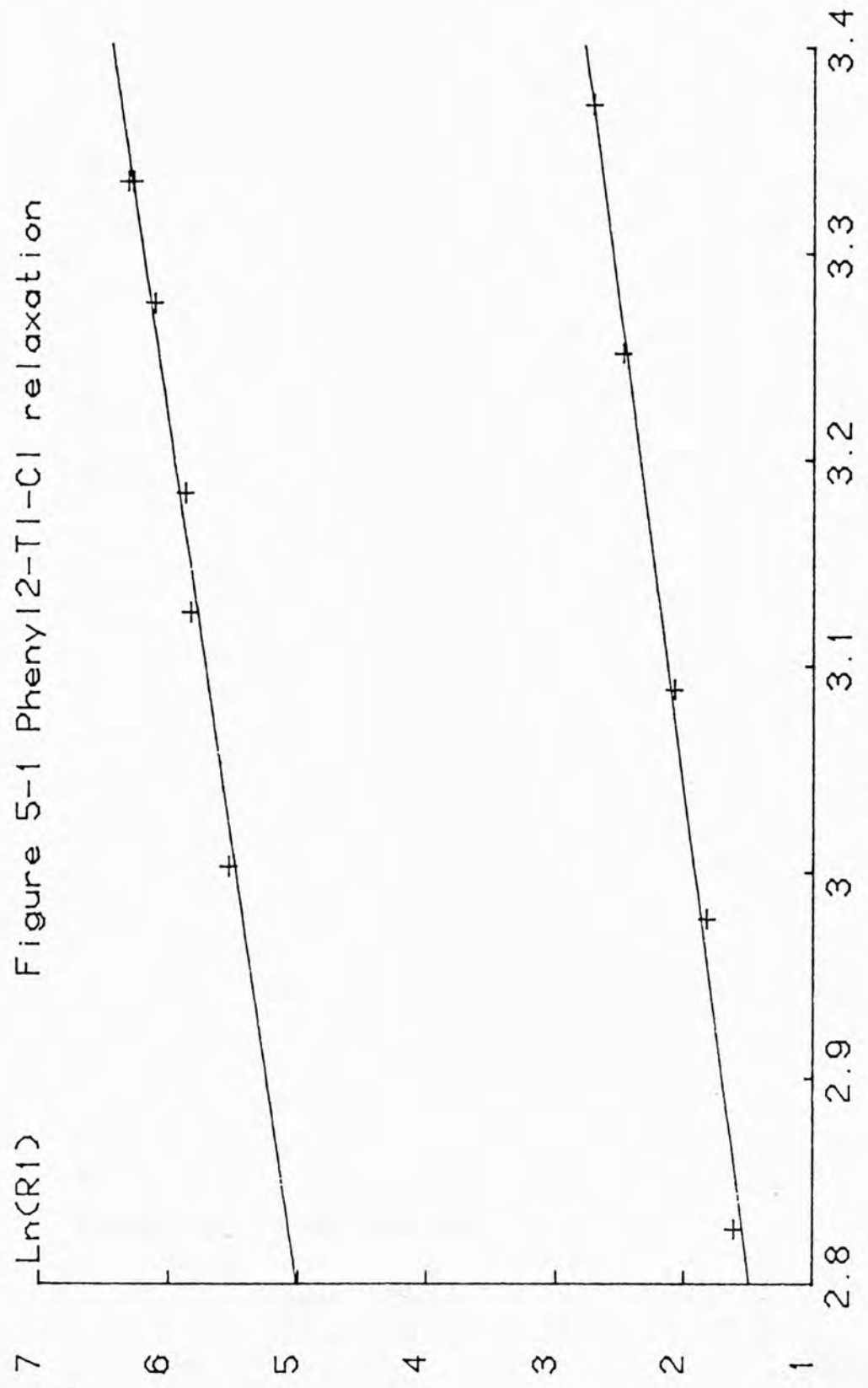

Figure 5-1 Phenyl2-Tl-Cl relaxation

larger value for the products of the effective reorientational correlation time τ_2^{EFF}, the square of the shielding anisotropy $\Delta\sigma$, and the asymmetry of the shielding tensor term $(1 + \eta^2/3)$. In the case of the axially symmetric dimethylthallium(III) cation $\eta = 0$, furthermore a knowledge of $\Delta\sigma$ allowed the calculation of τ_2^{EFF}.

However the lack of definitive knowledge of the position of the dissociation equilibrium in equation 5 - 1, implies difficulty in the estimation of these parameters; also the reorientational correlation time and shielding anisotropy would be expected to be different in the associated and dissociated forms. However it is still possible to derive limited ^{205}Tl shielding tensor information from the high field ^{205}Tl relaxation rates. Since the molecular reorientation lies within the extreme narrowing region then as discussed in Chapter Two $\omega_0\tau_2^{EFF} \ll 1$. Using the less restrictive relationship

$$\omega_0\tau_2^{EFF} < 1, \qquad \{5 - 4\}$$

allows the calculation of an upper bound for τ_2^{EFF} at 298 K, thus

$$\tau_2^{EFF} < 1/\omega_0 = 6.88 \times 10^{-10}\,s \qquad \{5 - 5\}$$

Thus a lower bound can be calculated for the product $\Delta\sigma^2(1 + \eta^2/3)$, using equation 5-3. If an effective anisotropy is defined as

$$\Delta\sigma^2_{EFF} = \Delta\sigma^2(1 + \eta^2/3) \qquad \{5 - 6\}$$

Then using $R_1(298K) = 561\ s^{-1}$, one obtains

$$\Delta\sigma_{EFF}^2 > 2.90 \times 10^{-6} \qquad \{5 - 7\}$$

or equivalently

$$|\Delta\sigma_{EFF}| > 1700 \text{ ppm} \qquad \{5 - 8\}$$

This calculation shows the ^{205}Tl nucleus to be in a highly anisotropic shielding environment. It must be emphasised that the value of 1700 ppm for the effective anisotropy is only a lower limit, the true value could be several times larger. This represents a weighted mean value due to the probable presence of associated and dissociated species in solution.

This situation contrasts with the known stability and linearity of the diphenylmercury molecule.[15] A study of the ^{199}Hg relaxation of this species in a mixed organic solvent has shown CSA to be the dominant relaxation mechanism at fields of 2.35T and 7.05T[17]. Measurements of the ^{13}C T_1 and ^{13}C $\{^1H\}$ NOE for the para carbon nucleus allowed calculation of a value for τ_2 which was 50 ps at 300K. With this value for τ_2 equation 5-3 was used to calculated $\Delta\sigma$ for the axially symmetric shielding tensor as 6800 $\pm$ 680 ppm.

Section 5.2 Dineopentylthallium(III) chloride.

5.2.1 Introduction.

The dineopentylthallium(III) chloride is the only representative of the higher dialkylthallium(III) compounds whose ^{205}Tl relaxation behaviour will be reported here. Information available in the literature on this class of compound includes reports on ^{205}Tl chemical shifts[1,3], $^{205}Tl-^{13}C$ coupling constants,[3] and $^{205}Tl - ^{1}H$ coupling constants[1,3-5,18-21]. The first reports of ^{205}Tl relaxation measurements of these compounds may be found in the thesis of Brady.[3]

Gillies et al.[22] have determined ^{13}C and ^{1}H NMR parameters for several dineopentylthallium(III) and bis-trimethylsilylthallium(III) derivatives. Molecular weight measurements suggest that both chloride derivatives are dimeric in chloroform solution[23]. Furthermore IR spectra of the latter compound suggest a bent C-Tl-C unit in solution and solid states.[24] A single crystal X-ray study of this compound has confirmed the dimeric structure, the four co-ordinate thallium atom is bonded to two bridging chlorine atoms and the C-Tl-C angle is 168^{o}. Double resonance $^{13}C\ \{^{1}H\}$ experiments were used to show that $J(^{205}Tl-^{13}C)$ and $J(^{205}Tl-^{1}H)$ are of opposite sign in the dineopentylthallium(III) compound.[22]

If one neglects the added complication of possible dimer formation in pyridine d^5 solution, then the dissociation equilibrium for the dineopentylthallium(III) chloride may be expressed by an equation analogous to equation 5 - 1. As was the case for the diphenylthallium(III)

chloride in the last section, the dissociation is not expected to be complete except at very low concentrations. This situation and the lack of available molecular interaction constants such as ^{205}Tl shielding anisotropies etc., implies that the interpretation of the ^{205}Tl relaxation rates may only be carried as far as the separation of individual relaxation mechanisms. Thus no attempt is made here to derive reorientational correlation times for the species studied.

5.2.2. Previous Relaxation Studies.

Brady[3] has performed the first ^{205}Tl relaxation measurements on the higher dialkylthallium(III) compounds. These studies were carried out at a ^{205}Tl resonance frequency of 34.7 MHz, using the modified Varian HA-60 instrument described in Chapter Three. The results obtained are described in Table 5 - 2 of his thesis, a brief summary of this work will now be given.

A series of ^{205}Tl spin lattice relaxation measurements were performed at a single temperature for the dimethyl, diethyl, di n-propyl, di n-butyl and di n-hexylthallium(III) nitrates in DMSO-d^6. It was observed that the spin-lattice rate increased monotonically with the size of the alkyl group. Such behaviour may be rationalised by simple hydrodynamic theory whereby increasing molecular volume leads to an increase in viscous drag, and to a correspondingly larger effective reorientational correlation time τ_2^{EFF}. It was proposed that the chemical shift anisotropy mechanism dominates the relaxation of the above series of compounds, and reorient-

ational correlation times were calculated, assuming an effective ^{205}Tl shielding anisotropy of 5300 ppm.

Variable temperature ^{205}Tl R_1 measurements were performed for 0.25 M di-isopropylthallium(III) isopropylate in pyridine d^5. The relaxation rate was observed to decrease with increasing temperature showing that a mechanism other than spin rotation is dominant. Previous experience suggests that this is CSA and correlation times were calculated using the assumptions just discussed.

In addition Brady performed a single temperature ^{205}Tl spin lattice relaxation measurement for 0.18M dineopentylthallium(III) chloride in pyridine d^5; a value of 5.2 s^{-1} at 39.9^{o}C was observed.

5.2.3 ^{205}Tl Spin Lattice Relaxation Measurements.

The temperature dependence of the relaxation rate R_1 of 0.18 M dineopentylthallium(III) chloride non-degassed in pyridine-d^5 (an identical sample to that studied by Brady) is reported here. These studies were performed at 34.7 MHz,field/frequency lock was achieved by ^{2}H lock at 9.2 MHz to the deuterated solvent.

The sample temperature was measured by observing the previously calibrated ^{205}Tl shift of a solution of $(CH_3)_2TlNO_3$ in D_2O, contained in a 5mm concentric tube.

The observed relaxation rate decreases steadily with increasing temperature, the results are shown in Table 5 - 4, and the CSA mechanism is implied.

Temperature(K)	$R_1(s^{-1})$	Temperature(K)	$R_1(s^{-1})$
281.8	9.04	317.8	5.10
288.6	8.00	328.5	4.38
295.7	6.82	334.5	4.29
303.6	5.85	342.5	3.92
308.7	5.51	343.7	3.99
310.8	5.72	362.9	3.80
310.8	5.12	-	-

Table 5.4 Variable temperature ^{205}Tl R_1 measurements for $((CH_3)_3 C CH_2)_2$ TlCl/pyridine d^5 at 34.7 MHz.

The plot of ln R_1 against inverse temperature in Figure 5.2 shows marked non linearity in the high temperature region and suggests a significant contribution from the spin rotation mechanism. At the highest temperature studied the ^{205}Tl R_1 reaches a minimum as a function of temperature.

5.2.4 Data Analysis and Discussion.

Although the sample was not degassed it will be assumed that the contribution from oxygen to the relaxation is not greater than that for the dimethylthallium-(III) case (~ 0.4 s^{-1}) and hence will be regarded as negigible. As before the total rate is taken as

$$R_{1\ TOT} = R_{1\ SR} + R_{1\ CSA}. \qquad \{5 - 9\}$$

expressing the relaxation rate for each mechanism in the form of equation 5 - 2, with $E_{CSA} = -E_{SR} = E_{ACT}$ the data have been fitted to equation 5 - 9 using the non-linear least squares method. The best fit parameters are shown

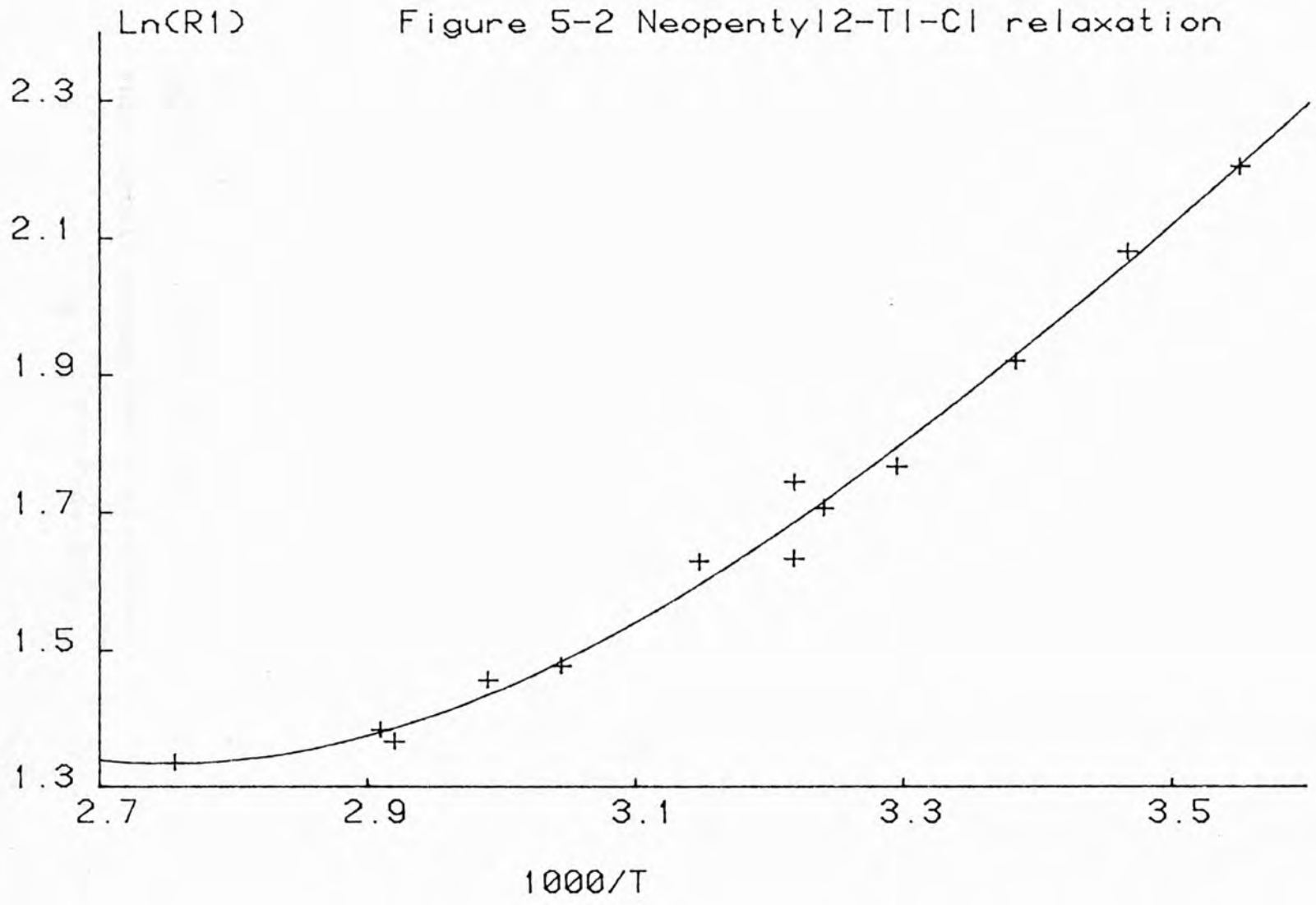

Figure 5-2 Neopentyl2-Tl-Cl relaxation

in Table 5.5.

R_1^{CSA} (298K)	=	6.00 ± 0.10 s^{-1}
R_1^{SR} (298K)	=	0.60 ± 0.05 s^{-1}
$E_{CSA} = -E_{SR}$	=	15.7 ± 0.8 KJ/mol.

Table 5.5. Dineopentylthallium(III) chloride relaxation parameters.

The parameters shown in the above table allow a calculation of R_1 (^{205}Tl) at other temperatures and field strengths. The field dependent relaxation measurements required to prove the presence of significant CSA relaxation have not been performed. However the next chapter will show how the presence of this mechanism can be implied by the observation of the ^1H spectrum of this compound at high field.

The parameters in Table 5.5 have been used to generate the curve in Figure 5.2. The calculated value of 5.2 s^{-1} for R_1 at 39.9°C is the same as that reported by Brady.(3)

The assumption of activation energies of equal magnitude for the CSA and SR mechanisms is a restrictive one necessitated by the lack of high field data where the relaxation would be dominated by CSA. Reference to the theory described in Chapter Two shows that if this assumption is true then

$$\tau_2 \, \tau_{SR} \, T = \text{Constant}, \qquad \{5 - 10\}$$

this may be compared to the Hubbard equation

$$\tau_2 \, \tau_{SR} = \frac{I}{6KT} \qquad \{5 - 11\}$$

Thus equality of the activation energies for CSA and SR mechanisms is consistent with the form of the Hubbard equation relating molecular reorientational and spin rotation correlation times.

REFERENCES CHAPTER FIVE

1. H.Koppell, J.Dallorso, G.Hoffman and B Walther, Z.Anorg.Allg.Chem., 427, 24 (1976).
2. K.Hildenbrand and H.Dreeskamp, Z.Phys.Chem.(N.F.), 69, 171 (1970).
3. F.Brady, PhD.Thesis, Polytechnic of North London, (1980).
4. J.P.Maher and D.F.Evans, J.Chem.Soc., 637 (1975).
5. J.P.Maher and D.F.Evans, Proc.Chem.Soc. 176 (1973).
6. A.McKillop, J.D.Hunt and E.C.Taylor, J.Organomet. Chem., 24, 77 (1970).
7. B.Walther, Z.Anorg.Allg.Chem., 395,112 (1973).
8. H.B.Stegmann, K.B.Ulmschneider and K.Scheffler, J.Organomet. Chem., 72, 41 (1974).
9. J.P.Maher, M.Evans and M.Harrison, J.Chem.Soc.Dalton, 188 (1972).
10. G.B.Deacon and I.K.Johnson, J.Organomet Chem., 112, 123 (1976).
11. H.Kurosawa, Chapter 8, Thallium,in Comprehensive Organometallic Chemistry, Pergamon Press (1982).
12. R.T.Griffin, K.Henrick, R.W.Matthews and M.McPartlin, J.Chem.Soc., Dalton, 1550 (1980).
13. H.B.Stegmann, K.B.Ulmschneider and K.Scheffler, J.Organomet.Chem., 101, 145 (1975).
14. G.A.Hammond and D.R.Pollard, J.Organomet.Chem., 36, 249 (1972).
15. B.Ziolkovska, R.M.Myasnikova and A.I.Kitaigorodski, J.Struct.Chem., USSR, 5, 678 (1964).

16. P.J.Burke, R.W.Matthews, I.D.Cresshull and D.G. Gillies, J.Chem.Soc.Dalton, 132 (1981).

17. D.G.Gillies, L.P.Blaauw, G.R.Hays, R.Huis and A.D.H.Clague, J.Magn.Reson., 42, 420 (1981).

18. G.D.Shier and R.S.Drago, J.Organomet.Chem., 5, 330 (1966).

19. J.V.Hatton, J.Chem.Phys., 40, 933 (1964).

20. D.W.Turner, J.Chem.Soc., 847 (1962).

21. H.Kurosawa and R.Okawara, J.Organomet.Chem., 10, 211 (1967).

22. F.Brady, K.Henrick, R.W.Matthews and D.G.Gillies, J.Organomet.Chem., 193, 21 (1980).

23. H.Kurosawa, S.Numata, T.Konishi and R.Okawara, Bull.Chem.Soc. Japan, 51, 1397 (1978).

24. H.Kurosawa, S.Numata and R.Okawara, J.Organomet. Chem., 70, C21 (1974).

CHAPTER SIX - EFFECT OF ^{205}Tl RELAXATION ON SPECTRA OF COUPLED NUCLEI.

Section 6.1 Introduction

6.1.1. Discussion of Scalar Relaxation.

The effects of enhanced ^{205}Tl relaxation at high field strengths on the spectra of coupled spin ½ nuclei have been discussed by Gillies et al.[1] These effects are not limited to the diorganothallium(III) derivatives or indeed to ^{205}Tl relaxation. However the best examples of these effects have been observed for diorganothallium(III) compounds because of the large anisotropies and large gyromagnetic ratio for thallium.

It is well known that the fast relaxation of a quadrupolar nucleus in a non spherically symmetric electric field gradient has a strong effect on the observed lineshape of coupled spin ½ nuclei such as protons[2]. When the quadrupolar relaxation rate R_{1Q} is less than the coupling constant $2\pi J$ then broadening effects may be observed in the lineshape of the coupled nucleus. At higher relaxation rates coalescence and collapse of the multiplet structure can occur[2,3].

These effects are due to scalar relaxation of the second kind as discussed in Chapter Two. The scalar spin-spin interaction is modulated by relaxation of the quadrupolar nucleus.

For the case of a collapsed multiplet ($\tau_{SC} << 1/J$) the scalar relaxation rates are given by the following equations[2,4]:

$$R_{1\ SC} = \frac{8\pi^2 J^2}{3} S(S+1) \left[\frac{\tau_{SC}}{1 + \Delta\omega^2 \tau^2_{SC}} \right], \quad \{6 - 1A\}$$

$$R_{2\ SC} = \frac{4\pi^2 J^2}{3} S(S+1) \left[\tau_{SC} + \frac{\tau_{SC}}{1 + \Delta\omega^2 \tau^2_{SC}} \right], \{6 - 1B\}$$

where S is the spin quantum number of the quadrupolar nucleus, $\Delta\omega$ is the difference in resonance frequency between the quadrupolar and spin ½ nucleus and τ_{SC} is the scalar correlation time which is a multiple of T_{1Q}. Often τ_{SC} is taken as T_{1Q} and this happens to be correct for the I = 3/2 case which applies to the common case of coupling to quadrupolar halogen nuclei. Scalar relaxation is a significant contributor to the R_2 and hence linewidth of the coupled nucleus because of the presence of the zero frequency spectral density term J(O) ($= \tau_{SC}$) in equation 6 - 1B. Similarly this mechanism seldom contributes to R_1 since the timescale of the modulation is typically much slower than the difference in the Larmor frequencies. This implies inefficient relaxation since $\Delta\omega^2 \tau_{SC}^2 >> 1$ in equation 6 - 1A.

These lineshape effects are not restricted to the requirement of a quadrupolar mechanism. Scalar coupling effects upon the lineshape of coupled nuclei may be induced by chemical exchange, this mechanism is known as scalar relaxation of the first kind.(2)

Scalar relaxation of the second kind may be induced by any relaxation mechanism, since it is an effect which depends on the finite lifetime of the nuclear states of the S nucleus.

6.1.2. Some examples of Scalar Relaxation.

Navon and Polak have investigated the effects of dissolved oxygen on the proton spin-spin multiplets of organic molecules.[5] They found that increased spin lattice relaxation of one set of nuclei causes an extra broadening and apparent reduction of the J coupling in the NMR spectrum of another set of coupled nuclei. A classical lineshape equation[2] was used to calculate first order multiplet lineshapes and it was concluded that for the well resolved multiplet in an A_mX_n system the broadening induced in each component is equal to $n/2T_{1X}$ s^{-1}. These phenomena have been dubbed "T_1 spin decoupling", by Navon and Polak. As discussed in Chapter Four, Lallemand et al.[6] have used the disappearance of ^{195}Pt-^{1}H and ^{195}Pt-^{13}C couplings and line broadening of ^{195}Pt spectra to imply a dominant CSA relaxation mechanism for some Pt(II) complexes. The collapse of couplings at high field strength is due to increased scalar R_2 relaxation arising from an enhanced ^{195}Pt R_1 relaxation. Similarly Ismail, Kerrison and Sadler[7] have observed broadening of ^{195}Pt satellites in the ^{1}H spectrum of a Pt(II) complex at high fields.

The ^{199}Hg nucleus is known to relax efficiently via the CSA mechanism in non spherically symmetric shielding environments[8,9]. Gillies et al.[8] have noted that the ^{199}Hg satellites in the ^{13}C spectrum of diphenylmercury are broader at 67.9 MHz than at 25.1 MHz. Similar effects have previously been noted for ^{31}P and ^{1}H spectra coupled to ^{199}Hg (10,11)

Section 6.2 Effects due to ^{205}Tl relaxation.

6.2.1. Broadening effects of ^{205}Tl relaxation in the slow relaxation limit.

Broadening effects similar to those just discussed may be observed for ^{1}H spectra of dialkylthallium(III) compounds. However the thallium nucleus has two magnetically active isotopes ^{205}Tl and ^{203}Tl with natural abundances of 70.5% and 29.5% respectively. Since the gyromagnetic ratios of these nuclei are in the ratio $\gamma(^{205}Tl)/\gamma(^{203}Tl) = 1.0098$, overlap of ^{1}H signals coupled to the two isotopes will occur in the compounds studied here. Brady et al.[12] have observed the dependence of the ^{1}H linewidth for $(CH_3)_2TlOCOCH_3$ in D_2O solvent, on the resonance frequency, ν_o, and found a linear relationship between the ^{1}H linewidth and ν_o^2.

Scalar relaxation of the second kind for a spin A differs from scalar relaxation of the first kind only in that it is rapid spin lattice relaxation of X, rather than chemical exchange which modulates the J coupling leading to spin-spin relaxation of A. The analogy may be extended to considering the effect of changes in the X spin state on the A spectrum of an AX spin system as a two site chemical exchange problem for A.[1] The sites are labelled by the α and β spin states of X, with lifetimes τ_α and τ_β respectively. The ratio of the transition probabilities for X is equal to the Boltzmann factor[13].

$$\frac{W_{\alpha\,\beta}}{W_{\beta\,\alpha}} = \frac{\tau_\beta}{\tau_\alpha} = \exp\left(h\nu_X / \kappa T \right) . \quad \{6 - 2\}$$

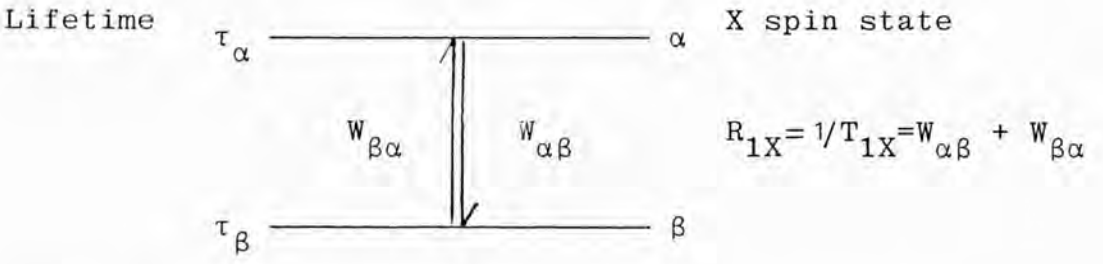

Figure 6-1. Spin states, lifetimes and transition probabilities for a single spin 1/2.

For the present purposes the Boltzmann factor may be taken as unity, hence the lifetimes of the α and β spin states of X are related to T_{1X} as

$$\tau_\alpha^{-1} = \tau_\beta^{-1} = W_{\alpha\beta} = W_{\beta\alpha} = 1/2\ T_{1X}. \quad \{6 - 3\}$$

The situation for the ^1H spectrum of dimethylthallium(III) derivatives is equivalent to the slow exchange limit $\tau_\alpha >> (2\pi J)^{-1}$, and a simple two site exchange analysis[3,13] shows that the broadening in Hz for each component of A is equal to $1/\pi\tau_\alpha$ or $1/2\pi T_{1X}$. Thus the observed linewidth in the A spectrum is given by the following expression[1].

$$\Delta\nu_{\frac{1}{2}}(A) = \frac{1}{\pi T^*_{2A}} + \frac{1}{2\ \pi T_{1X}} \quad \{6 - 4\}$$

where the term $1/\pi T^*_{2A}$ includes the natural linewidth of A and any contributions due to field inhomogeneity etc. The above expression may be derived from the results of Navon and Polak for an A_mX spin system in the slow exchange limit. Equation 6 - 4 may be particularly useful in the ^{195}Pt and ^{199}Hg cases where the linewidths

of signals associated with the central non magnetic Hg and Pt nuclei provide a direct measure of $1/\pi T^{*}_{2A}$.

As an example of the use of equation 6 - 4 the ^{1}H linewidth of a degassed solution of 0.8M $(CH_3)_2TlNO_3$ in D_2O at 300K and 400MHz, has been found to be 55 Hz. If the natural linewidth contribution in equation 6 - 4 is negligible compared to the scalar broadening, this equation predicts a ^{205}Tl R_1 of 345 s^{-1} under these conditions, which agrees within experimental error with the value of 322 s^{-1} calculated from the best fit parameters in Chapter Four.

The observed ^{205}Tl linewidth under these conditions was 140 Hz, corresponding to a value of 120 Hz predicted by the relationship $R_{2\ CSA} = 7/6\ R_{1\ CSA}$. The excess of 20 Hz is attributed to an effective inhomogeneity in sample temperature of $<0.2^{o}C$. The broadening in the proton spectrum should be 3/7 of the observed thallium linewidth i.e. 51.4 Hz, this corresponds favourably with the observed ^{1}H linewidth of 55 Hz.

6.2.2. Lineshape effects outside slow relaxation limit.

A further example of the effect of CSA induced ^{205}Tl relaxation on the ^{1}H spectrum of dialkylthallium(III) compounds is provided by the 360 MHz ^{1}H spectrum of dineopentylthallium(III) chloride in pyridine-d^5 solution shown together with the computed ^{1}H spectrum in Figures 6-2 and 6-3.[12,14] The ^{4}J (^{205}Tl-^{1}H) coupling is resolved only at higher temperatures where the CSA

mechanism is less efficient. The $^{2}J\ (^{205}Tl-^{1}H)$ coupling is resolved at both temperatures since the larger J value corresponds to a shorter NMR time scale.

The Pople exchange equations[3] for the case of two equally populated sites, were used to describe the ^{1}H scalar relaxation due to $^{203,205}Tl-^{1}H$ coupling. The exchange equation is,

$$S(\nu)= \frac{K\tau(\nu_A-\nu_B)^2}{\{\frac{1}{2}\ (\nu_A+\nu_B)-\nu\}^2 + 4\pi^2\tau^2(\nu_A-\nu)^2\ (\nu_B-\nu)^2} \quad , \quad \{6 - 5\}$$

where ν_A and ν_B are the site fequencies in Hz, and $\tau = \frac{1}{2}\tau_A = \frac{1}{2}\tau_B = T_1(^{203,205}Tl)$. For all proton types $\nu_A = \delta + J/2$ and $\nu_B = \delta - J/2$ respectively. The relevant shifts and coupling constants were taken from a 60 MHz ^{1}H spectrum[14], where the scalar broadening is considerably reduced. Thus

$$\delta(CH_3) = 1.09 \text{ ppm} \qquad ^{4}J(^{205}Tl - ^{1}H) = 31 \text{ Hz} \quad \{6 - 6A\}$$

$$\delta(CH_2) = 2.38 \text{ ppm} \qquad ^{2}J(^{205}Tl - ^{1}H) = 415 \text{ Hz} \quad \{6 - 6B\}$$

overlap due to ^{203}Tl and ^{205}Tl isotopes has been included, with the $^{203}Tl-^{1}H$ coupling constants reduced by the factor 1.0098. The natural ^{1}H linewidth was considered negligible. $R_1(^{205}Tl)$ and $R_1(^{203}Tl)$ are assumed equal, and the rates evaluated by extrapolating the CSA relaxation contribution given in Chapter Five to a field of 8.46 T.

Thus $R_1(300K) = 206.7\ s^{-1}$ and

$R_1(340K) = 99.6\ s^{-1}$.

Each theoretical spectrum is a sum of four expressions of the form of equation 6 - 5.

The full approach using exchange equations is necessary because $R_1(^{203,205}Tl)$ is of the order of $2\pi^4 J$

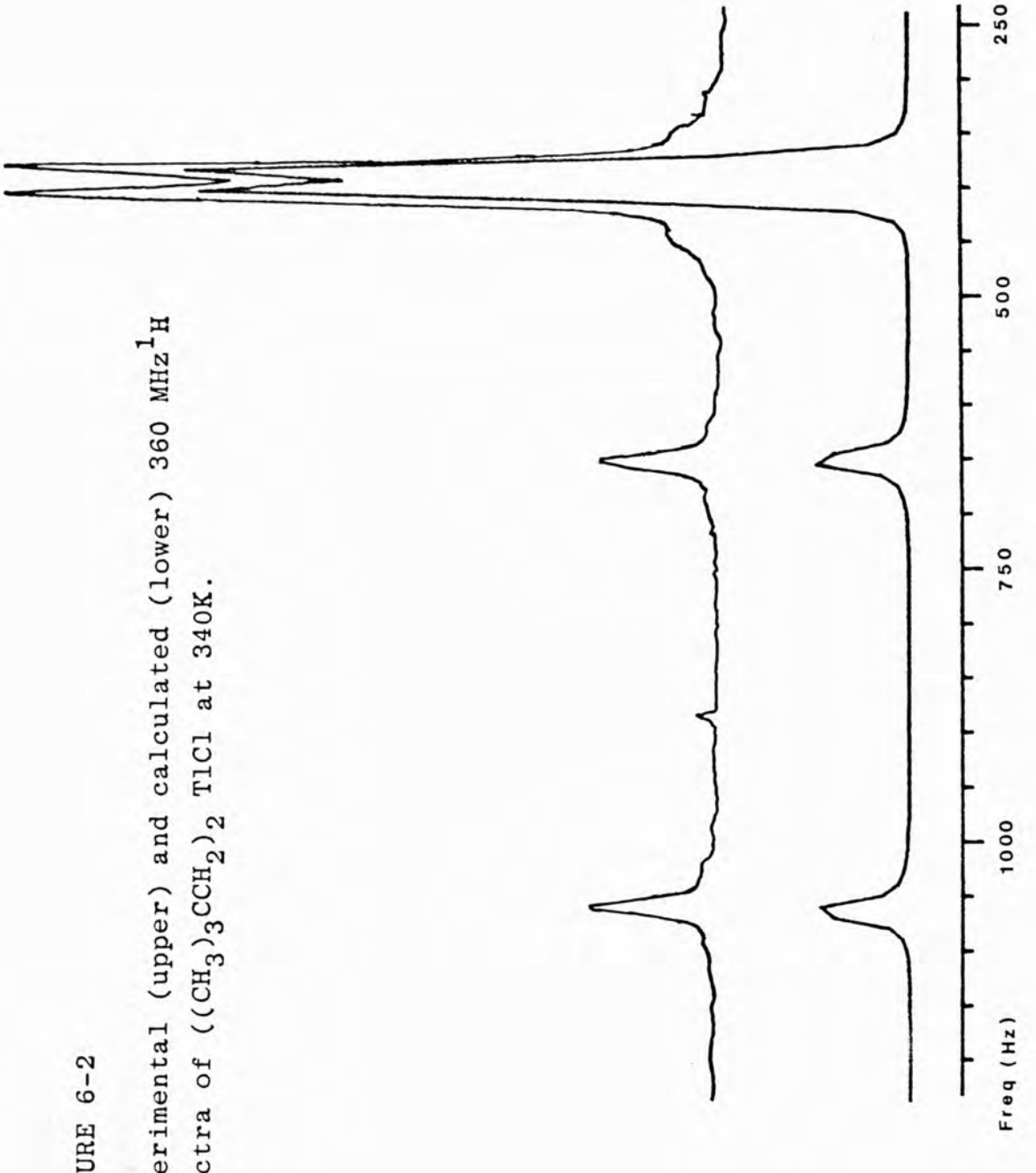

FIGURE 6-2

Experimental (upper) and calculated (lower) 360 MHz ^{1}H spectra of $((CH_3)_3CCH_2)_2$ TlCl at 340K.

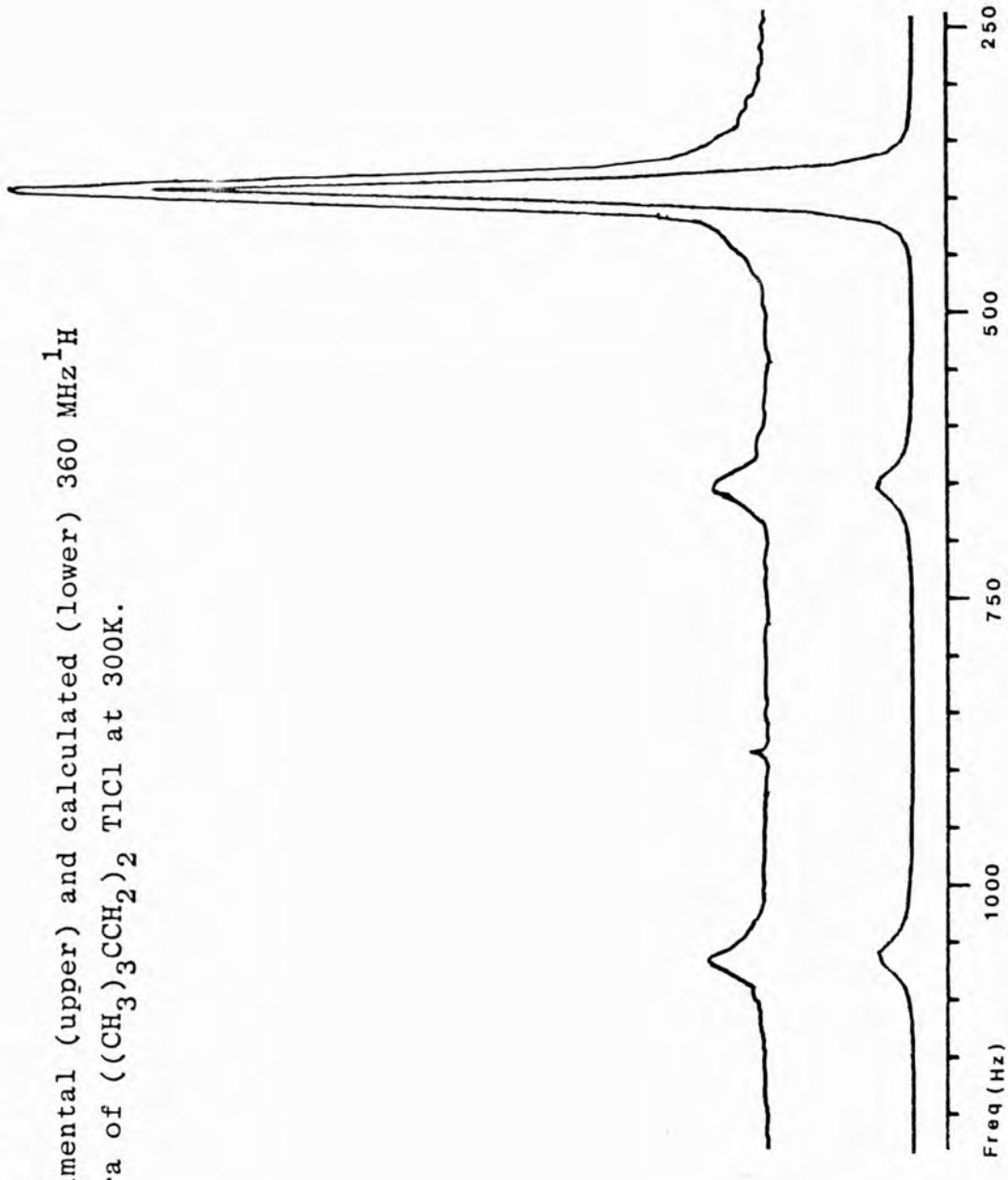

FIGURE 6-3

Experimental (upper) and calculated (lower) 360 MHz ^1H spectra of $((CH_3)_3CCH_2)_2$ TlCl at 300K.

whereas the simpler approach involving line broadening is applicable to the methyl protons which are in a slower timescale regime. The theoretical spectra reproduce well the spectra observed at both temperatures. Thus low field ^{205}Tl relaxation data at 34.73 MHz have been used to successfully reproduce the linewidth effects in the high field proton spectra at 360 MHz.

This work demonstrates the feasibility of deducing R_1 values for coupled nuclei by the fitting of proton bandshapes to exchange equations in suitably broadened spectra at high field.

REFERENCES. CHAPTER SIX

1. F.Brady, R.W.Matthews, M.J.Forster and D.G.Gillies, J.Chem.Soc., Chem.Comm., 911 (1981).

2. A.Abragam, The Principles of Nuclear Magnetism, Oxford University Press (1961).

3. J.A.Pople, W.G.Schneider and H.J.Bernstein, High Resolution Nuclear Magnetic Resonance, McGraw Hill, New York (1959).

4. J.R.Lyera and D.M.Grant, Chapter 5, Vol.4, MTP International Review Series - Physical Chemistry.

5. G.Navon and M.Polak, Chem.Phys.Lett., 25, 239 (1974).

6. J.Y.Lallemand, J.Soulie and J.C.Chottard, J.Chem.Soc., Chem.Comm., 436 (1980).

7. I.M.Ismail, S.J.S.Kerrison and P.J.Sadler, Polyhedron, 1,57 (1982).

8. D.G.Gillies, L.P.Blaauw, G.R.Hays, R.Huis and A.D.H.Clague, J.Magn.Reson., 42, 420 (1981).

9. C.R.Lassigne and E.J.Wells, Can.J.Chem., 55, 1303 (1977).

10. N.S.Ham, E.A.Jeffrey, T.Mole and S.N.Stuart, J.Chem.Soc., Chem.Comm., 254 (1967).

11. A.J.Brown, O.W.Howarth and P.Moore, J.Chem.Soc., Dalton, 1589 (1976).

12. F.Brady, R.W.Matthews, M.J.Forster and D.G.Gillies, Inorg.Nucl.Chem.Lett., 17, 155 (1981).

13. A.Carrington and A.D.McLachlan, Introduction to Magnetic Resonance, Harper and Row (1967).

14. F.Brady, Ph.D.Thesis, Polytechnic of North London (1980).

CHAPTER SEVEN - THALLIUM(I) COMPOUNDS.

Section 7.1 ^{205}Tl NMR Studies of Tl(I) ion solvation and complexation.

7.1.1 Tl^+ Solvation Phenomena.

The ^{205}Tl chemical shift is known to be an extremely sensitive probe of the solution environment of the thallium(I) cation, and ^{205}Tl NMR has been widely used as a tool to investigate solvation phenomena. The concentration and anion dependence of the $^{205}Tl^+$ chemical shift have been measured in aqueous[1-14] and non aqueous solvents,[15-24] and found to vary by up to 100 ppm. The dissociation equilibrium may be represented as

$$Tl^+ + A^- \rightleftharpoons TlA \quad . \qquad \{7 - 1\}$$

The rapid equilibrium leads to a weighted mean ^{205}Tl NMR signal given by

$$\delta_{OBS} = x_F \ \delta_F + x_{IP} \ \delta_{IP} \ , \qquad \{7 - 2\}$$

where x_F and x_{IP} are the mole fractions of free and ion paired thallium(I) cation respectively, and δ_F and δ_{IP} are the chemical shifts of these species at infinite dilution. In the above solvation studies the observed $^{205}Tl^+$ shifts are discussed in terms of ion pairing, using equations 7 - 1 and 7 - 2. The ion pair formation constant for the above equilibrium is defined as

$$K = [Tl\text{-}A] / \gamma_{\pm}^{\,2} [Tl^+] [A^-] \qquad \{7 - 3\}$$

where $\gamma_{\pm}$ is the mean actvity coefficient. The formation constants in several solvents for the thallium(I) cation with nitrate and perchlorate anions have been obtained by Hinton et al.[22] by fitting the data to equations

7 -2 and 7 - 3, the chemical shifts for the free and ion paired cation are obtained.

The solvent dependence of the $^{205}Tl^{+}$ chemical shift has been observed by Zink et al.[16,17] to be as large as 2600 ppm. It was found that in oxygen coordinating solvents the ^{205}Tl resonance was to low frequency of that in nitrogen coordinating solvents. Hinton et al.[24] have observed a correlation between the infinite dilution extrapolated resonance frequency and the Gutman donor number. This correlation implies that increasing solvent basicity shifts the $^{205}Tl^{+}$ resonance to high frequency.

The sensitivity of the ^{205}Tl shift to the nature of the solvent has been used to study preferential solvation in a number of mixed solvent systems. The statistical solvation model of Covington[25] assumes a fixed solvation number in pure and mixed solvents, that the chemical shift of solvate species are linearly related to the composition of the first solvation sphere, that solvent substitution is independent of the composition of the first solvation sphere, and that the equilibrium constants for the individual solvent exchange processes are statistically related to the overall stability constant. This theory has been used to analyse preferential solvation in pyrollidine-formamide, water-methanol[16], and DMSO-pyridine[18] mixtures. The solvating ability of a wide range of solvents has been measured relative to a chosen standard of DMF.[15] Hinton et al[24] have investigated

preferential solvation in aqueous-amide and amide-amide mixtures using the above theory. Covington and Thain[26] have introduced a modification to their theory which allows the substitution process to be dependent on the composition of the primary solvation sphere. This leads to a non statistical distribution of solvate species. This revised model has been used to reinvestigate Tl^+ solvation in nine binary solvent systems.[22] Equilibrium constants and free energies of preferential solvation have been obtained.

7.1.2. Tl(I) Complex Studies.

The field of Tl(I) complexation has been widely studied by ^{205}Tl NMR. Reuben and Kayne[27,28] have observed the effect of paramagnetic Mn^{2+} bound to pyruvate kinase on bound Tl^+ cation. The effects on the ^{205}Tl chemical shift, T_1 and T_2 indicate that the divalent and monovalent binding sites are close together. The Tl(I) ion complexation with the crown ethers 18-crown-6 and dibenzo 18-crown-6 have been studied by Dechter and Zink.[19,29] Selectivity sequences have been determined with the alkali metal cations as well as NH_4^+ and Ag^+. Formation constants for Tl^+ are too large to measure. The ^{205}Tl shift in these crown ethers is strongly solvent dependent, showing the open nature of the complexes, allowing solvent and anion interactions with the cation.

Formation constants of Na^+, Cs^+ and Tl^+ cations with the dibenzo-21-crown-7, dibenzo-24-crown-8 and dibenzo-29-crown-7 ethers have been determined.[30]

In a range of non aqueous solvents the stabilities are in the order $Tl^+ > Cs^+ > Na^+$.

The complexation of Tl(I) ion with the 221, 222 and 222B cryptands have been studied in water and several non aqueous solvents.[31] The ^{205}Tl shift is found to be independent of solvent and anion, but shifts to low frequency with an increasing number of complexing oxygen atoms. This indicates that the cation is protected from environmental effects by the surrounding cryptand.

Hinton et al. have studied Tl(I) complexation with the antibiotic ionophores lasalocid[32], valinomycin[33], monensin and nigericin[34] and with three actin ionophores.[35] In these studies the ^{205}Tl shift is indicative of the basicity of the functional groups involved with binding, and the effect of molecular oxygen on the ^{205}Tl T_1 shows how well the ionophore surrounds the cation. By use of variable temperature T_1 and NOE measurements the spin rotation, dipole-dipole and remaining chemical shift anisotropy contributions have been approximately separated. The magnitude of the dipole-dipole contribution indicates the closeness of protons in the complex to the thallium ion. A high CSA contribution to T_1 indicates a low thallium symmetry and vice versa. The results for the above studies are summarised in Table 7 - 1.[36]

Ionophore	^{205}Tl shift[a]	% CSA relaxation[b]	O_2 effect
Lasalocid	294	Probably dominant	-
Nigericin	128	<50	Yes
Monensin	107	<50	Yes
Nonactin	-262	~10	No
Monactin	-262	~10	No
Dinactin	-262	~10	No
Valinomycin	-540	~90	Yes

[a] ppm relative to infinite dilution Tl^+/H_2O

[b] At 51.9 MHz

Table 7 - 1. Summary of some Tl(I)-ionophore studies.

The solid state ^{205}Tl spectrum of the thallium(I) valinomycin complex has been obtained.[37] From the powder pattern lineshape, a ^{205}Tl shielding anisotropy was deduced assuming an axially symmetric shielding tensor. The anisotropy of 135 ppm thus found does not compare favourably with values of between 317 ppm and 976 ppm estimated from the fluid state ^{205}Tl relaxation study. Hinton et al. have also published a series of papers where ^{205}Tl NMR has been used to investigate the Tl(I)-gramicidin complex. A solution study in 1,4 dioxane has established a chemical shift of -675 ppm from infinite dilution Tl(I) ion in H_2O.[38] An association study of this complex in 2,2,2 trifluoroethanol has indicated that the dimer has two or more strong binding sites and one or more weak sites. The measurement of the temperature dependence of the strong site association constant allows

the measurement of the enthalpy and entropy of association. The values are ΔH = -8.77 kJ mol^{-1} and ΔS = 22.4 J $mol^{-1}K^{-1}$ respectively.[39] The Tl(I) ion gramacidin complex has been incorporated into micelles and the ^{205}Tl shift data interpreted in terms of a one site binding model. A binding constant of 900 M^{-1} was found at 30°C.[40] A recent association study of the system in DMSO has shown that Tl^+ binds to the monomer as a 1:1 complex.[41] The association enthalpy and entropy are -8.15 kJ mol^{-1} and 41.6 J $mol^{-1}K^{-1}$ respectively. The ^{13}C NMR spectrum of this complex indicates that the binding site is in the tryptophan carbonyl region.

Section 7.2. Previous $^{205}Tl(I)$ ion Relaxation Studies.

7.2.1 Relaxation in aqueous solutions.

The ^{205}Tl relaxation of the Tl(I) ion was first investigated by Gasser and Richards.[42] They observed a linear increase of the ^{205}Tl R_1 with added paramagnetic $Fe(CN)_6^{3-}$ ion in aqueous solution, up to a paramagnetic concentration of 0.01 M.

The effect of dissolved paramagnetic molecular oxygen on the ^{205}Tl R_1 and R_2 has been investigated by Reeves et al.[43,44], working at a ^{205}Tl frequency of 15.1 MHz. A linear dependence of R_1 and R_2 on the partial pressure of oxygen, up to five atmospheres was observed. It was found that R_2 and R_1 were equal within experimental error, which led to the proposal that the dominant relaxation mechanism is the electron nuclear dipole-dipole mechanism. For solutions free of

dissolved paramagnetics it was found that both relaxation rates were independent of resonance frequency, resonant spin (^{203}Tl or ^{205}Tl), anion, concentration, and substitution of H_2O for D_2O.[44] This latter observation is however not in agreement with their earlier report[43], which gave $R_1(D_2O)/R_1(H_2O)$ equal to the inverse viscosity ratio $\eta(H_2O)/\eta(D_2O)$, which differ by about 20%. The transient spin rotation mechanism was proposed as the dominant relaxation mechanism in solutions free of paramagnetic species. This mechanism was later placed on a firm theoretical footing by Schwartz[45], this mechanism arises from the rotational and collisional modulation of the spin rotation interaction of transient solvated species. As discussed in Chapter Two this mechanism is characterised by a transient spin rotation correlation time τ_{SR}, which increases with increasing temperature leading to faster spin relaxation. Such a temperature dependence was observed for the Tl(I) ion in aqueous solution by Hinton et al.[20]

Bangerter and Schwartz[46] have reported a linear dependence of the ^{205}Tl R_1 and R_2 in aqueous $TlNO_3$ on the concentration of the nitroxide radical 4-hydroxy-2,2,2,6 tetramethylpiperidine-1-oxyl (TANOL). At 51.75 MHz it was found that R_2 was significantly greater than R_1, and it was concluded that a strong scalar coupling exists between the unpaired electron spin of TANOL and the ^{205}Tl nucleus. The scalar hyperfine mechanism was considered to dominate the transverse relaxation, but not to contribute significantly to the longitudinal relaxation

where the electron-nuclear dipole-dipole mechanism was thought to dominate. The ^{205}Tl R_1 was observed to be temperature independent within experimental error in contrast to R_2 which decreased with increasing temperature.

Bangerter later reinvestigated the effect of dissolved O_2 on the ^{205}Tl R_1 and R_2 in aqueous solution.[47] Both relaxation rates were found to be linearly related to the partial pressure of oxygen. In contrast to previous reports[44] R_2 was observed to be greater than R_1 and similar conclusions were made to those described for the TANOL system. It should be noted, however, that the R_1 values observed by Bangerter[47] are less than those observed by Reeves under equal partial pressures of oxygen, unlike the R_2 values which were equal within experimental error.

7.2.2 Relaxation in non aqueous solutions.

The ^{205}Tl relaxation of the Tl(I) ion in non aqueous solutions has been well investigated. Chan and Reeves[44] have found that the effect of oxygen pressure on the ^{205}Tl relaxation is about a factor of four greater in methanol than in aqueous solution. This is explained by the greater solubility of oxygen in the former. R_2 and R_1 were observed to be the same within experimental error as in the aqueous case.

In aqueous solutions free of paramagnetic species the ^{205}Tl relaxation is dominated by the transient spin rotation mechanism, but in non aqueous solutions this may not be the case. Hinton et al.[48] have studied the

the concentration and temperature dependence of the ^{205}Tl R_1 of thallium(I) perchlorate in DMSO at concentrations up to 0.99M, spin rotation appears to be the dominant mechanism. However, at 2.99M another mechanism makes a significant contribution. Any ^{205}Tl-^{1}H dipolar mechanism can be disregarded since no change in the relaxation rate is found upon substituting DMSO-d^6 for DMSO. This was rationalised by suggesting that the other mechanism is transient CSA, a mechanism discussed in Chapter Two and first described theoretically by Schwartz.(45) The effect of transient counterion penetration of the Tl(I) ion solvation sphere is to induce a large perturbation of the thallium electronic environment and hence of the ^{205}Tl shielding tensor. Modulation of this interaction by transient ion pair encounters or reorientation of such a species can provide a mechanism for spin relaxation. These effects become more pronounced at increased concentrations. However, the field dependent measurements required to prove the presence of this mechanism have not been performed for ^{205}Tl.

The solvent dependence of the ^{205}Tl relaxation has been demonstrated by ^{205}Tl R_1 measurements for ca.0.2M Tl NO_3 solution in a range of nine solvents(20) at 52 MHz. R_1 was found to vary from 12.5 s^{-1} in butylamine to 0.55 s^{-1} in H_2O. It should be noted that the anion present was unmentioned in the original publication, but is documented in recent reviews.(49,50) A temperature dependent relaxation study of ca.0.2M Tl NO_3

in the solvent HMPA ($OP\{N(CH_3)_2\}_3$) has shown that a mechanism other than transient SR was dominant across the temperature range studied.

Section 7.3 ^{205}Tl Relaxation Mechanisms in Tl(I)-paramagnetic Systems.

7.3.1 Mechanisms considered.

The next section of this chapter will present ^{205}Tl relaxation results for the Tl(I) ion in aqueous solution in the presence of dissolved paramagnetic oxygen. In preparation for this a discussion of the relevant ^{205}Tl relaxation mechanisms will now be given. The unpaired electron(s) of the paramagnetic species can induce ^{205}Tl relaxation by either the dipole-dipole or scalar (contact hyperfine) interactions. Thus the observed relaxation rates may be described by the sum of three terms

$$R_{1,2} = R_{1,2\ DD} + R_{1,2\ SC} + R_{1,2\ OTHER}\ , \qquad \{7 - 4\}$$

where $R_{1,2\ OTHER}$ are the rates in the absence of the paramagnetic species. The dominance of the transient spin rotation mechanism in paramagnetic-free aqueous solutions has already been discussed in Section 7.2, thus in the following discussion $R_{1,2\ OTHER}$ will be taken to be equal to the spin rotation rates. This term is expected to be field independent but to increase with increasing temperature.[20,44] Since the paramagnetically induced dipolar and scalar mechanisms were not discussed in detail in Chapter Two and both are considered relevant to $^{205}Tl(I)$

ion relaxation, both mechanisms will now be discussed.

7.3.2 Electron Nuclear Dipole-Dipole Mechanism.

The presence of paramagnetic species in solution may induce nuclear spin relaxation via modulation of the electron nuclear dipolar interaction; the efficiency of this mechanism arises from the large electronic dipole moment. The interaction may be modulated by translational and reorientational motions or by electronic spin relaxation. The interpretation of the observed relaxation rates differ according to whether or not a Tl(I)-paramagnetic complex with an appreciable lifetime is formed. Bangerter[47] has noted that the nitroxide radical TANOL, is two orders of magnitude more effective in enhancing ^{205}Tl relaxation than is Mn^{2+} at the same concentration. This suggests the possibility of a TANOL-Tl(I) complex, although TANOL EPR and optical studies do not indicate any strong interaction. If such a complex were formed and the Tl(I) ion exchanges rapidly between bound and free environments, the electron induced relaxation rates would be describable in terms of the Solomon-Bloembergen equations.[51,52]

In this case the electron-nuclear dipole-dipole relaxation rates are given in S.I. units by equations 7 - 5A and 7 - 5 B,

$$R_{1\ DD} = \frac{2}{15}\left(\frac{\mu_o}{4\pi}\right)^2 \frac{S(S+1)\gamma_I^{\,2}\gamma_S^{\,2}\hbar^2 x}{r^6}\left[\frac{3\tau_c}{1+\omega_S^{\,2}\tau_c^{\,2}} + 7\tau_c\right], \quad \{7-5A\}$$

$$R_{2\ DD} = \frac{1}{15}\left(\frac{\mu_o}{4\pi}\right)^2 \frac{S(S+1)\gamma_I^{\,2}\gamma_S^{\,2}\hbar^2 x}{r^6}\left[\frac{13\tau_c}{1+\omega_S^{\,2}\tau_c^{\,2}} + 7\tau_c\right] \quad \{7-5B\}$$

μ_o is the permeability of free space and equals $4\pi \times 10^{-7}$ Hm^{-1}, γ_I and γ_S are the nuclear and electronic gyromagnetic ratios respectively, r is the mean electron-nucleus distance and τ_C is the dipolar correlation time. Both molecular reorientation and electronic relaxation can modulate the dipolar interaction, Solomon considered only a single electronic relaxation time τ_S hence

$$\tau_C^{-1} = \tau_S^{-1} + \tau_R^{-1} \qquad \{7\text{-}6\}$$

where τ_R is the thallium(I)- paramagnetic complex reorientational correlation time. The above equations were derived for the case of water ^1H relaxation in an aqueous solution of a paramagnetic metal ion; in this case x is the mole fraction of water in the first coordination sphere of an ion. In the case of a Tl(I) ion-paramagnetic complex, x will be the fraction of complexed thallium(I) ions.

In the absence of complex formation any dipole-dipole relaxation must be intermolecular in nature. This mechanism has been described theoretically by Abragam[53]; the relaxation rates R_1 and R_2 are given in S.I. units by the expressions

$$R_{1\ DD} = \tfrac{1}{2}\left(\frac{\mu_o}{4\pi}\right)^2 \gamma_I^2 \gamma_S^2 \hbar^2 S(S+1) \left[3J(\omega_I) + 7J(\omega_S)\right] \qquad \{7\text{-}7A\}$$

$$R_{2\ DD} = \tfrac{1}{2}\left(\frac{\mu_o}{4\pi}\right)^2 \gamma_I^2 \gamma_S^2 \hbar^2 S(S+1) \left[2J(0) + \frac{3}{2} J(\omega_I) + \frac{13}{2} J(\omega_S)\right], \qquad \{7\text{-}7B\}$$

where ω_I and ω_S are the nuclear and electronic resonance frequencies, and S is the spin quantum number of the paramagnetic. The spectral density functions $J(\omega)$ have been evaluated by Pfeiffer[54],

$$J(\omega)= \frac{8\pi N_S \tau_S^2}{45\, d^3 \tau_D (1+\omega^2\tau_S^2)} \left[\frac{2}{3}(V^2-U^2) + \frac{3U^2V-V^3}{U^2+V^2} \right.$$

$$+ \frac{5U^4V-10U^2V^3+V^5}{(U^2+V^2)^3} + \exp(-2V) \left[\frac{(3UV^2-U^3)\sin 2U + (3U^2V-V^3)\cos 2U}{U^2+V^2} \right.$$

$$+ \frac{(8UV^3-8U^3V)\sin 2U - (2U^4-12U^2V^2+2V^4)\cos 2U}{(U^2+V^2)^3}$$

$$\left. + \frac{(U^5-10U^3V^2+5UV^4)\sin 2U - (5U^4V-10U^2V^3+V^5)\cos 2U}{(U^2+V^2)^3} \right] \left. \right] \qquad \{7-8\}$$

where N_S is the number of S spin per cm^3, d is the distance of closest approach of I and S, τ_S is the electron spin-lattice relaxation time, and τ_D is the translational correlation time. This is defined in terms of the translational diffusion coefficients of the molecules carrying the spins I and S, as

$$\tau_D = \frac{d^2}{3(D_I + D_S)} \qquad \{7-9\}$$

Finally U and V are defined as

$$U = \left(\frac{3\tau_D}{2\tau_S} \left(1 + \omega^2\tau_S^2 - 1 \right)^{\frac{1}{2}} \right)^{\frac{1}{2}} \qquad \{7-10A\}$$

$$V = \left(\frac{3\tau_D}{2\tau_S} \left(1 + \omega^2\tau_S^2 + 1 \right)^{\frac{1}{2}} \right)^{\frac{1}{2}} \qquad \{7-10B\}$$

These complicated looking expressions describe many important features of this mechanism. The observed rates are proportional to the concentration of paramagnetic, i.e. N_S. This interaction may be modulated by electron spin relaxation or by the relative diffusion of I and S. The mechanism is dependent upon spectral densities at zero, nuclear, and electronic resonance frequencies

and the latter may be outside extreme narrowing. However, if the electronic relaxation is relatively slow then $\omega_S\tau_S << 1$ and the extreme narrowing criterion is valid. In this limit the intermolecular dipole-dipole relaxation may be more simply described. Equations that are more manageable than equation 7 - 8 have been given by Abragam[53] and Kivelson et al.[55]

7.3.3. Electron-Nuclear Scalar Relaxation.

The electron-nuclear scalar (or contact hyperfine) interaction can lead to nuclear spin relaxation if there is finite unpaired electron spin density at the observed nucleus. The coupling constant in rad s^{-1} is given by the expression[56]

$$A(r) = \frac{8\pi\hbar}{3} |\gamma_I||\gamma_S||\Psi(r)|^2, \qquad \{7 - 11\}$$

where $\Psi(r)$ is the probability of finding an unpaired electron at the nucleus when the separation of the nucleus and the centre of the paramagnetic species is r. It is a theoretical simplification to consider the distance dependence of A(r) as a switch function[57], i.e. for some critical distance R_o,

$$A(r) = A \quad \text{for} \quad |r| \leqslant R_o , \qquad \{7 - 12A\}$$

$$A(r) = 0 \quad \text{for} \quad |r| > R_o . \qquad \{7 - 12B\}$$

The nuclear relaxation rates due to the scalar interaction have been described by Bloembergen[52], Abragam[53] and Hertz[57],

$$R_{1\ SC} = \frac{2}{3}\ S(S+1)A^2 \times \left[\frac{\tau_{SC2}}{1 + (\omega_I-\omega_S)^2\tau_{SC2}^2}\right], \qquad \{7 - 13A\}$$

$$R_{2\ SC} = \frac{1}{3}\ S(S+1)A^2 \times \left[\tau_{SC1} + \frac{\tau_{SC2}}{1 + (\omega_I-\omega_S)^2\tau_{SC2}^2}\right] \qquad \{7 - 13B\}$$

Here x is the fraction of the observed nuclear spins experiencing the scalar interaction. Both translational modulation of A(r) and electron spin relaxation can modulate the scalar interaction. Hausser and Noack[58] have considered both contributions and if the electronic relaxation times τ_{S1} and τ_{S2} are different then the scalar correlation times are given as

$$\tau_{SC1,2}^{-1} = \tau_A^{-1} + \tau_{S1,2}^{-1} \quad . \qquad \{7 - 14\}$$

Thus it is the faster of the two modulating processes that controls the scalar relaxation mechanism.

It is proposed that the dominant relaxation mechanism for both ^{205}Tl spin-lattice and spin-spin relaxation in solutions of paramagnetics is the scalar mechanism for which there is strong evidence.

The proton relaxation in the water-oxygen system has been studied by Hausser and Noack[58], as a function of oxygen pressure (10^{-2} to 200 atm), proton resonance frequency (0.45 to 160 MHz) and temperature ($20^{o}C$ to $300^{o}C$). The dominant relaxation mechanism is the intermolecular electron-nuclear dipole-dipole mechanism. The data obtained were analysed using equations 7-7 and 7-10. The proton R_1 and R_2 were found to be linearly related to the oxygen pressure, the ration R_2/R_1 was found to tend to 7/6 at high oxygen pressure at 28 MHz. The observed relaxation rates were field dependent, and at an oxygen pressure of 21 atm and a temperature of $25^{o}C$, R_1 varied from a low field limit of approximately 8.9 s^{-1} to a high field

limit of approximately 2.7 s^{-1}.

The above work is of considerable interest in relation to the thallium(I)-oxygen system in aqueous solution. Since an effective molecular radius of 1.4 Å was used for H_2O by Hausser and Noack, and since this equals the ionic radius of the thallium(I) ion, then to a good approximation once can take the intermolecular dipole-dipole spectral density functions for the water-oxygen and thallium(I) ion-oxygen systems to be the same. If this is the case then the oxygen contribution to the ^{205}Tl R_1 due to the intermolecular dipole-dipole mechanism can be calculated quite easily. At a proton frequency of 21.89 MHz, oxygen pressure of 21 atm and 25°C the observed proton R_1 is about 7.1 s^{-1} and the oxygen induced contribution is 6.8 s^{-1}. Using equation 7.7 with a ratio $\{\gamma(^1H)/\gamma(^{205}Tl)\}^2 = 2.99$ and scaling to an oxygen partial pressure of 0.2 atm, the calculated contribution to the ^{205}Tl R_1 is 0.02 s^{-1}. This is completely negligible in comparison to the observed rate of 6.98 s^{-1} to be presented in the next section, and hence the intermolecular dipole-dipole mechanism can be safety neglected.

Further information on the relative importance of the dipolar and scalar mechanisms can be obtained from an electron-nuclear double resonance (ENDOR) experiment, where the intensity of the nuclear resonance is observed whilst irradiating the electron resonance.

This phenomenon is analogous to the nuclear Overhauser effect discussed by Noggle and Schirmer[59]

who considered a system of two weakly coupled spins with $I = S = \frac{1}{2}$. An enhancement of the intensity of the I resonance, from I_0 to I_z, can occur upon saturation of the S resonance if cross relaxation occurs between the two spins. Three relaxation mechanisms can give rise to cross relaxation effects. These are,

1. The I - S dipolar mechanism,
2. Scalar mechanism with interaction A $\hat{\underline{I}}\cdot\hat{\underline{S}}$ modulated by the time dependence of A (scalar relaxation of the first kind),
3. Scalar mechanism with interaction A $\hat{\underline{I}}\cdot\hat{\underline{S}}$ modulated by the time dependence of $\underline{S}$. (scalar relaxation of the second kind).

The signal enhancement factor of the NMR signal is defined as:

$$\eta = \frac{I_z - I_0}{I_o} \quad . \qquad \{ 7 - 15 \}$$

The enhancements produced in the ENDOR experiment, differ according to which of the above mechanisms dominates the nuclear spin lattice relaxation[53]. Under conditions of complete saturation of the S resonance, assuming that the dipolar mechanism is within the extreme narrowing region and that for scalar relaxation of the second kind

$$1/\tau_{S1} = 1/\tau_{S2} >> \omega_I, \omega_S,$$

the maximum enhancements achievable in the Endor experiment are given as:

$$\eta = \frac{-|\gamma_S|}{2\gamma_I} \quad \text{dipolar} \qquad \{7 - 16A\}$$

$$\eta = \frac{+|\gamma_S|}{\gamma_I} \quad \text{scalar 1st kind} \qquad \{7 - 16B\}$$

$$\eta = \frac{+|\gamma_S|}{2\gamma_I} \quad \text{scalar 2nd kind} \qquad \{7 - 16C\}$$

The Endor enhancements are a direct measure of which mechanism dominates the nuclear relaxation process. Since $|\gamma_S| >> |\gamma_I|$ then for a nucleus with positive $\gamma(^{205}Tl)$ the dipolar mechanism will lead to large negative enhancements, whereas the scalar mechanism should give large positive enhancements.

Conclusive evidence for the dominance of the scalar mechanism for ^{205}Tl relaxation in the presence of paramagnetics has been provided by Dwek et al.[60], who reported preliminary ^{205}Tl ENDOR enhancement measurements for thallium(I) acetate in methanol; thallium(I) nitrate in acetone, and diethylthallium(III) chloride in pyridine, each in the presence of galvinoxyl and tri-tertiarybutylphenoxyl (TTBP) radicals. In every case the enhancements were positive and were much greater for the thallium(I) than the diethylthallium(III) compound. Further, the broadening effects were much greater for the thallium(I) species. An enhancement of +600 was reported for thallium(I) acetate with TTBP in methanol. The value of +600 when considered with the value for $|\gamma_S|/\gamma_I$ of 1140 for ^{205}Tl is strongly indicative of scalar relaxation of the second kind (cf.equation 7 - 16C).

These important measurements appear to have been overlooked since their original publication.

Significant unpaired electron density can be achieved at the nuclear site even in the absence of long lived complexes by charge transfer and exchange polarisation mechanisms during radical-receptor molecule collisions.[61] Charge transfer may occur if the unpaired electron orbital has a higher energy than an unoccupied orbital in the receptor molecule. Partial electron donation may then take place. Exchange polarisation is the partial unpairing of an electron in a receptor molecule as it attempts to pair with the radical electron. These mechanisms may be invoked to explain how thallium(I) compounds are more strongly affected by radicals than dialkylthallium(III) compounds.[44,60] In the former the unpaired electron spin density may be transmitted to the ^{205}Tl nucleus via the $6S^2$ electrons; this orbital has a large probability density at the nucleus and hence produces a large scalar coupling constant. This scheme has been previously put forward by Bangerter.[47] In dialkylthallium(III) compounds the $6S^2$ electron pair is not present and other, less suitable, orbitals must be used for the scalar coupling process. Relative electron spin densities induced at the receptor nucleus by intermolecular coupling with free radicals have been calculated by Dwek et al.[62], and indicate a value for a thallium nucleus which is 575 times that for a hydrogen. Thus, on this basis, large intermolecular scalar couplings between the ^{205}Tl nucleus and unpaired electrons are highly likely.

Section 7.4 ^{205}Tl Relaxation in the Tl(I)-oxygen system in aqueous solution.

7.4.1 Measurements.

In the previous section it was proposed that the dominant ^{205}Tl relaxation mechanism for the thallium(I) ion in solutions containing paramagnetic species is the electron-nuclear scalar coupling mechanism. Observation of the frequency and temperature dependence of the ^{205}Tl relaxation in such a system allow further insight as to the nature of the scalar coupling mechanism and the parameters that control it. Therefore, using a sample of 1.47 M thallium(I) acetate in D_2O in equilibrium with a 0.2 atmospheres partial pressure of oxygen, the ^{205}Tl spin lattice relaxation rate has been measured as a function of temperature at 21.89 and 230.8 MHz. In addition the ^{205}Tl R_2 has been measured at two temperatures at 230.8 MHz, using the phase alternated Hahn spin echo pulse sequence. Sample temperatures at both fields were obtained using a solution of dimethylthallium(III) nitrate in D_2O contained in a concentric tube. Finally measurements of $R_{1\rho}$ the ^{205}Tl spin lattice relaxation rate in the rotating frame, have been performed at 230.8 MHz using selective excitation by means of the Dante pulse sequence described in Chapter Three.[63]

These selective excitation experiments were intended as a feasibility study for later measurements of the relaxation properties of the dimethylthallium(III) cation. Therefore only two measurements of $R_{1\rho}$ were performed, both at an instrument set temperature of 306K.

In this case the sample was 1.16M thallium(I) acetate in D_2O, again in equilibrium with oxygen at 0.2 atmospheres partial pressure.

The observed ^{205}Tl relaxation rates are shown in Tables 7.2 and 7.3.

Temperature (K)	^{205}Tl $R_1(s^{-1})$	Temperature (K)	^{205}Tl $R_1(s^{-1})$
283.8	7.41	319.6	6.86
295.7	6.92	332.3	6.12 [a]
297.2	6.92	344.1	5.00 [a]
300.3	7.05	ambient	5.39 [b]
306.4	7.09	ambient	6.61 [c]
313.0	6.96		

a) Rates time dependent, presumably through loss of oxygen, see text.
b) Ambient temperature is approximately 298K, measurement immediately after high temperature experiment.
c) After b) sample exposed to air for 2 hrs. before measurement.

Table 7 - 2. Temperature dependence of ^{205}Tl R_1 of 1.47M Tl $OCOCH_3/D_2O$ at 21.89 MHz.

Temperature (K)	R_1 (s^{-1})	$R_2(s^{-1})$	$R_{1\rho}(s^{-1})$
295.7	1.87	18.8	-
306 [a]	-	-	12.9
306 [a]	-	-	11.8
314.8	1.90	14.5	-
324.2	1.78	-	-

a) Instrument set temperature (all others by ^{205}Tl shift method)

Table 7 - 3 ^{205}Tl relaxation rates for 1.47M Tl $OCOCH_3/D_2O$ at 230.8 MHz.

The data obtained during or after the high temperature run (a,b,c in Table 7 - 2) are less reliable since the rates were decreasing with time presumably through progressive loss of oxygen. This is consistent with the observation of the reduced rate of 5.39 s^{-1} at ambient temperatures recorded immediately after the high temperature measurements, a value which increased with time to a value of 6.61 s^{-1} close to those previously observed.

The data at 21.89 MHz are shown in Figure 7 - 1 the straight line represents the mean value of all the rates except those at the two highest temperatures and the anomalous point at ambient temperature discussed previously. The data at 230.8 MHz were insufficient to warrant plotting.

The R_1 values are seen to be independent of temperature within experimental error at both frequencies over the range 10 to 50°C. The two R_2 values obtained at 231 MHz indicate a decrease with increased temperature.

7.4.2 Discussion of temperature and frequency dependence.

The observation of temperature independent R_1 values at two frequencies and the indication of decreasing R_2 values with increasing temperature are consistent with the results of Bangerter and Schwartz[46] for the Tl(I) ion in the presence of the TANOL radical. This indicates a common relaxation mechanism. The

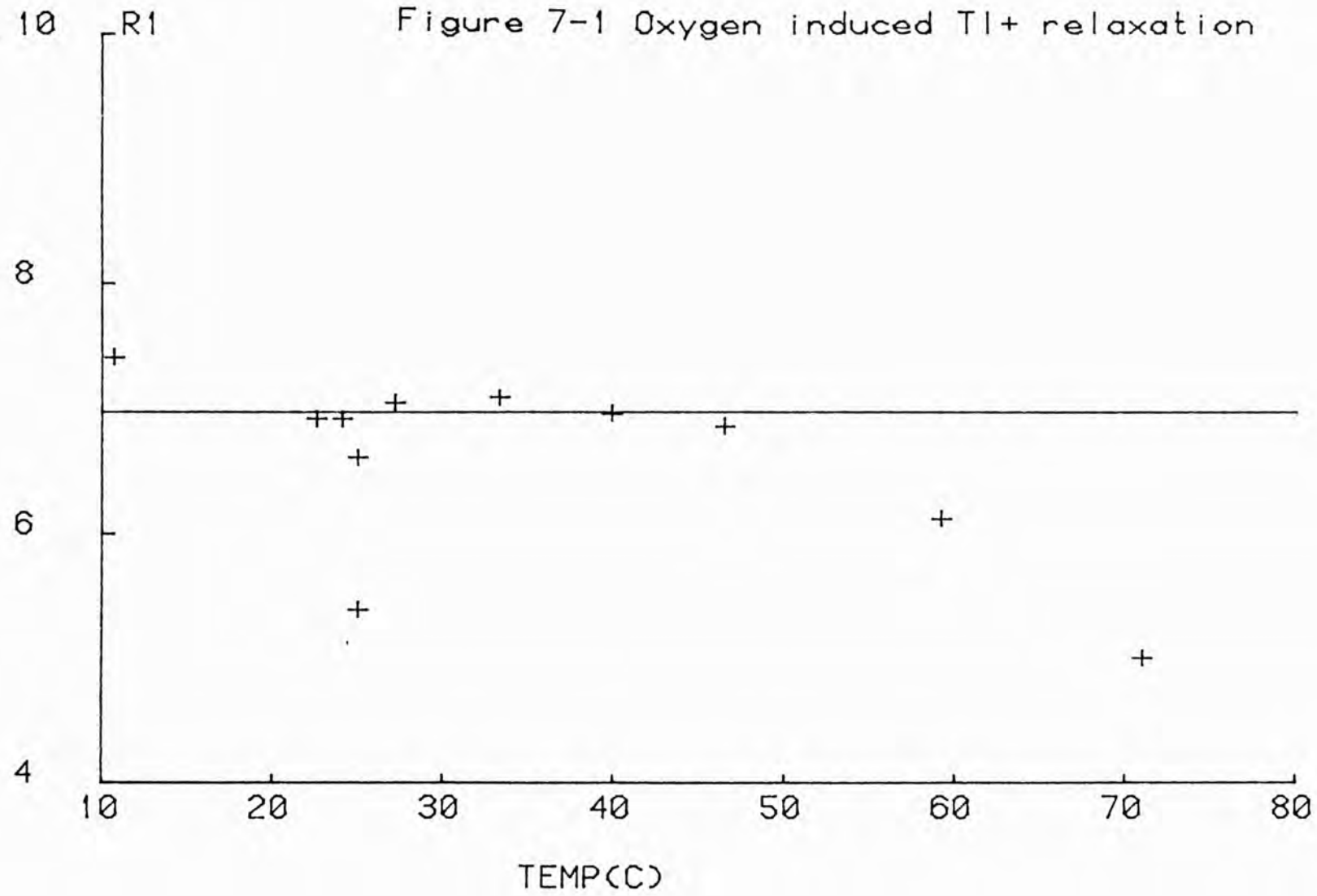

Figure 7-1 Oxygen induced Tl+ relaxation

differing temperature dependencies of R_1 and R_2 may be qualitatively explained in terms of the scalar coupling mechanism. If the lifetime of the Tl(I) ion-oxygen 'complex' is long in relation to the electronic relaxation times, then equation 7 - 14 shows that the correlation times for the scalar interaction are equal to the electronic relaxation times. Thus the scalar correlation times and hence the scalar relaxation rates, may have differing temperature dependencies if those of τ_{S1} and τ_{S2} are different. These observations imply that τ_{S2} is temperature independent whereas τ_{S1} must decrease with increasing temperature, but since the electronic relaxation mechanisms are unknown for TANOL and O_2 it is not possible to confirm these predictions.

The data reported here include measurements at 21.89 and 230.8 MHz and $T_{1\rho}$ measurements presented in Table 7 - 3 provide data at essentially zero frequency. It is now possible to consider results obtained by previous workers at other frequencies in order to gain insight into the overall frequency dependence. Both Bangerter[47] and Reeves[43,44] have performed single temperature ^{205}Tl relaxation measurements with variable oxygen pressures. Thus for the purposes of comparison, relaxation rates scaled to an oxygen partial pressure of 0.2 atmospheres may be calculated, and are presented in Table 7 - 4 along with the measurements performed here.

It should be noted that the data in

Table 7 - 4 represent various concentrations of Tl(I) ion but that measurements by Reeves[43,44] indicate no significant variation in R_1 or R_2 in changing the thallium concentration from 0.08M to 2.0M, with a fixed oxygen partial pressure. The rotating frame relaxation rates represent spin lattice relaxation in a magnetic field equal in magnitude to the spin locking field, and since this is of the order of 100 Hz it is effectively a zero field relaxation measurement performed on a high field instrument.

$\nu_o(^{205}Tl)$MHz	ω_s(rad s^{-1})	Temperature (K)	$R_1(^{205}Tl)$	$R_{1\ SC}$	$R_2(^{205}Tl)$	$R_{2\ SC}$	$R'_{2\ SC}$
3.37×10^{-5}	2.48×10^{5}	306	11.8	11.5	-	-	-
2.08×10^{-4}	1.49×10^{6}	306	12.9	12.3	-	-	-
15.1	1.08×10^{11}	299.0	7.80	7.23	7.80	7.23	3.61
21.89	1.57×10^{11}	297.5	6.98	6.41	-	-	-
51.75	3.71×10^{11}	unknown	2.41	1.84	9.35	8.78	7.86
230.8	1.65×10^{12}	295.9	1.87	1.30	18.8	18.2	17.5

Table 7 - 4 Frequency dependence of ^{205}Tl relaxation in O_2/Tl^+ system in aqueous solution. All rates in inverse seconds.

$R_{2\ SC}$ and $R_{1\ SC}$ are scalar relaxation rates induced by the presence of paramagnetic O_2. These rates are calculated by subtracting a spin rotational rate of 0.57 s^{-1} in accordance with equation 6 - 4. This is the average of the values measured by Bangerter[47] and Reeves[43].

From equation 7 - 13 it follows that a relaxation rate $R'_{2\ SC}$ may be written as

$$R'_{2\ SC} = R_{2\ SC} - \tfrac{1}{2}R_{1\ SC} = \frac{1}{3} S(S+1)A^2 x \tau_{SC1} . \quad \{7 - 17\}$$

The observed values of $R_{1\ SC}$ and $R_{2\ SC}$ are field dependent. $R_{1\ SC}$ decreases steadily with increasing field, whereas $R_{2\ SC}$ increases.

As discussed in Chapter Two, the nuclear-nuclear scalar coupling mechanism rarely contributes to the nuclear R_1 because typically $\Delta\omega\tau_{SC} >> 1$. The presence of this term in the denominator of the rate expression strongly impairs the efficiency of this mechanism. However the electronically induced mechanism should be more efficient, due to a greatly increased scalar coupling constant and also because electronic relaxation times are typically several orders of magnitude less than their nuclear counterparts.

The form of equations 7 - 13 suggests that $R_{1\ SC}$ and $R_{2\ SC}$ should decrease with increasing field, for $R_{1\ SC}$ this is as observed, but for $R_{2\ SC}$ the opposite behaviour is found.

The differing field dependencies of $R_{1\ SC}$ and $R_{2\ SC}$ must arise from the dependence of these rates on different correlation times, as shown in equations 7 - 13. The rate $R_{1\ SC}$ is controlled by τ_{SC2} alone, whereas $R_{2\ SC}$ is controlled by τ_{SC2} and τ_{SC1}. In order for τ_{SC1} and τ_{SC2} to differ it is necessary for any Tl(I)-paramagnetic complex formed to be long lived in relation to the electronic relaxation times, since in the limit of short lived complexes equation 7 - 14 yields $\tau_{SC1} = \tau_{SC2} = \tau_A$. The rate term $R'_{2\ SC}$ defined in equation 7 - 17 measures the secular portion of $R_{2\ SC}$ which is the zero quantum

spectral density term and reflects the effect of τ_{SC1} alone on the ^{205}Tl linewidth (R_2). Since $R'_{2\ SC}$ increases with increasing field as shown in Table 7 - 4 it follows that τ_{SC1} is increasing similarly. Hausser and Noack[58], however, did not discuss any frequency dependence of τ_{S1}. The present theory identifies τ_{SC1} as equal to τ_{S1} and τ_{SC2} as equal to τ_{S2}, hence the R'_{2SC} data imply that τ_{S1} increases with frequency. The rate $R_{2\ SC}$ consists of secular and non secular terms with differing dependencies on frequency.

7.4.3 Estimation of Electronic Relaxation Times.

If the electron-nuclear scalar mechanism dominates the ^{205}Tl relaxation the frequency dependence of $R_{1\ SC}$ should follow that of equation 7 - 13A. The discussion presented thus far has shown that this is qualitatively correct. The decrease of $R_{1\ SC}$ with increasing frequency implies that $\Delta\omega\tau_{SC} < 1$ in the low frequency region and $\Delta\omega\tau_{SC} > 1$ in the high frequency region. Thus at the higher frequencies the modulating process, which is electronic spin-spin relaxation may be described as being outside the extreme narrowing region. Thus by analogy with the ^{205}Tl relaxation study of the dimethylthallium(III) cation in aqueous glycerol, it should be possible to separate the interaction and modulation terms that control nuclear spin relaxation.

In order to try to obtain quantitative information a non linear least squares fit of the $R_{1\ SC}$ data in Table 7 - 4 to equation 7 - 13A has been performed,

using τ_{S2} and $\frac{2}{3} S(S+1)A^2x$ as variable parameters. The following best fit values were obtained,

$$\tau_{S2} = (6.4 \pm 0.8) \times 10^{-12} \text{ s} \quad , \qquad \{7 - 18A\}$$

$$\frac{2}{3} S(S+1)A^2x = (1.8 \pm 0.2) \times 10^{12} \text{rad}^2\text{s}^{-2} \qquad \{7 - 18B\}$$

The Lorentzian curve generated by these parameters and the observed data points are shown in diagram 7 - 2. It is seen that the fit is good for all points except that at the highest frequency, where the observed R_1 is much greater than expected. It is possible that there is a relaxation contribution due to a mechanism other than scalar relaxation which becomes relatively more efficient as R_{1SC} decreases.

Substitution of equation 7 - 18B into equation 7 - 17 enables the calculation of the electronic relaxation time τ_{S1} ($= \tau_{SC1}$), values of which are shown in Table 7 -5.

$\nu_o(^{205}\text{Tl})$MHz	$R'_{2SC}(s^{-1})$	τ_{S1}(ps)
15.1	3.61	4.0
51.75	7.86	8.7
230.8	17.5	19.4

Table 7 - 5. Estimated electronic spin-lattice relaxation times as a function of frequency.

These values compare favourably with the value of 10 ps obtained by Hausser and Noack[58] for molecular oxygen in water at 25°C from studies of ^{1}H relaxation, although no

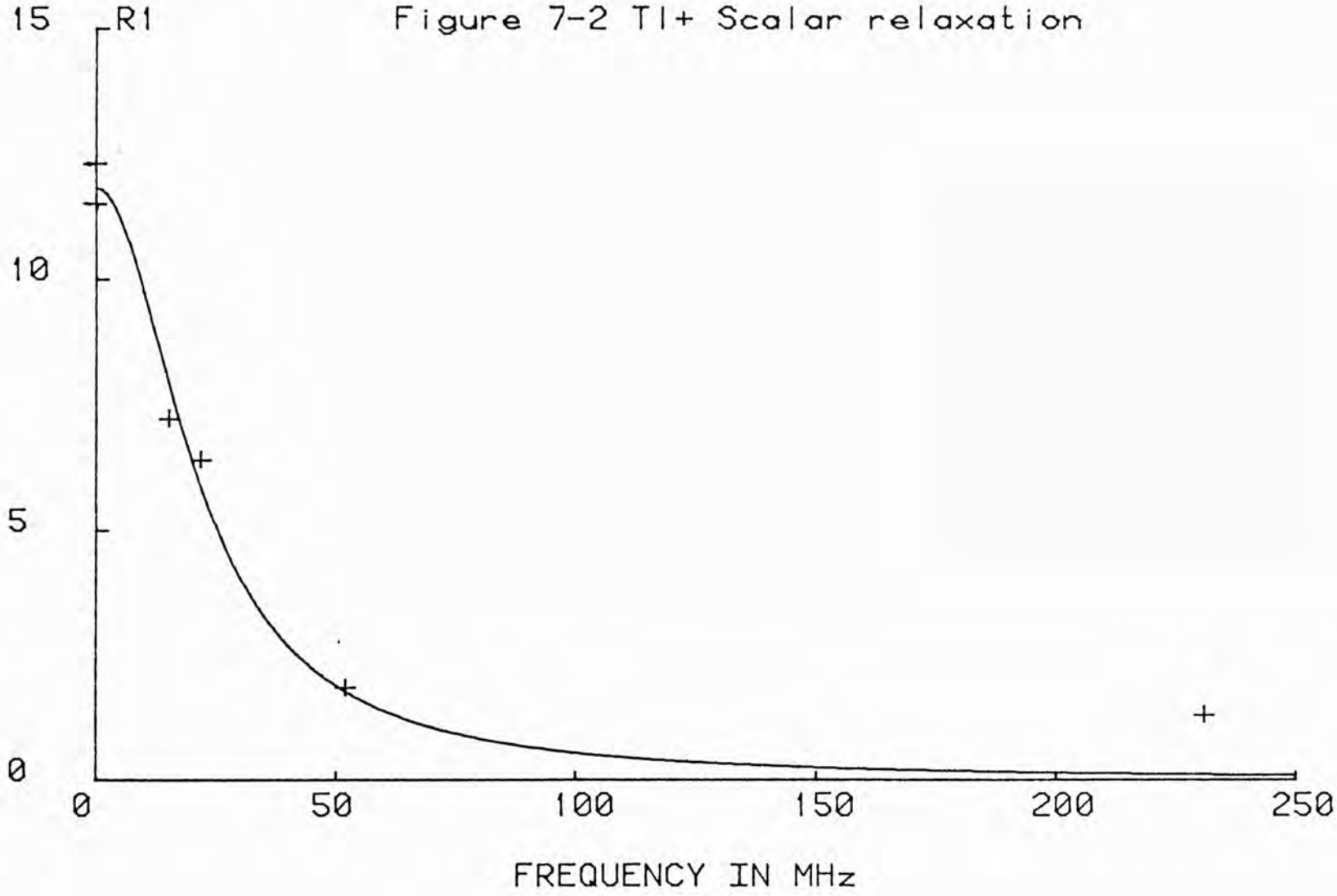

Figure 7-2 Tl+ Scalar relaxation

frequency dependence was reported. The frequency dependence of τ_{S1} contrasts with the (assumed) frequency independent value of 6.4 ps obtained for τ_{S2}.

It should be borne in mind that in the derivation of equations 7 - 13 it was assumed that the electron relaxation times which modulate the scalar interaction are much longer than the time characterising molecular reorientation[53], a condition that may well be violated here. Further more detailed measurements might provide a basis for a better understanding of the electron relaxation mechanisms.

Estimation of the electron-nuclear scalar coupling requires a knowledge of x, the fraction of Tl(I) ions experiencing a scalar interaction at any instant, and since there is no reliable estimate of this factor the magnitude of the scalar coupling constant remains unknown.

7.4.4. Electronic Relaxation and Effects on ^{205}Tl shift.

The mechanism of electronic relaxation of both nitroxide radicals and molecular oxygen are not completely understood. Percival and Hyde[64] have performed saturation recovery electronic spin-lattice relaxation studies of some simple nitroxides, including TANOL, in an organic solvent. Dominance of the spin rotation mechanism was suggested at high temperature, but at low temperatures the relaxation is faster than predicted by known mechanisms and the dominant mechanism

in this region remains unknown. Schwartz and Stillman[65] have noted that Heisenberg electronic exchange interactions may dominate the EPR lineshape of nitroxide radicals in solution and have discussed the extraction of the exchange frequency from these spectra. Strong Heisenberg exchange between nitroxide radicals and molecular oxygen has been found by Hyde et al. to take place in lipid bilayers[66].

The gas phase EPR spectrum of O_2 is well resolved at low pressures, but rapidly broadens with increasing pressure and has no fine structure at atmospheric pressure[67,68]. This suggests dominant Heisenberg exchange broadening of the electronic resonance, a process which should become more efficient with an increasing rate of collisions and hence pressure. Gardiner et al.[69] have carefully studied this collisional linewidth for 16 lines in the X-band of the EPR spectrum of molecular oxygen. There is a remarkable variation with pressure over the range 0.5 to 2.3 Torr.

The electron τ_{S1} of 10^{-11}S in aqueous solution found by Hausser and Noack[58], implies that the EPR spectrum will be unobservable under these conditions. Hence no direct EPR relaxation studies have been made for this species.

The ^{17}O NMR signal in liquid oxygen has been observed by Dundon[70] at 77K and an ^{17}O frequency of 5.99 MHz (0.822T). An ^{17}O linewidth of 44 $\pm$ 3 KHz ($7.1 \pm 0.5 \times 10^{-3}$T) was obtained. It was suggested

that the ^{17}O relaxation is dominated by a scalar hyperfine interaction modulated by electronic relaxation due to electronic Heisenberg exchange.

Other possible electronic relaxation mechanisms to be considered include modulation of the anisotropic hyperfine and electronic g tensors by molecular reorientation. The latter process is the electronic equivalent of CSA relaxation. Since the ground electronic state of molecular oxygen is a triplet state (labelled $^3\Sigma$), in which the two electronic spins are parallel, it is possible for a strong zero field splitting to exist between the two electrons.(56) This interaction is so named because the electron-electron dipolar interaction lifts the degeneracy of the triplet wave functions even in zero field, in transition metal complexes with triplet ground states this interaction arises from spin orbit coupling rather than a dipolar interaction. Modulation of this interaction typically leads to very fast relaxation for triplet radicals or ions.

It is clear that the mechanism of electronic relaxation has a direct effect on the observed ^{205}Tl relaxation behaviour in systems containing paramagnetics. Since these mechanisms are not well understood, especially for O_2, then it follows that ^{205}Tl relaxation has considerable utility as a probe for electronic relaxation which is not easy to study directly.

The electronic spin-lattice relaxation rates are fast in relation to the inverse of scalar

couplings constants and hence no scalar hyperfine coupling is resolved in NMR spectra. The nucleus experiences a field proportional to the mean of the Z component of the electronic spin operator $\langle S_Z \rangle$. This is non zero because the α and β electronic spin states have appreciably different populations. This leads to a paramagnetically induced shift called the contact shift.[56] Often this shift, expressed in field units B, is proportional to the applied field[71] in field independent units,

$$\frac{\Delta B}{B} = \frac{xA\langle S_Z \rangle}{\gamma_I \hbar} = - \frac{\gamma_S \times A \, S(S+1)}{\gamma_I \, 3 \, k T} \quad \{7 - 19\}$$

Thus the contact shift is to high frequency (low field) if A is positive, and should shift to low frequency with increasing temperature. The dominance of the ^{205}Tl relaxation by the scalar mechanism implies that a ^{205}Tl contact shift should be present.

A detailed study of the Tl(I) shift in oxygenated vs degassed solutions would be required to enable a determination of the hyperfine coupling constant, A, and the mole fraction of complexed species x from equation 7 - 13A which gives A^2x and equation 7 - 19 which gives Ax.

REFERENCES. CHAPTER SEVEN

1. R.P.H.Gasser and R.E.Richards, Mol.Phys. 2, 357 (1959).
2. R.Freeman, R.P.H.Gasser, R.E.Richards and D.H. Wheeler, Mol.Phys. 2, 75 (1959).
3. E.B.Baker and L.W.Burd, Rev.Sci.Instr., 34, 238 (1968).
4. R.E.Sheriff and D.Williams, Phys.Rev. 82, 651 (1951).
5. H.L.Poss, Phys.Rev., 72, 637 (1947).
6. H.L.Poss, Phys.Rev., 75, 600 (1949).
7. W.G.Proctor, Phys.Rev., 75, 522 (1949).
8. H.S.Gutowsky and B.R.McGarvey, Phys.Rev., 91, 81 (1953).
9. D.Herbison-Evans and B.R.McGarvey, J.Chem.Soc., 6170 (1965).
10. R.Freeman, R.P.H.Gasser and R.E.Richards, Mol.Phys., 2, 301 (1959).
11. R.W.Vaughan and D.H.Anderson, J.Chem.Phys., 52, 5287 (1970).
12. S.Hafner and N.H.Nachtrieb, J.Chem.Phys., 42, 631 (1965).
13. N.H.Nachtrieb and R.K.Momii, in Reactive Solids Proc. 6th Wt. Symp. (Ed.J.W.Mitchell) Wiley, New York, 675 (1969).
14. H.Köppel, J.Dallorso, G.Hoffmann and B.Walther, Z.Anorg.Allgem.Chem.,427, 24 (1976).
15. J.J.Dechter and J.I.Zink, Inorg.Chem., 15, 1690 (1976).

16. J.J.Dechter and J.I.Zink, J.Amer.Chem.Soc., 97, 2937 (1975).

17. J.J.Dechter and J.I.Zink, J.Chem.Soc.Chem.Comm., 96 (1974).

18. J.F.Hinton and R.W.Briggs, J.Magn.Reson., 19, 393 (1975).

19. J.J.Dechter and J.I.Zink, J.Amer.Chem.Soc., 98, 845 (1976).

20. J.F.Hinton and R.W.Briggs, J.Magn.Reson., 25, 379 (1979).

21. J.J.Dechter, Diss.Abstr.Int.B. 36, 3944 (1976).

22. R.W.Briggs, K.R.Metz and J.F.Hinton, J.Solution Chem., 8, 479 (1979).

23. J.F.Hinton and K.R.Metz, J.Solution Chem., 9, 197 (1980).

24. R.W.Briggs and J.F.Hinton, J.Solution Chem., 6, 827 (1977).

25. A.K.Covinton, T.H.Lilley, K.E.Newman and G.A. Porthouse, J.Chem.Soc., Faraday I, 963 (1973).

26. A.K.Covington and J.M.Thain, J.Chem.Soc., Faraday I, 1879 (1974).

27. F.J.Kayne and J.Reuben, J.Amer.Chem.Soc., 92, 220 (1970).

28. F.J.Kayne and J.Reuben, J.Amer.Chem.Soc., 246, 6227 (1971).

29. C.Srivanavit, J.I.Zink and J.J.Dechter, J.Amer. Chem.Soc., 99, 5876 (1977).

30. M.Shamispur, G.Rounaghi and A.Popov, J.Solution Chem., 9, 701 (1980).

31. D.Gudlin and H.Schneider, Inorg.Chim.Acta., 33, 205 (1979).

32. R.W.Briggs, F.A.Etzkorn and J.F.Hinton, J.Magn.Reson., 37, 523 (1980).

33. R.W.Briggs and J.F.Hinton, J.Magn.Reson., 32, 155 (1978).

34. R.W.Briggs and J.F.Hinton, Biochemistry 17, 5576 (1978).

35. R.W.Briggs and J.F.Hinton, J.Magn.Reson., 33, 363 (1979).

36. J.J.Dechter, NMR of Metal Nuclides, Prog.Inorg. Chem., 29, 285 (1982).

37. J.F.Hinton, K.R.Metz and F.S.Millet, J.Magn.Reson., 44, 217 (1981).

38. J.F.Hinton, G.L.Turner and F.S.Millet, J.Magn. Reson., 45, 42 (1981).

39. J.F.Hinton, G.Young and F.S.Millet, Biochemistry, 21, 646 (1982).

40. J.F.Hinton, G.Young and F.S.Millet, Biochemistry, 21, 651 (1982).

41. J.F.Hinton, G.L.Turner and F.S.Millet, J.Magn. Reson., 51, 205 (1983).

42. R.P.H.Gasser and R.E.Richards, Mol.Phys., 2, 357 (1959).

43. M.Bacon and L.W.Reeves, J.Amer.Chem.Soc., 95, 272 (1973).

44. S.O.Chan and L.W.Reeves, J.Amer.Chem.Soc., 96, 404 (1974).

45. R.N. Schwartz, J.Magn.Reson., 24, 205 (1976).

46. B.W.Bangerter and R.N.Schwartz, J.Chem. Phys., 60, 333 (1974).

47. B.W.Bangerter, J.Magn.Reson., 28, 141 (1977).

48. J.F.Hinton, and K.N.Ladner, J.Magn.Reson., 32, 303 (1978).

49. J.F.Hinton, K.R.Metz and R.W.Briggs, Ann.Rep. NMR Spectry., 13, 211 (1983).

50. J.F.Hinton and R.W.Briggs, NMR and the Periodic Table, p.288, Editors R.K.Harris and B.Mann.

51. I.Solomon, Phys.Rev., 99, 559 (1955).

52. N.Bloembergen, J.Chem.Phys., 27, 572 (1957).

53. A.Abragam, The Principles of Nuclear Magnetism. Oxford University Press. (1961).

54. H.Pfeiffer, Ann.Phys., Liepzig, 8, 1 (1961).

55. B.Berne and D.Kivelson, J.Chem.Phys., 83, 1401 (1979).

56. A.Carrington and A.D.McLachlan, Introduction to Magnetic Resonance. Harper and Row. (1967).

57. H.G.Hertz in 'Water a Comprehensive Treatise', 4, 301 (1973) Plenum Press.

58. R.Hausser and F.Noack, Z.Naturforsch, 20A, 1668 (1965).

59. J.H.Noggle and R.E.Schirmer, The Nuclear Overhauser Effect. Academic Press. (1971).

60. R.A.Dwek, R.E.Richards and D.Taylor, Ann.Rev. NMR Spectry., 2, 293 (1969).

61. R.L.Glazer and E.H.Pointdexter, J.Chem.Phys., 55, 4548 (1971).

62. R.A.Dwek, Adv.Mol.Relax.Processes, 4, 1 (1972).

63. G.A.Morris and R.Freeman, J.Magn.Reson., 29, 433 (1978).

64. P.W.Percival and J.S.Hyde, J.Magn.Reson., 23, 249 (1976).

65. A.E.Stillman and R.N.Schwartz, J.Magn.Reson., 22, 269 (1976).

66. W.K.Subczynski and J.S.Hyde, Biochim. Biophys.Acta, 643, 283 (1981).

67. P.B.Ayscough, Electron Spin Resonance in Chemistry. Methuen. (1967).

68. R.S.Alger, EPR: Techniques and Applications. Wiley (1968).

69. W.C.Gardiner Jr., H.M.Pickett and M.H.Proffit, J.Chem.Phys., 74, 6037 (1981)

70. J.M.Dundon, J.Chem.Phys., 76, 2171 (1982).

71. H.M.McConnell and D.B.Chesnut, J.Chem.Phys., 28, 107 (1958).

CHAPTER EIGHT - THALLIUM(I) ETHOXIDE.

Section 8.1. Structure of Thallium(I) Alkoxides.

8.1.1. Molecular Weight, Spectroscopic and X-Ray Studies.

The structures of thallium(I) alkoxides have been investigated by several experimental techniques. Sidgwick and Sutton[1] have performed relative molecular mass measurements for several thallium(I) alkoxides by freezing point depression and boiling point elevation methods. Their results imply the presence of tetramers $\{Tl(OR)\}_4$ for methyl, ethyl and phenylmethyl alkoxides in benzene solution as well as for the thallium(I) ethoxide in ethanol. Results obtained for the thallium(I) cyclohexyloxide in benzene and thallium(I) methoxide in methanol suggest that the predominant species in these solutions are the trimer and monomer respectively. Similar experiments later performed by Bradley[2] indicate a tetramer for the thallium(I) 1,1 dimethylpropoxide, $Tl\text{-}OC(CH_3)_2CH_2CH_3$, in benzene solution. A cubic structure for the thallium(I) alkoxides was proposed by Sidgwick and Sutton with the thallium and oxygen atoms at alternate corners of the cube. Thus the respective sets of four thallium and four oxygen atoms form regular interpenetrating tetrahedra.

Raman and infra red spectra of liquid thallium(I) ethoxide and solid thallium(I) propoxide have been reported by Maroni and Spiro[3]. These spectra were consistent with tetramer formation and the bands were assigned on this basis. The similarity between the

thallium(I) alkoxides and the tetrameric $\{Pb(OH)^{+}\}_4$ was discussed. The latter is isoelectronic with the Tl_4O_4 unit in the alkoxides. In both cases the spectral analysis indicates strong metal-metal interactions.

A single crystal X-ray study of thallium(I) methoxide by Dahl et al.[4] has confirmed tetramer formation in the solid state with the thallium atoms occupying the corners of a regular tetrahedron with an average Tl-Tl distance of 384 pm. A distorted cubic structure was proposed in which the Tl-O-Tl angle is $>90^{o}$ and the O-Tl-O angle is $<90^{o}$.

8.1.2 NMR Studies.

Schneider and Buckingham[5] have made a ^{203}Tl and ^{205}Tl NMR spectroscopic study of the structure of pure thallium(I) ethoxide. These spectra were obtained by the frequency sweep CW method at ^{205}Tl and ^{203}Tl resonance frequencies of 15.91 and 15.75 MHz respectively. Symmetrical seven and five-line spectra were observed for the respective isotopes. No change other than intensity reduction was observed upon diluting the sample to a concentration of 20 mole % in cyclohexane. The ^{1}H NMR spectrum showed the characteristic ethyl group pattern and no ^{1}H- $^{203,205}Tl$ coupling was observed over the temperature range $-70^{o}C$ to $+20^{o}C$. These data are consistent with the tetrameric model of Sidgwick and Sutton; the multiplet structure arises from ^{203}Tl- ^{205}Tl coupling within the tetramer. If a mixture of isotopomers are present and all nuclei of the same isotopic species are magnetically

equivalent then the theoretical NMR spectra for both thallium isotopes can be calculated. The normalised abundances of the possible isotopomers are given by the terms of the binomial expansion(5)

$$(a + b)^4 = a^4 + 4\,a^3b + 6a^2b^2 + 4ab^3 + b^4 \qquad \{8 - 1\}$$

where a = 0.705 is the fractional isotopic abundance of ^{205}Tl and b = 0.295 is that of ^{203}Tl.

Using this expression Schneider and Buckingham have calculated the abundances of each isotopomeric tetramer and their table is presented as Table 8 - 1.

Isotopomer[a]	Normalised Abundance	^{205}Tl Spectrum	^{203}Tl Spectrum
5-5-5-5	0.247	Singlet	-
5-5-5-3	0.413	Doublet	Quartet
5-5-3-3	0.260	Triplet	Triplet
5-3-3-3	0.072	Quartet	Doublet
3-3-3-3	0.008	-	Singlet

a) Labels 5 and 3 represent ^{205}Tl and ^{203}Tl respectively.

Table 8 - 1. Isotopomeric abundances and spectral multiplicities for $\{Tl(OR)\}_4$ tetramer, taken from Reference 5.

The observed ^{205}Tl and ^{203}Tl NMR spectra are superimpositions of the spectra due to each isotopomer. Thus calculated intensities and those observed by Schneider and Buckingham are shown below.

^{205}Tl spectrum

Calculated intensity	0.07:1 : 5.0 : 9.6 : 5.0 : 1 : 0.07
Observed intensity	- :1 : 4.7 : 9.4 : 4.7 : 1 : -

^{203}Tl spectrum

Calculated intensity	1 : 2.5 : 5.1 : 5.6 : 5.1 : 2.5 : 1
Observed intensity	1 : 2.3 : 4.1 : 4.5 : 4.1 : 2.3 : 1

Thus, within experimental error, these ratios confirm tetramer formation in liquid thallium(I) ethoxide.

Gillies et al.[6] have reported both frequency swept and pulsed Fourier transform ^{205}Tl NMR spectra, at a ^{205}Tl frequency of 34.7 MHz, for a range of eleven thallium(I) alkoxides in toluene solution and a further two in benzene solution. The ^{205}Tl spectra for ca. 1M toluene solution of the alkoxides Tl(OR) with alkyl groups C_2H_5, nC_4H_9, nC_5H_{11}, nC_6H_{13}, $CHCH_3(CH_2)_2CH_3$, $CHCH_3(CH_2)_3CH_3$ or $CH_2C_6H_5$ are all consistent with the dominance of tetrameric species in solution. This is also the case for 0.5M and 1.8M $TlOCH_2C_6H_5$ and 4M $TlOC_2H_5$ solutions in benzene. However for ca 1M toluene solutions of the alkoxides Tl(OR) with alkyl groups nC_3H_7, iC_3H_7, $CH_2CH(CH_3)_2$ or $C(CH_3)_2CH_2CH_3$, the relative peak areas could not be measured with a sufficient degree of accuracy to discount the possibility of some trimer or hexamer formation.

All ^{203}Tl- ^{205}Tl coupling constants measured were in the range 2170 Hz - 2769 Hz and the ^{205}Tl chemical shift was found to span a range of 434 ppm for these alkoxides. ^{205}Tl linewidths at half height varied from

120 Hz to 500 Hz, the broadness of these lines limiting the accuracy with which ^{205}Tl shifts and peak areas can be measured. In addition it was suggested that these large linewidths are the result of chemical exchange processes.

Section 8.2 ^{205}Tl Spin Lattice Relaxation.

8.2.1. Method.

There are no previously reported ^{205}Tl relaxation measurements for thallium(I) alkoxides. ^{205}Tl R_1 measurements have now been made on liquid thallium(I) ethoxide as a function of temperature, at ^{205}Tl resonance frequencies at 21.95 MHz and 231.5 MHz. The sample was degassed by the freeze pump thaw technique and sealed in a 5mm tube under an argon pressure of 680 mm Hg.

Sample temperatures at both fields were obtained using the calibrated ^{205}Tl shift of a sample of dimethylthallium(III) nitrate in D_2O, contained in a concentric tube.

The modified Varian XL-100 spectrometer used for the low field measurements allowed a maximum spectral width of 5KHz which complicated observation of the central features of the ^{205}Tl spectrum by aliasing of less intense peaks outside the spectral window. This factor, along with the broadness of the ^{205}Tl lines caused some difficulty in the choice of a spectral baseline. Nevertheless, the ^{205}Tl relaxation rates were still found to be reproducible within an experimental error of $\pm$ 10%. All components of the multiplet appeared to relax at the same rate and hence the intensity of the central feature provides a valid measure of the magnitude of the magnetisation vector.

8.2.2. ^{205}Tl R_1 Results and CSA Contribution.

^{205}Tl spin-lattice relaxation data are shown in Tables 8 - 2 and 8 - 3. The ^{205}Tl nucleus is observed to relax considerably faster at high field than at low, implying a significant contribution to the R_1 from the CSA mechanism. This is as might be expected for a covalently bound ^{205}Tl nucleus in an anisotropic electronic environment. In order to extract the activation energy for the relaxation process the data have been fitted to equations of the form

$$R_1(T) = R_1(298K).\ \mathrm{Exp}\left(\frac{E_{ACT}}{R}\left(\frac{1}{T} - \frac{1}{298}\right)\right) \qquad \{8 - 1\}$$

Using $R_1(298K)$ and E_{ACT} as variable parameters. At high field the best fit parameters thus obtained are

$$R_1(298K) = 512 \pm 15\ s^{-1} \qquad \{8 - 2A\}$$

$$E_{ACT} = 16.2 \pm 1.4\ \ kJ\ mol^{-1} \qquad \{8 - 2B\}$$

These parameters are used to generate the conventional linear plot of $\ln R_1$ against inverse temperature shown in Figure 8 - 1.

Temperature (K)	$R_1(s^{-1})$	Temperature (K)	$R_1(s^{-1})$
281.1	29.7	334.7	7.90
283.5	27.0	336.4	5.90
292.3	17.3	341.4	5.35
297.6	15.1	345.9	4.56
298.7	14.4	347.5	4.96
310.8	10.2	353.1	4.59
311.1	8.84	358.7	4.52
322.7	9.00	-	-

Table 8 - 2. Temperature dependence of ^{205}Tl R_1 at 21.95 MHz.

Temperature (K)	$R_1(s^{-1})$
294.6	537
305.3	469
314.7	368
333.5	250
342.8	207

Table 8 - 3. Temperature dependence of ^{205}Tl R_1 at 231.5 MHz.

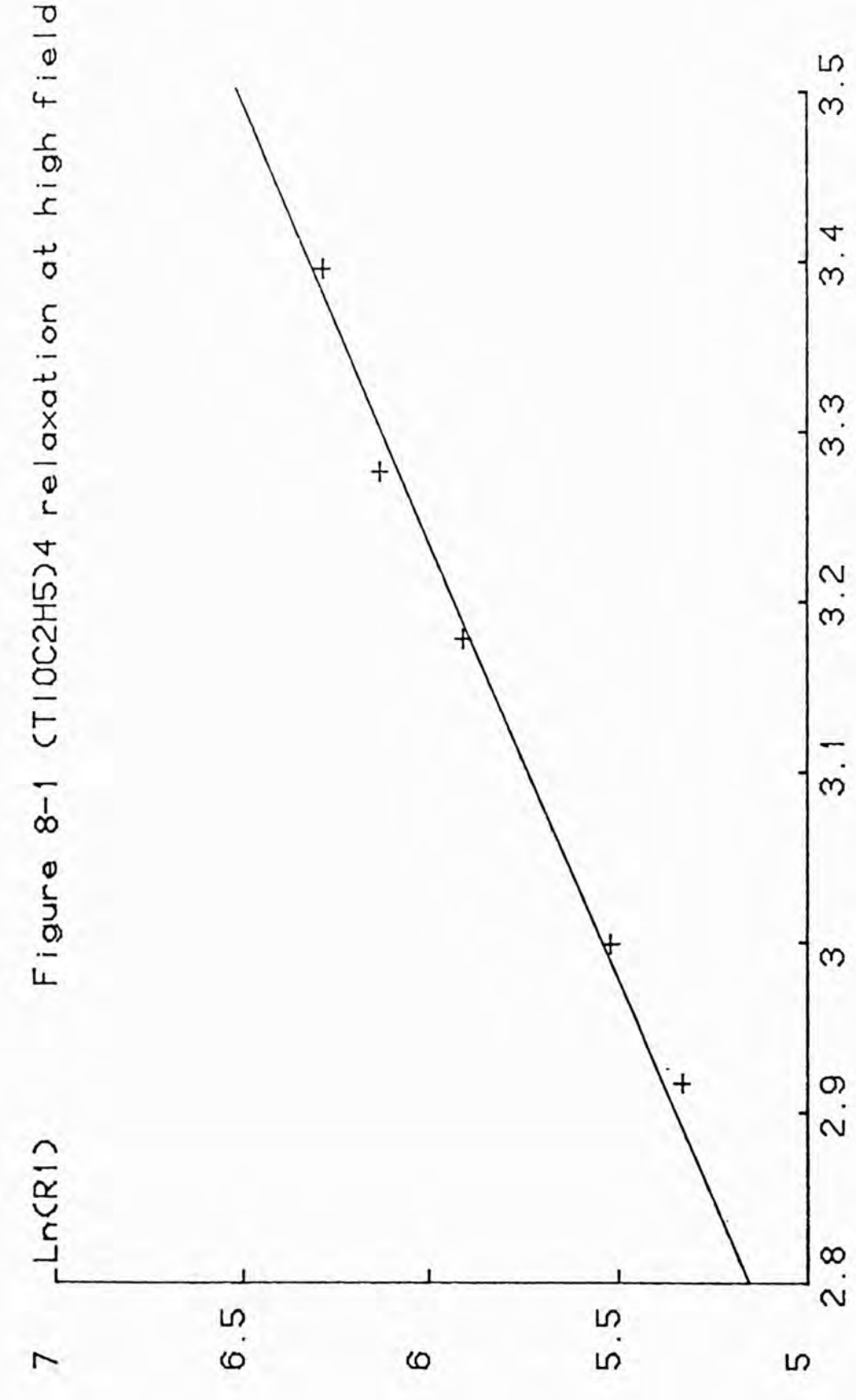

Figure 8-1 (T10C2H5)4 relaxation at high field

Consideration of the relaxation data in Tables 8 - 2 and 8 - 3 shows that CSA is the dominant mechanism at high field. The linear plot in Fig. 8 - 1 shows that the reorientatinal motion is within the extreme narrowing limit, thus from Chapter Two

$$R_{1\ CSA} = \frac{2}{15}\gamma^2 B_o^2 \Delta\sigma^2 (1 + \eta^2/3)\tau_2^{EFF} \qquad \{8 - 3\}$$

Thus the parameters in equation 8 - 2 represent $R_{1\ CSA}(298K)$ and the activation energy for τ_2^{EFF} respectively.

As was the case for the diphenylthallium(III) measurements, lack of knowledge of the anisotropy and asymmetry of the ^{205}Tl shielding tensor prevents a direct calculation of τ_2^{EFF}. As in Chapter Five defining an effective anisotropy $\Delta\sigma_{EFF}$ as

$$\Delta\sigma_{EFF}^2 = \Delta\sigma^2 (1 + \eta^2/3), \qquad \{8 - 4\}$$

and using $\omega_o\tau_2^{EFF} < 1$ allows the calculation of a lower bound for $\Delta\sigma_{EFF}$ as

$$\Delta\sigma_{EFF}^2 > 2.64 \times 10^{-6} \qquad \{8 - 5\}$$

or

$$|\Delta\sigma_{EFF}| > 1600 \text{ ppm}. \qquad \{8 - 6\}$$

Although this shielding tensor information is very limited, it once again indicates the large shielding anisotropies associated with the ^{205}Tl nucleus.

8.2.3. Other ^{205}Tl Relaxation Mechanisms.

The above discussion has shown that the high field spin-lattice relaxation is dominated by the CSA mechanism. Thus using equation 8 - 3 the CSA relaxation

rate can be calculated at lower field strengths. Thus at 21.95 MHz a value of 4.6 s^{-1} for $R_{1\ CSA}(298K)$ is obtained. This is sufficient to show that CSA is not the dominant mechanism at low field. If the sum of the contributions due to other mechanisms is represented by a term $R_{1\ OTHER}$ then one has

$$R_{1\ TOTAL} = R_{1\ CSA} + R_{1\ OTHER}. \qquad \{8 - 7\}$$

Using the parameters of equation 8 - 2 to calculate $R_{1\ CSA}$ at low field allows the calculation of $R_{1\ OTHER}$ at each temperature in Table 8 - 2. Using these values a fit to equation 8 - 1 produces the best fit parameters

$$R_{1\ OTHER}(298K) = 11.3 \pm 0.4\ s^{-1} \qquad \{8 - 8A\}$$

$$E_{OTHER} = 26.9 \pm 1.9\ kJ/mol. \qquad \{8 - 8B\}$$

The temperature dependence of the CSA and other mechanisms are represented by the lower and centre lines respectively in Figure 8 - 2. The upper line represents the total relaxation rate at this field.

Thus it may be seen that the other mechanism(s) dominate the ^{205}Tl spin-lattice relaxation at low field. One might consider an intermolecular Tl-Tl dipolar mechanism, this is,however, likely to be inefficient due to the large Tl-Tl distance which is 384 pm in solid $(TlOCH_3)_4$ [4].

The ^{205}Tl - ^{203}Tl scalar interaction may be modulated by either chemical exchange or ^{203}Tl relaxation and hence provide a ^{205}Tl relaxation mechanism. The effects of this interaction on the ^{205}Tl lineshape are to be discussed in the next section. If the scalar correlation time τ_{SC2} is much shorter than the inverse of the coupling

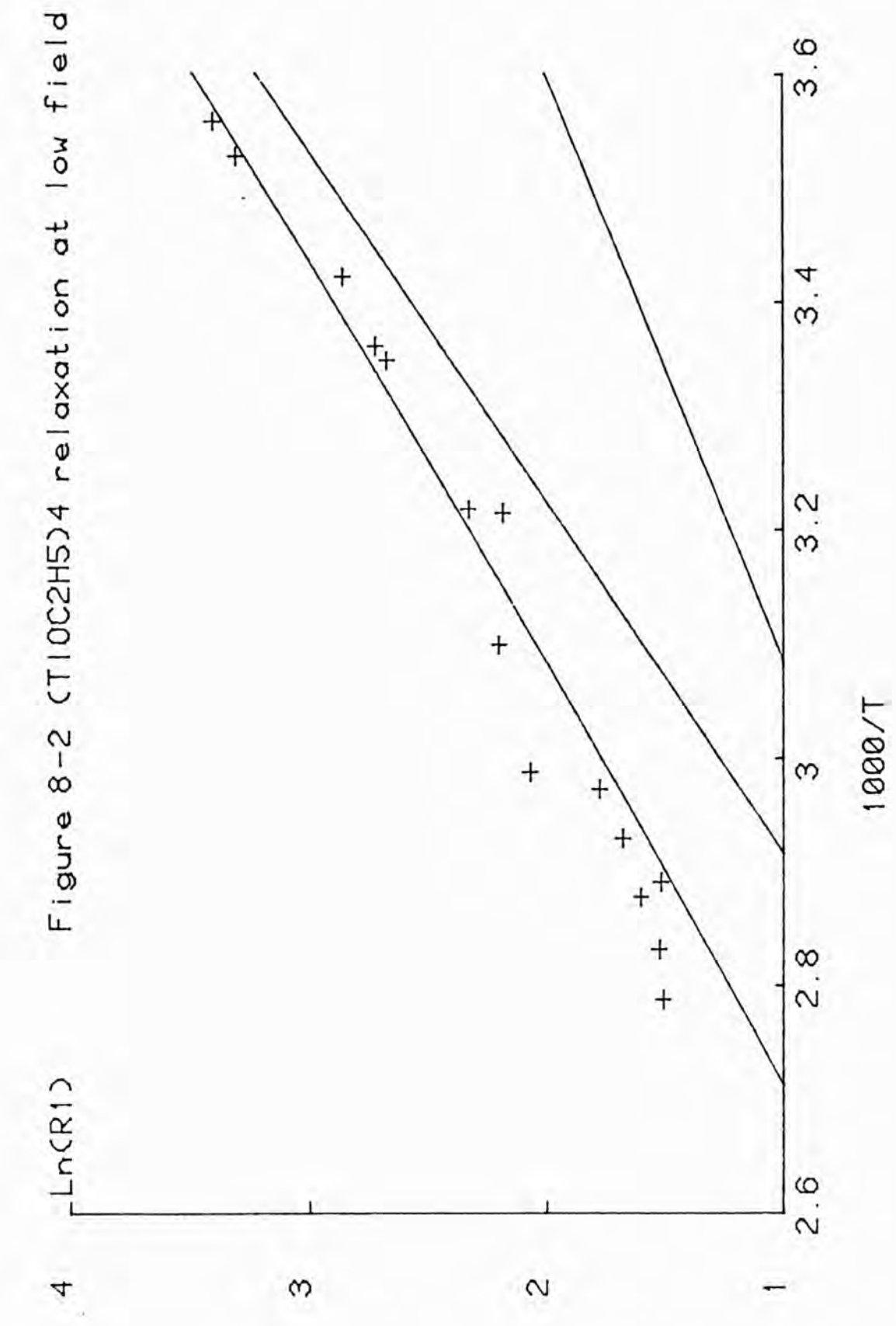

Figure 8-2 (T1OC2H5)4 relaxation at low field

constant J, then the contribution $R_{1\ SC}$ to the ^{205}Tl spin lattice relaxation is as described in Chapter Two.

$$R_{1\ SC} = \frac{8\pi^2 J^2 S(S+1)}{3} \quad \frac{\tau_{SC2}}{1 + \Delta\omega^2 \tau^2_{SC2}} \qquad \{8 - 9\}$$

The nuclear-nuclear scalar coupling mechanism is not usually observed to contribute measurably to R_1. In this case however, the mechanism might be relatively efficient due to the large coupling constant and small difference in resonance frequencies between the two thallium isotopes. At high fields this relaxation mechanism should be relatively less efficient since $\Delta\omega$ is proportional to the applied field strength. The contribution of this mechanism to the ^{205}Tl R_1 could be quantified by a ^{205}Tl $\{^{203}Tl\}$ double resonance experiment. Irradiation of the ^{203}Tl resonance will lead to a reduction of the ^{205}Tl peak area if this mechanism contributes significantly. Dominance of the ^{205}Tl spin-lattice relaxation by this mechanism would lead to disappearance of the ^{205}Tl signal since the signal area is given by the expression(7)

$$I_z = I_0 \left[1 - \frac{\gamma_{IRRAD}}{\gamma_{OBS}} \right] . \qquad \{8 - 10\}$$

Finally consider the ^{205}Tl-^{1}H dipolar mechanism, the total contribution of intermolecular and intramolecular ^{205}Tl-^{1}H dipolar relaxation to the ^{205}Tl R_1 may be established by a ^{205}Tl $\{^{1}H\}$ NOE measurement. The maximum effect would be an enhancement of approximately 88% since the ^{205}Tl signal area is described by the equation

$$I_z = I_0 \left[1 + \frac{\gamma_{IRRAD}}{2\ \gamma_{OBS}} \right] . \qquad \{8 - 11\}$$

Section 8.3 ^{205}Tl Lineshape Phenomena.

8.3.1 Factors affecting the ^{205}Tl lineshape.

During the course of the previously described ^{205}Tl spin-lattice relaxation experiments, considerable changes in the nature of the ^{205}Tl lineshape were observed as a function of temperature and magnetic field strength. Figure 8 - 3 shows the temperature variation of the ^{205}Tl spectrum of liquid $(TlOC_2H_5)_4$ at 21.95 MHz. As the temperature is increased the distinct ^{205}Tl lines broaden, coalesce and collapse. This temperature variation is characteristic of chemical exchange processes and is the opposite of that previously discussed for the scalar broadening of ^{1}H lines coupled to fast relaxing thallium nuclei. At high field strength however the ^{203}Tl - ^{205}Tl coupling is not resolved at any of the temperatures. The broad spectral envelope has a linewidth of ca. 3800 Hz at 295K decreasing to ca. 2500 Hz at 343K. In order to interpret these observations correctly one needs to carefully consider the various processes that can affect the ^{205}Tl spectrum.

8.3.2. ^{205}Tl Relaxation.

Although all processes that affect the ^{205}Tl lineshape are correctly described as ^{205}Tl relaxation processes it is convenient to discuss chemical exchange and scalar relaxation separately (see Sections 8.3.3 and 8.3.4).

At high field it has been shown that the CSA mechanism dominates the spin-lattice relaxation and that the molecular motion is within the extreme narrowing

FIGURE 8-3.

Temperature variation of the ^{205}Tl spectrum of $(TlOC_2H_5)_4$ at 21.95 MHz. All temperatures in ^{o}C. 200 scans and 64 Hz linebroadening used for spectrum at 25.6^{o}C.

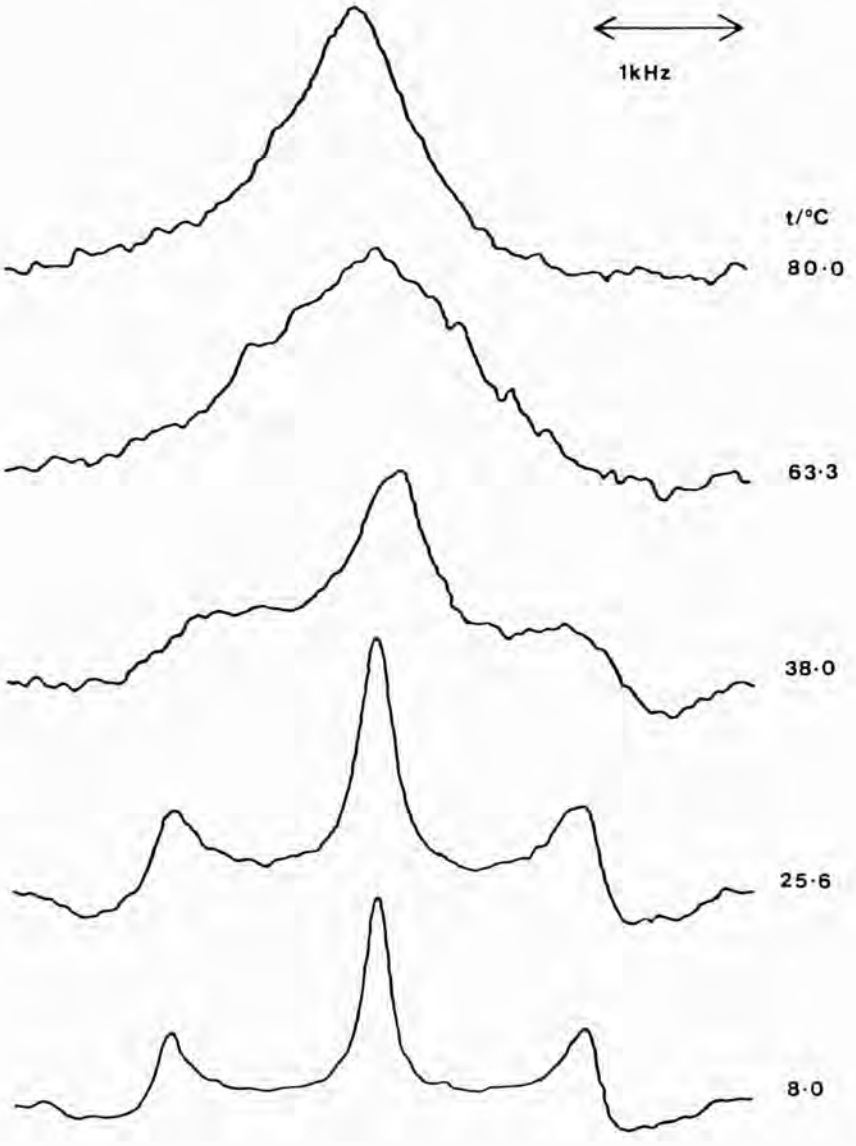

region. Under these conditions equation 8 - 3 describes the behaviour of $R_{1\ CSA}$ and the CSA contribution to R_2 is given by

$$R_{2\ CSA} = \frac{7}{6} R_{1\ CSA} = \frac{7}{45} \gamma^2 B_0^2 \Delta\sigma^2 (1 + \eta^2/3) \tau_2^{EFF} . \{8 - 12\}$$

The best fit value of 512 s^{-1} for $R_{1\ CSA}$(298K) allows the calculation of $R_{2\ CSA}$(298K) as 597 s^{-1}. Thus at high field at 298K the CSA relaxation process leads to a ^{205}Tl linewidth contribution of about 190 Hz and hence is not a major contributor to the observed ^{205}Tl linewidth. Similarly at low field the value of R_1 (298K) is ca. 16 s^{-1} and the associated linewidth contribution of ca. 5Hz is therefore insignificant.

8.3.3. Chemical Exchange.

If exchange of $TlOC_2H_5$ units takes place between different isotopomeric tetramers then this process can modulate the large ^{205}Tl - ^{203}Tl coupling constant thus leading to scalar relaxation of the first kind[7] (chemical exchange averaging). It is usually assumed in chemical exchange studies that the time required for an exchange to occur is negligible. In this case it should be noted that exchange of ethoxide anions could not account for the observed low field spectra since this process would not modulate the ^{205}Tl - ^{203}Tl coupling and could not provide the averaging observed at high temperature. Exchange between thallium(I) ethoxide tetramers and monomers might also be considered but no significant amounts of monomer have been detected in this sample by NMR or other means and its existence need not be invoked to explain the observed

spectra at low field.

There are several facets to the chemical exchange problem in this system. A general isotopomer may be represented by the formula $(^{205}TlOC_2H_5)_{4-n}$ $(^{203}TlOC_2H_5)_n$ and has a ^{205}Tl subspectrum with n + 1 lines due to the ^{205}Tl-^{203}Tl coupling.

Firstly, consider exchange of a $^{205}TlOC_2H_5$ unit with the reservoir of all other tetramers. If a $^{205}TlOC_2H_5$ unit is received there will be no observed change in the ^{205}Tl spectrum since the structure of the tetramer is unchanged. However if the incoming unit is ^{203}Tl then the formula of the isotopomer becomes $(^{205}TlOC_2H_5)_{3-n}$ $(^{203}TlOC_2H_5)_{n+1}$ and the multiplicity of the ^{205}Tl subspectrum increases by one. Secondly, the consequences of chemical exchange involving the loss of a $^{203}TlOC_2H_5$ unit must be considered. If a $^{205}TlOC_2H_5$ unit is received the multiplicity of the ^{205}Tl spectrum decreases by one. There are however two possibilities to be considered if the incoming unit is a $^{203}TlOC_2H_5$. If the arriving ^{203}Tl nucleus has the same spin as the departing ^{203}Tl nucleus then no change in the ^{205}Tl spectrum is expected. If the arriving ^{203}Tl nucleus has differing spin then the resulting change in ^{203}Tl spin state is equivalent to ^{203}Tl relaxation and can modulate the ^{205}Tl-^{203}Tl scalar coupling thus leading to chemical exchange averaging.

Broadening of the ^{205}Tl and ^{203}Tl NMR signals by ^{205}Tl, ^{203}Tl exchange interactions was observed in the thallium NMR study of Tl_2O_3 and thallium metal by Bloembergen and Rowland[8]. They observed the ^{205}Tl and ^{203}Tl

linewidths as a function of isotopic abundance of both nuclei and observed that enrichment of a given nucleus sharpened its signal and broadened that of the other nucleus. It was concluded that spin exchange between unlike nuclei contributes to the second moment and linewidth of the nuclear resonances whilst that between like nuclei does not.

8.3.4 ^{203}Tl Relaxation.

The effects of chemical exchange on the ^{205}Tl- ^{203}Tl scalar coupling interaction have been discussed above and the effects of rapid ^{203}Tl relaxation on this coupling will now be considered. The possibility that this process may contribute to the ^{205}Tl R_1 was discussed in Section 8.2 and is given quantitatively by equation 8 - 9; similarly the scalar contribution to R_2 is given by

$$R_{2\ SC} = \frac{4}{3}\pi^2 J^2 S(S+1)\left[\tau_{SC1} + \frac{\tau_{SC2}}{1 + \Delta\omega^2\tau_{SC2}^2}\right] . \{8 - 13\}$$

This equation is only strictly applicable in the fast relaxation limit in which the relaxation times T_1, T_2 ($= \tau_{SC1}, \tau_{SC2}$) of the relaxing nucleus are much less than the inverse of the scalar coupling constant J.

$$T_1,\ T_2 << 1/J, \qquad \{8 - 14A\}$$

or

$$R_1,\ R_2 >> J \quad . \qquad \{8 - 14B\}$$

Since the ^{203}Tl and ^{205}Tl nuclei have similar gyromagnetic ratios and the difference in electronic structure and shielding anisotropies due to isotopic effects will be negligible it is reasonable to suggest that at high field

both will have equal values of R_1, due to dominance by the CSA mechanism. Thus the value of 512 s^{-1} for $R_1(^{203}Tl)$ at 298K will be taken as correct. The difference in resonance frequencies for ^{205}Tl and ^{203}Tl is about 2MHz at high field, hence for any reasonable τ_{SC2} in equation 8 - 13 $\Delta\omega\tau_{SC2} >> 1$, and the single quantum is negligible in comparison to the zero quantum term. The inequality in 8 - 14 thus becomes $R_1 >> J$. Since J is about 2560 Hz it appears that this inequality does not hold and hence this mechanism does not appear efficient enough to collapse the ^{205}Tl - ^{203}Tl coupling at high field and ambient temperature. Thus no explanation is available for the dramatic increase in the observed ^{205}Tl linewidth at high field.

REFERENCES CHAPTER EIGHT

1. N.V.Sidgwick and L.E.Sutton, J.Chem.Soc., 1461 (1930).

2. D.C.Bradley, J.Chem.Soc., 4780 (1958).

3. V.A.Maroni and J.G.Spiro, Inorg.Chem., 7, 193 (1968).

4. L.F.Dahl, G.L.Davis, D.L.Wampler and R.West, J.Inorg.Nucl.Chem., 24, 357 (1962).

5. W.G.Schneider and A.D.Buckingham, Disc.Farady Soc., 34, 147 (1962).

6. P.J.Burke, R.W.Matthews and D.G.Gillies, J.Chem.Soc., Dalton, 1439 (1980).

7. A.Abragam, The Principles of Nuclear Magnetism, O.U.P., (1961).

8. N.Bloembergen and T.J.Rowland, Phys.Rev., 97, 1679 (1955).

APPENDIX 1.

GEOMETRY AND INERTIAL PROPERTIES OF $(CH_3)_2Tl^+$.

The geometry and moments of inertia of the dimethylthallium(III) cation have been assumed in Chapter Four in the discussion of models of molecular motion. This brief Appendix shows how these properties may be calculated from first principles.

Consider a $(CH_3)_2Tl^+$ cation with a linear C-Tl-C skeleton as shown in Figure A1 - 1. If a Cartesian axis system is superimposed on this and is centred on the Tl atom, then this has coordinates (0,0,0). The calculations presented here use the bond lengths given by Lee and Reeves.(1)

$$r\ (C\text{-}Tl) = 2.019 \times 10^{-10}\ m \qquad \{A1 - 1\}$$

$$r\ (C\text{-}H) = 1.097 \times 10^{-10}\ m \qquad \{A1 - 2\}$$

along with a tetrahedral angle taken as,

$$\theta = \cos^{-1}(-1/3) \qquad \{A1 - 3\}.$$

The carbon and hydrogen atom coordinates may be calculated by simple geometry and are shown in the Tables below.

Atom	x	y	z
C_1	-2.019	0	0
C_2	+2.019	0	0
H_1	-2.385	+1.034	0
H_2	-2.385	-0.517	-0.896
H_3	-2.385	-0.517	+0.896
H_4	+2.385	+1.034	0
H_5	+2.385	-0.517	-0.896
H_6	+2.385	-0.517	+0.896

Table A1 - 1. Atomic coordinates in units of 10^{-10}m

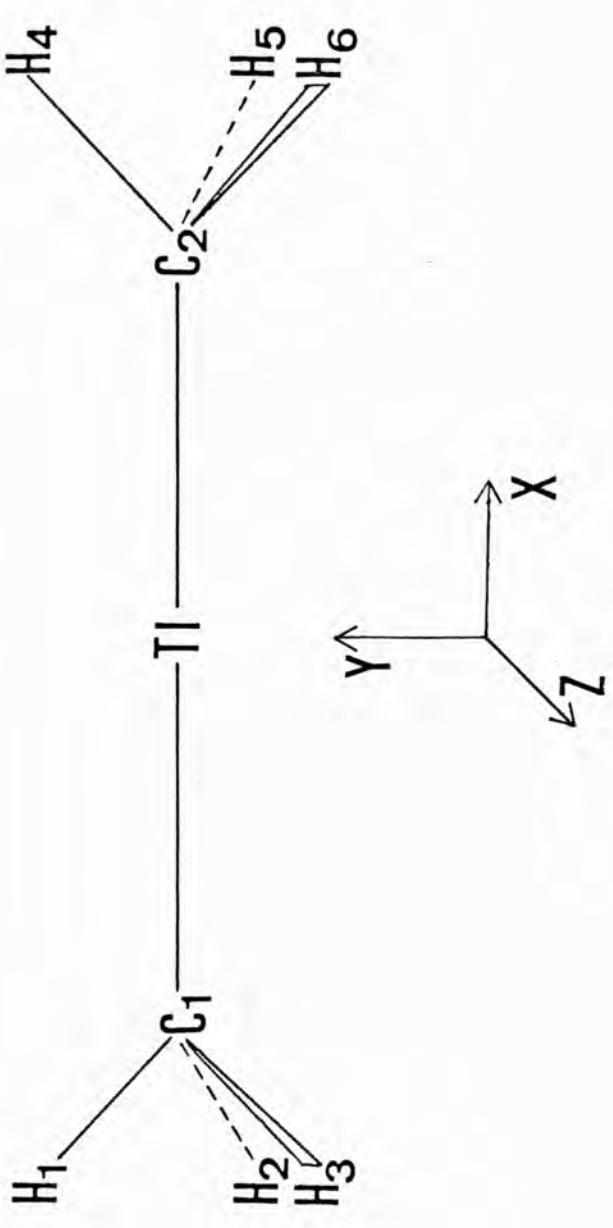

FIGURE A1 - 1 Representation of $(CH_3)_2Tl^+$ Cation.

The inter-proton distance within a methyl group, is of importance in the calculation of intramolecular dipolar relaxation for protons and is found to be

$$r\ (H\text{-}H) = 1.791 \times 10^{-10} m \qquad \{A1 - 4\}.$$

The moment of inertia about a given axis is defined as

$$I = \sum_i m_i r_i^2 \qquad \{A1 - 5\}$$

where the summation is over all atoms and r_i is the perpendicular distance from the chosen axis, e.g. the perpendicular distance from the y axis is given by

$$r_i = (x_i^2 + z_i^2)^{\frac{1}{2}} \qquad \{A1 - 6\}$$

analogous equations hold for the other axes.

Using standard values for the atomic weights of carbon and hydrogen the moments of inertia are calculated to be

$$I_y = I_z = I_\perp = 2.251 \times 10^{-45}\ kg\ m^2 \qquad \{A1 - 7\}$$

$$I_x = I_\parallel = 1.074 \times 10^{-46}\ kg\ m^2 \qquad \{A1 - 8\}.$$

The inertial anisotropy ε is defined as

$$\varepsilon = (I_\perp - I_\parallel)/I_\parallel \qquad \{A1 - 9\}$$

Using the moments of inertia above one finds,

$$\varepsilon = 19.96 \qquad \{A1 - 10\}.$$

This is the value assumed in Chapter Four.

REFERENCE APPENDIX 1.

1. Y.Lee and L.W.Reeves, Can.J.Chem., 53, 161 (1975).

APPENDIX 2.

NON LINEAR REGRESSION ANALYSIS.

The non linear least squares fitting technique has been extensively used in this thesis to derive best fit parameters of physical significance from experimental data. The method used herein is known as the Gauss-Newton linearisation procedure and is distinct from the Simplex and steepest descent techniques.

The problem requires the adjustment of variable parameters A_k that are inherent in the chosen functional form

$$Y = F(x, A_1, A_2, \ldots . A_m) \qquad \{A2 - 1\},$$

in order to minmise the sum of the residual errors squared

$$S = \sum_{i=1}^{n} \left[y_i - F(x_i) \right]^2 \qquad \{A2 - 2\}.$$

Where x_1, y_1 x_2, y_2 .... x_n, y_n are the pairs of experimental data points.

The minimisation criterion requires the derivative of the sum of errors squared with respect to each parameter to be equal to zero.

$$\frac{\partial S}{\partial A_k} = 0 \qquad k = 1,2, \ldots m \qquad \{A2 - 3\}.$$

Thus a system of m non linear simultaneous equations are generated. These equations may be linearised by expanding the fitting function as a truncated Taylor series about a set of initial parameter estimates A_k^o.

$$F(x_i) = F^o(x_i) + \sum_{k=1}^{m} \frac{\partial F^o(x_i)}{\partial A_k} . \Delta A_k \qquad \{A2 - 4\}.$$

The m x m system of linear equations may be written in matrix form as

$$P\ \Delta A = Z \qquad \{A2 - 5\}$$

where P is the m x m matrix of partial derivatives,

$$P_{jk} = \sum_{i=1}^{n} \frac{\partial F_o(x_i)}{\partial A_j} . \frac{\partial F_o(x_i)}{\partial A_k} \qquad \{A2 - 6\}$$

Z is the m x 1 row vector with elements,

$$Z_r = \sum_{i=1}^{n} \{ y_i - F^o(x_i)\} . \frac{\partial F_o(x_i)}{\partial A_r} \qquad \{A2 - 7\}$$

and ΔA is 1 x m column vector of correction terms A_k for the initial parameter estimates A_k^o. The system of linear equations is solved by matrix inversion of P thus

$$\Delta A = P^{-1} Z \qquad \{A2 - 8\}$$

followed by addition of the correction terms.

$$A_k = A_k^o + \Delta A \qquad \{A2 - 9\}.$$

These new parameter values may now be taken as improved initial estimates and the process repeated until convergence is obtained.

If ε is an arbitrary convergence criterion then convergence is defined by the condition.

$$\sum_{k=1}^{m} \left| \frac{\Delta A_k}{A_k} \right| < \varepsilon \qquad \{A2 - 10\}.$$

Having achieved convergence the variance of the fit is given by

$$\sigma^2 = \frac{\sum_{i=1}^{n} \{y_i - F(x_i)\}^2}{n-m-1} \qquad \{A2 - 11\}$$

and the estimated standard deviation for each parameter is equal to

$$\sigma(A_k) = \{\sigma^2 P_{kk}^{-1}\}^{\frac{1}{2}} \quad k = 1,2,...m \quad \{A2 - 12\}$$

where P_{kk}^{-1} is the kth diagonal element of the matrix P^{-1}. The error bounds given for the best fit parameters shown in this thesis are $\pm$ one standard deviation.

Non linear least squares fit programs have been written in BASIC language on Tektronix 4052 and BBC Model B microcomputers. Listing one shows the BBC BASIC program used to analyse IRFT data and fits to the three parameter exponential function described in Chapter Three. In order to fit to other functions the derivative and function procedures in lines 790-890, the prompts in lines 170-200, and the print statements in lines 640-660 should be changed.

LISTING ONE

```
 10 MODE7
 20 PRINT"This program calculates the spin"
 30 PRINT"lattice relaxation rate R1, from"
 40 PRINT"experimental peak areas and tau values"
 50 PRINT"found from the inversion recovery "
 60 PRINT"pulse sequence."
 70 NPARAM%=3
 80 INPUT"number of data points=",NPOINTS%
 90 DIM X(NPOINTS%),Y(NPOINTS%)
100 DIM P(NPARAM%,NPARAM%),PINV(NPARAM%,NPARAM%),Z(NPARAM%)
110  DIM ACOR(NPARAM%),A(NPARAM%),DERIV(NPARAM%),SDEV(NPARAM%)
120  DIM B(NPARAM%,NPARAM%),D(NPARAM%,NPARAM%)
130 PRINT"enter tau values, peak areas"
140 FOR POINT%=1 TO NPOINTS%
150   INPUT X(POINT%),Y(POINT%)
160   NEXT POINT%
170 PRINT"enter initial,parameter estimates."
180 INPUT"Magnetisation at long time=",A(1)
190 INPUT"Magnetisation at zero time=",MZERO
200 A(2)=MZERO-A(1)
210 INPUT"R1=",A(3)
220 PRINT"ITERATING"
230 PRINT"EXIT WHEN CONVERGENCE CRITERION<0.001"
240 PRINT"CONV__________________SUM-OF-ERRORS^2-"
250 TIME=0
260 REM ITERATIONS LOOP
270 REPEAT
280   PROCZCALC
290   PROCPCALC
300   REM NOW CALC INCREMENTS
310   PROCMATINV
320   FOR K%=1 TO NPARAM%
330     ACOR(K%)=0
340     FOR J%=1 TO NPARAM%
350       ACOR(K%)=ACOR(K%)+PINV(K%,J%)*Z(J%)
360       NEXT J%:NEXT K%
370   REM ADD CORRECTIONS AND CALC CONV
380   CONV=0
390   FOR K%=1 TO NPARAM%
400     A(K%)=A(K%)+ACOR(K%)
410     CONV=CONV+ABS(ACOR(K%)/A(K%))
420     NEXT K%
430   PROCERROR2
440   PRINT;CONV;TAB(25);SUMSQ
450   UNTIL CONV<0.001
460 PRINT"ITERATION COMPLETE"
470 WAIT$=INKEY$(200)
480 CLS
490  PRINT
500 PRINT"X(OBS) ______Y(OBS) _____Y(CALC) ________"
510 FOR POINT%=1 TO NPOINTS%
520   PROCFUNC(X(POINT%))
530   PRINT ;X(POINT%);TAB(12);Y(POINT%);TAB(23);F
```

```
540   NEXT POINT%
550 PRINT"PARAMETER___VALUE______STD_DEV_________"
560 PROCERROR2
570 SIGMA2=SUMSQ/(NPOINTS%-NPARAM%-1)
580 FOR K%=1 TO NPARAM%
590   PROCMATINV
600   SDEV(K%)=SQR(SIGMA2*PINV(K%,K%))
610   PRINT ;K%;TAB(8);A(K%);TAB(23);SDEV(K%)
620   NEXT K%
630 PRINT
640 PRINT"parameter 1 =M(infinity)"
650 PRINT"parameter 2 =M(zero)-M(infinity)"
660 PRINT"parameter 3 =R1 in /seconds"
670 PRINT"PRESS ANY KEY FOR GRAPHICS"
680 CLS
690 WAIT$=GET$
700 INPUT"GRAPH TITLE=";T$
710 INPUT"X AXIS PLOT MIN,MAX=";XMIN,XMAX
720 INPUT"TIC MARK INCREMENT=";XINC
730 INPUT"Y AXIS PLOT MIN,MAX=";YMIN,YMAX
740 INPUT"TIC MARK INCREMENT=";YINC
750 MODE0
760 PROCGRAPH
770 END
780 REM_________________________________
790 DEF PROCFUNC(X)
800 F=A(1)+A(2)*EXP(-A(3)*X)
810 ENDPROC
820 REM_________________________________
830 DEF PROCDERIV(X)
840 LOCAL K%
850 DERIV(1)=1
860 DERIV(2)=EXP(-A(3)*X)
870 DERIV(3)=-A(2)*X*EXP(-A(3)*X)
880 ENDPROC
890 REM_________________________________
900 DEF PROCZCALC
910 FOR J%=1 TO NPARAM%
920   Z(J%)=0
930   FOR POINT%=1 TO NPOINTS%
940     PROCFUNC(X(POINT%))
950     PROCDERIV(X(POINT%))
960     Z(J%)=Z(J%)+(Y(POINT%)-F)*DERIV(J%)
970     NEXT POINT%:NEXT J%
980 ENDPROC
990 REM_________________________________
1000 DEF PROCPCALC
1010 FOR J%=1 TO NPARAM%:FOR K%=1 TO NPARAM%
1020     P(J%,K%)=0
1030     FOR POINT%=1 TO NPOINTS%
1040       PROCDERIV(X(POINT%))
1050       P(J%,K%)=P(J%,K%)+DERIV(J%)*DERIV(K%)
1060       NEXT POINT%:NEXT K%:NEXT J%
1070 ENDPROC
```

```
1080 REM_______________________________
1090 DEF PROCMATINV
1100 LOCAL I%,J%,K%,L%
1110 FOR L%=1 TO NPARAM%:FOR M%=1 TO NPARAM%
1120     D(L%,M%)=P(L%,M%):B(L%,M%)=0:B(L%,L%)=1
1130     NEXT M%:NEXT L%
1140 NO%=NPARAM%-1
1150 FOR J%=1 TO NPARAM%
1160   FOR K%=1 TO NO%
1170     JO%=K%+1
1180     FOR L%=JO% TO NPARAM%
1190       B(L%,J%)=B(L%,J%)-(P(L%,K%)*B(K%,J%)/P(K%,K%))
1200       FOR M%=JO% TO NPARAM%
1210         P(L%,M%)=P(L%,M%)-(P(L%,K%)*P(K%,M%)/P(K%,K%))
1220         NEXT M%:NEXT L%:NEXT K%
1230   FOR K%=1 TO NPARAM%
1240     JO%=NPARAM%-K%+1
1250     JOP%=NPARAM%-K%+2
1260     PINV(JO%,J%)=B(JO%,J%)
1270     IF JOP%>NPARAM% THEN 1310
1280     FOR I%=JOP% TO NPARAM%
1290       PINV(JO%,J%)=PINV(JO%,J%)-P(JO%,I%)*PINV(I%,J%)
1300       NEXT I%
1310     PINV(JO%,J%)=PINV(JO%,J%)/P(JO%,JO%)
1320     NEXT K%
1330   FOR L%=1 TO NPARAM%:FOR M%=1 TO NPARAM%
1340       P(L%,M%)=D(L%,M%)
1350       NEXT M%:NEXT L%:NEXT J%
1360 ENDPROC
1370 REM_______________________________
1380 DEF PROCGRAPH
1390 REM GRAPHICS SUBROUTINE
1400 LOCAL X:REM HERE PLOT VARIABLE
1410 CLS
1420 REM DRAW AXES
1430 MOVE 1200,100
1440 DRAW 200,100
1450 DRAW 200,900
1460 XPLOT0=200
1470 PROCFUNC(XMIN)
1480 YPLOT0=(F-YMIN)*800/(YMAX-YMIN)+100
1490 MOVE XPLOT0,YPLOT0
1500 FOR X=XMIN TO XMAX STEP (XMAX-XMIN)/100
1510   XPLOT=(X-XMIN)*1000/(XMAX-XMIN)+200
1520   PROCFUNC(X)
1530   YPLOT=(F-YMIN)*800/(YMAX-YMIN)+100
1540   DRAW XPLOT,YPLOT
1550   NEXT X
1560  REM DRAW TIC MARKS
1570 FOR X1=XMIN TO XMAX STEP XINC
1580   X2=(X1-XMIN)*1000/(XMAX-XMIN)+200
1590   MOVE X2,100:DRAW X2,80
1600   MOVE X2,60:VDU 5:PRINT "";X1
1610   NEXT X1
```

```
1620 FOR Y1=YMIN TO YMAX STEP YINC
1630   Y2=(Y1-YMIN)*800/(YMAX-YMIN)+100
1640   MOVE 200,Y2:DRAW 180,Y2
1650   MOVE 10,Y2:VDU 5:PRINT "";Y1
1660   NEXT Y1
1670 REM PLOT POINTS
1680 FOR POINT%=1 TO NPOINTS%
1690   XPLOT=(X(POINT%)-XMIN)*1000/(XMAX-XMIN)+200
1700   YPLOT=(Y(POINT%)-YMIN)*800/(YMAX-YMIN)+100
1710   MOVE XPLOT,YPLOT+25
1720   DRAW XPLOT,YPLOT-25
1730   MOVE XPLOT-25,YPLOT
1740   DRAW XPLOT+25,YPLOT
1750   NEXT POINT%
1760 REM PRINT TITLE
1770 MOVE 400,1000:VDU 5:PRINT T$
1780 ENDPROC
1790 DEF PROCERROR2
1800 SUMSQ=0
1810 FOR POINT%=1 TO NPOINTS%
1820   PROCFUNC(X(POINT%))
1830   SUMSQ=SUMSQ+(Y(POINT%)-F)^2
1840   NEXT POINT%
1850 ENDPROC
```

PUBLICATIONS

1. Thallium-205 Spin Lattice Relaxation in Dialkylthallium(III) derivatives: importance of Chemical Shift anisotropy Relaxation and Effects on NMR spectra of Coupled Nuclei.
   F.Brady, R.W.Matthews, M.J.Forster and D.G.Gillies, Inorg. Nucl.Chem.Letters, 17, 155 (1981).
2. Broadening of N.M.R. Signals of Nuclei Coupled to Fast Relaxing Spin-½ Nuclei: An Example of T_1 Spin-decoupling.
   F.Brady, R.W.Matthews, M.J.Forster and D.G.Gillies, J.C.S. Chem.Comm., 911 (1981).

INORG.NUCL.CHEM.LETTERS Vol.17, No.5/6, pp.155-159, 1981. 0020-1650/81/060155-05$02.00/0
Printed in Great Britain.

THALLIUM-205 SPIN LATTICE RELAXATION IN DIALKYLTHALLIUM(III) DERIVATIVES : IMPORTANCE OF CHEMICAL SHIFT ANISOTROPY RELAXATION AND EFFECTS ON NMR SPECTRA OF COUPLED NUCLEI.

Frank Brady and Ray W Matthews
Department of Chemistry, Polytechnic of North London, Holloway, N7 8DB, UK.

and

Mark J Forster and Duncan G Gillies
The Bourne Laboratory, Department of Chemistry, Royal Holloway College, University of London, Egham Hill, Egham, Surrey, TW20 OEX, UK.

(*Received* 18 *November* 1980)

Abstract: A dominant contribution from the chemical shift anisotropy relaxation mechanism to ^{205}Tl spin-lattice relaxation in some dialkylthallium(III) derivatives is demonstrated by measurements at two different fields and is also reflected in nmr linewidths of coupled protons, hence suggesting a new and facile method for monitoring changes in ^{205}Tl T_1 values.

The chemical shift anisotropy (C.S.A.) mechanism has been suggested as a significant contributor to spin-lattice relaxation processes of several heavier spin-1/2 nuclei (i.e. ^{77}Se (1), ^{113}Cd (2), ^{199}Hg (3), ^{205}Tl (4),) but in only two cases (^{195}Pt (5) and ^{207}Pb (6)) have the appropriate variable field experiments (7) been used to confirm this. We report here variable field ^{205}Tl and ^{1}H nmr spectra which demonstrate that thallium-205 spin-lattice relaxation in some dialkylthallium(III) derivatives is dominated by the C.S.A. mechanism.

Component linewidths of proton-coupled ^{205}Tl nmr spectra for $(CH_3)_2TlNO_3$ in D_2O increase from about 4 to 140 Hz on raising the field from 1.41 T to 9.40 T (Fig.1). Field dependence of this order is consistent with domination of spin-spin relaxation by the C.S.A. mechanism as given by equation (1) for the extreme narrowing condition and axial symmetry (7). (The symbols are defined in ref.7).

$$T_1^{-1}(C.S.A.) = (6/7)T_2^{-1}(C.S.A.) = (2/15)\gamma^2 B_o^2(\sigma_{\parallel}-\sigma_{\perp})^2\tau_c \qquad (1)$$

The temperature dependence of T_1 for $(CH_3)_2TlNO_3$ in D_2O at 34.7 MHz* (Fig. 2) indicates (7) that the substantial contribution from the spin-rotation (S.R.) mechanism at high temperatures gives way to C.S.A. and/or other contributions at lower temperatures. (Similar results were

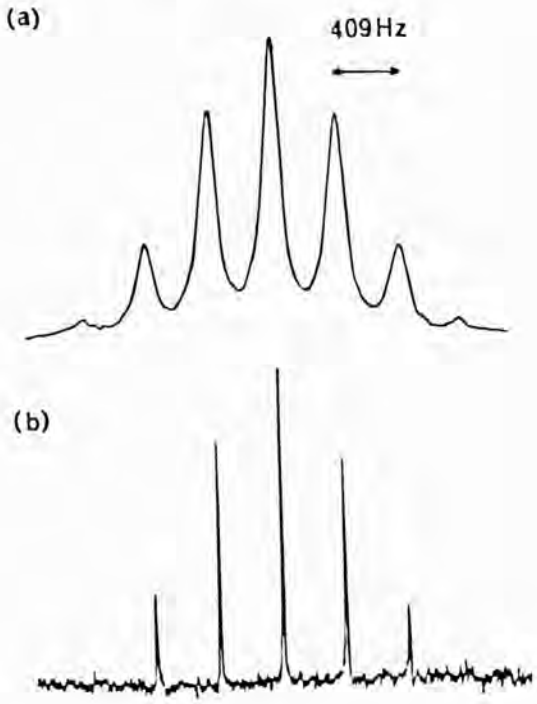

FIG. 1
^{205}Tl spectra of $(CH_3)_2TlNO_3$ in D_2O at 9.40 T (231.5 MHz) (a), and 1.41 T (34.7 MHz) (b). Same scale in Hz cm^{-1}.

obtained for $(CH_3)_2TlOAc$ in D_2O). Assuming only S.R. and C.S.A. contributions, we have obtained a least squares fit of these results to the Arrhenius-type equation (2) where the pre-exponential factors, A, and the activation energies, $E^{\neq}$, are treated as variables. The

$$T_1^{-1} = A_{SR}e^{-E^{\neq}_{SR}/RT} + A_{CSA}e^{-E^{\neq}_{CSA}/RT} \qquad (2)$$

separate contributions are indicated in Fig. 2 and at 295 K, for example, are T_1^{-1}(S.R.) = 12% and T_1^{-1}(C.S.A.) = 88%. Preliminary measurements of T_1 for this solution at 231.5 MHz* yield T_1 ca. 2.9 ms at 295 K. Assuming that ^{205}Tl relaxes solely by the C.S.A. mechanism at the higher field, the lower field rate can be calculated (equation (1)) as T_1^{-1}(C.S.A.) = 7.7 s^{-1}. This is in good agreement with the low field value of 8.0 s^{-1} obtained from the fitting procedure, and positively identifies C.S.A. as the dominant contribution to T_1.

The dominance of the C.S.A. contribution to ^{205}Tl T_1's is also observable through the field dependence of linewidths of thallium-coupled components in ^{1}H nmr spectra of dialkylthallium(III) derivatives. Thus component linewidths for $(CH_3)_2TlOAc$ in D_2O increase linearly with the square of the observing frequency (Fig. 3), and demonstrate that the proton linewidths are determined by spin-lattice relaxation at the coupled thallium nucleus. Linewidths used

* T_1 values were obtained from inversion-recovery experiments.

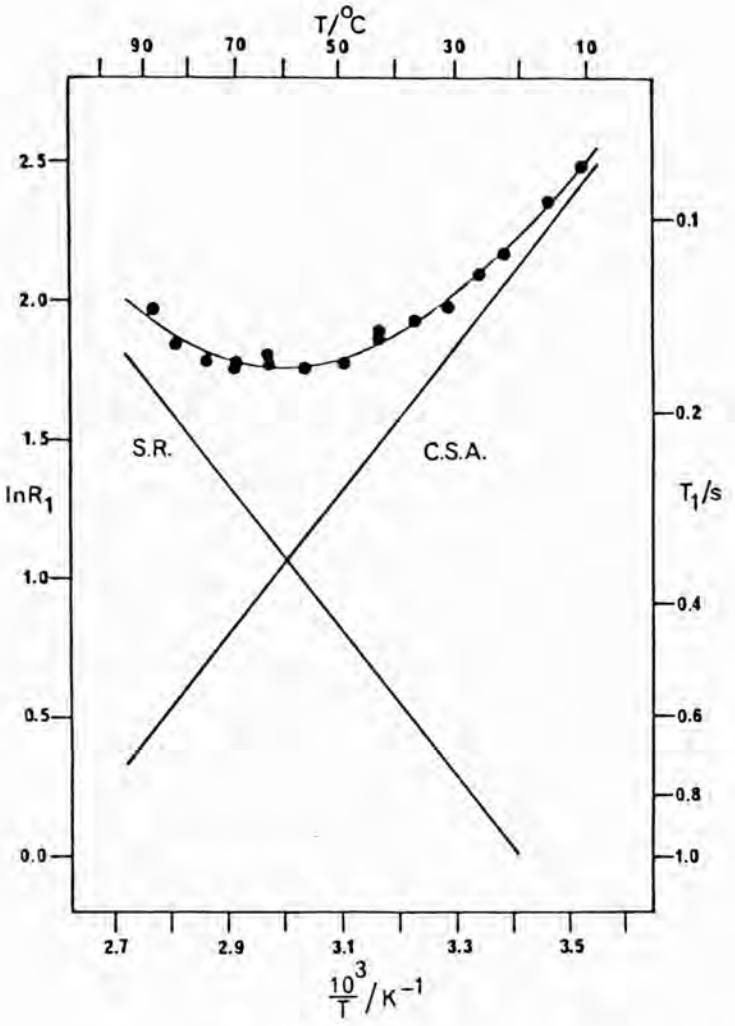

FIG. 2

Temperature dependence of ^{205}Tl spin-lattice relaxation for $(CH_3)_2TlNO_3$ in D_2O (0.16 mol dm^{-3}, sample not degassed) at 34.7 MHz. The solid curve represents the least squares fit to equation (2) and the derived C.S.A. and S.R. contributions are indicated. (The effect on T_1 of degassing is within experimental error, ± 10%).

in Fig. 3 are uncorrected for (i) overlap of components coupled to ^{205}Tl and ^{203}Tl (natural abundance 70.5% and 29.5% respectively; $\gamma(^{205}Tl)/\gamma(^{203}Tl) = 1.0098$) and (ii) the 'intrinsic' linewidths of the proton signals in the absence of broadening due to coupling to thallium. These corrections are clearly feasible and suitably corrected linewidths provide a potentially convenient way of monitoring changes in thallium spin-lattice relaxation in proton-thallium coupled systems (e.g. preliminary results for ^{1}H linewidths of thallium-coupled components as a function of temperature, at constant field, for $(CH_3)_2TlOAc$ in D_2O parallel the temperature

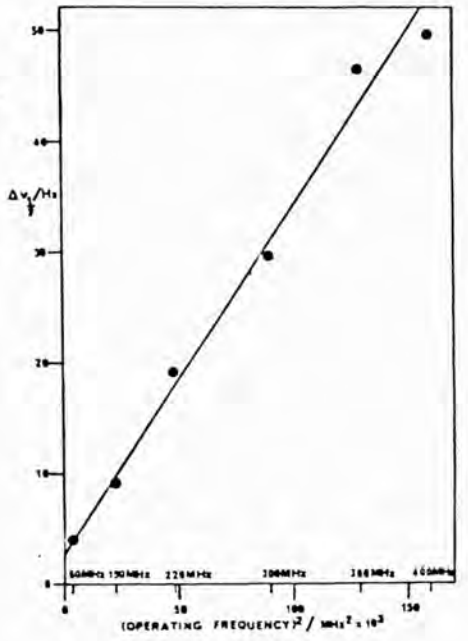

FIG. 3

Dependence of ^{1}H thallium-coupled component linewidths ($\Delta\nu_{\frac{1}{2}}$) on observation frequency for $(CH_3)_2TlOAc$ in D_2O (0.2 mol dm^{-3}; temperature was 27 °C for all points except at 300 MHz (29 °C) and 60 MHz (35 °C); sample not degassed).

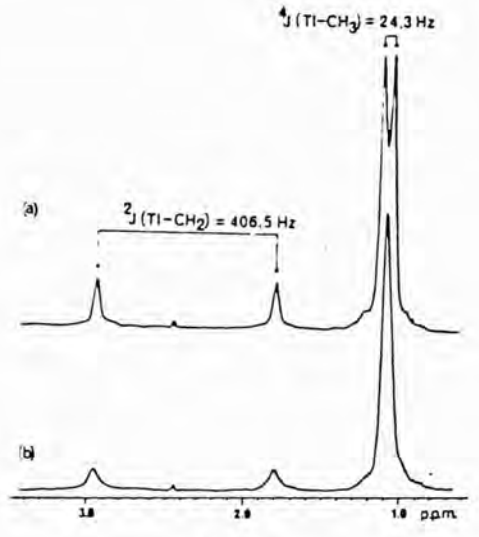

FIG. 4

^{1}H spectra of $[(CH_3)_3CCH_2]_2TlCl$ in C_5D_5N (0.18 mol dm^{-3}) at 360 MHz and 67 °C (a), and 27 °C (b).

dependence of $T_1^{-1}(^{205}Tl)$ for this solution). We have also observed similar effects on linewidths of thallium-coupled components in ^{13}C nmr spectra of these derivatives.

A further manifestation of the same effect is provided by the ^1H spectra of $[(CH_3)_3CCH_2]_2TlCl$ at 360 MHz (Fig. 4) as a function of temperature. The doublet arising from $^4J(Tl-H)$ is resolved only at the higher temperature where $T_1^{-1}(^{205}Tl)$ is reduced through a decrease in the correlation time, τ_c, as a result of increasing the temperature.

These effects on the spectra of the coupled nuclei may be general for several spin-½ nuclei with relatively fast relaxation (c.f. ^{195}Pt (5)). While providing some observational problems, they also present the opportunity for facile study of relaxation processes at the fast relaxing nucleus.

Acknowledgements: We thank the S.R.C. for studentships to F.B. and M.F.

REFERENCES

1. W-H.PAN and J.P.FACKLER, J. Amer. Chem. Soc., 100, 578 (1978); O.A.GANSOW, W.D.VERNON and J.J.DECHTER, J. Magn. Reson., 32, 19 (1978); J.D.ODOM, W.H.DAWSON and P.D.ELLIS, J. Amer. Chem. Soc., 101, 5815 (1979).

2. J. DALTON, J.D.KENNEDY, W. McFARLANE and J.R.WEDGR, Mol. Phys. 34, 215 (1977); M. HOLZ, R.B.JORDAN and M.D.ZEIDLER, J. Magn. Reson., 22, 47 (1976); A.D.CARDIN, P.D.ELLIS, J.D.ODOM and J.W.HOWARD, J. Amer. Chem. Soc., 97, 1672 (1975).

3. M.A.SENS, N.K.WILSON, P.D.ELLIS and J.D.ODOM, J. Magn. Reson., 19, 323 (1975); J.D.KENNEDY and W.McFARLANE, J.C.S. Faraday II, 1653 (1976); C.R.LASSIGNE and E.J.WELLS, Can. J. Chem., 55, 1303 (1977).

4. J.F.HINTON and K.H.LADNER, J. Magn. Reson., 32, 303 (1978); R.W.BRIGGS and J.F.HINTON, ibid., 32, 155 (1978); 33, 363 (1979); R.W.BRIGGS, F.A.ETZKOM and J.F.HINTON, ibid., 37, 523 (1980).

5. J.Y.LALLEMAND, J.SOULIE and J.C.CHOTTARD, J.C.S. Chem. Comm., 436 (1980).

6. R.M.HAWK and R.R.SHARP, J. Chem. Phys., 60, 1522 (1974).

7. T.C.FARRAR and E.D.BECKER, Pulse and Fourier Transform NMR, chpt. 4, Academic Press, London (1971).

911 J.C.S. CHEM. COMM., 1981

Broadening of N.M.R. Signals of Nuclei Coupled to Fast Relaxing Spin-$\frac{1}{2}$ Nuclei: An Example of T_1 Spin-decoupling

By FRANK BRADY and RAY W. MATTHEWS*
(*Department of Chemistry, The Polytechnic of North London, Holloway, London* N7 8DB)
and MARK J. FORSTER and DUNCAN G. GILLIES*
(*The Bourne Laboratory, Department of Chemistry, Royal Holloway College, University of London, Egham Hill, Egham, Surrey* TW20 0EX)

Summary Broadening effects in the spectra of spin-$\frac{1}{2}$ nuclei, A, coupled to fast relaxing spin-$\frac{1}{2}$ nuclei, X, have been related to the T_1 value of X and hence provide a new method for measuring this parameter at high field on account of enhanced relaxation by the chemical shift anisotropy mechanism.

EVIDENCE is accumulating to show that linewidths of spin-$\frac{1}{2}$ nuclei, A, (*e.g.* A = ^{1}H, ^{13}C, ^{31}P) coupled to fast relaxing spin-$\frac{1}{2}$ nuclei, X, (*e.g.* ^{195}Pt,[1] ^{199}Hg,[2] ^{205}Tl[3]) may be dominated by relaxation at X, particularly at high field. Specification of the relationship between the broadening effects in the A spectrum and relaxation at X provides a new and facile means of determining the spin–lattice relaxation of X.

These lineshape phenomena are examples of the T_1 spin-decoupling effect noted previously[4] for the effect of dissolved oxygen on proton spin–spin multiplets. The spin–lattice relaxation of the X nuclei produces an effect analogous to that of chemical exchange on the multiplet and hence a useful insight may be gained by treating the effect of changes in the X spin-state on the A spectrum of an AX spin system in terms of two-site exchange. Assigning the two A components respectively to the α and β spin states of X, standard exchange equations may be applied noting that the lifetimes of the equally populated spin states, τ_α and τ_β, are related to the transition probability, $W_{\alpha\beta}$, and spin–lattice relaxation of X, T_{1X},[5a] by $\tau_\alpha^{-1} = \tau_\beta^{-1} = W_{\alpha\beta} = (2T_{1X})^{-1}$. The most usual situation corresponds to the slow exchange limit when $\tau_\alpha >> (2\pi J)^{-1}$. In this case the broadening of each A component is just $(\pi\tau_\alpha)^{-1}$ or $(2\pi T_{1X})^{-1}$. Thus the observed line width is given by equation (1), were $(\pi T'_{2A})^{-1}$ is the sum

$$\Delta\nu_{\frac{1}{2}}(A) = (\pi T'_{2A})^{-1} + (2\pi T_{1X})^{-1} \quad (1)$$

of the natural linewidth of A and magnetic field inhomogeneity broadening. The general treatment of Navon and Polak[4] for first-order A_mX_n spectra yields the same result in

the slow exchange limit for the A_mX case, and also provides a means of calculating A-multiplet lineshapes for faster exchange rates, although other formulations of the exchange problem could of course be used.

It should be noted that although scalar relaxation of the second kind[4a] is undoubtedly responsible for the broadening, the usual expressions[4b] for relaxation at A are inappropriate in the case of non-overlapping A-components where the condition[4a] $(2\pi J)^{-1} >> T_{1X}$, implying collapse to a single resonance, clearly does not apply. The situation is analogous, however, to broadened, non-overlapping components of a spin-$\frac{1}{2}$ nucleus coupled to a quadrupolar nucleus (*e.g.* ^1H–^{14}N)[4b] although in this case differential broadening arises from unequal lifetimes of the quadrupolar nuclear spin-states.

The value of $(\pi T'_{2A})^{-1}$ can be obtained from non-coupled signals in the A spectrum and, for some X nuclei (*e.g.* ^{195}Pt, ^{199}Hg), the central uncoupled signal arising from A connected to the 'n.m.r. inactive' isotope of X provides a particularly convenient measure. The ability of equation (1) to yield T_{1X} with accuracy increases with increasing $(2\pi T_{1X})^{-1}$, *i.e.* with increasing relaxation rate of X. The situation will be especially favourable for X nuclei which relax significantly *via* the chemical shift anisotropy (C.S.A.) mechanism and where the A spectra are determined at high magnetic field, B_0, because $(T_{1X})^{-1}$ (C.S.A.) $\propto B_0^2$ [$(\pi T'_{2A})^{-1}$ is essentially field independent]. Equation (2) gives the C.S.A. contribution for the extreme narrowing condition and axial symmetry,[7] and indicates that the applicability of this method for determining T_{1X} also depends on the value of γ_X and the chemical shift anisotropy in the particular molecular species.

$$(T_{1X})^{-1}(\text{C.S.A.}) = (6/7)(T_{2X})^{-1}(\text{C.S.A.}) = (2/15)\gamma_X^2 B_0^2 (\sigma_\parallel - \sigma_\perp)^2 \tau_c \quad (2)$$

Illustrating the use of equation (1) we have obtained $\Delta\nu_{\frac{1}{2}}(H) = 55$ Hz for $Tl(CH_3)_2NO_3$ in D_2O (degassed) at 400 MHz and 300 K. Without allowances for $(\pi T'_{2B})^{-1}$ and the effect of overlapping components coupled to ^{203}Tl and ^{205}Tl (together $<ca.$ 4 Hz), equation (1) predicts $T_{1(Tl)} = ca.$ 2·9 ms in good agreement with a preliminary $T_{1(Tl)}$ for this solution of *ca.* 2·9 ms at 295 K and the same magnetic field.

Where the C.S.A. contribution to relaxation of X is 100%, combination of equations (1) and (2) and neglecting $(\pi T'_{2A})^{-1}$ yields $\Delta\nu_{\frac{1}{2}}(A) = (3/7)\Delta\nu_{\frac{1}{2}}(X)$, where $\Delta\nu_{\frac{1}{2}}(X) = (\pi T_{2X})^{-1}$. For the thallium solution noted above, $\Delta\nu_{\frac{1}{2}}(Tl) = ca.$ 140 Hz at 231·5 MHz[3] which is consistent with the predicted value of $(7/3)\Delta\nu_{\frac{1}{2}}(H) = 128$ Hz. The additional broadening in the ^{205}Tl spectrum can be ascribed to the effects of temperature inhomogeneity at high field [temperature coefficient of chemical shift for Tl $(CH_3)_2NO_3$ in $H_2O = 0.44$ p.p.m. K^{-1}].[8] In cases where the relaxation of X is not totally dominated by the C.S.A. mechanism, the relative contributions of other mechanisms (*e.g.* spin rotation) may be ascertained by observation of broadening effects on A as a function of temperature and magnetic field.

We thank the S.R.C. for studentships to F.B. and M.F. and the U.L.I.R.S. WH-400 N.M.R. Service at Queen Mary College for spectra.

(*Received*, 10*th June* 1981; *Com.* 682.)

[1] J. Y. Lallemand, J. Soulie, and J. C. Chottard, *J. Chem. Soc., Chem. Commun.*, 1980, 436.
[2] N. S. Ham, E. A. Jeffery, T. Mole, and S. N. Stuart, *Chem. Commun.*, 1967, 254; A. J. Brown, O. W. Howarth, and P. Moore, *J. Chem. Soc., Dalton Trans.*, 1976, 1589; L. P. Blaauw, A. D. H. Clague, D. G. Gillies, G. R. Hays, and R. Huis, *J. Magn. Reson.*, 1981, **42**, 420.
[3] F. Brady, M. J. Forster, D. G. Gillies, and R. W. Matthews, *Inorg. Nucl. Chem. Lett.*, 1981, **17**, 155.
[4] G. Navon and M. Polak, *Chem. Phys. Lett.*, 1974, **25**, 239.
[5] J. A. Pople, W. G. Schneider, and H. J. Bernstein, 'High-resolution Nuclear Magnetic Resonance,' McGraw-Hill, New York, 1959; (a) p. 24; (b) p. 228.
[6] A. Abragam, 'The Principles of Nuclear Magnetism,' Oxford University Press, London, 1961; (a) p. 309; (b) p. 311.
[7] T. C. Farrar and E. D. Becker, 'Pulse and Fourier Transform N.M.R.,' Academic Press, London, 1971, ch. 4.
[8] P. J. Burke, I. D. Cresshull, D. G. Gillies, and R. W. Matthews, *J. Chem. Soc., Dalton Trans.*, 1981, 132.